JOURNAL OF BIOLOGICAL REGULATORS & HOMEOSTATIC AGENTS
Volume 29, No. 3, July - September, 2015

CONTENTS

JOURNAL OF BIOLOGICAL REGULATORS & HOMEOSTATIC AGENTS Vol. 29, no. 3, 521-526 (2015)

EDITORIAL

PRESBYOPIA OPTOMETRY METHOD BASED ON DIOPTER REGULATION AND CHARGE COUPLE DEVICE IMAGING TECHNOLOGY

Q. ZHAO, XX. WU, J. ZHOU, X. WANG, RF. LIU and J. GAO

Department of Ophthalmology, the Second Hospital of Dalian Medical University, Dalian, Liaoning Province, China

Received May 28, 2015 – Accepted July 20, 2015

With the development of photoelectric technology and single-chip microcomputer technology, objective optometry, also known as automatic optometry, is becoming precise. This paper proposed a presbyopia optometry method based on diopter regulation and Charge Couple Device (CCD) imaging technology and, in the meantime, designed a light path that could measure the system. This method projects a test figure to the eye ground and then the reflected image from the eye ground is detected by CCD. The image is then automatically identified by computer and the far point and near point diopters are determined to calculate lens parameter. This is a fully automatic objective optometry method which eliminates subjective factors of the tested subject. Furthermore, it can acquire the lens parameter of presbyopia accurately and quickly and can be used to measure the lens parameter of hyperopia, myopia and astigmatism.

As a biological optic system, human eyes can be emmetropic, hyperopic, myopic and astigmatic, which vary from person to person (15-16). All of them will negatively influence the vision of human eyes except emmetropia, which is called vision deficiency or diopter abnormity (1). Vision deficiency is normally adjusted by optometry a well as surgery, laser operation and drug therapy. In the last decade, as photoelectric technology and single-chip microcomputer technology has developed, objective (automatic) optometry has become increasingly more precise to the point that it can completely eliminate the subjective factors of the tested subject and acquire the lens parameter accurately and quickly (17-18).

CCD was invented by Bell Laboratory in the late 1960s. It is a special semiconductor consisting of several independent light sensors which are normally in matrix arrangement (2-4). At first, CCD was used as a new PC storage circuit. But soon it had many other potential applications, such as signal and image (light sensitivity of silicon) management (5). Most digital cameras use CCDs as their photosensitive elements.

Presbyopia usually occurs with age and is caused by the variation of physiological functions (19). The conventional method of presbyopic optometry uses different lens for trial after an estimation is based on age and empirical data (6). To date, there is no objective measuring method. This paper proposed a method to measure the near and far point on the basis of diopter regulation principle and then designed an

Key words: visual optics, diopter regulation, CCD devices, image identification

Mailing address: Dr Qi Zhao,
Department of Ophthalmology,
the Second Hospital,
Dalian Medical, University, Dalian,
Liaoning Province,
116023, China
e-mail: zq2395@163.com

0393-974X (2015)

DISCLOSURE: ALL AUTHORS REPORT NO CONFLICTS OF INTEREST RELEVANT TO THIS ARTICLE.

objective optometry unit of optical system based on CCD imaging technology.

DIOPTER REGULATION OF HUMAN EYES AND IMAGING PROPERTY OF PRESBYOPIA

Human eyes automatically adjust focal lengths when observing objects at different distances to make the image projected onto the retina, thus we can see things clearly. The automatic adjustment of focal length is called diopter regulation (7). The diopter regulation range is the difference between far point diopter and near point diopter, which varies as age grows. Far point diopter is the reciprocal of the furthest distance (in m) human eyes can see clearly when they are relaxed. The furthest distance that relaxed emmetropic eyes can project a clear image on the retina is infinity, hence the far point diopter is 0. If the furthest distance myopic eyes can see clearly is - 2 m, then the near point diopter is - 0.5. Near point diopter is the reciprocal of the nearest distance human eyes can see with the maximum regulation (8). The near point distance of a 20-year-old human's emmetropic eye is – 100 mm, and the near point diopter is – 10 while the far point distance is infinity, thus the maximum regulation range is 10 diopter.

When emmetropic eyes become presbyopic, the far point distance stays as infinity and the relevant far point diopter is 0, whereas the near point distance becomes further and the absolute value of relevant near point diopter decreases, thus the regulation range narrows. The near point distance of emmetropic eye of a 50-year-old human is – 400 mm of which the relevant near diopter is – 2.5, thus the regulation range is 2.5 diopter. The narrowing of regulation range is the symptom of presbyopia, and is a physiological phenomenon which relates to age and occurs in all the elderly.

Imaging property of presbyopia is shown in Fig. 1. The imaging of infinite object point falls on the retina (expressed as fine solid line) and the imaging of finite object point falls on the F point which is behind the retina (expressed as light ray with an arrow), and a light spot is formed on the retina, hence the image is blurry. If a convex lens is put before the eye, the object point at infinite distance forms clear imaging on the retina (dash line). The convex lens is known as a presbyopic lens, which replaces the convex crystalline lens to adjust presbyopia.

Since presbyopia is characterized by the narrowing of regulation range, and the diopter regulation range is the difference between far point and near point, thus we can acquire the presbyopic lens parameter by measuring the far point diopter and near point diopter of the eye and applying the clinical experiential formula of ophthalmology (9).

The near point of presbyopic subjects becomes further away, so objects can be perceived clearly when things are placed further from the eye. But if the object is small and placed too far away, even beyond the distinguishability extremity, things can not be seen clearly either. So, in order to read and see normally, we have to adjust presbyopia with lens.

THE CORRELATION BETWEEN FAR POINT AND NEAR POINT DIOPTER AND PRESBYOPIC DIOPTER

The regulation range (ability) of the human eye is the difference between the far point and near

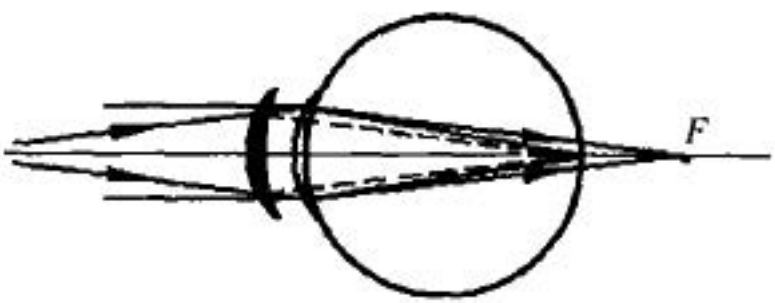

Fig. 1. *Imaging property of presbyopia.*

point diopter, i.e., ΔD=DY – DJ (10-11). In clinical experience, the presbyopic symptom of the human eye is void or slight when ΔD ≥3D (D refers to diopter unit) and the presbyopic symptom is severe when ΔD <3D (12). Presbyopia is usually corrected by wearing presbyopic glasses to move the near point into an appropriate distance through the power of convex lens instead of regulation. In practice, the presbyopia diopter (lens diapoter) is defined as

DL =DJ - D0 + ΔD /3 (i)

where, D0 is the diopter which is relevant to reading distance. Reading distance is normally –m/3, thus D0 = -3D.

Fig. 2, showing the equation (1), demonstrates clearly that when the human eye is relaxed, it can clearly see objects at far point PY, and with some regulation ability it can see the object at P1 (P1 is within the regulation range). Then after being adjusted with a lens (diopter value is DL), the eye can see the object clearly at reading point P0. Here, near point PJ is beyond P0.

In equation (i), the configuration of ΔD /3 is reasonable because it is a clinical experiential datum of ophthalmology and its value is 1/3 of the remaining regulation ability (ΔD). Its physical meaning is to adjust presbyopia with lens and make sure 2/3 of the remaining regulation ability can be invoked. If a man with presbyopia reads without applying regulation ability, but is directly adjusted from PY to P0 with lens, crystalline lens will be in a dormant state for a long time and thus cause the acceleration of eye senility. On the contrary, if we invoke all the regulation ability, our eyes get tired easily.

If an eye has lost all the regulation ability, which means ΔD = 0 and its far point coincides with near point. The equation of presbyopia changes from equation (i) to:

DL =DJ - D0 (ii)

The physical meaning of equation (ii) is that the far point of the relaxed eye is directly adjusted from PY (also PJ) to P0 with lens.

OPTICAL SYSTEM AND THE MEASUREMENT OF FAR POINT AND NEAR POINT OF THE HUMAN EYE

The optical system shown in Fig. 3 can measure the far point diopter and near point diopter as well as directly measure the degree of hyperopia, myopia and astigmatism. In Fig. 3, sequence 100 is projected light path, sequence 200 is measurement light path and sequence 300 is fixation light path. Near-infrared source 101 lights up diaphragm 105, forms ringlike image and then enters the eyeball 112. To emmetropic eyes, the image may be projected on the retina and be reflected from there; then the image goes back through the previous pathway and reflects on spectral 201. After that, the image refracts to diaphragm 202 which eliminates stray lights and forms a ring-like image on the area array CCD. The image has a fixed diameter. If the tested eye is abnormal, the scanner consisting of 109 and 110 compensates the light

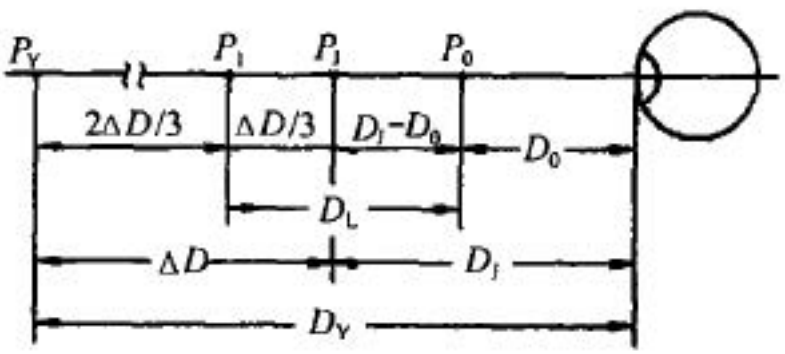

Fig. 2. *Diagram of presbyopia adjustment.*

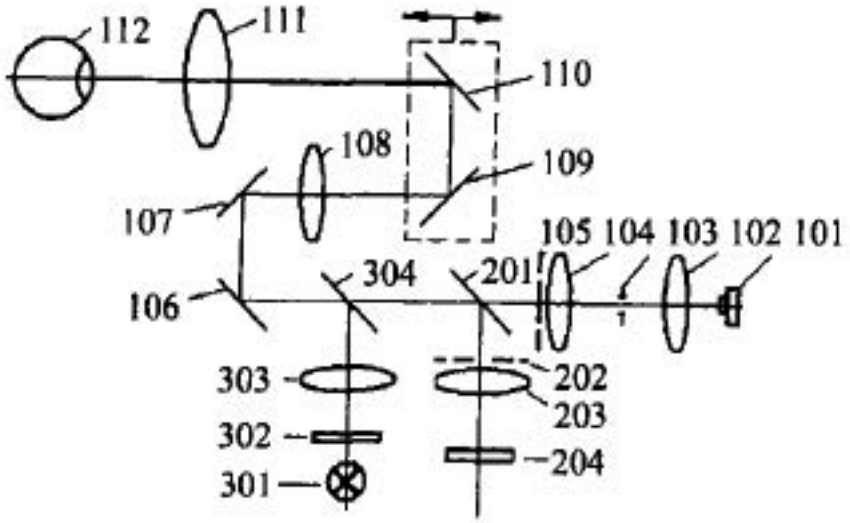

Fig. 3. *Optical system.*

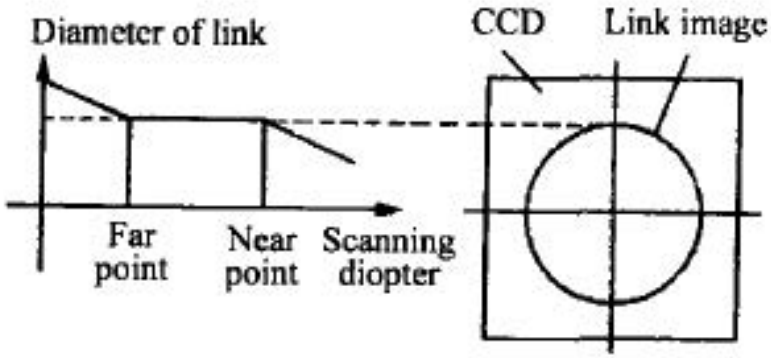

Fig. 4. *The correlation between scanning diopter and diameter of ring-like image.*

and still projects the ring-like image on the retina. Then we get ring-like images of the same diameters and the compensation amount of the scanner is the diopter of the far point and near point. If the tested eye is astigmatic, the image on CCD will be ellipse and we can get astigmatic degree and axial angle parameter from the length, minor axis and gradient of the ellipse.

In fixation light path, the fixation vision image 302 is lightened by visible light source 301, then it reflects on splitter 304 and refracts to the tested eye. The tested eye stares at fixation vision image and regulates the diopter with the scanning of the scanner to get clear vision of fixation vision image, thus we can get the diopter of the far point and near point. The process is shown in Fig. 4.

Fig. 4 shows that first, as scanning is performed beyond the regulation range of the tested eye, the tested eye can not see things clearly and can not follow the fixation vision image. Thus the diopter value is fixed and focal length of the optical system changes during the scanning (or scanning diopter) which leads to the variation of diameter of the ring-like image on CCD.

Secondly, between the far point and near point, scanning is within the regulation range of the tested eye. As the eye can see things clearly and it can regulate during the scanning when it is following the fixation vision image, the diopter value changes during this process. The diopter value variation of

the tested eye neutralizes the scanning diopter, so the diameter of the ring-like image on CCD stays the same.

The far point and near point of the tested eye are at the two scanning positions where the diameter of ring-like image changes. At this time, the scanning diopter equals to the far point diopter and near point diopter of the tested eye (13-14). The acquired far point and near point diopters in equation (i) are substituted to get the presbyopia diopter. Characteristics of the ring-like image are recognized by the Single Chip Microcomputer, and the whole process is performed by the system automatically without the consciousness of the tested subjects.

CONCLUSIONS

To sum up, we can arrive at three conclusions from this study:

(a) a fully automatic objective presbyopia optometry method is described by measuring the far point and near point diopter and calculating the presbyopia diopter with a scientific calculating method;

(b) through the analysis of the optical system, we find that this method is competent for measuring the lens parameter of hyperopia, myopia and astigmatism, which is multifunctional;

(c) the traditional fully automatic objective optometry unit used for measuring myopia, hyperopia and astigmatism only needs the tested eye to be relaxed and no diopter regulation is required, which accomplishes the whole measurement within 1 second. The presbyopia method of this paper which is based on human eye diopter regulation and CCD imaging technology needs a bit more time. It takes some time for the tested eye to focus on the fixation vision image and regulate the diopter during the scanning. So it needs in-depth research and experiment to determine the scanning time. However, this uncertainty does not influence the validity and feasibility of this method.

REFERENCES

1. Palomino C, Carmona D, Castillo A, Genol I, Clariana A. Visual quality after presbyopia surgery. J Emmetropia 2010; 1:74-80.
2. Artigas JM, Menezo JL, Peris C, Felipe A, Díaz-Llopis M. Image quality with multifocal intraocular lenses and the effect of pupil size: comparison of refractive and hybrid refractive-difractive designs. Cataract Refract Surg 2007; 34:1056-57.
3. Güell JL, Pujol J, Arjona M, Diaz-Douton F, Artal P. OQAS: A new instrument for an objective clinical evaluation of the ocular optical quality. Cataract Refract Surg 2004; 30:1598-99.
4. Díaz-Doutón F, Benito A, Pujol J, Arjona M, Güell JL, Artal P. Comparision of the retinal image quality with a Hartmann-Shack wavefront sensor and double-pass instrument. Invest Ophthalmol Vis Sci 2006; 47:1710716.
5. Kawamorita T, Uozato H. Modulation transfer function and pupil size in multifocal and monofocal intraocular lenses in vitro. Cataract Refract Surg 2005; 31:2379-85.
6. Luque SO, Díaz-Doutón F, Lapuente V, Pujol J, Arjona M, Artal P. Estimating intraocular scattering from combined Hartmann-Shack and double-pass measurements. Presented at ARVO 2006 annual meeting.
7. Montes-Micó R, España E, Bueno I, Charman WN, Menezo JL. Visual performance with multifocal intraocular lenses; mesopic contrast sensitivity under distance and near conditions. Ophthalmol 2004; 111:85-96.
8. Rawer R, Stork W, Spraul CW, Lingenfelder C. Imaging quality of intraocular lenses. Cataract Refract Surg 2005; 31:1618-31.
9. Altmann GE, Nichamin LD, Lane SS, Pepose JS. Optical performance of 3 intraocular lens designs in the presence of decentration. Cataract Refract Surg 2005; 31:574-85.
10. Castillo-Gómez A, Carmona-González D, Martínez-de-laCasa JM, Palomino-Bautista C, García-Feijoo J. Evaluation of image quality after implantation of 2 diffractive multifocal intraocular lens models. Cataract Refract Surg 2009; 35:1244-1250.
11. JA Monsoriu, WD Furlan, G Saavedra, F Giménez. Devil's lenses. Optics Express 2007; 15:13858-64.
12. Taketani F, Matura T, Yukawa E, Hara Y. Influence of intraocular lens tilt and decentration on wavefront aberrations. Cataract Refract Surg 2004; 30:2158-62.
13. Koretz JF, Cook CA, Kaufman PL. Aging of the

human lens: Changes in lens shape at zero-diopter accommodation. Journal of the Optical Society of America A-Optics and Image Science and Vision 2001; 18(2):265-72.

14. Tognetto D, Sanguinetti G, Sirotti P, Cecchini P, Marcucci L, Ballone E, Ravalico G. Analysis of the optical quality of intraocular lenses. Invest Ophthalmol Vis Sci 2004; 45:2682-2690.

JOURNAL OF BIOLOGICAL REGULATORS & HOMEOSTATIC AGENTS Vol. 29, no. 3, 527-531 (2015)

EDITORIAL

PHYSIOPATHOLOGY OF OSTEOPOROSIS: FROM RISK FACTORS ANALYSIS TO TREATMENT

A. DEL PUENTE[1], A. ESPOSITO[1], A. DEL PUENTE[2], L. COSTA[1], F. CASO[1] and R. SCARPA[1]

[1]Rheumatology Unit, "Federico II" University, Naples, Italy; [2]Rehabilitation Unit, "Federico II" University, Naples, Italy

Received March 24, 2015 Accepted June 5, 2015

Osteoporosis represents a relevant health issue, being the first cause of bone fractures in the elderly with subsequent implications in terms of survival and social costs. The improved knowledge about the physiopathology of this disease has led to a new definition of Osteoporosis, which shifts the attention from the "decrease in bone mass" to several elements related to what has globally been defined as bone quality. In fact, it has been shown that clinical risk factors affecting bone homeostasis coincide with osteoporosis risk factors. The evaluation of such clinical risk factors is an important element in the assessment of the global fracture risk. The availability of instruments for the assessment of the global fracture risk also suggests a change in the clinical perspective and raises new questions as yet unanswered.

Osteoporosis affects millions of people and is the major underlying cause of bone fractures in postmenopausal women and the elderly, representing a dramatically growing problem in terms of human and social costs (1).

The definition of osteoporosis has been recently revised from the one formulated in 1993 which identified the "decrease in bone mass" as the major characteristic of the pathology (2). The new definition includes several elements that are all affected by the interaction with life style factors, which represent risk factors for osteoporosis development (3).

Particularly in the older age groups, for example, it has been shown that non-skeletal risk factors play a very relevant role in determining the fracture risk (4). This evidence outlines the importance of paying attention to these factors in the clinical practice. Obviously, the focus has to be on modifiable risk factors, which represent a field where the collaboration between patient and physician can be effective and has to be improved.

HOMEOSTATIC SYSTEMS

Factors that affect bone homeostasis coincide with osteoporosis risk factors. Calcium Cycle and Coupling are the two main homeostatic systems in bone metabolism.

Calcium cycle

Calcium is an essential threshold nutrient (5). It is important to understand that the goal of calcium homeostasis is not to protect against bone loss, but rather to maintain ionic calcium in the plasma within

Key words: osteoporosis treatment, osteoporosis risk factors, calcium

Mailing address: Prof. Antonio del Puente,
Rheumatology Unit,
"Federico II" University,
via Pansini 5,
80131 Naples, Italy
Tel.: +39 081 746 3773 Fax: +39 081 546 3445
e-mail: delpuent@unina.it

0393-974X (2015)

DISCLOSURE: ALL AUTHORS REPORT NO CONFLICTS OF INTEREST RELEVANT TO THIS ARTICLE.

narrow physiologic concentration. This is one of the most tightly regulated constants in physiology and is consistent with the important role of intracellular calcium in cell biology as a signal transducer (6). Indeed, bone loss can occur as a compensatory mechanism to maintain a constant serum ionic calcium concentration. All ingress and egress of calcium from the body passes through a rapidly miscible calcium pool that includes plasma, extracellular fluids, and components of bone, probably bone surfaces. This pool represents approximately 1% of the 1,000 grams of calcium in the skeleton of an average-sized woman. Calcium enters the pool either by intestinal absorption of dietary calcium or by bone resorption. Calcium leaves the pool mainly by secretion into the intestine (endogenous fecal calcium), by urinary losses, and by bone formation. Approximate daily rates for these fluxes for a person on a dietary calcium intake of 1,000 mg is 300 mg for intestinal calcium absorption, 100 mg for endogenous fecal calcium, 200 mg for urinary calcium excretion, 200 mg for bone formation, and 200 mg for bone resorption. In addition, there are dermal losses, which in the past have been estimated to be about 20 mg/day, but which more recently have been estimated about 60 mg/day. These fluxes are regulated by changes in plasma concentration of a number of hormones, especially 1,25 dihydroxyvitamin D3 ($1,25(OH)_2$ D_3), the physiological form of vitamin D. Vitamin D also regulates changes in calcium absorption and parathyroid hormone (PTH), which regulates the level of bone resorption and tubular reabsorption of calcium. These homeostatic changes maintain a constant concentration of serum ionic calcium (7). The role of other vitamins at present seems less determinant and potential causes of hypovitaminosis other than vitamin D are definitely less frequent (8). An adequate evaluation of vitamin D status is mandatory in patient management and supplementation must be provided when required (9, 10).

Coupling cycle

Bone remodeling is essential for various necessities: to refill the calcium pool, to adapt skeleton segments to increased activity, to periodically repair micro-fractures. For these reasons, the entire skeleton undergoes a turnover every year in the child and every seven years in the adult.

The Coupling cycle consists of different steps. As a rule, mineralized bone surface is covered by dormant osteoblasts. Bone is subdivided into remodeling units: volumetric units each managed by a certain number of osteoblasts. Osteoblasts regularly bare bone surface that is instantaneously covered by osteoclasts. Osteoclasts generate a resorption cavity of definite dimensions. In the last step, osteoblasts are recruited on the resorption cavity surface and they fill it with osteoid matrix and grow factors.

Going into details, osteoblasts expose RANK-Ligand (RANK-L) that interacts with RANK receptor on osteoclast precursors. Osteoblasts also secrete Osteoprotegerin (OPG), a decoy receptor that is the soluble form of RANK, in order to modulate RANK-L activity.

RANK/RANK-L bond activates osteoclasts that become polarized cells (11). They tightly adhere to bone surface (12, 13) and, under the adhesion area, they secrete high doses of hydrogen ions and enzymes, among which Catepsin-K (14). In this way, they create a chemical microenvironment able to destroy bone within that area (15). From eroded bone, growth factors are released which act on osteoblast precursors triggering WNT/β-Catenin signaling pathway, transforming mesenchymal precursors into mature osteoblasts (11, 16, 17).

Whilst laying matrix, some osteoblasts are incorporated into the matrix that mineralizes and they become osteocytes. Osteocytes are connected by cytoplasmic prolongations, forming a syncytium. Osteocytes act as mechanoreceptors: they perceive load stimulation and modulate the Coupling cycle by the production of Sclerostin which hinders the activation of WNT pathway, blocking osteoblast maturation and thus making bone resorption prevail (18).

Summarizing, the Coupling cycle consists of two arms: resorption (RANK/RANK-L/ osteoclasts) and formation (sclerostin/WNT/osteoblasts). Sexual hormones, PTH, calcitonin, vitamin D, and physical activity influence these two homeostatic systems.

CLINICAL RISK FACTORS

Factors affecting these homeostatic systems are the same which represent risk factors for osteoporosis and fracture. An illustrative example

of this is represented by inflammatory cytokines. On the one hand, they activate the RANK/RANK-L pathway with an increase of osteoclast activity, on the other hand, they contemporarily act on TNFα, increasing the WNT antagonist dickkopf-1 (DKK-1) levels, which inhibit osteoblasts maturation (19, 20). Therefore, inflammatory cytokines increase bone resorption and reduce bone formation. Overall, these actions may determine an increased osteoclast activity that is not sufficiently well balanced by osteoblast-forming activity, causing alterations on bone architecture. Trabecula alterations and interruptions are not properly repaired and this may compromise the statics of skeletal segments (21). It is well known, in fact, that a structure formed by horizontal and vertical supports is not able to bear the same weight if removing horizontal supports, reducing approximately 12-fold the load bearing capacity, which is the reason why structure alterations may determine an increased fracture risk even without significantly reduced bone mass (22, 23). Several risk factors determine a significant increase of fracture risk independently from bone mass variations, including the body mass index, previous fractures, familiarity for fragility fractures, smoking, steroid use, excessive alcohol consumption, and chronic inflammatory diseases. Thus, the evaluation of clinical risk factors is an important element in the assessment of the global fracture risk. In particular, clinical risk factors and age modulate the global fracture risk which is an expression of bone strength. With regard to this point, it is important to outline the importance of an assessment of bone mineral density with appropriate devices and in centers which perform adequate and periodical calibration measurements. Surrogate indexes of bone quality, such as spinal deformity index, are promising but still under evaluation (24).

Recently, the scientific community has been devoting a considerable effort in order to define and to find how to express the global fracture risk. At present, two main kinds of instruments are available. The first one is the record of high-risk cases, which defines clinical profiles with high fracture risk. In Italy this approach is represented, for example, by the cases listed in the so-called "nota 79" recently appropriately revised (25). In this case, the list has mainly a normative value in relation to the drug reimbursement. A second approach is represented by several algorithms which have been developed (26). They are mathematical functions that combine the effects of the various clinical risk factors in the same subject in order to evaluate the global fracture risk. Most of them express this risk in percentage probability of fractures in a defined time.

The availability of these instruments is also suggesting a change in the clinical perspective. The prevalent attitude of trying to identify patients deserving treatment, the so-called "target to treat" approach, should be accompanied by an attempt to treat patients in order to modify their risk profile and reduce the global fracture risk, the so-called "treat to target" approach. Patient management should aim at moving the patient profile from a higher risk category to a lower one.

However, two key questions emerge while using clinical risk factors with this approach. First question: is the risk profile, identified in this way, reversible with treatment? This is a crucial point especially when using algorithms, because all the drugs available at present have been tested for their efficacy in reducing fractures due to their mechanism of action on bone mass.

The second question is a consequence of the first: we should try to better understand, of the drugs now available and for those coming, which are the determinants of the anti-fracture efficacy.

Several analyses have already reevaluated the results of the studies on different drugs with the intention to evaluate whether the treatment was actually able to shift subjects from a high-risk category to a lower risk one according to the most used algorithm, FRAX, showing a better effect in the patients in high risk categories. Only a few drugs (Clodronate, Bazedoxifene, Denosumab) proved to be able to do this, the others did not, even though all examined studies had reported significant reduction in fracture incidence in the treated groups (27-32).

In the management of osteoporosis today, these two questions remain as critical elements. Therefore, a more complex and more complete approach to patients with osteoporosis is necessary. This approach will have to consider both drug efficacy and drug capacity to act on other parameters besides bone mass (and at present this is still not evident for any of the available drugs). Moreover, it will

be necessary to enlarge the therapeutic approach including, in a more determined way, the action on the other modifiable risk factors with the aim not only of increasing bone mass, but also at improving the risk profile of patients.

In conclusion, the new definition of osteoporosis results as being more appropriate (3). It includes several elements related to what has globally been defined as bone quality. These elements, macroarchitecture, connectivity, microarchitecture, material properties of the matrix, are all affected by the interaction with clinical risk factors. Instead of focusing on the reduction of bone mass, osteoporosis is currently defined as a reduction of "bone strength", thus taking into account these complex variables.

REFERENCES

1. Kanis JA and the WHO Study Group: World Health Organization Study Document. Assessment of fracture risk and its application to screening for postmenopausal osteoporosis: synopsis of a WHO report. Osteoporosis Int 1994; 4:368-81.
2. Consensus development conference: diagnosis, prophylaxis, and treatment of osteoporosis. Am J Med 1993; 94(6):646-50.
3. NIH Consensus Development Panel on Osteoporosis Prevention, Diagnosis, and Therapy. Osteoporosis prevention, diagnosis, and therapy. JAMA 2001; 285(6):785-95.
4. Dennison E, Eastell R, Fall CHD, Kellingray S, Wood PJ, Cooper C. Determinants of bone loss in elderly men and women: prospective population-based study. Osteoporos Int 1999; 10:384-91.
5. Heaney RP. Low calcium intake among African Americans: effects on bones and body weight. J Nutr 2006; 136(4):1095-8.
6. Edel KH, Kudla J. Increasing complexity and versatility: How the calcium signaling toolkit was shaped during plant land colonization. Cell Calcium 2015; 57(3):231-46.
7. NIH Consensus conference. Optimal calcium intake. NIH Consensus Development Panel on Optimal Calcium Intake. JAMA 1994; 272(24):1942-8.
8. Hamidi MS, Gajic-Veljanoski O, Cheung AM. Vitamin K and bone health. J Clin Densitom. 2013;16(4):409-13.
9. Rosen CJ. The Epidemiology and Pathogenesis of Osteoporosis. In: De Groot LJ, Beck-Peccoz P, Chrousos G, et al, editors. Endotext [Internet]. South Dartmouth (MA): MDText.com, Inc.; 2000.
10. Del Puente A, Esposito A, Savastano S, Carpinelli A, Postiglione L, Oriente P. Dietary calcium intake and serum vitamin D are major determinants of bone mass variations in women. A longitudinal study. Aging Clin Exp Res 2002; 14(5):382-8.
11. Cappariello A, Maurizi A, Veeriah V, Teti A. Reprint of: The great beauty of the osteoclast. Arch Biochem Biophys 2014; 561:13-21.
12. Marchisio PC, Cirillo D, Naldini L, Primavera MV, Teti A, Zambonin-Zallone A. Cell-substratum interaction of cultured avian osteoclasts is mediated by specific adhesion structures. J Cell Biol 1984; 99:1696-705.
13. Saltel F, Chabadel A, Bonnelye E, Jurdic P. Actin cytoskeletal organisation in osteoclasts: A model to decipher transmigration and matrix degradation. Eur J Cell Biol 2008; 87:459-68.
14. Zaidi M, Troen B, Moonga BS, Abe E. Cathepsin K, osteoclastic resorption, and osteoporosis therapy (Editorial). J Bone Miner Res 2001; 16:1747-49.
15. Peruzzi B, Teti A. The physiology and pathophysiology of the osteoclast. Clin Rev Bone Miner Metab 2012; 10:71-97.
16. Takeshita S, Kaji K, Kudo A. Identification and characterization of the new osteoclast progenitor with macrophage phenotypes being able to differentiate into mature osteoclasts. J Bone Miner Res 2000; 15(8):1477-88.
17. Rosenberg N, Rosenberg O, Soudry M. Osteoblasts in bone physiology-mini review. Rambam Maimonides Med J 2012; 3(2):e0013.
18. You L, Chen L, Pan L, Gu W, Chen J. Zinc finger protein 467 regulates Wnt signaling by modulating the expression of sclerostin in adipose derived stem cells. Biochem Biophys Res Commun 2015; 456(2):598-604.
19. Weitzmann MN, Roggia C, Toraldo G, Weitzmann L, Pacifici R. Increased production of IL-7 uncouples bone formation from bone resorption during estrogen deficiency. J Clin Invest 2002; 110(11):1643-50.
20. Goldring SR, Gravallese EM. Bisphosphonates: en-

vironmental protection for the joint? Arthritis Rheum 2004; 50(7):2044-7.
21. Parfitt AM. Trabecular bone architecture in the pathogenesis and prevention of fracture. Am J Med 1987; 82(1B):68-72.
22. Carballido-Gamio J, Harnish R, Saeed I, et al. Proximal femoral density distribution and structure in relation to age and hip fracture risk in women. J Bone Miner Res 2013; 28(3):537-46.
23. Carballido-Gamio J, Harnish R, Saeed I, et al. Structural patterns of the proximal femur in relation to age and hip fracture risk in women. Bone 2013; 57(1):290-9.
24. Di Somma C, Rubino M, Faggiano A, Vuolo L, Contaldi P, Tafuri N, Andretti M,Savastano S, Colao A. Spinal deformity index in patients with type 2 dibetes. Endocrine 2013; 43(3):651-8.
25. AIFA http://www.agenziafarmaco.gov.it/it/content/nota-79
26. Siris ES, Baim S, Nattiv A. Primary care use of FRAX: absolute fracture risk assessment in postmenopausal women and older men. Postgrad Med 2010; 122(1):82-90.
27. McCloskey EV, Johansson H, Oden A, et al. Ten-year fracture probability identifies women who will benefit from clodronate therapy-additional results from a double-blind, placebo-controlled randomised study. Osteoporos Int 2009; 20:811-17.
28. Cummings SR, Donaldson ML, Palermo L, et al. Efficacy of alendronate for reducing nonvertebral and clinical fractures by FRAX score. J Bone Miner Res 2009; 24(S1):S10.
29. Kanis JA, Johansson H, Oden A, et al. A meta-analysis of the efficacy of raloxifene on all clinical and vertebral fractures and its dependency on FRAX. Bone 2010; 47:729-35.
30. Kanis JA, Johansson H, Oden A, et al. Bazedoxifene reduces vertebral and clinical fractures in postmenopausal women at high risk assessed with FRAX. Bone 2009; 44(6):1049-54.
31. Kanis JA, Johansson H, Oden A, et al. A meta-analysis of the effect of strontium ranelate on the risk of vertebral and non-vertebral fracture in postmenopausal osteoporosis and the interaction with FRAX® Osteoporos Int 2011; 22(8):2347-55.
32. McCloskey EV, Johansson H, Oden A, et al. Denosumab reduces the risk of osteoporotic fractures in postmenopausal women, particularly in those with moderate to high fracture risk as assessed with FRAX. J Bone Miner Res 2012; 27(7):1480-86.

JOURNAL OF BIOLOGICAL REGULATORS & HOMEOSTATIC AGENTS Vol. 29, no. 3, 533-545 (2015)

EDITORIAL

CLINICAL APPLICATION OF SHOCK WAVE THERAPY IN MUSCULOSKELETAL DISORDERS: PART I

R. SAGGINI[1], A. DI STEFANO[2], A. SAGGINI[3] and R.G. BELLOMO[4]

[1]Department of Neuroscience and Imaging, "G. D'Annunzio" University, Chieti, Italy; [2]School of Specialties in Physical Medicine and Rehabilitation "G. D'Annunzio" University, Chieti, Italy; [3]Department of Dermatology, University of Rome Tor Vergata, Rome, Italy; Pathology, University of California San Francisco, San Francisco, California, USA; [4]Department of Medicine and Science of Aging, "G. D'Annunzio" University, Chieti, Italy

Received February 18, 2015 – Accepted July 1, 2015

The shock wave has been widely recognized in literature as a biological regulator; therefore we carried out a review on the activity performed by shock waves on the bone-myofascial tissue system. To date, the application of Shock Wave Therapy (SWT) in musculoskeletal disorders has been primarily used in the treatment of tendinopathies (proximal plantar fasciopathy, lateral elbow tendinopathy, calcific tendinopathy of the shoulder, and patellar tendinopathy, etc.) and bone defects (delayed- and non-union of bone fractures, avascular necrosis of femoral head, etc.). Although the mechanism of their therapeutic effects is still unknown, the majority of published papers have shown positive and beneficial effects of using SWT as a treatment for musculoskeletal disorders, with a success rate ranging from 65 to 91%, while the complications are low or negligible. The purpose of this paper is to inform the reader about the published data on the clinical application of SWT in the treatment of musculoskeletal disorders. In this paper, with the help of a literature review, indications and success rates for SWT in the treatment of musculoskeletal disorders are outlined, while adequate SWT parameters (e.g., rate of impulses, energy flux density, etc.) are defined according to the present state of knowledge. Given the abundance of the argument, it seems appropriate to subdivide the review into two parts, the first concerning the evidence of Extracorporeal Shock Wave Therapy (ESWT) on bone disorders, the second concerning findings on tendon and muscle treatment.

A Shock Wave (SW) is defined as an acoustic wave, at the front of which pressure rises from the ambient value to its maximum within a few nanoseconds (1, 2). Shock Waves are characterized by high peak-pressure amplitudes (500 bar) with rise times of less than 10 nanoseconds, a short lifecycle (<10 ms) and a frequency spectrum ranging from 16 Hz to 20 MHz (3). After reaching the positive peak, the pressure rapidly drops to negative values within microseconds. Both the positive and the negative phase of a shockwave have an effect on interfaces between tissues with different density (acoustic impedance). During the positive phase, shock waves with high pressure may hit an interface, leading to

Key words: skeletal diseases, therapeutics, bone, shock wave, biological regulator

Mailing address: Prof. Raoul Saggini,
Department of Neuroscience and Imaging,
"G. D'Annunzio" University,
V.le Abruzzo 322, 66100 Chieti Scalo, Italy
Tel.: +39 0871 3553005 – 3553007
Fax: +39 0871 3553224
e-mail: saggini@unich.it

0393-974X (2015)

reflections, or they may pass and gradually become absorbed. The negative (tensile) phase of the shock wave causes cavitation at the tissue interfaces. During cavitation air bubbles are formed as a result of the negative pressure. These bubbles subsequently implode with high speed, generating a second wave of shock waves or microjets of fluid. These events cause the direct (physical) and indirect (biological) effects of the shock waves on the treated tissue (4, 5). Since their introduction in clinical settings, several commercially available shock wave generators have been developed. Depending on the commercial generator, electromagnetically, electrohydraulically, piezoelectrically, or electropneumatically derived energy is transformed into a shock wave. Focused shock waves can be electromagnetically, electrohydraulically or piezoelectrically generated. Some electromagnetic and electrohydraulic generators convert the acoustic wave into planar or defocused (soft-focused) waves, which retain the same physical characteristics but deliver the energy to a larger surface area. The depth of penetration will obviously be lower and, therefore, therapeutic use is limited to superficial lesions such as cutaneous ulcers (6).

Electromagnetic systems use an electromagnetic coil and an opposing metal membrane. A high current pulse is released through the coil to generate a strong magnetic field, which induces a high current in the opposing membrane, accelerating the metal membrane away from the coil to the 100,000-fold of gravity, thus producing an acoustic pulse in surrounding water. The pulse generates a cylindrical wave which is focused through a parabolic reflector, to direct the shock wave energy to the target tissue. The lens controls the focus size and the amount of energy produced within the target.

Piezoelectric systems are characterized by mounting piezoelectric crystals to a spherical surface. When a high voltage is applied to the crystals they immediately contract and expand, thus generating a pressure pulse in the surrounding water. The pulse is focused by means of the geometrical shape of the sphere.

Electrohydraulic systems incorporate an electrode, submerged in a water-filled housing comprised of an ellipsoid and a patient interface. The electrohydraulic generator initiates the shock wave by an electrical spark produced between the tips of the electrode. Vaporization of the water molecules between the tips of the electrode produce an explosion, thus creating a spherical shock wave. The wave is then reflected from the inside wall of a metal ellipsoid to create a focal point of shock wave energy in the target tissue. The size and shape of the ellipsoid control the focal size and the amount of energy within the target.

Each operator aims to couple the generated pressure pulse to the tissue while minimizing energy loss, concentrating the shock waves so that they can be applied in sufficient quantity to stimulate a desired tissue response (3-5).

For their clinical use, the head of the shock-wave generators are positioned over the area to be treated, which can be determined on the basis of previous diagnostic images or, if available on the device, by radiographic or ultrasound positioning systems. Once the position of the targeting site has been located, the treatment area is prepared with a coupling gel to minimize the loss of shock wave energy at the interface between the head of the device and the skin. Shock waves are dispersed from the application site and then may be absorbed, reflected, or dissipated depending on the properties of the tissue through which they spread (2).

The energy at the focal point of the shock wave per pulse is called the "Energy Flux Density" (EFD) and is recorded as joules per area. The effective total energy of a treatment is defined by the number and EFD of the single pulses and by the geometrical measurement of the focal point. Focused shock waves have a high (>0.2mJ/mm^2) EFD, while the defocused shock waves have a low (<0.2mJ/mm^2) EFD. The EFD is one of the most important physical parameters of shock wave therapy for the treatment of musculoskeletal disorders (7), in fact, high- and low-energy SWT sessions can yield equivalent EFD: a high-energy session using an energy level of 0.3 mJ/mm^2 and 1,000 shocks and a low-energy session using 0.1 mJ/mm^2 and 3,000 shocks yield an equivalent EFD of 300 mJ/mm^2 each (6). The number of shocks, intervals between shocks, number of treatments, and intervals between treatments are additional parameters that can determine the therapeutic response (4, 8). Focused SW concentrate the acoustic energy on a well-defined point of the

target tissue, with varying focal volume, depth of penetration, level of energetic flux density (EFD) and total energy administered (1, 2). The use of focused SW, especially when high energy levels are used, requires accurate identification of the area to be treated. This allows the most favourable therapeutic effect and avoids damage to the surrounding tissue. For this purpose, radiographic or ultrasound guidance is necessary. In the treatment of soft tissues, patient feedback is usually sufficient.

With regard to defocused SW therapy, some electromagnetic and electrohydraulic generators convert the acoustic wave into planar or defocused (soft-focused) waves, which retain the same physical characteristics but deliver the energy to a larger surface area. The depth of penetration will obviously be lower and, therefore, therapeutic use is limited to superficial lesions, such as cutaneous ulcers (9). Pneumatic generators produce radial waves, or pressure waves, whose physical properties significantly differ from those of focused SW. The linear pressure, the low energy values, the relatively low velocity of propagation and, above all, the long duration of the rise time differentiate radial waves from focused SW (10). In radial SW generators, the compressed air strikes a bullet contained in a cylinder. At the top of this cylinder is the applicator. The energy produced by the pressure wave is highest at the skin surface, diverging and weakening as it penetrates deeper. In radial shock wave therapy (rSWT) the focal point is not centered on the target zone as occurs in focused SWT, but on the tip of the applicator. We do not include radial waves within the initial classification because, due to their specific mechanism of action, i.e. the generation of pressure waves (4-5 Bar) and not high-energy acoustic waves (500 Bar), they cannot be considered as real shock waves.

The mechanisms of Extracorporeal Shock Wave Therapy (ESWT), by which an acoustic signal is converted into a biological reaction, is not fully understood. However, it is possible to hypothesize that mechanotransduction is the basis of the biological response to shock wave pulse. Mechanotransduction is the mechanism by which reactive cells recognize and respond to mechanical stimulation, converting physical forces into biochemical signals. Mechanotransduction stimulates extracellular matrix binding proteins and the nucleus via the cytoskeleton resulting in response leading to tissue regeneration. In recent years, cells have been the subject of detailed studies showing that they can transpose mechanical forces and convert them into biological responses, and it has long been known how biological and biochemical signals may influence the cellular ability to transpose, generate and bear mechanical forces. Studies on cellular biomechanics have quickly evolved over the past decades, with important implications for medical biotechnology.

The analysis of the cellular mechanotransduction, namely the mechanism by which cells convert mechanical signals into biochemical responses, has focused on the identification of mechano-sensitive molecules and cellular components. It was demonstrated how ion channels activated by stress, integrins, cadherins, growth receptors, myosin filaments of the cytoskeleton, nucleus, extracellular matrix, and numerous other structures and signaling molecules contribute to the response to mechanotransduction (11).

A model of the mechano-sensitivity considers cells as a sort of "hard wire mesh", describing the cytoplasmic space as interconnected by a network of elastic fibers which allows internal structures, such as chromatin, to respond directly and immediately to forces applied to the cell membrane (12). The most suitable structural micro-anatomic model to describe the cytoskeleton of adherent cells was proposed by Stamenovic et al. in 1996 under the name of tensegrity or tension integrity (13).

Other models are the networking model of the cell poking connection and the open-cell foam (14).

Several other studies have shown that the activation of conventional secondary messengers, such as an increase of the concentration of intracellular $Ca2^{+}$ (15), occurs after mechanical stress, suggesting that mechanical stimuli can report their cellular effects through messages used by intracellular soluble ligands.

When applied to the human body, the acoustic energy determines physical and chemical changes that can be embodied in the concept of mechanotransduction. The shock waves work through the acoustic phenomena generating a phenomenon of mechanotransduction. Recent histologic, biochemical, and immunologic basic science

studies have greatly advanced the understanding of how shock waves affect tissue regeneration (16-20). In a recent work, Saggini et al. described the effects of mechanotransduction on pain (21). Different hypotheses were formulated with regard to the analgesic effect of the shock waves. Among the most reliable is the theory of hyperstimulation analgesia. According to this theory, a particularly intense painful stimulation, as in the case of shock waves, transmitted to the central nervous system through the posterior column of the spinal cord, may activate the descending inhibitory system that blocks a subsequent transmission of nociceptive stimuli in the posterior column. The obtained analgesia allows to improve joint function. Shock waves also create overstimulation of nerve fibers, blocking the increase of the painful stimulus thus intensifying the analgesic effect (Gate Control Theory).

Another biological mechanism through which the shock waves cause a reduction in pain is degeneration of nerve fibers that originate from small neurons immunoreactive to activating transcription factor 3 (ATF3), a protein linked to the activation of genes related to protein pro-inflammatory coding, which seems to derive a relieved pain. The release of bioactive substances [in particular substance P and calcitonin gene-related peptide (CGRP)] released at the level of sensory nerve endings plays an important role in the maintenance of pain and chronic inflammation (22).

Substance P acts as a neuro-hormone and mediates nerve transmission in the type C nerve endings of peripheral origin, which causes excitation of the postsynaptic element. It is, in fact, believed that when the C fibers make synapses in the dorsal horn of the spinal cord, they release substance P as neurotransmitter, which is a neuropeptide formed slowly at the synapse and is also slowly destroyed; therefore, after the start of pain stimulation, its concentration in the synaptic space increases for several seconds, and lasts for a few minutes after the stimulation is ended, thus explaining why slow chronic pain gradually increases in intensity with time and persists even after the cessation of the painful stimulus (23). CGRP is a marker of sensory neurons, typically involved with pain perception, and was isolated, along with substance P, in capsaicin sensitive axons.

The literature shows that the unmyelinated fibers of the peripheral nervous system play a central role in the maintenance of pain due to musculoskeletal disorders. The activation of the small diameter peripheral fibers results in local depolarization: axonal reflexes with involvement of the dorsal roots and increase in substance P and CGRP. Both act on peripherals target cells such as mast cells, immune cells and vascular smooth muscle cells, causing inflammation. This phenomenon is called neurogenic inflammation (22).

It was found that chronic inflammation contributes to the etiology of pain, for example in epicondylitis, chronic plantar fasciitis and tendinous disorders of the rotator cuff (24, 25). Furthermore, one study revealed the contribution of substance P (as interleukin 1 alpha and transforming growth factor beta1) in the pathogenesis of tennis elbow, without any apparent infiltration of inflammatory cells (26).

The reduction of pain associated with these diseases after ESWT is related to the induction of changes in the levels of substance P and Calcitonin Gene Related Peptide (CGRP). The effect of ESWT would be damaging to small unmyelinated fibers with immediate release of substance P and this explains the appearance of pain during the application.

The above has been demonstrated *in vitro*: after stimulation with high-intensity shock waves the appearance was detected of vacuoles and alterations of small unmyelinated fibers. Furthermore, after the application high levels of substance P were found even at the level of the central nervous system.

The destruction of the peripheral unmyelinated fibers that control the release of substance P determines the resolution of the symptoms in the following weeks, in some experimental protocols there was a significant reduction of pain 4-6 weeks after treatment. Other nerve fibers are not affected by the damage by ensuring a safe and repeatable application of treatment.

Moreover, the application of shock waves on the trigger point (TP) causes a reduction in pain by acting: i) on the hyper-irritability of the trigger with a mechanical disruption of terminations of sensory nerves mediating the activity of TP, and removal of sensitizing substances; ii) on the increase in vasodilation mediated by the sympathetic system.

The stimulation of muscle nociceptors strongly activates the efferent fiber motor gamma at the level of muscle spindles, contributing indirectly to alter the circle; and iii) on reducing spasm-contracture-bandeletta**?** of muscle fibers.

Shock waves reduce muscle tension and generate vaso-activation, allow a reduction of edema and therefore pain, from the early treatments giving a tangible comfort to the patient. The analgesic effect is also given by the stimulation of the production of endorphins (substances which play a fundamental role in decreasing pain sensitivity), and by the inhibition of some specific receptors responsible for the activation of pain. The mechanisms of action of shock waves in the treatment of musculoskeletal pain have not been defined in a single pathogenetic mechanism: to explain the clinical success in the treatment of muscle pain reference is usually made to:

-release of the actin-myosin bridges of the hyper-contracted areas due to the mechanical action of the energy of shock waves with energy applied perpendicular to the direction of muscle fibers;

-improvement in blood circulation through the reactive hyperemia and neoangiogenesis dilutes the inflammatory metabolites;

-modulation of pain by the release of endogenous analgesic substances P and CGRP;

-modulation of pain by the release and synthesis of nitric oxide

-selective degeneration of C fibers involved in the genesis and perpetuation of the painful stimulus

-pain modulation according to the Gate Control Theory.

Research conducted on muscle pain during recent years and the experience gained on shock wave therapy on skeletal muscle pain, confirms the important role of this advanced physical therapy as a conservative treatment option, which can be extended to other diseases characterized by functional disorders and pain syndromes (27).

SWT FOR BONE DISORDERS

Several studies investigated the effects of SWT on acute fracture healing, delayed unions, non-unions, and avascular necrosis. Experimental models demonstrate that SWT promotes bone healing through a typical biological response characterized by the up-regulation of bone growth factors and bone morphogenetic proteins. It has been shown that the growth of bone marrow mesenchymal cells, and their differentiation into osteoblasts is mediated by TGF-β 1 and vascular endothelial growth factor (VEGF), induced by SWT (19, 21). The signal transduction in bone cells induced by SWT could be mediated by cyclin E2/CDK2 complex, (28) and ERK and p38 kinase activity (29). Early local production of angiogenic factors, including endothelial nitric oxide synthase and vascular endothelial growth factor (VEGF), was observed after SWT (30, 31).

The importance of the biological stimulus induced by SWT was confirmed by a clinical study reporting that patients with non-union who failed to heal after SWT, were those showing lower concentrations of bone turnover markers, such as osteocalcin and bone-specific alkaline phosphatase (32).

Non-unions and delayed unions

Several studies exploring the effects of SWT on non-unions and delayed unions of long bone fractures reported promising results with a success rate ranging from 50% to 85% (33-38). Valchanou et al. (37) reported bone healing in 70 of 82 patients with delayed or chronic non-union of fractures at various locations. Schaden et al. (22) reported, with a follow-up ranging from 3 months to 4 years, a healing of 87 of 115 patients (75.7%) with non-unions or delayed unions of various fractures who were treated with high-energy SWT and immobilization. Rompe et al. (38) reported their experience using high-energy SWT to treat 43 patients with either a tibial or femoral diaphyseal non-union. They noted bony healing in 31 of 43 patients (72%) after an average of 4 months post-treatment. Wang et al. (35) used high-energy SWT as a treatment of 72 non-unions of long-bone fractures. A 12-month follow-up was available for 55 patients, of these 44 (80%) healed.

Cacchio et al. (33) in a randomized clinical trial, compared 3 groups of patients. Groups 1 and 2 received SWT (4 treatments of 4000 shocks) with an EFD of 0.4 mJ/mm^2 and 0.7 mJ/mm^2, respectively. Patients in group 3 were treated with surgery. At 6 months post-intervention, 70% of non-unions in group 1, 71% in group 2, and 73% of in group 3 had healed. It was concluded that SWT was as effective

as surgery in stimulating union of long-bone non-unions. The analysis of the literature data indicate that SWT is more successful for hypertrophic non-unions than for atrophic ones.

Wang et al. (35), found a success rate of 40% at three months, 61% at six months, and 80% at twelve months for hypertrophic non-unions but only 27% for atrophic non-unions. Beutler et al. (39) reported a success rate of 53% for hypertrophic non-unions but only 25% for atrophic non-unions. Xu et al. (40) reported an overall healing rate of 75.4% in their series of 69 non-unions, but none of the atrophic non-unions healed.

In a randomized controlled trial, Cacchio et al. (33) reported that drop-out rate was greater for the patients with atrophic non-union (11 of 34; 32%) than it was for those with hypertrophic ones (4 of 92; 4%). Moreover, of the 23 atrophic non-unions that remained, 13 were treated with SWT; of these 6 healed while 7 did not. Non-unions are usually treated with 2000 to 6000 shocks using an EFD between 0.3 mJ/mm^2 and 0.6 mJ/mm^2. The total number of pulses is usually divided along the proximal and distal margins of the non-union. The total number of treatments (typically ranging from 1-4) and the interval between treatments (typically ranging from 1-4 weeks) vary from center to center.

Although treatment for the non-unions is performed with a high EFD, a retrospective clinical study on the efficacy of low-EFD (0.09 mJ/mm^2) SWT compared with that of a standard surgical procedure to treat pseudo-arthrosis of the carpal scaphoid, reported that the radiographic consolidations and clinical results of SWT (75.9% and 86.3%, respectively) are comparable with those of surgical stabilization (76.7% and 83.4%, respectively) (26). Thus, currently, in the clinical setting, the procedure for SWT in bone disorders is similar to that used in soft tissue disorders: deeper structures should be treated with high EFD, whereas more superficial structures with either a high- or low-EFD protocol.

Moretti et al. (41) reported their results regarding treatment of both non-unions and fresh fractures with ESWT. He included 204 cases of pseudoarthrosis of different bony segments and 16 cases of fresh closed fracture of tibia treated by external fixation. In the treatment of the pseudoarthrosis a range of energy flow density (EFD) was used between 0.22 and 1.10 mJ/mm^2 as tolerated and 4000 pulses by an electromagnetic device (Minilith SL1-STORZ). Following SWT, non-union was immobilized with a plaster cast or plaster splint, even if this immobilization was not necessary when the pseudoarthrosis was treated with appropriate osteosynthesis devices without evidence of loosening upon clinical and radiological examination. In fresh fractures, ESWT was performed within a month from the surgery of external fixation and the patients were forbidden to load on the fractured leg. The EFD was between 0.07 and 0.17 mJ/mm^2 (low EFD) in order to induce a neoangiogenetic effect; the number of pulses was the same used for pseudoarthrosis. Follow-up was between a minimum of 45 days and a maximum of 3 months. Bone union was achieved in 174 (85%) of non-unions and 50 (80%) of fractures. In the treatment of pseudoarthrosis the best results were obtained both at high and at low EFD ($p < 0.05$). The bone segments showed consolidation as following: 100% in clavicle and metatarsus, 96% in ulna, 80% in femur and carpal scaphoid, 78% in humerus and tibia. Males (87%) had better results than females (83%), as did patients aged over 60 years (89%) in comparison with younger subjects (83%). The results of shock-wave treatment of fresh fractures were compared with a control-group. Fracture healing was assigned when it was possible to recognize at least 3 out of 4 bone cortexes by plain radiograph. The average of the bone cortex was 3.25 in the ESWT group and 2.54 in the control group.

The analysis of the results in pseudoarthrosis treatment offers useful information to the expert practitioner in the choice of patient and protocol to successfully apply ESWT. High energy induces periosteal detachment and trabecular fractures with hemorrhages, which in turn stimulate callus formation and subsequent fracture healing; low-middle energy induces mesenchymal stem cell recruitment and differentiation into osteoblasts for bone formation (41). The high Energy Flux Density (EFD) can be useful for atrophic non-unions in which shock waves produce the periosteal detachment and trabecular fractures (non-surgical cruentation), instead the low EFD for hypertrophic ones in which this treatment allows angiogenesis and osteogenesis (40). The choice of a lower energy of ESWT in the

treatment of fresh fractures is based on the rationale that ESWT induces nitric oxide (NO) liberation even at low energy (42).

There is a link between NO and osteogenesis via the seven day expression of the core binding factors such as core binding factor 1(cbfa1) (43). Consequently, the choice of applying lower energy shock wave stimulates bone growth by nitric oxide production.

According to literature data, patients treated with ESWT showed good clinical and functional results. This technique represents a safe method of treatment with few complications and a high percentage of success. The efficacy of shock-waves in the treatment of fractures and pseudoarthrosis must be based on the association of the biological stimulation of ESWT and the mechanical stabilization of fixation or cast. Therefore, ESWT can be considered a good therapeutic choice in the management of fractures and hypertrophic non-unions, in association with an adequate mechanical stabilization of bone edges.

Bone marrow edema

In a recent study, D'Agostino et al. (44) described the effectiveness of ESWT in bone marrow edema syndrome of the hip. The term bone marrow edema (BME) describes a wide range of focal bone lesions of different origin and is most likely a vascular reaction to external or internal disorders (45). Although the correlations with other diseases, such as aseptic osteonecrosis, algodistrophy, trabecular microfractures and osteoporosis of pregnancy, are still debated, bone marrow edema syndrome (BMES) is now an accepted clinical entity. It is typified by an "inflammatory pattern" in MRI (low signal intensity in T1-W and high signal intensity in T2-W sequences). BMES usually affects the epiphyses of weight-bearing joints—hip, knee, foot and ankle—although it may manifest itself as a "migratory" BME with multiple episodes in different locations (46). The hip is the most common site of BMES. BMES is normally spontaneously self-limiting within 4–24 months; however, there is a risk of fracture due to the weakened bone architecture (47). Progression to avascular osteonecrosis (AVN) is a rare occurrence, although it has been described in the literature (48).

There is no gold standard for the treatment of BMES; treatment is traditionally conservative and includes reduced weight-bearing, physical therapy, analgesics and vasoactive prostacyclin analog drugs like iloprost (IP), although some authors have even resorted to treating the condition surgically, performing a bone core decompression (49). However, there is consensus regarding the importance of an early treatment to relieve pain and to avoid weakening the bone trabeculae which could potentially lead to a collapse of the subchondral bone.

Given the proven effectiveness of ESWT in other musculoskeletal disorders, due to its angiogenic, analgesic and anti-inflammatory effects, D'Agostino performed a perspective study aimed at evaluating the effectiveness of ESWT in relieving pain and normalizing the MRI appearance of BMES. The therapeutic protocol consisted of two sessions of shock wave therapy, 48 h apart, using a shock wave electromagnetic source (Modulith SLK Storz Medical, Switzerland) fitted with a double ecographic and radiographic pointing device. Each treatment consisted of 4,000 shots at high-energy level, with mean energy flux density (EFD) value of 0.5 mJ/mm^2 (range 0.4–0.6 mJ/mm^2). Results showed a dramatic improvement in Harris Hip Score (HHS) at t1 (2 months post-treatment), and almost all patients continued to improve over the follow-up period. The mean improvement in HHS over the course of the study was of 58.5±14.9 points (range 31.2–81.5, $p < 0.0001$). The mean improvements were strongly statistically significant between t0 and t1 and between t1 and t2 ($p < 0.0001$) and less significant between t2 and t3 ($p < 0.01$). The mean improvement was not significant between 6 months (t3) and final follow-up.

The MRI findings demonstrated the progressive regression of the BME. Before treatment, the mean edema area of the cohort was 981.9±453.2 mm^2. The largest improvement was seen at t1, when the mean edema area had more than halved, to 469.5±306.8 mm^2. At the final MRI examination at t3, the mean edema area had reduced to 107.8±248.1 mm^2. These reductions were highly statistically significant at both time points ($p>0.0001$).

A quick positive response to the therapy was therefore observed. The most marked clinical improvement occurred at 2 months post-treatment, where the mean HHS values were significantly higher

than those recorded before treatment ($p < 0.001$). From 3 to 6 months post-treatment, the improvement in scores was more gradual, but still statistically significant with a gain of 10.6 points ($p < 0.001$) at t2 and of 3.35 points ($p < 0.01$) at t3. Although the area of edema on MRI had not disappeared in all cases, the functional results were all good or excellent. On this basis D'Agostino hypothesized that the early clinical response to high-energy dose treatment may be due to the direct, nonenzymatic production of NO as experimentally observed *in vitro* with high-energy values. The results show that ESWT can be effective in the treatment of BMES, bringing a swift clinical improvement, followed by a progressive normalization of the MRI appearance. Consequently, it seems possible that it might also prevent the, admittedly rare, development to AVN of the femoral head. Furthermore, ESWT is a non-invasive technique that is well tolerated and with no side effects. Since this was the first study to describe the use of SW in BMES, further controlled studies, with different treatment protocols in terms of number of shots, energy level and frequency employed, and the number of treatments, are needed to establish the optimal regimen and to confirm these new data (54).

Avascular necrosis

Avascular necrosis (AVN) is a progressive condition characterized by bone death due to vascular insufficiency. Although its etiology remains unclear, several risk factors such as trauma, surgery, steroid use, alcoholism, coagulopathy, systemic lupus erythematosus (SLE), and hyperlipidemia have been found. Conservative treatments include administration of bisphosphonates, anticoagulation, and activity modification, but are generally ineffective. Core decompression with or without bone grafting is considered the gold standard of surgical procedures (50). Several studies reported the positive effects of SWT for AVN, usually of the femoral head (51-53). Wang et al. (51) in a previous study in 2005 compared at three time intervals (1, 2 and 9 years) 29 hips treated with SWT and 28 hips treated by core decompression with non-vascularized fibular bone grafting. Significant improvements in pain and function were noted at each time intervals in favor of SWT. Moreover, total hip arthroplasty was performed in 3% and 21% ($p=0.039$) of patients at 1 year, 10% and 32% ($p=0.044$) at 2 years, and 24% and 64% ($p=0.002$) at 9 years of follow-up for the SWT group and the surgical group, respectively. The same authors (37) compared 26 hips in patients with SLE with 29 hips of non-SLE patients. Total hip arthroplasty was performed in 12% and 14% of patients respectively, and there were no differences in pain and function between the two groups. In this study the authors concluded that the rate of success of SWT on AVN in patients with SLE was comparable to that obtained in non-SLE patients.

In a further and more recent study, Wang et al. demonstrated that ESWT appears to be more effective than core decompression and bone grafting for early Osteonecrosis of the Femoral Head (ONFH) with 8-to 9-year long-term follow-up. The cohort study consisted of 48 patients with 57 hips including 23 patients with 29 hips in the ESWT group and 25 patients with 28 hips in the surgical group. Patients in the ESWT group received shockwave therapy to the affected hip. Patients in the surgical group underwent core decompression and autogenous cancellous bone and allogenous fibular graft. The average length of follow-up was 103.5±3.4 (ranged 93-106) months and 104.5±4.3 (range 95-108) months for the ESWT and the surgical group, respectively. The evaluations included clinical assessment for pain and function, X-ray and MRI of the affected hips. The overall clinical results were 76% good or fair and 24% poor for the ESWT group; and 21% good or fair and 79% poor for the surgical group. Total Hip Arthroplasty (THA) was performed in 3% and 21% at one year, 10% and 32% at 2 years and 24% and 64% at 8-9 years for ESWT and the surgical group respectively. Significant differences in pain and Harris hip scores were observed at different time intervals favoring the ESWT group. There was a trend of decrease in the size of the lesion in the ESWT group when compared with the surgical group. Lin et al. (52) reported successful treatment of a 19-year-old patient with SLE who developed bilateral avascular necrosis of the femoral head. At 3-year follow-up, the authors noted that both hips had an improvement in pain, Harris hip scores, and range of motion; moreover, MRI showed substantial reduction in bone marrow edema and no collapse of the subchondral bone. Vulpiani et al. (54) reported the results of SWT in 36 patients with unilateral AVN of the femoral head. Ten

patients with stage I, eleven with stage II, and fifteen with stage III of AVN were treated with 4 sessions of high-energy (0.50 mJ/mm^2) SWT with 2,400 pulses. Follow-up examinations were scheduled at 3, 6, 12 and then 24 months. At all scheduled follow-ups, stage I and II patients showed significantly better results than stage III patients as regards pain score, Harris hip score, and Roles and Maudsley score. During the study period, 10 of the 15 stage III patients, but none of stage I and II patients, received a total hip arthroplasty.

Yin et al. in 2011 (55) showed how ESWT significantly enhanced the angiogenic and osteogenic effects of BMSCs mediated through the NO pathway in hips with osteonecrosis *in vitro*. Bone marrow stromal cells (BMSCs) were harvested from the bone marrow cavity of the proximal femur in six patients with osteonecrosis of the femoral head. The specimens were divided into four groups, the control, shockwave, shockwave plus nω-nitro-L-arginine methyl ester (L-NAME) and a nitric oxide (NO) donor (NOC18) groups. The control group received no shockwaves and was used as the baseline. The shockwave group received 250 shockwave impulses at 14 Kv (equivalent to 0.18 mJ/mm^2 energy flux density). The shockwave plus LNAME group was pre-treated with L-NAME before receiving shockwaves. The NOC18 group received NOC18 after cell culture for 48 hours. The evaluations included cell proliferation (MTT) assay, alkaline phosphatase, real time reverse transcriptase-polymerase chain reaction analysis of vessel endothelial growth factor (VEGF), bone morphogenic protein (BMP)-2, RUNX2 and osteocalcin mRNA expression and von Kossa stain for mineralized nodules. The shockwave group showed significant increases in MTT, VEGF, alkaline phosphatase, BMP2, RUNX2 and osteocalcin mRNA expression and more mature mineralized nodules compared with the control group. Pre-treatment with L-NAME significantly reduced the angiogenic and osteogenic effects of ESWT and the results were comparable with the controls. Administration of NOC18 significantly enhanced the angiogenesis and osteogenesis effects compared with the control group and the results were comparable with the shockwave group.

Wang also investigated the effects of shockwave on systemic concentrations of nitric oxide (NO) level, angiogenic and osteogenic and anti-inflammatory factors in hips with osteonecrosis of the femoral head (ONFH). Forty-seven hips with ONFH were treated in his study. Each hip was treated with 6,000 impulses of shockwave at 28 kV in a single session. Ten milliliters of peripheral blood was obtained for the measurements of serum NO level, angiogenic factors (VEGF, vWF- von Willebrand factor, Fibroblast growth factor basic (FGF)- and transforming growth factor (TGF)-1-, beta 1); osteogenic factors (BMP-2 - Bone morphogenetic protein 2, osteocalcin, alkaline phosphatase, DKK-1 - Dickkopf-related protein 1 and IGF- insulin-like growth factor); and antiinflammatory markers (sICAM and sVCAM - Intercellular Adhesion Molecule) before treatment and at 1, 3, 6 and 12 months after treatment. The hips were evaluated with clinical assessment, serial radiograph and Magnetic Resonance Imaging (MRI). At 12 months, in the overall results, 83% showed improvement and 17% no improvement. Total hip replacement was performed in 4 cases (8.5%). Serum NO3 level showed significant elevation at 1 month after treatment, but the changes at 3, 6 and 12 months were not significant. For angiogenesis, significant elevations of VEGF, vWF and FGF basic and a decrease in TGF-1 were observed at 1 month, but the changes at 3, 6 and 12 months were non-significant. For osteogenesis, BMP-2, osteocalcin, alkaline phosphatase and IGF were significantly elevated, while DKK-1 was decreased at 1 month, but the changes at 3, 6 and 12 months were not significant. For anti-inflammatory markers, significant decreases in sICAM and sVCAM were noted at 1 month after treatment, but the changes at 3, 6 and 12 months were not significant. Local ESWT application results in significant elevation of serum NO levels, angiogenic and osteogenic and anti-inflammatory factors in ONFH (56).

Stress fractures

Stress fractures are overuse injuries of bone which can be common among athletes. These fractures, which may be nascent or complete, result from repetitive sub-threshold loading that, over time, exceeds the bone's intrinsic ability to repair itself. Currently, no prospective, randomized, blinded studies evaluating SWT as a treatment of chronic stress fractures have been published. However, SWT

has been used in the treatment of chronic stress fractures and has shown encouraging results.

Taki et al. (57) reported their experience in using focused SWT to treat 5 athletes with chronic stress fractures who had found no improvement after 6 to 12 months of traditional therapy. The fractures included the middle third of the tibia (N.=2), the base of the fifth metatarsal (N.=1), the inferior pubic ramus (N.=1), and the medial malleolus of the ankle (N.=1). A single high-energy treatment (0.29 mJ/mm^2-0.4 mJ/mm^2) was used in each case. All fractures healed after SWT with time to radiographic union ranging from 2 to 3.5 months post-treatment. All athletes were able to return to their sporting activities in a time ranging from 3.5 to 6 months post-treatment. No complications or recurrent stress fractures in any of the 5 cases was reported. Moretti et al. (58) reported on 10 male soccer players ranging in age from 19 to 29 years and suffering from either tibial or fifth metatarsal stress fractures who received 3 (for the metatarsus) to 4 (for the tibia) sessions of SWT with low-middle EFD (0.09-0.17 mJ/mm^2) and high number of pulses (N.=4000). At a mean of 8 weeks post-treatment, a 100% healing rate was noted. All athletes were able to return to their pre-injury level of sporting activity. Albisetti et al. (59) treated 18 dancers with stress fractures of the base of the metatarsal bones with ESWT; all them were treated non-operatively with rest and ESWT (Wolf Piezoson 300 lithotripter, with 6.5 MHz ultrasounds; 2,000 pulses 0.06–0.28 mJ/mm^2, three to five times in a month), depending on clinical and anatomical factors, age of the dancers and type of stress fracture. The progress of the patients was weekly monitored by testing the tenderness in the area localised over the metatarsal. When local pain lessened, return to activity was gradually allowed, avoiding jumps and pirouette en pointe. At 2.2 years mean follow-up (range 1.3–3.3 years) all dancers healed without any midfoot pain. The authors showed that shockwave therapy allows dancers to return to practice about 4.6 weeks (range 3–5.3 weeks) after the first application. All of the dancers returned to full activities after a mean time of 18 days (range 14–23 days) following the end of treatment (6.3 weeks from the onset of the symptoms). No fractures developed non-union and no re-fracture occurred. The authors concluded that medium energy external shockwave therapy gives good results in young dancers. If properly diagnosed and treated early, stress fractures do not recur, and they only entail a relatively short period of rest from the patients' activities.

CONCLUSION

Over the last decade several reviews were carried out on ESWT in skeletal disorders, which have shown conflicting evidence on its efficacy. Today it is possible to say that ESWT can be a substitute in certain circumstances of bone surgery. Future scientific works will have to be extremely accurate with regard to the parameters, in order to make the data homogeneous and reproducible.

REFERENCES

1. Ueberle F. Shock wave technology. In: Siebert W, Buch M, eds. Extracorporeal shock waves in orthopaedics. Springer. Berlin, 1997; p. 59-87.
2. Wess O, Ueberle F, Duhrsen RN, et al. Working group technical developments – consensus report. In: Chaussy C, Eisenberger F, Jocham D, Wilbert D, editors. High energy shock waves in medicine. Thieme. Stuttgart, 1997; p. 59-71.
3. Rompe JD. Shock wave applications in musculoskeletal disorders. Thieme Verlag. Stuttgart, 2002; p. 1-4.
4. Ogden JA, Toth-Kischkat A, Schultheiss R. Principles of shock wave therapy. Clin Orthop 2001; 387:8-17.
5. Furia JP, Rompe JD, Cacchio A, Maffulli N. Shock wave therapy as a treatment of non-unions, avascular necrosis, and delayed healing of stress fractures. Foot Ankle Clin N Am 2010; 15:651-62.
6. Mittermayr R, Antonic V, Hartinger J, et al. Extracorporeal shock wave therapy (ESWT) for wound healing: technology, mechanisms, and clinical efficacy. Wound Repair Regen 2012; 20:456-65.
7. Wang C-J. Extracorporeal shockwave therapy in musculoskeletal disorders. J Orthop Surg Res 2012; 7:11.
8. Wang CJ, Yang KD, Wang FS, Hsu CC, Chen HH. Shock wave treatment shows dose-dependent enhancement of bone mass and bone strength after

fracture of the femur. Bone 2004; 34:225-30.
9. Romeo P, Lavanga V, Pagani D, Sansone V. Extracorporeal shock wave therapy in musculoskeletal disorders: a review. Med Princ Pract 2014; 23(1):7-13.
10. Van der Worp H, de Poel HJ, Diercks RL, van den Akker-Scheek I, Zwerver J. ESWT for tendinopathy: technology and clinical implications. Knee Surg Sports Traumatol Arthrosc 2012; 21:1451-58.
11. 11.Fung YC. Biomechanics: mechanical properties of living tissues. 2nd ed. New York, Springer, 2010 pp . 392-423
12. Maniotis AJ, Chen CS, Ingber DE. Demonstration of mechanical connections between integrins, cytoskeletal filaments, and nucleoplasm that stabilize nuclear structure. Proc Natl Acad Sci U S A. 1997; 94(3):849-54.
13. Stamenović D, Fredberg JJ, Wang N, Butler JP, Ingber DE. A microstructural approach to cytoskeletal mechanics based on tensegrity. J Theor Biol 1996; 181(2):125-36.
14. Satcher RL Jr, Dewey CF Jr. Theoretical estimates of mechanical properties of the endothelial cell cytoskeleton. Biophys J 1996; 71(1):109-18.
15. Munevar S, Wang YL, Dembo M. Regulation of mechanical interactions between fibroblasts and the substratum by stretch-activated Ca2+ entry. J Cell Sci 2004; 117(Pt 1):85-92.
16. Maier M, Milz S, Tischer T, et al. Influence of extracorporeal shock-wave application on normal bone in an animal model in vivo. Scintigraphy, MRI and histopathology. J Bone Joint Surg Br 2002; 84:592-9.
17. Maier M, Averbeck B, Milz S, Refior HJ, Schmitz C. Substance P and prostaglandin E2 release after shock wave application to the rabbit femur. Clin Orthop Relat Res 2003; 406:237-45.
18. Martini L, Giavaresi G, Fini M, Torricelli P, de Pretto M, Schaden W, Giardino R. Effect of extracorporeal shock wave therapy on osteoblastlike cells. Clin Orthop Relat Res 2003; 413:269-80.
19. Wang FS, Yang KD, Chen RF, Wang CJ, Sheen-Chen SM. Extracorporeal shock wave promotes growth and differentiation of bone-marrow stromal cells towards osteoprogenitors associated with induction of TGF-beta1. J Bone Joint Surg Br 2002; 84:457-61.
20. Wang FS, Yang KD, Kuo YR, Wang CJ, Sheen-Chen SM, Huang HC, Chen YJ. Temporal and spatial expression of bone morphogenetic proteins in extracorporeal shock wave-promoted healing of segmental defect. Bone 2003; 32:387-96.
21. Saggini R., Buoso S., Pestelli G. Dolore e Riabilitazione. Minerva Medica 2014; 3 p. 85-91.
22. Richardson JD, Vasko MR. Cellular mechanisms of neurogenic inflammation. J Pharmacol Exp Ther 2002; 302(3):839-45.
23. Snijdelaar DG, Dirksen R, Slappendel R, Crul BJ. Substance P. Eur J Pain 2000; 4(2):121-35.
24. Schepsis AA, Leach RE, Gorzyca J. Plantar fasciitis. Etiology, treatment, surgical results, and review of the literature. Clin Orthop Relat Res 1991; (266):185-96.
25. Roetert EP, Brody H, Dillman CJ, Groppel JL, Schultheis JM. The biomechanics of tennis elbow. An integrated approach. Clin Sports Med 1995; 14(1):47-57. Review.
26. Uchio Y, Ochi M, Ryoke K, Sakai Y, Ito Y, Kuwata S. Expression of neuropeptides and cytokines at the extensor carpi radialis brevis muscle origin. J Shoulder Elbow Surg 2002; 11(6):570-5.
27. Hofmann A, Ritz U, Hessmann MH, Alini M, Rommens PM, Rompe JD. Extracorporeal shock wave-mediated changes in proliferation, differentiation, and gene expression of human osteoblasts. J Trauma 2008; 65:1402-10.
28. Tamma R, dell'Endice S, Notarnicola A, et al. Extracorporeal shock waves stimulate osteoblast activities. Ultrasound Med Biol 2009; 35:93-100.
29. Chen YJ, Kuo YR, Yang KD, et al. Activation of extracellular signal-regulated kinase (ERK) and p38 kinase in shock wave-promoted of bone formation segmental defect in rats. Bone 2004; 34:466-77.
30. Chen YJ, Wurtz T, Wang CJ, Kuo YR, Yang KD, Huang HC, Wang FS. Recruitment of mesenchymal stem cells and expression of TGFbeta 1 and VEGF in the early stage of shock wave-promoted bone regeneration of segmental defect in rats. J Orthop Res 2004; 22:526-34.
31. Wang FS, Wang CJ, Chen YJ, et al. RAS induction of superoxide activates ERK-dependent angiogenic transcription factor HIF-1alpha and VEGF-A expression in shock wave-stimulated osteoblasts.

Journal Biol Chem 2004; 279:10331-7.
32. Cacchio A, De Blasis E, Rosa F, De Blasis D, de Paulis F, Santilli V, Calvisi V. Response of bone turnover biochemical markers to extracorporeal shock wave therapy in the management of long-bone non-unions. Clin Chem 2009; 55:195-6.
33. Cacchio A, Giordano L, Colafarina O, et al. Extracorporeal shock-wave therapy compared with surgery for hypertrophic long-bone non-unions. J Bone Joint Surg Am 2009; 91:2589-97.
34. Elster EA, Stojadinovic A, Forsberg J, Shawen S, Andersen RC, Schaden W. Extracorporeal shock wave therapy for non-union of the tibia. J Orthop Trauma 2010; 24:133-41.
35. Wang CJ, Chen HS, Chen CE, Yang KD. Treatment of non-unions of long bone fractures with shock waves. Clin Orthop Rel Res 2001; 387:95-101.
36. Schaden W, Fischer A, Sailer A. Extracorporeal shock wave therapy of non-union or delayed osseous union. Clin Orthop 2001; 387:90-4.
37. Valchanou VD, Michailow P. High-energy shock waves in the treatment of delayed and non-union of fractures. Int Orthop 1991; 151:181-4.
38. Rompe JD, Rosendahl T, Schollner C, Theis C. High-energy extracorporeal shock wave treatment of non-unions. Clin Orthop 2001; 387:102-11.
39. Beutler S, Regel G, Pape HC, et al. Extracorporeal shock wave therapy for delayed union of long bone fractures - preliminary results of a prospective cohort study. Unfallchirurg 1999; 102:839-47.
40. Xu ZH, Jiang Q, Chen DY, Xiong J, Shi DQ, Yuan T, Zhu XL. Extracorporeal shock wave treatment in non-unions of long bone fractures. Int Orthop 2009; 33:789-93.
41. Moretti B, Notarnicola A, Moretti L, Patella S, Tatò I, Patella V. Bone healing induced by ESWT. Clin Cases Miner Bone Metab 2009; 6(2):155-8.
42. Altland OD, Dalecki D, Suchkova VN, Francis CW. Low-intensity ultrasound increases endothelial cell nitric oxide synthase activity and nitric oxide synthesis. J Thromb Haemost 2004; 2(4):637-43.
43. Zaragoza C, López-Rivera E, García-Rama C, et al. Cbfa-1 mediates nitric oxide regulation of MMP-13 in osteoblasts. J Cell Sci 2006; 119:1896-902.
44. d'Agostino C, Romeo P, Lavanga V, Pisani S, Sansone V. Effectiveness of extracorporeal shock wave therapy in bone marrow edema syndrome of the hip. Rheumatol Int 2014; 34(11):1513-8.
45. Blum A, Roch D, Loeuille D, Louis M, Batch T, Lecocq S, Witte Y. L'oedema meddullaire: definition, valeur diagnostique et pronostique. J Radiol 2009; 90:1789-811.
46. Vande Berg BC, Lecouvet FE, Koutaissoff S, Simoni P, Malghem J. Bone marrow edema of the femoral head and transient osteoporosis of the hip. Eur J Radiol 2008; 67:68-77.
47. Guardiano SA, Katz J, Schwartz AM, Brindle K, Curiel R. Fracture complicating the bone marrow edema syndrome. J Clin Rheumatol 2004; 10:269-74.
48. Radke S, Kenn W, Eulert J. Transient bone marrow edema syndrome progressing to the avascular necrosis of the hip - a case report and a review of the literature. Clin Rheumatol 2004; 23:83-88.
49. Aigner N, Petje G, Schneider W et al. Bone marrow edema syndrome of the femoral head: treatment with the prostacyclin analogue iloprost vs core decompression. An MRI-controlled study. Wien Klin Wochenschr 2005; 117(4):130-35.
50. Parsons JS, Stelle N. Osteonecrosis of the femoral head: part 2-options for treatment. Curr Orthop 2008; 22:349-58.
51. Wang CJ, Wang FS, Huang CC, Yang KD, Weng LH, Huang HY. Treatment for osteonecrosis of the femoral head: comparison of extracorporeal shock waves with core decompression and bone-grafting. J Bone Joint Surg Am 2005; 87:2380-87.
52. Lin PC, Wang CJ, Yang KD, Wang FS, Ko JY, Huang CC. Extracorporeal shockwave treatment of osteonecrosis of the femoral head in systemic lupus erythematosis. J Arthroplasty 2006; 21:911-5.
53. Wang CJ, Wang FS, Yang KD, et al. Treatment of osteonecrosis of the hip: comparison of extracorporeal shockwave with shockwave and alendronate. Arch Orthop Trauma Surg 2008; 128:901-8.
54. Vulpiani MC, Vetrano M, Trischitta D, et al. Extracorporeal shock wave therapy in early osteonecrosis of the femoral head: prospective clinical study with long term follow-up. Arch Orthop Trauma Surg 2012; 132:499-508.
55. Yin TC, Wang CJ, Yang KD, Wang FS, Sun YC. Shockwaves enhance the osteogenetic gene expression in marrow stromal cells from hips with

osteonecrosis. Chang Gung Med J 2011; 34(4):367-74.
56. Wang CJ, Yang YJ, Huang CC. The effects of shockwave on systemic concentrations of nitric oxide level, angiogenesis and osteogenesis factors in hip necrosis. Rheumatol Int 2011; 31(7):871-7.
57. Taki M, Iwata O, Shiono M, Kimura M, Takagishi K. Extracorporeal shock wave therapy for resistant stress fractures in athletes. Am J Sports Med 2007; 35:1188-92.
58. Moretti B, Notarnicola A, Garofalo R, Moretti L, Patella S, Marlinghaus E, Patella V. Shock waves in the treatment of stress fractures. J Ultrasound Med Biol 2009; 35:1042-9.
59. Albisetti W, Perugia D, De Bartolomeo O, Tagliabue L, Camerucci E, Calori GM. Stress fractures of the base of the metatarsal bones in young trainee ballet dancers. Int Orthop 2010; 34(1):51-5.

EDITORIAL

MANAGEMENT OF PSORIATIC ARTHRITIS: SHOULD THE INTERACTION BETWEEN DERMATOLOGISTS AND RHEUMATOLOGISTS IN CLINICAL PRACTICE BE INTENSIFIED?

A. MIGLIORE[1], F. CUSANO[2], G. BIANCHI[3], G. MALARA[4], O. EPIS[5] and O. DE PITÀ[6]

[1]U.O. Reumatologia, Ospedale San Pietro, Roma, Italy; [2]U. O. C. Dermatologia, Azienda Ospedaliera "G. Rummo", Benevento, Italy; [3]U.O. Reumatologia, ASL3, Azienda Sanitaria Genovese, Genova, Italy; [4]U.O. Dermatologia Ospedale Papardo, Messina Italy; [5]U.O. Reumatologia, Ospedale Niguarda Ca' Granda, Milano Italy; [6]Istituto Dermopatico dell'Immacolata, Roma Italy

Received April 28, 2015 – Accepted July 24, 2015

Psoriatic arthritis is an inflammatory seronegative spondyloarthropathy that occurs in approximately 25% of patients with psoriasis and is a progressive and severely disabling disease. Most patients have had psoriasis for several years before the development of arthritis or develop the joint and skin condition simultaneously. Given the absence of specific diagnostic test for psoriatic arthritis, clinical findings remain the standard criteria for the diagnosis. Patients with psoriasis presenting to the dermatologist for management of their skin disease may have joint symptoms related or not to psoriatic arthritis and similarly arthritic patients presenting to a rheumatologist for the management of psoriatic arthritis may have skin lesions related or not to psoriasis. In this paper an expert panel of specialist belonging to the "Associazione Dermatologi Ospedalieri Italiani" (ADOI) and "Collegio dei Reumatologi Ospedalieri Italiani" (CROI) analysed the international literature and scientific recommendations and also investigated the Italian setting. It has been demonstrated in the literature that a multidisciplinary clinical setting may benefit patients with psoriatic arthritis from both diagnostic and therapeutic points of view. The comparative analysis of the Italian clinical records used by ADOI and CROI have highlighted some substantial differences. Collaboration between the dermatologist and rheumatologist allows for a more complete appreciation of the overall skin and musculoskeletal disease burden, and subsequently leads to a more comprehensive treatment approach.

PSORIATIC ARTHRITIS

Background

Psoriatic arthritis (PsA) is a progressive and severely disabling disease. About 40% of patients with PsA develop radiographic evidence of erosive joint disease. The joint involvement in patients with PsA causes a decrease in quality of life. Approximately 10–30% of patients with psoriasis have been diagnosed with PsA, and an additional 27% suffer from joint pain and stiffness. The condition affects men and women equally and can occur at

Key words: psoriatic arthritis, psoriasis, dermatologist, rheumatologist, management

Mailing address: Prof. Alberto Migliore,
U.O. Reumatologia,
Ospedale San Pietro
Via Cassia 600, 00189 Roma, Italy
Tel.: +39 06 3358 5802
Fax: +39 06 3325 1424/ +39 335 85802
e-mail: reumafbf@libero.it

0393-974X (2015)

DISCLOSURE: ALL AUTHORS REPORT NO CONFLICTS OF INTEREST RELEVANT TO THIS ARTICLE.

any time during the course of psoriasis, although its onset is earlier in women than in men (1).

PsA is characterized by morning stiffness, fatigue, pain, swelling and tenderness of the joints as well as ligaments and tendons and most often by psoriasis. In fact, the onset of psoriatic lesions precedes the arthritis in about 70% of cases, whereas the arthritis is manifested before the skin disease in only 15% of cases. Rarely, the skin and joint conditions present simultaneously (2).

Psoriatic lesions can appear anywhere on the body, but most often affect the scalp, nails (up to 90% of patients with PsA may have nail changes), the trunk, the elbows, and knees. Although the prevalence of PsA increases in patients with severe psoriasis, even those with mild or no evident skin involvement can suffer from severe PsA (1).

Unfortunately, a significant proportion of psoriasis patients have joint involvement without a diagnosis of PsA (3), since involvement of joints or juxta-articular tendons may be unpredictable, heterogeneous, and often insidious. Given the absence of a diagnostic test for PsA, the standard criteria for the diagnosis remain the clinical findings. The recognition of PsA and its distinction from other types of arthritis may be a challenge since several types of joint damage, such as osteoarthritis and gout, often coexist with psoriasis and mimic the presentation of PsA. Contrariwise, patients with psoriasis-like skin lesions and a concomitant inflammatory arthritis, such as rheumatoid arthritis or ankylosing spondylitis, may be misdiagnosed with PsA. Patients with psoriasis presenting to the dermatologist for the management of their skin disease may have joint symptoms related or not to PsA; similarly, arthritic patients presenting to a rheumatologist for management of arthritis may have skin lesions related or not to psoriasis.

One relevant clinical goal is to determine how dermatologists and rheumatologists should best collaborate in the diagnosis and management of these patients. The arthritis associated with psoriasis complicates management of the skin disease. Dermatologists and rheumatologists may have complementary roles to play in managing the skin and joint lesions which may affect patients. Moreover, new treatment options for PsA and psoriasis have become available over recent years. Several different biological agents are currently labelled for the treatment of PsA and also moderate-to-severe plaque-type psoriasis. Some of these drugs have been shown not only to reduce skin and joint symptoms, but also to prevent the progression of bone destruction in PsA, and to dramatically improve health-related quality of life. In addition, recent data show that patients should be treated early in the course of their disease in order to achieve the best symptomatic results and the possibility of halting the structural bone damage (1). Unfortunately no common and universally accepted guidelines are available in literature since dermatologists and rheumatologists have different resources for evaluating and managing joint symptoms. Taking into account this scenario the "Associazione Dermatologi Ospedalieri Italiani" (ADOI) and "Collegio dei Reumatologi Ospedalieri Italiani" (CROI) have started to investigate the international framework and to analyse the Italian setting.

The aim of this work is to describe how rheumatologists interact with dermatologists, and *vice versa*, in addressing and identifying skin and joint symptoms and signs in PsA patients in order to improve the management of patients with PsA.

Methodology

A group of experts on PsA, 4 dermatolgists and 4 rheumatologists, were appointed respectively by ADOI and CROI in order to study the interaction between dermatologists and rheumatologists in the management of psoriatic arthritis. This expert panel decided to focus this question in 4 items: 1) Overview of the international literature; 2) to compare record forms used in clinical practice by specialist members of both ADOI and CROI; 3) to compare the profile of patients with psoriasis and psoriatic arthritis from the specialist's point of view, both dermatologist and rheumatologist; 4) to analyse the recommendations on the management of patients with psoriatic arthritis produced by both dermatologic and rheumatologic associations.

Overview of the international literature

Laws et al. (4) reviewed the criteria for the diagnosis of PsA, looking at the clinical indications for referral to a rheumatologist and discussing evolving treatment options relevant to both conditions. It is

well-known that patients with psoriasis experience more joint pain than non-psoriatic subjects and this pain may be non-inflammatory in nature. However, a history of potential inflammatory arthritis (joint swelling, morning stiffness) should lead to a correct diagnosis. The initial assessment should help to restrict the likely diagnosis but anyone with a history or examination findings consistent with inflammatory joint disease should be referred to a rheumatologist.

The authors suggest that joint pain without evidence of inflammatory arthritis may be managed with simple analgesics, while more severe or persistent symptoms should be promptly referred to a rheumatologist. This process could be better performed if imaging studies and soluble biomarkers have already been assessed. Since the erythrocyte sedimentation rate and C-reactive protein level may be normal in up to 50% of patients with PsA, these markers should not be used to exclude patients from seeking rheumatology advice. Because treatment needs to be tailored to control the numerous factors relevant to the disease, the involvement of a multidisciplinary team, including a rheumatologist, physiotherapist, orthopaedist and an occupational therapist, is expected to offer the best results.

In 2009 Taylor et al. (5) surveyed ten rheumatologists to determine what role they suggest dermatologists should play in the evaluation and management of joint pain and other joint symptoms in patients with skin psoriasis. Although a consensus was not reached among the rheumatologists, the survey provided a range of opinions regarding how dermatologists can better address PsA in their psoriatic patients. Rheumatologists suggested that obvious joint warmth, joint swelling, and joint erythema must be recorded. Additionally, dermatologists should consult a rheumatologist when psoriasis patients complain of joint pain not responsive to non-steroidal anti-inflammatory drugs (NSAIDs) or when psoriasis patients experience swollen joints. Moreover, patients with disabling joint symptoms, patients whose joint symptoms do not improve on disease-modifying anti-rheumatic drug (DMARD) therapy for skin disease, and patients who might have other causes of joint pain should also be referred to rheumatologists. In the opinion of the rheumatologists, dermatologists should not need to perform laboratory and radiographic studies to evaluate joints and dermatologists should be comfortable offering patients prescription NSAIDs and treating psoriasis patients' skin disease with DMARDs such as methotrexate or biologic therapies. Finally, the rheumatologists suggested that DMARD therapy for joint disease should be left to the rheumatologist when skin disease does not warrant such therapy.

In 2009 a total of 1,511 patients were enrolled in a German observational prospective cross-sectional cohort study in 48 centres (6). Demographic and medical parameters were recorded, including severity of skin symptoms, Psoriasis Area Severity Index (PASI), treatments, concomitant diseases, and the impact of psoriasis on quality of life. Patients with joint symptoms were referred to a rheumatologist for diagnosis and to record the activity and pattern of their arthritis; in 85% of the cases PsA was newly diagnosed. Of these patients more than 95% had active arthritis and 53% had five or more joints affected. The authors' conclusion was that the findings are consistent with a high prevalence of undiagnosed cases of active PsA among patients with psoriasis seen by dermatologists. As many of these patients also have significant skin symptoms, treatment strategies are required that are equally effective in the control of skin and joint symptoms of psoriasis. In 2012, Kraishi et al. (7) also tried to quantify the prevalence of PsA in psoriasis patients seen in a dermatology practice and to define their characteristics using the validated Psoriatic Arthritis Screening Questionnaire (PASQ). A small cohort of 66 patients with definite plaque psoriasis (as determined by a dermatologist) completed the self-administered PASQ, and patients with a score >7 or >9 were assessed by a rheumatologist to ascertain the diagnosis of PsA according to the CASPAR (Classification Criteria for Psoriatic Arthritis) criteria. Using PASQ cut-off scores of 7 and 9, the estimated prevalence of PsA was 40.9% (29.0–52.8%) and 36.4% (24.8–48.0%), respectively. In this case, too, the estimated prevalence of PsA in psoriasis patients from a population of patients drawn from a dermatology practice was greater than in most previous estimates. This finding illustrates the importance of screening for PsA in psoriasis patients and indicates that an easy-to-administer screening tool for PsA should probably be incorporated in

the initial assessment of patients with psoriasis, facilitating these patients' correct and early referral and effective treatment and consequently improving their outcome.

In 2012, Velez et al. (8) reported the experience of multidisciplinary clinical care of patients by both a rheumatologist and a dermatologist. In October 2003, the Department of Dermatology and Division of Allergy, Immunology and Rheumatology at Brigham and Women's Hospital (Boston, MA, USA) created the Center for Skin and Related Musculoskeletal Diseases (SARM). The goal was to provide comprehensive, multidisciplinary care, one half-day per week, with an attending dermatologist and rheumatologist working synchronously at the point of service, evaluating and managing patients together (9). One of the first clinics of its kind nationwide, SARM has provided a unique referral service for both primary care physicians and specialists caring for patients with challenging skin and musculoskeletal diseases. In the retrospective chart review of 510 patients evaluated between October 2003 and October 2009 in the SARM, 268 patients had psoriasis and/or PsA. The prevalence of comorbidities was high (45% hypertension, 46% hyperlipidaemia, 19% diabetes). Interestingly, being assessed in the SARM led to a revised diagnosis that diverged from the previous diagnosis at outside clinics in 46% of cases. Patients were more likely to receive systemic medication after evaluation in than SARM as compared to before. This experience confirmed that multidisciplinary care offers a more comprehensive treatment approach for patients with both psoriasis and PsA and may facilitate the diagnosis of the joint disease.

Recently, Mease et al. (10) estimated the prevalence of PsA in patients with plaque psoriasis in 34 dermatology centres in seven European and North American countries. Nine hundred and forty-nine patients were evaluated by dermatologists for plaque psoriasis and subsequently by rheumatologists for PsA. The presence of PsA was determined first based on the rheumatologists' assessment of medical history and physical examination, and then laboratory tests. Overall, in the various countries, 285 patients (30%) were found to be affected by PsA based on the rheumatologists' assessment: Canada, 54/299 (18%); United States, 35/98 (36%); Belgium, 6/33 (18%); Denmark, 49/117 (42%); France, 12/44 (27%); Germany, 65/189 (34%); and Hungary, 64/169 (38%). The diagnosis of PsA changed in 1.2% of patients when diagnostic laboratory tests were added to the medical history and physical examination. Of the 285 patients given the diagnosis of PsA by a rheumatologist in this study, 41% had not previously been diagnosed as having PsA, suggesting under-diagnosis of this incapacitating joint disease in patients with psoriasis evaluated in dermatology practice. This study underscores the high prevalence of undiagnosed PsA, and indicates that clinical evaluation alone is often adequate to identify PsA. Increased awareness of this joint condition among patients with psoriasis and their dermatologists may be a critical step in reducing the potential for disability in this population.

Given that clinical evaluation may underestimate joint damage and that early treatment can delay progression of PsA, screening psoriasis patients with imaging tools that can detect early PsA changes would have clear benefits. In this context, De Simone et al. (11) compared the ability of X-ray and ultrasound examinations to reveal morphological abnormalities consistent with early PsA in patients with psoriasis, using rheumatological evaluation as the gold standard for diagnosis. Ultrasound proved valuable in detecting joint and/or tendon abnormalities in the fingers and toes of psoriasis patients with joint pain. The dermatologist should consider ultrasound to obtain an accurate assessment of suspicious findings.

In conclusion, multidisciplinary clinical care may benefit psoriasis patients from both diagnostic and therapeutic points of view. Collaboration between a dermatologist and rheumatologist allows for a more complete appreciation of the overall skin and musculoskeletal disease burden, and subsequently leads to a more comprehensive treatment approach. There is a high rate of undiagnosed cases of PsA among patients in dermatological care for psoriasis. The high estimate of the prevalence of PsA in the population studies described above underscores the importance of early screening for PsA in those patients already diagnosed with psoriasis. As many of these patients also have significant skin symptoms, treatment strategies are required that are equally effective in the control of skin and joint symptoms

of psoriasis. The high prevalence of newly diagnosed PsA emphasizes the need to facilitate the diagnosis of PsA among dermatologists and to encourage an interdisciplinary management of this subgroup of patients.

A COMPARISON OF DERMATOLOGICAL AND RHEUMATOLOGICAL DATA COLLECTION FORMS: PSODIT AND REUMARECORD

Psodit and Reumarecord are computerised clinical records, respectively used in clinical practice by ADOI and CROI. In these records the data collected for the management of patients with psoriasis (Psodit) and psoriatic arthritis (Reumarecord) are reported. Even if they are still not widely used, they represent a common view of how each discipline approaches these patients. The comparative analysis of the two clinical records highlights some substantial differences (Table I).

Psodit is a more complete tool than Reumarecord with regards to the collection of purely dermatological data. The data collected include the date of onset of the psoriasis, first- or second-degree relatives affected, an evaluation of disease activity and site and possible involvement of the nails, assessed with the Nail Psoriasis Severity Index (NAPSI). Another feature of Psodit is the use of questionnaires which evaluate skin involvement, such as the Dermatology Life Quality Index (DLQI) and PSOdisk. The drug history is centred on the use of drugs for psoriasis and not for joint disease.

In the Reumarecord data collection form, more attention is paid to assessing the joints and the patient's general health status through the use of questionnaires such as the Functional Assessment of Chronic Illness Therapy (FACIT), the Short Form (36) health survey (SF-36) and the Health Assessment Questionnaire (HAQ). One particular feature of Reumarecord is that it includes some automatically calculated compound indices such as the Clinical Disease Activity Index (CDAI) and the Simplified Disease Activity Index (SDAI), used to evaluate the activity of the arthritis. The drug history is very detailed and includes an evaluation of current and past drug use (steroidal and non-steroidal anti-inflammatory agents, traditional and biological DMARDs) for arthritis, but does not take into consideration drugs used for psoriasis.

The Psodit and Reumarecord forms do, therefore, give two completely different views of the patient's clinical condition. From the rheumatological point of view, the skin disease is neglected, while from the dermatological point of view, the arthritic component is neglected. This highlights the need to create a unified clinical record that incorporates the minimum data necessary from both the previously described records. This should aid a more valid therapeutic approach. However, collecting the data for integrated clinical records could prolong the duration of the assessment excessively. This could be avoided by defining a shorted list of shared variables and/or using patient-reported outcomes.

It is important to define the most useful indicators for both the dermatologist and rheumatologist which will make up the scales for the creation of a single

Table I. *A comparison between dermatological and rheumatological data collection forms: PSODIT and REUMARECORD.*

PSODIT	REUMARECORD
Computerised clinical record that collects the data for the management of patients with psoriasis	Computerised clinical record that collects the data for the management of patients with psoriatic arthritis
Arthritic component neglected	Skin disease neglected
Questionnaires for evaluation of skin involvement (DLQI, PSOdisk)	Questionnaires for assessing the joints and the patient's general health status (FACIT, SF-36, HAQ)
	Presence of automatically calculated compound indices for evaluation of the arthritis activity (CDAI, SDAI)
Drug history centred on the use of drugs for psoriasis	Drug history includes evaluation of current and past drug use for arthritis

instrument (record/chart) for the two specialities, constructed for the management of PsA. One limitation is the lack of shared information between the dermatologist and rheumatologist, a problem which could be overcome by setting up training to increase the information available to the two groups of specialists on the management of PsA.

THE DERMATOLOGICAL AND RHEUMATOLOGICAL DIAGNOSIS OF PSORIATIC ARTHRITIS

The profile of patients with psoriasis from the specialist's point of view

Psoriasis is a common chronic inflammatory immuno-mediated disease which involves the skin and joints and which affects approximately 2% of the population. Its aetiology is still unknown, while a complex interplay between genetic susceptibility, environmental factors (excess alcohol, smoking, psychological distress, streptococcal infections and certain drugs) and immunological disorders are believed to be the basis of its pathogenesis (12).

According to current understanding (knowledge), the pathogenesis of psoriasis is based on the interplay between acquired and innate immunity. At the onset of the disease, dendritic cells (DCs) in the epidermis and dermis are activated; among other effects, these cells produce messenger proteins including tumor necrosis factor (TNF)-α and interleukin (IL)-23, which in turn, promote the development of T helper (Th)1, and Th17 cells. These T cells secrete mediators that contribute to the vascular and epidermal changes of psoriasis (12). It is been well known that IL-23 functions as a key cytokine for the maintenance and development of Th17 cells (13). Th17 cells and their downstream effector molecules, which include IL-17A, IL-17F, IL-22, IL-21 and TNF-a, are found at increased levels in psoriatic skin and circulation, and are known to play a crucial role in psoriasis (14-16).

In addition to the T cells already known, more attention has recently been given to some innate immune cells, such as gamma delta (gd) T cells, natural killer (NK) cells and natural killer T (NKT) cells, because of their potential role in psoriasis. After IL-23 stimulation, gd T cells, are demonstrated to be the biggest IL-17 producer in the skin and are therefore considered to have a crucial function in psoriasis pathogenesis. Among several of their other functions, they amplify conventional immune response (17).

Further innate immune cells involved in psoriasis are NK and NKT cells. NKT cells, a heterogenous subset of T cells, share characteristics of both T cells and NK cells. NK and NKT cells have been found to be significantly increased in psoriatic lesions (18, 19). Additionally, psoriatic NK cells might have increased cytotoxicity through the release of cytotoxic granules such as perforin, which were found to be upregulated in psoriatic lesions (19).

Finally, Treg lymphocytes are a subset of T cells that suppress not only auto-immune responses but also other aberrant or excessive immune responses to non-self-antigens (20). Tregs have been found to be functionally deficient in suppressing effector T-cell responses (21). Both *in vitro* and *in vivo* experiments have suggested that Tregs did not function properly in psoriatic plaques and this is probably due to the pro-inflammatory cytokine milieu (especially IL-6 secreted from endothelial cells, DCs and Th17 cells), which inhibit Treg activity, avoiding the suppression of infiltrated T effector cells (22).

Psoriasis can be divided into type 1 and type 2, depending on the age of the patients. Type 1 typically arises in the second or third decade of life and accounts for more than 75% of cases. It is strongly associated with human leucocyte antigen (HLA)-Cw6, is usually more severe and tends to affect a greater number of family members. Type 2 normally begins in patients over 40 years old (23).

There are several psoriasis phenotypes, the most common, psoriasis vulgaris, affects approximately 85 to 90% of all patients with the disease. It is characterized by raised, well-demarcated, erythematous plaques covered with adherent silvery scales which are most frequent on the scalp, elbows, knees and sacral region. Over time the plaques can develop into:

- psoriasis gyrate - with predominant curved linear patterns;
- annular psoriasis - ring-like lesions secondary to central clearing;
- psoriasis follicularis - little scaly papules present at the openings of pilosebaceous follicles
- rupioid psoriasis - small hyperkeratotic plaques resembling limpet shells;

· ostraceous psoriasis - hyperkeratotic plaques with a slightly concave centre, similar to an oyster shell.

Other clinical forms are guttate, erythrodermic and pustular (localized or generalised), each of which can coexist or even convert into one of the other forms. In addition, specific nail changes occur in around 50% of all those affected and are more common in patients with PsA (23).

Several studies have identified risk factors for development and progression of PsA; in general, patients with moderate-to-severe psoriasis may have a higher risk of inflammatory arthritis than patients with mild psoriasis (24). Recently, physical trauma in patients with psoriasis known as the deep Koebner phenomenon, as well as acute life stressors, were found to be associated with onset of PsA. In addition, a significantly strong association between some psoriasis features (nail dystrophy, scalp and intergluteal/perianal lesions) and the onset of PsA was frequently seen (25).

Finally, patients with psoriasis have a remarkable worsening of quality of life similar to other chronic conditions including diabetes or even ischaemic heart disease (26). Very often psoriatic patients suffer from anxiety, depression and suicidal ideation (27).

Intriguingly there is no relationship between either the severity of the clinical features or anatomical location of psoriasis and psychological disability (28). Furthermore, these above-mentioned psychological complaints are often considered detrimental for the success of any therapy.

A wide variety of assessments is available to evaluate the severity of psoriasis. The PASI is a clinical tool based on a calculation of the severity of individual psoriasis plaques and the extent of the body surface area involved. Body Surface Area (BSA) is an instrument to estimate the extent of psoriatic involvement; an area of skin the size of the palm represents 1% of the total body surface area. DLQI and SF-36 are instruments which measure how psoriasis affects quality of life (29).

Several studies suggest that psoriasis is associated with comorbidities such as metabolic syndrome, increased cardiovascular risk, type 2 diabetes mellitus, Crohn's disease, non-alcoholic fatty liver disease, chronic obstructive lung disease, depression, sleep disorders/insomnia, smoking, gastroesophageal reflux disease, multiple sclerosis and PsA. This last is the most common comorbidity among those just mentioned (30).

There is, however, some controversy over the skin condition and arthritis: is PsA a different manifestation of the same disease, a natural clinical progression of psoriasis, or a concomitant condition? Genetic evidence as well as immunological findings suggest that they might be two different conditions, although with similar underlying inflammation and immune dysregulation (30).

Dyslipidaemia, coronary atherosclerosis, increased levels of C-reactive protein, and hyperhomocysteinemia are often found in psoriasis patients (31). Several studies have proposed a possible link between psoriasis and its comorbidities. It is thought that inflammation is the common milieu underlying all these conditions; in other words, psoriasis and concomitant diseases share a chronic inflammatory state, a common pathogenic pathway and additionally genetic susceptibility loci and environmental influences (32). These above-mentioned comorbidities can cause serious morbidity, have a negative impact on quality of life and can, ultimately, increase the risk of mortality. They must, therefore, be taken into account when prescribing any medications to psoriasis patients (30).

When choosing the best therapeutic options, the main targets of treatment should be to obtain prompt control of the disease without relapses or side effects, and to improve the patient's quality of life. It is important to match the treatment to the severity of the disease according to the European Consensus which defines mild psoriasis as a BSA, PASI and DLQI $\leq$10, and moderate to severe psoriasis as a BSA or PASI and DLQI >10. Treatment goals (assessed after 10-16 weeks) are a reduction of PASI $\geq$75% and DLQI 0 or 1 (65). If a treatment regimen results in a reduction of PASI $\geq$75% or PASI $\geq$50% to <75% combined with a DLQI $\leq$5, treatment is effective and therapy should be continued. When there is a reduction in PASI <50% or PASI $\geq$50% to <75% combined with a DLQI >5, treatment modifications should be considered, such as increasing the drug dosage, reducing intervals between each administration, combining therapies or changing the drug (34).

Nowadays, a wider range of effective treatment is available for psoriasis. Conventional systemic drugs, such as methotrexate, cyclosporine, acitretin and phototherapy, are frequently prescribed but are not indicated for long-term treatment because of their photo-carcinogenesis and their organ toxicity (especially liver and renal). During the past decade, new highly selective biological drugs for the management of inflammatory immune-mediated diseases, including psoriasis, have been approved. They are called "biologics" and are recombinant molecules and include tumour necrosis factor-alpha blockers (etanercept, infliximab and adalimumab) and an anti-interleukin 12/23 monoclonal antibody, ustekinumab. These drugs are given in the case of contraindications or intolerance or lack of response to traditional treatments and have been designed for long-term use (35).

The profile of patients with psoriatic arthritis from the specialist's point of view

The rheumatological evaluation of a patient affected or potentially affected by PsA is essentially centred on the search for signs and/or symptoms of joint or tendon disorders, using the following procedure:

· *family history*, collecting information on first- and second-degree relatives with a history of rheumatological disorders and psoriasis, dermatitis, scurf, etc.

· *personal past clinical history*, in which besides assessing previous non-rheumatological disorders, details of the joint problems are collected. Questions are asked about past episodes of joint swelling (mono- or pauci-articular involvement); if present, their site and how often they occurred, the duration of the episodes and whether they resolved spontaneously or in response to pharmacological treatment. Furthermore, it is noted whether these episodes were associated with stiffness that decreased with movement. Any axial disease is evaluated, that is, whether the patient has had episodes of inflammatory-type lower back pain (spine pain associated with prolonged morning stiffness), in what period and for how long; past episodes of unilateral or alternating sciatica (in particular pseudo-sciatica) are assessed. Tendon pain (particularly at the insertions) is assessed, with special attention to some particular sites such as the epicondyles, trochanters, knees and heels, in the absence of known trauma, and whether the pain is recurrent. Any episodes of swelling of a whole finger or toe, with a "sausage" appearance, is noted. A careful history is then taken to pick up any manifestations that might have occurred in other organs such as the eyes (uveitis), bowel (diarrhoea), genitals (sores, infections) and skin (psoriasis, folliculitis, purpura).

· *recent clinical history,* given that the patient requesting a rheumatologic consultation usually has an active joint or tendon problem. The patient may have pain and/or swelling of one or more joints, not responsive to NSAIDs (usually self-administered in the initial stages); he or she may complain of lower back pain that may have been present for years and has the characteristics of inflammatory pain. Sometimes the patient presents because of the development of dactylitis (usually recurrent episodes in the absence of a known cause).

· *clinical examination,* in which a full examination is usually performed, including a global rheumatological evaluation, with particular attention to the musculoskeletal apparatus and the skin. All the joints are evaluated, using manoeuvres that highlight acute conditions rather than chronic ones. The peripheral joints are evaluated, but also the axial skeleton, with assessment of the spine as well as the sacro-iliac joints. Entheses are examined to detect any swelling and/or pain. Particular attention is also given to the search for psoriatic skin lesions over the whole body, particularly if the past history is negative but the clinical picture is suggestive of this disease. The clinical examination is often completed by ultrasound studies that can show changes in the joints and tendons which are often not detectable clinically, especially in the early stages.

The arthritic patient is, therefore, an individual with a history characterized by pain, swelling and joint stiffness (mono- or pauci-articular) or involvement of the axial skeleton, or tendon involvement. Often the rheumatological evaluation is requested when the disease has been present for some time, particularly when the axial skeleton is affected, when there may be a diagnostic "delay" of some years.

There are various profiles of arthritic patients:

1. the patient with very active, polyarticular

arthritis, with considerable functional limitation. In this case, given the severity of the disease, the patient usually requests a rheumatological assessment quickly;

2. the patient with occasional episodes of joint pain and swelling (usually of a single joint or a few joints), which often resolve or improve with the aid of self-medication. The patient treats himself and the rheumatological consultation is requested some months after the onset of the first episode of joint problems;

3. the patient with lower back pain, whose rheumatological assessment is performed months/ years after the onset of the disorder. Lower back pain is an extremely common disorder; often the problem is undervalued, leading to diagnostic delay. The patients complain of an inflammatory-type of back pain, present for years sometimes with episodes of sciatica, which further confuses the clinical picture and raises the suspicion of a disc disorder. This is often a pseudo-sciatica and can be alternating;

4. the patient with tendon involvement, who reports episodes of pain (often inflammatory) at some tendon insertions; in the early stages, the pain is often related to physical activity;

5. the patient with dactylitis, who reports of episodes of "sausage"-like swelling of the fingers or toes, related in the early stages to possible trauma.

The management of PsA is advancing, owing to recent progress in treatment strategies and outcome assessment. We now know that early referral, diagnosis and initiation of treatment are crucial for the best management strategies for PsA. As in the management of rheumatoid arthritis, the treated-to-the-target approach to remission or to the alternative target of low disease activity is the suggested strategy also in PsA.

The first step in the treatment of PsA are NSAIDs and local corticosterods. Various studies support the efficacy of NSAIDs which are currently used to treat patients with PsA (36). NSAIDs are useful in all patients with mild disease, especially in the absence of risk factors for disease progression, which should be treated with NSAIDs to control disease activity. Intra-articular and local corticosteroid injections are useful in managing local flares according to the international recommendations (37).

In cases where patients do not have a clinical response they should be given DMARDs. Conventional DMARDs are used to treat patients with peripheral manifestations, but these drugs are not effective for treating axial disease. Methotrexate (7.5–25 mg per week) is the most widely used DMARD, even if studies of methotrexate treatment for PsA are scarce and their conclusions often contradictory (38,39).

When a response to DMARDs is lacking, TNF inhibitors are the next step. They reduce signs and symptoms of inflammation in both peripheral and axial disease. Currently four drugs are available (etanercept, infliximab, adalimumab, and golimumab) and all these agents have demonstrated significantly better response rates than placebo in randomized controlled trials (40).

The management of PsA is therefore improving and is now similar to the management of RA. As in RA, the early diagnosis and initiation of therapy are crucial for the effective treatment of patients with PsA.

Also pharmacological therapy is evolving, and new anti-TNF biologic agents, such as certolizumab pegol and ustekinumab, will be soon available. Furthermore, new data suggest that both targeting the IL-17 pathway with secukinumab and inhibiting the phosphodiesterase isozyme-4 with aprelimast could be additional therapeutic options.

ANALYSIS OF GUIDELINES OR RECOMMENDATIONS ON THE MANAGEMENT OF PATIENTS WITH PSORIATIC ARTHRITIS

There are currently adequate guidelines and recommendations in the fields of both dermatology and rheumatology for the diagnostic and therapeutic approach to the psoriatic patient on the one hand and the patient with PsA on the other hand. There is, however, a poorly defined borderline area including psoriatic patients with arthritis who are not adequately treated because of their complexity. An analysis of guidelines or recommendations on the management of patients with psoriatic arthritis is reported in Table II.

The heterogeneity of the joint manifestations of PsA has led to the suggestion that the term "psoriatic

disease" is better adapted to reflect the constellation of symptoms and different clinical pictures (41). Although each manifestation can be considered separately, in reality, individual patients often have overlapping clinical pictures, and it can be difficult to evaluate the relative importance of each component, particularly at the time of making therapeutic choices. This aspect is further complicated if the involvement of different organs (skin, joints, bowel, eye) and any comorbidities are also considered (42).

Ideally, a validated instrument to determine disease activity and therapeutic response should therefore be able to evaluate globally the single domains involved and reflect the effect of the disease on all dimensions of the patient. However, to date, only single domains, such as the skin or the joints, have been used to develop guidelines; this leads to the risk of underestimating the severity of the disease and, perhaps, any therapeutic response. For example, a patient with not severe, but simultaneous, involvement of the skin, joints and bowel would not be eligible for biologic therapy, despite having an overall significantly compromised quality of life. This problem of underestimating the disease and therapy response is made extremely complicated by a series of factors. First of all, although there is agreement on the evaluation of peripheral arthritis, the same cannot be said for dactylitis, enthesitis and spinal involvement. Furthermore, it is important to establish whether the evaluation should be aimed

Table II. *Analysis of guidelines or recommendations on the management of patients with psoriatic arthritis.*

Mumtaz A, FitzGerald O. Application of the GRAPPA psoriatic arthritis treatment recommendations in clinical practice. Curr Rheumatol Rep 2010; 12(4):264-71.	The term "psoriatic disease" is better adapted to reflect the heterogeneity of joint manifestations and different clinical pictures of PsA.
Sistema Nazionale Linee Guida Istituto Superiore di Sanità, Associazione Dermatologi Ospedalieri Italiani. Linea Guida "Il trattamento della psoriasi nell'adulto", Maggio 2013.	Patients with PsA often have overlapping clinical pictures making difficult the therapeutic choices. The involvement of different organs and any comorbidities further complicates this aspect.
Ritchlin CT, Kavanaugh A, Gladman DD, Mease PJ, Helliwell P, Boehncke WH, de Vlam K, Fiorentino D, Fitzgerald O, Gottlieb AB, McHugh NJ, Nash P, Qureshi AA, Soriano ER, Taylor WJ; Group for Research and Assessment of Psoriasis and Psoriatic Arthritis (GRAPPA). Treatment recommendations for psoriatic arthritis. Ann Rheum Dis 2009; 68:1387-94.	A validated instrument to determine disease activity and therapeutic response should be able to evaluate globally the single domains involved. The GRAPPA has established five domains that should be evaluated in patients with "psoriatic disease". The treatment recommendations were formulated individually for each domain and a grid was developed to classify the manifestations as mild, moderate or severe individually and overall.
Mumtaz A, Gallagher P, Kirby B, Waxman R, Coates LC, Veale J D, Helliwell P, FitzGerald O. Development of a preliminary composite disease activity index in psoriatic arthritis. Ann Rheum Dis 2011; 70:272-7.	Development of CPDAI a composite index that provides a measure of the activity of the disease and response to therapy. It can be used in randomised controlled trials.
FitzGerald O, Helliwell P, Mease P, Mumtaz A, Coates L, Pedersen R, Nab H, Molta C. Application of composite disease activity scores in psoriatic arthritis to the PRESTA data set. Ann Rheum Dis 2012; 71:358-62	Validation of CPDAI in PRESTA study.
Finlay AY. Current severe psoriasis and the rule of tens. Br J Dermatol 2005; 152:861-7.	Development of an instrument named "the rule of tens" that combined PASI score, BSA index, and DLQI. If BSA, PASI and DLQI are all <10, the psoriasis is considered mild; if the BSA and/or PASI and/or DLQI are >10, the psoriasis is defined as moderate-severe. Further distinction can be made between moderate psoriasis (BSA 10-25% and/or PASI 10-20 and/or DLQI ≥10) and severe psoriasis (BSA >25% and/or PASI >20 and/or unstable and rapidly progressive psoriasis).

at determining the extent of the involvement, the potential evolution of the disease or the functional limitation/impairment in quality of life. Finally, since not all treatments necessarily act in the same way on all the systems involved, should the evaluation be based on the worst clinical picture or on a model that integrates the various problems present? The Group for Research and Assessment of Psoriasis and Psoriatic Arthritis (GRAPPA) (42, 43), has established a set of domains that should be evaluated in patients with "psoriatic disease": peripheral joints, skin, axial involvement, enthesitis and dactylitis. The treatment recommendations were then formulated individually for each of the five domains and a grid was developed to classify the manifestations as mild, moderate or severe individually and overall, thereby giving a global, composite assessment of the disease (Composite Psoriatic Disease Activity Index - CPDAI) (44). The CPDAI is a composite index that provides a measure of the activity of the disease and response to therapy and can be used in randomised controlled trials. This index was validated in the Psoriasis Randomized Etanercept Study in Subjects with Psoriatic Arthritis (PRESTA) (45).

The need to have an index of severity that also takes account of the impact of the disease on the quality of life of the patient led to the creation of a simple and easily used instrument that combines the PASI score, the extent of the lesions expressed by the BSA index and the degree of social and psychological distress related to the presence of the disease evaluated by the DLQI. This instrument, named "the rule of tens" (46), sets out that:

- if the three parameters (BSA, PASI and DLQI) are all <10, the psoriasis is considered mild;
- if the BSA and/or PASI and/or DLQI are >10, the psoriasis is defined as moderate-severe.

Although of little practical use, a further distinction can be made between moderate psoriasis (BSA 10-25% and/or PASI 10-20 and/or DLQI ≥10) and severe psoriasis (BSA >25% and/or PASI >20 and/or unstable and rapidly progressive psoriasis). It should, however, be noted that specific clinical situations can cause a worsening in the severity of psoriasis, independently of the PASI score. In fact, involvement of visible areas (such as the face and hands) or the genital region can lead to psoriasis being considered as moderate or severe. Finally, in the light of the previously mentioned concept of "psoriatic disease", psoriasis associated with related extracutaneous inflammatory disorders (joint disease, chronic inflammatory bowel diseases, uveitis) is considered as severe.

INTEGRATED MANAGEMENT OF THE FOLLOW-UP OF PSORIATIC PATIENTS

As already described, PsA is a complex and heterogeneous disease which involves skin, nails and several musculoskeletal structures such as entheses, synovial joints, synovial tendon sheet and the axial skeleton. Several different clinical subsets of PsA have been identified and, as described by Moll and Wright, may coexist, making it difficult to recognize PsA. The clinical complexity can result, at best, in a delay in diagnosis and therefore treatment and, at worst, in a complete failure to diagnose the illness. This leads to the onset of chronic inflammation with progressive joint damage and permanent disability (1).

Dermatologists or other physicians including rheumatologists, who often deal with psoriasis, are in an ideal position to recognize PsA early and to start appropriate therapy as soon as possible (47). However, the management of PsA depends on the correct diagnosis, precise assessment of disease activity and its impact on the quality of life and function and, finally, coordination between dermatologists and rheumatologists in order to choose the best treatment strategy.

In most patients, psoriasis precedes joint involvement by approximately 10 years. However, occult PsA is still widely prevalent. Physicians have more chance of discovering a previously undiagnosed PsA by asking some key questions regarding joint symptoms, morning stiffness and function and by having patients fill in questionnaires such as the Toronto PsA screening questionnaire (ToPAS), the Psoriatic Arthritis Screening and Evaluation (PASE) or the Psoriasis and Arthritis Questionnaire (PAQ). This can easily be done either in the waiting room or even at home (48). However, these questionnaires have yet to be universally validated, although they are currently being standardized by GRAPPA.

Since the introduction of the Moll and Wright

classification, several other criteria have been proposed for the correct diagnosis and classification of the arthritis related to psoriasis, one of the best examples being CASPAR. These criteria, which were developed by experts from 30 rheumatology centres in 13 countries, are based on a prospective study of 500 patients and have a higher specificity and sensitivity than those previously used. In addition, they allow the diagnosis of PsA in spite of the presence of rheumatoid factor and the absence of psoriasis. The CASPAR criteria are not, however, useful for the diagnosis of a PsA of recent onset as they were obtained from a cohort of patients with chronic disease (35, 47, 48).

Apart from the need to identify PsA as soon as possible, clinical monitoring and assessment of response to treatment are also important. These can be done by using scores normally employed for the evaluation of rheumatoid arthritis, such as the Disease Activity Score 28 (DAS28), American College of Rheumatology 20 (ACR20), Psoriatic Arthritis Response Criteria (PsARC), European League Against Rheumatism (EULAR), HAQ or finally the disease-specific Psoriatic Arthritis Quality of Life (PsAQoL) score (47). For this reason, recently, rheumatologists, dermatologists and non-clinical members have joined GRAPPA, with the aim of validating and standardizing outcome assessment tools in PsA and psoriasis, both for clinical practice and for therapeutic investigative studies (49).

Finally, rheumatologists as well as dermatologists can accurately monitor PsA patients through the use of imaging modalities such as magnetic resonance imaging and ultrasonography.

A large number of treatments is now available thanks to the growing understanding of the pathophysiology of PsA and psoriasis. These range from symptomatic drugs such as NSAIDs, corticosteroids or even DMARDs (methotrexate, cyclosporine) to biologics. Biological drugs currently approved for PsA include anti-tumor necrosis factor agents such as infliximab, etanercept, adalimumab, golimumab and ustekinumab, a recently approved anti-interleukin 12/23. All these compounds are highly selective therapeutic options which increase the relevance of striving for a quick diagnosis and prompt therapy because of their ability to change the natural course of arthritis, avoiding progressive joint damage (35, 48, 50).

CONCLUSIONS

It is clear from the foregoing that more intense collaboration between the dermatologist and rheumatologist is necessary to optimise the diagnostic process of PsA.

It is known that skin psoriasis precedes the joint disease in 80% of cases, so the initial phase of the diagnostic process is usually performed by the dermatologist, who does, therefore, play a fundamental role in making an early diagnosis of PsA. Besides the large number of psoriatic patients who develop PsA, there is an equally large number of patients with psoriasis whose PsA is not diagnosed during the dermatological assessments, so that, to guarantee a prompt diagnosis, collaboration between dermatologists and rheumatologists, either synchronously or through referral of patients, should be intensified and should include imaging studies. The dermatologist should, therefore, consider ultrasonography as a diagnostic instrument and should work within a multidisciplinary context. In other words, attention should given to the joint symptoms of psoriatic patients as well as to their cutaneous symptoms, fostering multidisciplinary care and early screening for PsA. Reaching the correct diagnosis of PsA is a fundamental prerequisite for planning its optimal management, particularly in patients who do not have striking clinical manifestations.

REFERENCES

1. Lloyd P, Ryan C, Menter A. Psoriatic arthritis: an update. Arthritis 2012; 2012:176298.
2. Garg A, Gladman D. Recognizing psoriatic arthritis in the dermatology clinic. J Am Acad Dermatol 2010; 63:733-48.
3. Radtke MA, Reich K, Blome C, Rustenbach S, Augustin M. Prevalence and clinical features of psoriatic arthritis and joint complaints in 2009 patients with psoriasis: results of a German national survey. J Eur Acad Dermatol Venereol 2009; 23:683-91.
4. Laws P, Barton A, Warren RB. Psoriatic arthritis--what the dermatologist needs to know. J Eur Acad

Dermatol Venereol 2010; 24:1270-77.
5. Taylor SL, Petrie M, O'Rourke KS, Feldman SR. Rheumatologists' recommendations on what to do in the dermatology office to evaluate and manage psoriasis patients' joint symptoms. J Dermatolog Treat 2009; 20:350-3.
6. Reich K, Krüger K, Mössner R, Augustin M. Epidemiology and clinical pattern of psoriatic arthritis in Germany: a prospective interdisciplinary epidemiological study of 1511 patients with plaque-type psoriasis. Br J Dermatol 2009; 160:1040-7.
7. Khraishi M, Chouela E, Bejar M, Landells I, Hewhook T, Rampakakis E, Sampalis JS, Abouchehade K. High prevalence of psoriatic arthritis in a cohort of patients with psoriasis seen in a dermatology practice. J Cutan Med Surg 2012; 16:122-7.
8. Velez NF, Wei-Passanese EX, Husni ME, Mody EA, Qureshi AA. Management of psoriasis and psoriatic arthritis in a combined dermatology and rheumatology clinic. Arch Dermatol Res 2012; 304:7-13.
9. Mody E, Husni ME, Schur P, Qureshi AA. Multidisciplinary evaluation of patients with psoriasis presenting with musculoskeletal pain: a dermatology: rheumatology clinic experience. Br J Dermatol 2007; 157:1050-51.
10. Mease PJ, Gladman DD, Papp KA, et al. Prevalence of rheumatologist-diagnosed psoriatic arthritis in patients with psoriasis in European/North American dermatology clinics. J Am Acad Dermatol 2013; 69:729-35.
11. De Simone C, Caldarola G, D'Agostino M, Carbone A, Guerriero C, Bonomo L, Amerio P, Magarelli N. Usefulness of ultrasound imaging in detecting psoriatic arthritis of fingers and toes in patients with psoriasis. Clin Dev Immunol 2011; 2011:390726. doi: 10.1155/2011/390726. Epub 2011 Feb 8.
12. Nestle FO, Kaplan DH, Barker J. Psoriasis. N Engl J Med 2009; 361:496-509.
13. Kastelein RA, Hunter CA, Cua DJ. Discovery and biology of IL-23 and IL-27: related but functionally distinct regulators of inflammation. Annu Rev Immunol 2007; 25:221-42.
14. Boniface K, Guignouard E, Pedretti N, et al. A role for T cell-derived interleukin 22 in psoriatic skin inflammation. Clin Exp Immunol 2007; 150:407-15.
15. Caruso R, Botti E, Sarra M, et al. Involvement of interleukin-21 in the epidermal hyperplasia of psoriasis. Nat Med 2009; 15:1013-5.
16. Kagami S, Rizzo HL, Lee JJ, Koguchi Y, Blauvelt A. Circulating Th17, Th22, and Th1 cells are increased in psoriasis. J Invest Dermatol 2010; 130:1373-83.
17. Cai Y, Shen X, Ding C, et al. Pivotal role of dermal IL-17-producing gammadelta T cells in skin inflammation. Immunity 2011; 35:596-610.
18. Ottaviani C, Nasorri F, Bedini C, de Pità O, Girolomoni G, Cavani A. CD56brightCD162 NK cells accumulate in psoriatic skin in response to CXCL10 and CCL5 and exacerbate skin inflammation. Eur J Immunol 2006; 36:118-28.
19. Kastelan M, Prpic Massari L, Gruber F, Zamolo G, Zauhar G, Coklo M, Rukavina D. Perforin expression is upregulated in the epidermis of psoriatic lesions. Br J Dermatol 2004; 151:831-6.
20. Wing K, Sakaguchi S. Regulatory T cells exert checks and balances on self tolerance and autoimmunity. Nat Immunol 2010; 11:7-13.
21. Sugiyama H, Gyulai R, Toichi E, Garaczi E, Shimada S, Stevens SR, McCormick TS, Cooper KD. Dysfunctional blood and target tissue CD41CD25high regulatory T cells in psoriasis: mechanism underlying unrestrained pathogenic effector T cell proliferation. J Immunol 2005; 174:164-73.
22. Goodman WA, Levine AD, Massari JV, Sugiyama H, McCormick TS, Cooper KD. IL-6 signaling in psoriasis prevents immune suppression by regulatory T cells. J Immunol 2009; 183:3170-6.
23. Langley RGB, Krueger GG, Griffiths CEM. Psoriasis: epidemiology, clinical features, and quality of life. Ann Rheum Dis 2005; 64(Suppl II):ii18-ii23.
24. Gisondi P, Malara G, Ardigò M. The psoriatic patient profile for infliximab. Eur Rev Med Pharmacol Sci 2011; 15:1445-51.
25. Wilson FC, Icen M, Crowson CS, Mcevoy MT, Gabriel SE, Kremers HM. Incidence And Clinical Predictors Of Psoriatic Arthritis In Patients With Psoriasis: A Population-Based Study. Arthritis Rheum 2009; 61(2):233-9.
26. Finlay AY, Kelly SE. Psoriasis-an index of disability. Clin Exp Dermatol 1987; 12:8-11.
27. Gupta MA, Schork NJ, Gupta AK. Suicidal ideation in psoriasis. Int J Dermatol 1993; 32:188-90.

28. Kirby B, Richards HL, Woo P, Hindle E, Main CJ, Griffiths CE. Physical and psychologic measures are necessary to assess overall psoriasis severity. J Am Acad Dermatol 2001; 45(1):72-6.
29. Feldman SR, Krueger GG. Psoriasis assessment tools in clinical trials. Ann Rheum Dis 2005; 64 (Suppl 2):ii65-8.
30. Daudén E, Castañeda S, Suárez C, et al; Grupo de Trabajo en Comorbilidades asociadas a la Psoriasis. Integrated approach to comorbidity in patients with psoriasis.Working Group on Psoriasis-associated Comorbidities. Actas Dermosifiliogr 2012; 103(Suppl 1):1-64.
31. Onumah N, Kircik LH. Psoriasis and its comorbidities. J Drugs Dermatol 2012; 11(5 Suppl):s5-10.
32. Baeten D, van Hagen M, Magro F, Filipe P, Fonseca JE. Immune-mediated inflammatory diseases: a new multidisciplinary concept. Acta Reumatol Port 2009; 34:457-9.
33. Mrowietz U, Kragballe K, Reich K, et al. Definition of treatment goals for moderate to severe psoriasis: a european consensus. Arch Dermatol Res 2011; 303:1-10.
34. Mrowietz U, Elder JT, Barker J. The importance of disease associations and concomitant therapy for the long-term management of psoriasis patients. Arch Dermatol Res 2006; 298:309-19.
35. American Academy of Dermatology Work Group, Menter A, Korman NJ, Elmets CA, et al. Guidelines of care for the management of psoriasis and psoriatic arthritis: section 6. Guidelines of care for the treatment of psoriasis and psoriatic arthritis: case-based presentations and evidence-based conclusions. J Am Acad Dermatol 2011; 65(1):137-74.
36. Gossec L, Smolen JS, Gaujoux-Viala C, et al; European League Against Rheumatism. European League Against Rheumatism recommendations for the management of psoriatic arthritis with pharmacological therapies. Ann Rheum Dis 2012; 71(1):4-12.
37. Eder L, Chandran V, Ueng J, Bhella S, Lee KA, Rahman P, Pope A, Cook RJ, Gladman DD. Predictors of response to intra-articular steroid injection in psoriatic arthritis. Rheumatology (Oxford) 2010; 49(7):1367-73.
38. Ceponis A, Kavanaugh A. Use of methotrexate in patients with psoriatic arthritis. Clin Exp Rheumatol 2010; 28(5 Suppl 61):S132-7.
39. Mease PJ. Spondyloarthritis: Is methotrexate effective in psoriatic arthritis? Nat Rev Rheumatol 2012; 8(5):251-2.
40. Olivieri I, D'Angelo S, Palazzi C, Padula A. Advances in the management of psoriatic arthritis. Nat Rev Rheumatol 2014; 10(9):531-42.
41. Mumtaz A, FitzGerald O. Application of the GRAPPA psoriatic arthritis treatment recommendations in clinical practice. Curr Rheumatol Rep 2010; 12(4):264-71.
42. Sistema Nazionale Linee Guida Istituto Superiore di Sanità, Associazione Dermatologi Ospedalieri Italiani. Linea Guida "Il trattamento della psoriasi nell'adulto", Maggio 2013.
43. Ritchlin CT, Kavanaugh A, Gladman DD, et al; Group for Research and Assessment of Psoriasis and Psoriatic Arthritis (GRAPPA). Treatment recommendations for psoriatic arthritis. Ann Rheum Dis 2009; 68:1387-94.
44. Mumtaz A, Gallagher P, Kirby B, Waxman R, Coates LC, Veale J D, Helliwell P, FitzGerald O. Development of a preliminary composite disease activity index in psoriatic arthritis. Ann Rheum Dis 2011; 70:272-7.
45. FitzGerald O, Helliwell P, Mease P, Mumtaz A, Coates L, Pedersen R, Nab H, Molta C. Application of composite disease activity scores in psoriatic arthritis to the PRESTA data set. Ann Rheum Dis 2012; 71:358-62.
46. Finlay AY. Current severe psoriasis and the rule of tens. Br J Dermatol 2005; 152:861-7.
47. Mease PJ. Measures of psoriatic arthritis: Tender and Swollen Joint Assessment, Psoriasis Area and Severity Index (PASI), Nail Psoriasis Severity Index (NAPSI), Modified Nail Psoriasis Severity Index (mNAPSI), Mander/Newcastle Enthesitis Index (MEI), Leeds Enthesitis Index (LEI), Spondyloarthritis Research Consortium of Canada (SPARCC), Maastricht Ankylosing Spondylitis Enthesis Score (MASES), Leeds Dactylitis Index (LDI), Patient Global for Psoriatic Arthritis, Dermatology Life Quality Index (DLQI), Psoriatic Arthritis Quality of Life (PsAQOL), Functional Assessment of Chronic Illness Therapy-Fatigue

(FACIT-F), Psoriatic Arthritis Response Criteria (PsARC), Psoriatic Arthritis Joint Activity Index (PsAJAI), Disease Activity in Psoriatic Arthritis (DAPSA), and Composite Psoriatic Disease Activity Index (CPDAI). Arthritis Care Res (Hoboken) 2011; 63(Suppl 11):S64-85.

48. Anandarajah AP, Ritchlin CT. The diagnosis and treatment of early psoriatic arthritis. Nat Rev Rheumatol 2009; 5:634-41.
49. Cauli A, Porru G, Piga M, Vacca A, Mathieu A. Psoriatic arthritis (Psa) and outcome measures. Rev Latinoam Psoriasis Artritis Psoriásica 2012, 5:1-10.
50. Levine D, Strober BE. The treatment of moderate-to-severe psoriasis: prescreening and monitoring psoriatic patients on biologics. Semin Cutan Med Surg 2010; 29:28-34.

EDITORIAL

IMMUNOMODULATORY EFFECTS OF VITAMIN D ON SKIN INFLAMMATION

E. TONIATO[1], E. SPINAS[2], A. SAGGINI[3], S.K. KRITAS[4], A. CARAFFA[5], P. ANTINOLFI[5], R. SAGGINI[6], F. PANDOLFI[7] and P. CONTI[8]

[1]Department of Medical, Oral and Biotechnological Sciences, University G. D'Annunzio, Chieti-Pescara, Italy; [2]Department of Surgery and Odontostomatological Sciences, University of Cagliari, Italy; [3]Department of Dermatology, University of Rome Tor Vergata, Rome, Italy; [4]Department of Microbiology and Infectious Diseases, School of Veterinary Medicine, Aristotle University of Thessaloniki, Macedonia, Greece; [5]Orthopedic Division, University of Perugia, Perugia, Italy; [6]Department of Neurosciences and Imaging, Faculty of Medicine and Surgery, G. D'Annunzio University Chieti-Pescara, Chieti, Italy; [7]Catholic University of Rome, Italy; [8]Immunology Division, Post Graduate School of Medicine, Chieti, Italy

Received June 18, 2015 - Accepted August 31, 2015

Vitamin D has a major role in calcium absorption and maintenance of healthy bones. Vitamin D is also involved in cancer, cardiovascular system, allergic diseases, immune regulation and immune disorders. Irradiation of food as well as animals produces vitamin D and more than 90% of previtamin D3 synthesis in the skin occurs in the epidermis. Vitamin D receptor has been found in many cells including T and B lymphocytes, macrophages, mast cells, NK cells and Tregs, and it selectively binds with high affinity to its ligand. Vitamin D binds its receptor VDR, resulting in transcription of a number of genes playing a role in inhibition of MAPK. Its effect may be also mediated by the direct activation of PKC. Vitamin D has the ability to suppress inflammatory cytokines such as TNF, IL-1, IFN-gamma and IL-2; while it increases the generation of anti-inflammatory cytokines IL-4 and IL-10. In B cells, vitamin D3 have also been shown to suppress IgE antibody class switch partly through the inhibition of NF-kB. Here we discuss the relationship between vitamin D, immunity and skin disorders.

In 1912, the term "vitamin" was first used by Polish biochemist Funk to describe an accessory food factor. In 1922, McCollum discovered the fat-soluble vitamin D, and in 1926 Steenbock showed that irradiation of food as well as animals produced vitamin D2 (ergocalciferol), an active form of vitamin D. After irradiation, there are about 10 pro-vitamins that form compounds having anti-rachitic properties and 1,25-dihydroxyvitamin D, the hormonally active form of vitamin D, is produced by a number of different cell types (1-2). The irradiation of food has allowed the isolation and characterization of vitamin D2 form the provitamin ergosterol; while the irradiation of skin produces vitamin D3 (cholecalciferol) (Fig. 1) from the provitamin 7-dehydrocholesterol. It is well documented that

Key words: vitamin D, skin, immunity, inflammation

Mailing address: Dr Pio Conti,
Affiliated Professor, Molecular Immunopharmacology and Drug Discovery Laboratory,
Tufts University, Boston, MA 02111, USA;
Professor of Immunology, Post Graduate School of Medicine, University of Chieti-Pescara, Viale Unità d'Italia, 73
66100 Chieti, Italy
e-mail: pconti@unich.it

0393-974X (2015)

DISCLOSURE: ALL AUTHORS REPORT NO CONFLICTS OF INTEREST RELEVANT TO THIS ARTICLE.

more than 90% of previtamin D3 synthesis in the skin occurs in the epidermis, and 7-dehydrocholesterol formed in the skin after irradiation is absorbed through the skin and transported by the bloodstream at relatively low concentrations (Table I). The pro-vitamin D, 7-dehydrocholesterol, is synthesized in the sebaceous gland of the skin and is secreted on the surface where it is re-absorbed into the epidermis. The greatest concentration of 7-dehydrocholesterol is found in the Malpighi layers. Therefore, physical factors that reduce the exposure of the skin to UV light reduce the biosynthesis of vitamin D. This vitamin has a major role in calcium absorption and maintenance of healthy bones (3). A deficiency of vitamin D results in rickets, characterized by a decreased of calcium and phosphorus in cartilage and bone. In adults, osteomalacia is the counterpart of rickets. Vitamin D is the generic descriptor for all steroids and contains the intact "A" "C" and "D" steroid rings, being ultimately derived *in vivo* by photolysis of the "B" ring of 7-dehydrocholesterol (Fig. 1). Clinical signs of vitamin D deficiency includes inhibition of growth, weight loss, reduced appetite, muscular disorders, and congenital malformation in the new born. Vitamin D is available in two forms, vitamin D2 of plant origin, and vitamin D3 of animal origin, which serves as a protective antioxidant. To prevent hypocalcemia, supplemental vitamin D3, the metabolically active form of vitamin D, has been used.

Most of vitamin D is absorbed in the duodenum and ileum. Vitamin D, similar to other steroids, is transported in the plasma associated with proteins, and almost 90% of vitamin D enters the lymphatic circulation associated with the alpha-globulin fraction. The hydroxylated form of vitamin D is distributed intracellularly, and is present in the nucleus and cytoplasm. Intracellular vitamin D receptors are found in a wide variety of cells in human and other animals and their functions are associated with the induction of generation of calcium-binding proteins. Vitamin D deficiency causes epithelial lesions, nervous disorders and dermatological signs such as alopecia, seborrheic inflammation, epidermal hyperkeratosis, dysfunction of sebaceous glands and degeneration of myelin which can be potentially fatal. On the other hand, vitamin D at very high concentrations may provoke anorexia, hypercalcemia, bone abnormalities, myopathy, cardiac dysfunction, renal calcinosis and hyperphosphatemia.

In addition, a large number of reports indicated that vitamin D is involved in cancer, cardiovascular system, allergic diseases, immune regulation and immune disorders (Table II). These effects are linked to the innate and adaptive immune systems, which include immune cells such as macrophages, mast cells, NK cells, CD4 and CD8 cells, Treg cells and B cells.

In the skin, vitamin D undergoes several hydroxylation steps to generate the biologically-active form of vitamin D, 1,25(OH)2D which binds to the vitamin D receptor.

The vitamin D receptor has been found in many cells including lymphocytes, and it selectively binds with high affinity to its ligand 1,25 (OH) 2D. Vitamins D2 and D3 are sensitive to oxygen and light, and show strong UV absorption. Vitamin D is formed in humans by the action of 285/315 nm UV light on 7-dehydrocholesterol in the skin.

CHOLESTEROL → 7-DEHYDROCHOLESTEROL→UV→PRE-VITAMIN D3→VITAMIN D3

In mice, UV radiation causes tumors, systemic changes and immune suppression by acting mainly on the helper cells TH1, TH2 and TH17 (4)

In skin cells, UV radiation activates multiple signaling cascades including p38 MAPK, Jun N-terminal kinase, and NFkB pathways, an effect which may be linked to the regulation of TNF generation released from skin cells.

The effect of vitamin D3 may be mediated by the direct activation of PKC (5). In addition, it has been found (Nutchey et al.) that JNK activity (but not extracellular signal-regulated kinase (ERK) 1-2), is required for vitamin D3 to induce CYP24 gene expression. In innate immunity, mediated by the TLRs, vitamin D has an antimicrobial action through the stimulation of beta-defensin and cathelicidin and therefore the inhibition of pro-inflammatory cytokines. It has been reported that vitamin D3 has an anti-cancer activity, and promotes cell survival. Vitamin D3 produces at least 10 metabolites, and acts as endogenous regulators of skin functions and

Table I. *Synthesis of 1,25-dihydroxyvitamin D3 (1,25(OH)$_2$D3) pathway.*

UV → Epidermis → Vitamin D3 → Liver → 25-hydroxylase → 25(OH)2D3 → Kidney → 1-alpha-hydoxylase → 1,25(OH)2D3 → SYSTEMIC (calcium and phosphate regulation) AND LOCAL EFFECTS (reduces proliferation and increases cell differentiation in immune cells)

Table II. *Some biological effects of vitamin D.*

Decreases:
- dendritic cell maturation and migration
- IgE production and plasma cell differentiation in B lymphocytes
- IL-12 in Th1 cells
- IL-23
- Th17 cells

Increases:
- phagocytosis
- cathelicidin
- chemotaxis
- IL-4, IL-5, IL-10
- Treg and conversion of CD4+ cells to Treg

as a good candidate for treatment of inflammatory and skin cancer.

Moreover, vitamin D3 fights infections by increasing the generation of nitric oxide and expression of inducible nitric oxide synthase by macrophages.

Regarding mast cells, there is a growing body of evidence that vitamin D provokes an increase of the anti-inflammatory cytokine IL-10; while IL-12 mRNA transcription and translation protein decreases. These effects contribute to inhibiting inflammatory cells in inflammatory diseases, such as atherosclerosis, and skin disorders (6).

In adaptive immunity, Treg cells (derived from naive CD4+ T cells), which regulate and inhibit immune cells by acting on IL-10 and TGF-beta, are also induced by vitamin D3. A dysfunction of Treg is found in certain inflammatory and immune disorders including atopic dermatitis; therefore, Tregs are capable of alleviating clinical signs of immediate-type hypersensitivity reactions in IgE-mediated skin allergy.

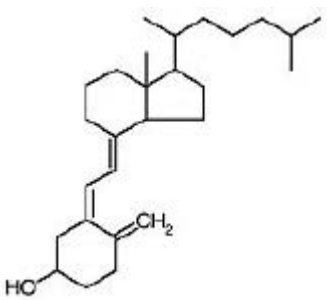

Fig. 1. *Cholecalciferol (vitamin D3).*

Epidermal and dermal cells produce several cytokines such as TNF, IL-1, IL-4, IL-6, IL-8, IL-10, IL-12 and IL-15. A number of reports indicated

that vitamin D has the ability to suppress the IL-2 in T-lymphocyte proliferation, TNF and IFN-gamma, while it increases the generation of anti-inflammatory IL-4, IL-10 and IL-5. In B cells, vitamin D3 has also been shown to suppress IgE antibody class switch partly through the inhibition of NF-kB.

Vitamin D decreases the expression of immune receptors, differentiation, maturation, chemotaxis, antigen presentation and stimulatory molecules, inhibiting dendritic cell and mast cell activation by antigens. In addition, vitamin D helps to defend the skin from opportunistic infections by stimulating macrophage phagocytosis. Moreover, vitamin D binds its receptor VDR, resulting in transcription of a number of genes playing a role in inhibition of MAPK, induction of apoptosis and cell-cycle inhibition in many cells. Apoptosis is also induced via the IGFR1/PI3K-Akt signalling pathway and by inhibiting telomerase (7).

Therefore, vitamin D down-regulates several cytokine genes including IL-1 and IL-12, TNF, IFN-gamma and EGF-R while it up-regulates many genes such as those coding for RANKL, Calbindin-9k, IGFBP and β3 integrin, osteopontin, and others (7)

Vitamins D3 and D2 inhibit keratinocyte proliferation and induce keratinocyte differentiation. For this reason they have been used as topical therapy in psoriasis patients. Psoriasis is worsened by acute stress and the plaques contain increased levels of VEGF compared with normal skin. Several different VEGF polymorphisms are associated with an increased risk of developing psoriasis. Psoriasis characterized by increased epidermal vascularization, keratinocyte hyperproliferation, and inflammation (8) is mediated by neuropeptides such as substance P. Increased numbers of mast cell were seen in lesional psoriatic skin which also has augmented AMP levels and increased inflammatory markers IL-17A, IL-17F, and IL-8. In humans, using vitamin D as topical therapy inhibits beta-defensin (HBD)2, HBD3, IL-17A, IL-17F, IL-8 and Treg cells in psoriatic patients.

Vitamin D shows an effect in non-immune cells, such as keratinocytes, against ionizing radiation as well as immune cells including mast cells, dendritic cells and T helper cells, and the absence of its receptor makes the cells more vulnerable to cancer (9). In fact, vitamin D decreases overall cancer risk and confers protection against melanoma via its receptor found also in NK cells. Vitamin D has positive effects on: risk factor for myocardial infarction, psoriasis, autoimmune disease, prevention on type I diabetes mellitus, multiple sclerosis, infectious periodontal diseases, bacterial infections (including upper respiratory tract infections) and skin diseases.

In the skin, ultraviolet light irradiation provokes $1,25(OH)_2D3$ release which can directly influence intrinsic functions of keratinocytes and other cells, and enhance the ability of Langerhans cells and dermal dendritic cells to induce FOXP3 expression and IL-10 secretion from T_{reg} cells.

Mast cells and Langerhans cells represent an immune barrier and can be activated by neurotransmitters such as substance P, growth factors, TNF-α, IL-1β, chemokines, and other inflammatory cytokines probably generated by activated keratinocytes, with the consequence of T-cell activation and therefore the enhancement of immune responses by multiple pathways.

In the skin, vitamin D provokes recruitment of T cells through the increase of expression of the chemokine receptor 10 (CCR10) and inhibits dendritic cell migration and IL-12 and IL-23 cytokine production.

T helper cells are divided into Th1, Th2, Th9, Th17 and Th22 cells and are characterized by specific cytokine generation patterns. All these cells and other immune cells own vitamin D receptor, where vitamin D can be linked and then decrease pro-inflammatory cytokines released from T helper cells and other immune cells such as mast cells and keratinocytes. Therefore, vitamin D influences the innate immune response by stimulating the production of cathelicidin, which is an anti-microbial peptide activated through toll-like receptors TLR2 and TLR4 (10).

Chronic inflammatory skin diseases, such as atopic dermatitis (AD) which includes eczema, asthma and allergic rhinitis, show an impaired cutaneous barrier function due to abnormalities in the skin. Clinical and basic immunological studies and epidemiological investigations on atopic dermatitis (AD) (11-12) have suggested a link between vitamin D deficiency and allergic skin diseases. Vitamin D deficiency is associated with higher risk of contracting AD, the severity of which may be improved by the administration of vitamin D with unknown

mechanism, but the benefit is often not statistically significant. Moreover, vitamin D-deficient mice have an increased contact hypersensitivity response compared to those with normal vitamin D.

Therefore, vitamin D enhances barrier function in the skin and often ameliorates atopic skin disease, however, in several studies the influence of this vitamin expression on skin allergies shows conflicting results.

In conclusion, vitamin D promotes mucosal barrier function, suppresses inflammatory cells, inhibits inflammatory cytokine and pro-allergic immune responses and promotes immunologic tolerance.

Since vitamin D provokes an increase of innate and acquired immunity, and has a possible role in cancer risk reduction, an association between deficient levels of vitamin D3 and several types of cancer is therefore pertinent. Data are accumulating to support the idea that vitamin D protects against inflammatory disorders and development and progression of many cancers, including melanoma.

However, more data are necessary to be considered to clarify this important relationship between cellular immunity, vitamin D and skin disorders.

REFERENCES

1. Hart PH, Gorman S, Finlay-Jones JJ. Modulation of the immune system by UV radiation: more than just the effects of vitamin D? Nat Rev Immunol2011; 11:584-96.
2. Wieczorek K, Braczkowski RS, Skrzypek M, Stryjewski PJ, Kuczaj A, Al-Srory G. The comparison between vitamin D concentration in upper silesia patients with prostate cancer and with benign prostatic hyperplasia. J Biol Regul Homeost Agents 2015; 29(1):207-11.
3. Need AG, Kemp A, Giles N, Morris HA, Horowitz M, Nordin BE. Relationships between intestinal calcium absorption, serum vitamin D metabolites and smoking in postmenopausal women. Osteoporos Int 2002; 13(1):83-8.
4. Mattner F, Smiroldo S, Galbiati F, et al. Inhibition of Th1 development and treatment of chronic-relapsing experimental allergic encephalomyelitis by a non-hypercalcemic analogue of 1,25-dihydroxyvitamin D(3). Eur J Immunol 2000; 30(2):498-508.
5. Suaini NH, Zhang Y, Vuillermin PJ, Allen KJ, Harrison LC. immune modulation by vitamin D and its relevance to food allergy. Nutrients 2015; 7(8):6088-108.
6. Malek HA, Shata A. Effect of a high dose of vitamin D on a rabbit model of atherosclerosis. Int J Immunopathol Pharmacol 201; 27(2):195-201.
7. Field S, Newton-Bishop JA. Melanoma and vitamin D. Mol Oncol 2011; 5(2):197-214.
8. Theoharides TC, Zhang B, Kempuraj D, et al. IL-33 augments substance P-induced VEGF secretion from human mast cells and is increased in psoriatic skin. Proc Natl Acad Sci U S A 2010; 107(9):4448-53.
9. Miller J, Gallo RL. Vitamin D and innate immunity. Dermatol Ther 2010; 23(1):13-22.
10. Santos-Martins M, Sameiro-Faria M, Ribeiro S, et al. TLR4 and TLR9 polymorphisms effect on inflammatory response in end-stage renal disease patients Eur J Inflamm 2014; 12:521-29.
11. Brough HA, Liu AH, Sicherer S, et al. Atopic dermatitis increases the effect of exposure to peanut antigen in dust on peanut sensitization and likely peanut allergy. J Allergy Clin Immunol 2015; 135(1):164-70.
12. Esposito S, Patria MF, Spena S, et al. Impact of genetic polymorphisms on paediatric atopic dermatitis. Int J Immunopathol Pharmacol 2015; 28(3):286-95.

PROTEOMIC CHANGES OF RECOMBINANT YEAST: PHARMACO-INDUSTRIAL POTENTIAL

P-H. MAO[1,3], J. LÜ[1,2] and C-L. CAI[3]

[1]Center of Ion Beam Biotechnology, College of Physics Science and Technology, Xinjiang University, Urumqi, People's Republic of China; [2]Laboratory of Molecular Ecology, College of Resource and Environment Sciences, Xinjiang University, Urumqi, People's Republic of China; [3]Research Center of Ion Beam Biotechnology and Biodiversity, Xi'an Technological University, Xi'an, People's Republic of China

Received April 14, 2015 – Accepted May 25, 2015

The original yeast strain *Hansenula anomala* 2340 was implanted by low-energy nitrogen ion (N+) to obtain the mutant strain N6076. The mutant strain produced a red quinone compound, not synthesized by the parent strain. Two-dimensional fluorescence difference gel electrophoresis (2-D DIGE) and mass spectrometry (MS) were utilized to analyze the protein profile of the mutant strain N6076. The proteome changes were compared to those of the original strain to assess the amount of change that the metabolic pathways underwent in the mutant strain. The results indicated the detection of 57 different expressed proteins ($P < 0.05$) when the N6076 mutant strain was cultured in the liquid medium for 96 h as compared to that of the original strain. Of these different expressed protein spots, 27 were upregulated, and 30 were down-regulated. Also, 56 protein spots were identified with the aid of MALDI-TOF and tandem (TOF-TOF) MS. The protein score confidence interval (CI) of the protein profiling in the down-regulated protein spots 273 and 1294 were 81.371% and 12.864%, respectively, by bioinformatic analysis. This probably points to the fact that the irradiation by N+ contributed to the mutation of these two proteins.

The biologic effects of ion irradiation were recognized and demonstrated experimentally for the first time in the mid-1980s by the Ion Beam Bioengineering Key Lab, the Institute of Plasma Physics, and the Chinese Academy of Sciences (1). Ion beam technology has been extensively employed as a new mutation method in organisms for mutation breeding, the creation of aneuploids, ion beam etching-mediated structural analyses of organisms and gene (genetic) transformation (2-3). Compared to the other physical radiation types, low-energy ion beam implantation varies significantly in terms of lower energy, charge transfer, and mass deposition, whereas X-rays display no charge transfer or mass deposition, but only have the energy (4). However, there are some disputes regarding the biologic effects of low-energy ion irradiation as the ion energies used in such experiments were at least of three-fold lower magnitude than the typical energies used in conventional heavy-ion experiments (5). It is commonly assumed that low-energy ions have a short, penetrating range in complex organisms that

Key words: 2-D DIGE, Hansenula anomala, protein profiling, recombinant, yeast

Mailing address: Prof. Pei-Hong Mao,
Center of Ion Beam Biotechnology,
College of Physics Science and Technology,
Xinjiang University, Urumqi 830046,
People's Republic of China
Tel./Fax: +86 991 8582405
e-mail: drwangion@outlook.com

0393-974X (2015)

would make it difficult for them to reach the genetic material and thus induce any conceivable biologic effect. Interaction mechanisms between low-energy ion irradiation and organisms have been studied extensively in the interdisciplinary field of ion beam biotechnology. The technology of the implanted low-energy nitrogen beam has been applied to improve the yield of rice seedlings (6). Low-energy nitrogen ion (N+) implantation in maize has also led to mutator transposable element system reactivation (7). In the past 20 years, the utilization of microbial breeding by low-energy ion irradiation has developed rapidly (4). The technology has been successfully utilized to screen for high-yielding *Bacillus subtilis* mutants from the strain Bs-916, the biocontrol bacterium. Subsequently, the mutant strain Bs-H74 was found to be more adept as a biocontrol agent than the parent strain (8). Improvements in chitosanase production and thermostable α-amylase activity have been shown by the mutagenesis breeding utilizing low-energy ion implantation (9, 10). Mutagenesis induced by ion beam implantation could identify two new rifampicin-resistance determining sites in *E. coli* within the rpoB gene (11). It is not yet established whether the low-energy ion implantation-induced stimulatory effect is passed on to the next generation or not; but the present generation can significantly benefit from it.

However, the molecular mechanisms concerning organism mutation induced by ion irradiation remain entirely unexplored, and more work on this interdisciplinary field, Ion Beam Bioengineering, is required to delineate such mechanism.

In 1891, Hansen for the first time described *Hansenula anomala*. The isolation of *H. anomala* from a child, who died of interstitial pneumonia, identified it to be a human pathogen (12). *H. anomala* is an ascosporogenous Ascomycete of the *Saccharomycetaceace* family and can be recognized by its biochemical pattern and ascospore production (13). It is usually found as a transient flora of the digestive tract, throat and skin in humans, and in soil, plants and fruits. A relatively few reported cases of *H. anomala* infections have been observed. It has been shown to ferment sucrose, glucose, and at times even maltose, galactose while it assimilates sucrose, glucose, cellobiose, raffinose, trehalose, melezitose, ethanol, soluble starch, glycerol, α-methyl-D-glucoside, D-glucitol, D-mannitol, erythritol, salicin, succinate, nitrate, citrate and DL-Lactate (14). It shows a negative Crabtree effect and is tolerant of low pH and high osmotic pressure (15). Nengguo et al. thus successfully isolated a *P. anomala* strain that showed bioethanol producing potential being tolerant of high ethanol concentrations (16). *H. anomala* extracellular material has even found application in gold nanoparticle synthesis as a bioreductant (17). Furthermore, it has been shown to be able to decrease growth of *P. agglomerans*, *E. coli* and mold growth in cereal grains (15, 19). With such a wide array of activities in its repertoire, low-energy ion implantation mediated mutagenesis to produce better strains of *H. anomala* becomes a natural choice.

In our previous study, ion irradiation methods were used to induce mutations in *Hansenula anomala* 2340 to create mutants for studying the mutation mechanisms induced by ion irradiation. Following N+ irradiation, many phenotypic variations of mutants were obtained, along with the isolation of an interesting mutant, which can produce a new red quinone compound (19). To investigate the mutational mechanisms of low-energy ion irradiation, we chose the new red quinone compound-producing mutant as target, and combined a two-dimensional fluorescence difference gel electrophoresis (2-D DIGE) approach with mass spectrometry (MS) to compare protein expression alterations between the mutant and the original strain in the present study.

MATERIALS AND METHODS

Sample preparation

The yeast mutants and the control cells were inoculated into the liquid medium from test tubes and grown at 28-30°C for 96 h at 230 r/min. After incubation, the yeast cells were collected following centrifugation at 12000 × *g* for 2 min. The yeast cells were ground into fine powder after immersing them in liquid nitrogen; the cells were then transferred into two 50 mL centrifuge tubes. The samples were precipitated with 25 mL trichloroacetic acid (TCA)/acetone (1:9), containing 65 mM DTT, at -20°C for 1 h. The mixture was then centrifuged at 12,000 × *g* at 4°C for 45 min. The pellets were washed with 100% ice-cold acetone, precipitated at -20°C for 1 h and air-dried.

Precipitated proteins (200 mg) were weighed and solubilized in the lysis buffer (7 M urea, 2 M thiourea,

0.2% v /v IPG buffer (GE Healthcare), 4% CHAPS). The mixtures were shaken for 10 min in an ultrasonic bath and centrifuged at 12,000 × *g* at 4°C for 45 min. The supernatants were filtered through a membrane filter of 0.22 µm and stored at -80°C.

CyDye DIGE fluors and labeling kits (Amersham Biosciences, Uppsala, Sweden) were used according to the manufacturer's protocol for 2-D DIGE. A total amount of 50 µg of protein taken from the mutant and control samples were labeled with 400 pmol of Cy3 or Cy5, respectively. Cy2 was used to label the same amount of internal standard, resulting from the pooling of aliquots of mutant and control. Labeling was performed on ice, in the dark for 30 min. The reaction was then quenched by incubating the mixtures above with 1.5 mL of 10 mM lysine on ice, in the dark for 10 min. Three independent biologic replicates were performed.

Three labeled protein samples (pooled standard, mutant, and control) were then combined (150 µg) and diluted with rehydration buffer (8 M urea, 2% CHAPS, 18 mM dithiothreitol (DTT), 0.5% carrier ampholyte, pH 3-10 NL) to 250 µl. The combined samples were then loaded on a pH gradient strip (13 cm, pH 3-10, non-linear) for isoelectric focusing (IEF) on an Ettan IPGphor system (Amersham Biosciences, Uppsala, Sweden).

After active rehydration for 12 h at 30 V and 20°C, IEF was performed as follows: 500 V for 1 h; 1000 V for 1 h; 8000 V for 8 h; 500 V for 4 h. The temperature was maintained at 20°C. After IEF, the strips were equilibrated in the equilibration buffer (50 mM Tris-HCl (pH 8.8), 6 M urea, 30% v/v glycerol, 2% w/v SDS, traces of bromophenol blue, and 1% w/v DTT) for 15 min and later in the same buffer except that DTT was replaced by 4% (w/v) iodoacetamide for a further 15 min. Following equilibration, the IPG strips were transferred to the top of a 12.5% polyacrylamide gel and sealed with 0.5% low melting agarose. Electrophoresis was conducted for 20 min at 1.5 W per gel and 3 W per gel constant current overnight until the bromophenol blue front reached the bottom of the gels. Analytical gels were scanned using a TyphoonTM 9400 laser scanner (GE Healthcare, UK) fluorescence scanner device (Amersham Biosciences, Uppsala, Sweden). For CyDye-labeled analytical gels, a 488 nm laser and 520 nm emission filters for Cy2 images, a 532 nm laser and 580 nm emission filters for Cy3 images, and a 633 nm laser and 670 nm emission filters for Cy5 images were used, respectively.

The images were analyzed using Differential In-gel Analysis (DIA) and Biologic Variation Analysis (BVA) modules of DeCyder software version 6.5 (Amersham Biosciences, Uppsala, Sweden). The gel with the highest spot count was assigned as the master gel. In DIA, the Cy2, Cy3, and Cy5 images for each gel were merged; spot boundaries were automatically detected, and normalized spot volumes (protein abundance) were finally calculated. During spot detection, the estimated number of spots was set at 2000. In BVA, the inter-gel variability was corrected by normalization of the internal standard present in each gel, and the normalized protein spots were matched among the different gels. Selection criteria for the detection of significantly changed protein spots include: protein spots were present in at least two of the three analyzed gels (in six of nine analyzed images), and the standardized average spot volume ratios exceeded 1.2 with statistical significance (Student's *t*-test, $P < 0.05$).

Protein digestion and mass spectrometry

For mass spectrometric analysis, two preparative gels loaded with 1 mg mutant and control samples were run in the same condition and stained with ammoniacal silver nitrate (20). Different expressed protein spots of interest were excised from the DIGE analytic and preparative gels with the help of an Ettan Spot Picker (Amersham Biosciences, Uppsala, Sweden) and subjected to in-gel digestion with trypsin. The gel plugs were stained with 30% acetonitrile in 100 mM ammonium bicarbonate (NH_4HCO_3) for 20 min and vacuum dried, followed by the addition of digestion buffer (20 ng/µl trypsin in 20 mM NH_4HCO_3); the proteins were then kept for overnight digestion at room temperature. Peptides were extracted twice with a solution containing 60% acetonitrile (ACN) and 0.1% trifluoroacetic acid (TFA). The extracted peptides were dried and re-suspended in 50% ACN and 0.1% TFA. Equal volumes of sample and α-HCCA matrix (5 mg/ml) were spotted and mixed. Peptide mixtures were analyzed with an AutoFlex MALDI-TOF mass spectrometer (Bruker Daltonics, Bremen, Germany) in positive ion reflector mode. The accelerating potential was 20 kV with eight shots per second. Each spectrum was internally calibrated using trypsin autolysis peaks (m/z 842.51 or 2211.10).

For peptide mass fingerprint (PMF) identification, the tryptic peptide mass maps were transferred to the MS BioToolsTM program (Bruker Daltonics) using Applied Biosystems software (Applied Biosystems). The National Center for Biotechnology non-redundant database was searched. The following search parameters were used: trypsin was used as the cutting enzyme, one missing cleavage was allowed, mass tolerance for average peptide window was set to ± 1 Da, the MS/MS tolerance window was set to ± 0.8 Da, while carbamidomethyl cysteine and oxidized methionine were chosen as fixed and variable modifications, respectively.

Analysis of identified proteins

To analyze all the differently expressed proteins of the

mutant strain N6076, the following databases were used:

a) MIPS (http://www.mips.biochem.mpg.de/proj/yeast/);

b) SGD (http://genome-www.stanford.edu/saccharomyces/);

c) YPD (http://www.proteome. com/databases/index.html); and

d) KEGG (http://www.genome.jp/kegg/).

We could thereby identify the function of different expressed proteins analyzed by MS and could predict the changing process of the metabolic pathways in the mutant strain.

The Cytoscape plug-in in conjunction with Gene Ontology was used to analyze the highly expressed protein gene cellular components and molecular functions in the mutant strain N6076.

Since no formal ethics committee is available, we assert that the research was conducted according to the principles of the Declaration of Helsinki.

RESULTS

To compare proteins differently expressed between the original strain 2340 and the mutant strain N6076, the proteins were fluorescence-labeled, followed by a 2-D DIGE separation.

The resulting gel images were obtained (Fig. 1) Using a TyphoonTM 9400 laser scanner, (GE Healthcare, UK). The gel images were analyzed with DeCyder differential analysis software, Version 6.5 (Amersham Biosciences, Uppsala, Sweden), and 57 significantly different spots ($P < 0.05$) were detected (Fig. 2). The range of protein expression change for the mutant strain 6076 was 1.2-fold higher or lower than that of the original strain 2340 as found through three separate biologic experiments. In the mutant strain N6076, we found 26 upregulated protein spots, whereas 30 upregulated protein spots were seen in the original strain 2340. One of them could not be identified by MALDI-TOF and tandem (TOF-TOF) MS (Table I).

Through a structure diagram of the cellular components, it could be seen that in the mutant strain N6076, the genes for highly expressed

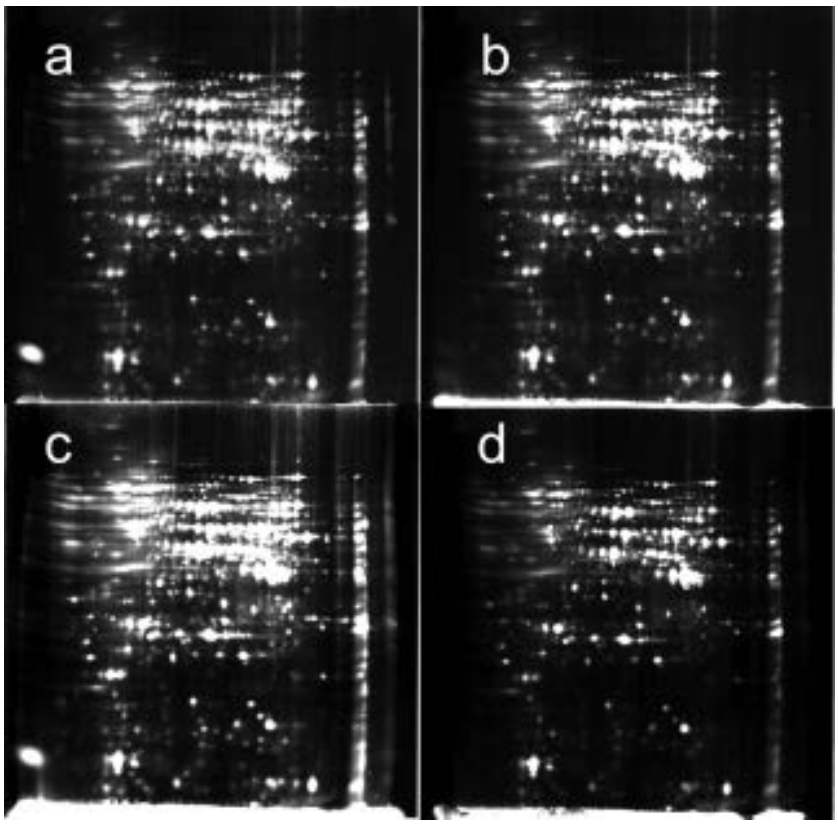

Fig. 1. *Reference 2-D DIGE electrophoretic patterns of the yeast protein extracts obtained from the mutant and control.* ***a****) Labelled proteins were visualized for all of the fluorophores.* ***b****) Cy2, mixing equal amounts of all of the proteins as the internal standard.* ***c****) Cy3, for the protein sample of mutant.* ***d****) Cy5, for the protein sample of control.*

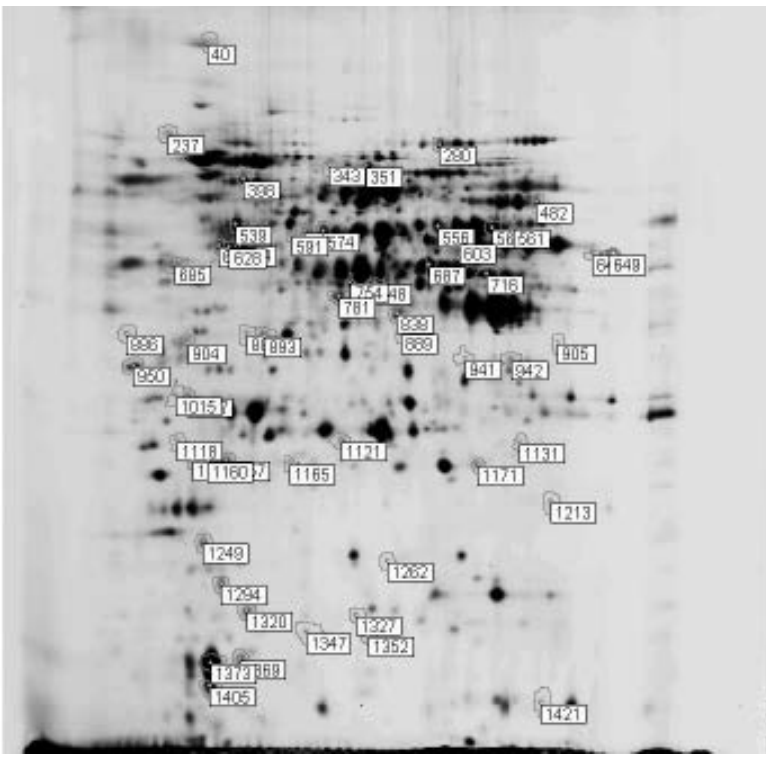

Fig. 2. *Representative gel of the differently expressed proteins of the mutant strain producing the red quinone compound. The gel was post-stained with ammoniac-silver nitrate. The numbers indicate spots associated with mutation.*

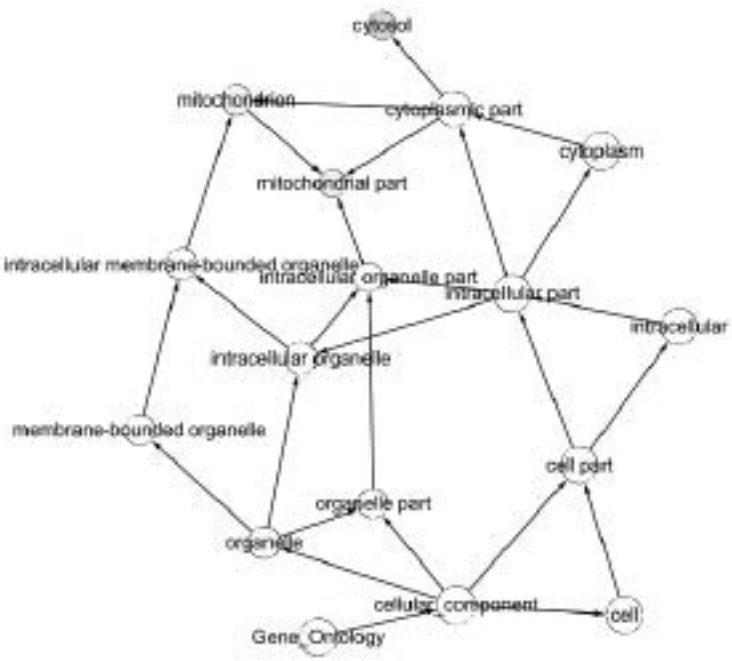

Fig. 3. *Structure diagram of the mutant strain 6076 high expression protein gene cellular component constructed with Cytoscape.*

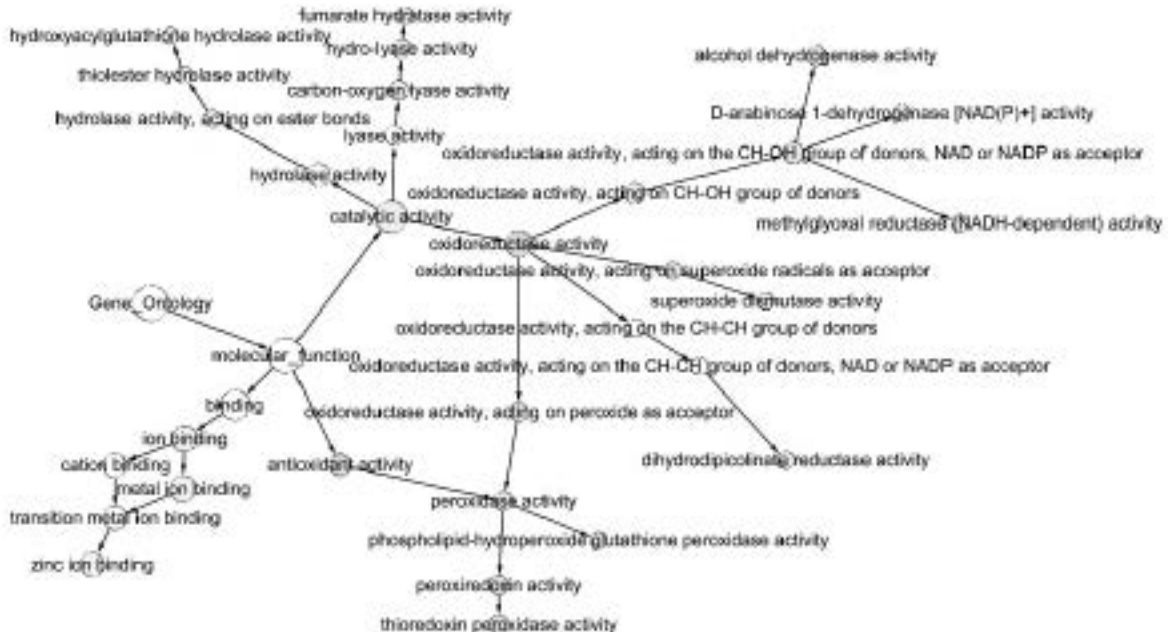

Fig. 4. *Structure diagram of mutant strain 6076 high expression protein gene molecular function constructed with Cytoscape.*

Table I. *Differently expressed proteins in mutant 6076 identified by MALDL-TOF PMF after DIGE analysis.*

Spot number	NCBI ID	Protein homologue	*P* value	Average ratio	Protein Score CI %
Carbohydrate and energy metabolic process					
482	gi|307568098	Chain A, Refined Structure of Yeast F1c10 Atpase Complex To 3 A Resolution	0.0046	4.65	100
556	gi|39654415	Chain A, Reverse Protonation Is The Key To General Acid-Base Catalysis In Enolase	0.047	1.23	100
560	gi|6321693	Eno1p	0.00069	1.31	100
561	gi|171523	fumarase	0.017	1.25	100
573	gi|6321968	Eno2p	0.049	-1.39	100
574	gi|6321968	Eno2p	0.03	-1.25	100
603	gi|6319426	Cor1p	0.0078	1.21	100
687	gi|6324486	Adh1p	0.0031	1.28	100
716	gi|6323961	Adh2p	0.003	1.31	100
754	gi|6322790	Fba1p	0.029	-1.4	100
781	gi|6319625	Ara1p	0.0032	1.26	100
838	gi|6321583	Thi4p	0.026	1.39	100
887	gi|6319483	Ipp1p	0.0096	-1.25	100
893	gi|6319483	Ipp1p	0.049	-1.21	100
942	gi|6324614	Glo4p	0.015	1.2	100
1294	gi|6324328	Cit1p	0.015	-1.61	12.864
1327	gi|20151124	Chain G, Yeast Cytochrome Bc1 Complex With Bound Substrate Cytochrome C	0.0043	1.41	100
Protein metabolism					
237	gi|50593216	Dsd1p	0.025	-1.51	81.371

280	gi|6320936	Met6p	0.033	-1.21	100
398	gi|6324804	Wtm1p	0.021	-1.23	100
591	gi|6324899	Pro2p	0.04	-1.2	100
614	gi|51013823	YDR502C	0.0056	-1.25	100
620	gi|51013823	YDR502C	0.039	-1.29	100
628	gi|51013823	YDR502C	0.022	-1.35	100
1007	gi|172043	Egd2p	0.0068	-1.62	100
1015	gi|49258825	Chain E, Structure of The Ribosomal 80s-Eef2-Sordarin Complex From Yeast Obtained By Docking Atomic Models For RNA And Protein Components Into A 11.7 A Cryo-Em Map. This File, 1s1h, Contains 40s Subunit. The 60s Ribosomal Subunit Is In File 1s1i	0.013	-1.4	100
1156	gi|6324670	Rps7ap	0.018	1.34	100
1157	gi|6324670	Rps7ap	0.0061	1.38	100
1160	gi|6324670	Rps7ap	0.0036	1.4	100
1262	gi|6325220	Egd1p	0.0011	-1.59	100
1320	gi|49258828	Chain I, Structure Of The Ribosomal 80s-Eef2-Sordarin Complex From Yeast Obtained By Docking Atomic Models For RNA And Protein Components Into A 11.7 A Cryo-Em Map. This File, 1s1h, Contains 40s Subunit. The 60s Ribosomal Subunit Is In File 1s1i	0.0031	-1.45	100
1369	gi|18479209	12 kDa heat shock protein	0.041	-1.31	100
1373	gi|18479209	12 kDa heat shock protein	0.015	-1.5	100
Cell signaling					
40	gi|6319978	Hbt1p	0.01	-1.78	100
539	gi|6322581	Atp2p	0.0029	1.26	100
685	gi|6325253	Lsp1p	0.000093	-1.3	100
748	gi|14277713	Chain B, Structure Of The Yeast Cytochrome Bc1 Complex Co-Crystallized With An Antibody Fv-Fragment	0.0084	1.29	100
886	gi|1945336	CLC1	0.017	-1.9	100
889	gi|6321583	Thi4p	0.0027	1.87	100
950	gi|6321571	Phb1p	0.049	1.3	100
Nucleotide biosynthesis and salvage					
343	gi|6321013	Pab1p	0.035	-1.31	100
351	gi|6321013	Pab1p	0.029	-1.24	100
904	gi|6320304	Bmh2p	0.044	-1.29	100
905	gi|6319315	Efb1p	0.004	1.33	100
1347	gi|10383793	Rps14ap	0.013	-1.48	99.986
1405	gi|6321879	Rtc3p	0.029	-1.58	100
Stress response					
1165	gi|6323613	Tsa1p	0.0014	1.32	100
1171	gi|223570	dismutase,Mn superoxide	0.022	1.25	100
1213	gi|6322228	Hyr1p	0.024	1.34	100
Unknown					
648	gi|6322055	Om45p	0.0017	2	100
649	gi|6322055	Om45p	0.02	1.49	100
1118	gi|6323208	Ylr179cp	0.02	-1.37	100
1121	gi|6323737	Ymr090wp	0.0029	1.39	100
1131	gi|6324975	Hsp32p	0.029	1.54	100
1249	gi|6323737	Ymr090wp	0.0023	-1.55	99.563
1352	gi|6323754	Spg4p	0.011	-1.36	100
Unsuccessful identification					
1421	□	□	0.00085	1.5	0

(a): The spot numbers correspond to the position number in the BVA module of the Decyder software.
(b): t-test indicates significant difference in expression of these proteins during red compound production in yeast mutant 6076.

proteins existed mainly in mitochondria and cytosol. The highly expressed proteins that occurred in mitochondria are related primarily to providing energy to the yeast cells. Thus, the metabolism for mutant strain N6076 following a 96-h liquid culture was more vigorous than the original strain (Fig. 3). Regarding molecular functions, it could be seen that the primary features of highly expressed genes were fumarate hydratase, hydroxyacylglutathione hydrolase, D-arabinose 1-dehydrogenase, methylglyoxal reductase, dihydrodipicolinate reductase and thioredoxin peroxidase expression (Fig. 4). However, it is difficult to analyze the direct relationship between the metabolism of red substances and the endogenous highly expressed genes of *Hansenula anomala*.

The results of MS identification are shown in Table I. We searched the 56 identified differential proteins in NCBI, SGD, and KEGG. Subsequently, we classified the differently expressed proteins. The functions of these proteins mainly referred to metabolic processes, cell signaling, nucleotide biosynthesis, salvage, and stress response; with functions of some proteins among these groups unknown. Four protein spots could be identified: 273, 1249, 1294 and 1347, which have protein score confidence interval (CI) of 81.371%, 99.563%, 12.864%, and 99.986%, respectively.

DISCUSSION

Secondary microbial metabolites are important sources of innovative new drugs and their precursor compounds (21). Many multi-enzyme systems involved in the biosynthesis of secondary metabolites are composed of individually separated functional regions with significant spatial structures.

Genetic recombination may change the biosynthetic pathway of secondary metabolites and generate new metabolic bypasses to form new compounds (22). We have detected that the mutant strain N6076 could produce a new red quinone compound (19), which indicated that its metabolic pathway had changed due to the N+ irradiation. The volatile compound, 2-phenylethanol obtained from *P. anomala*, has been previously shown to inhibit the aflatoxin genes from *Aspergillus flavus* (23). *H. anomala* genome shuffling has been carried out to obtain a mutated strain that showed improved flavor formation of soy sauce (24). Thus, the mutant *H. anomala* strain N6076 obtained could be beneficial in some aspects. Suppression subtractive hybridization (SSH) technology was used to discuss the gene expression of the mutant strain N6076 (25). A total of 14 gene fragment sequences with high expression levels were obtained from the strain N6076, which included nine different genes.

Here, we combined 2-D DIGE with MS identification analysis and compared the proteome changes of the mutant strain to that of the original strain 2340. Altogether, 57 differently expressed protein spots in the mutant strain N6076 were compared to those of the original strain 2340. Bioinformatic analysis of four proteins showed that the protein score CIs were less than 100%. This was probably due to the possibility of ion irradiation of *Hansenula anomala* 2340 causing mutations in amino acid residue sequences.

Except for four protein spots, the protein score CI of MS-identified proteins by the bioinformatic analysis was 100%. Among these, however, the protein score CI of the protein spots 273 and 1294 were 81.371% and 12.864%, respectively. Thus, we believe that the protein score CI is less than 95% for this model organism and that the search results were unauthentic. The question remains whether this difference is the result of irradiation-induced mutagenesis through N+ or due to other factors. If these two proteins were mutated because of N+ irradiation, the original biologic functions of these two proteins would also have changed. Also, these two differentially expressed proteins were down-regulated in the mutant strain N6076. It could be speculated that these two proteins may block the original metabolic pathway due to their changed function. This could alter the metabolic pathways of the mutant yeast strain and thus accumulate or produce new metabolites.

In conclusion, mutated strains of organisms with pharmaco-industrial significance modify metabolic pathways, enable production or accumulation of new metabolites, i.e. active therapeutics. Further research is needed to determine whether the mutation of the structure of these proteins changed their original functions. These researches should also determine whether a lower expression of the mutation of the structure of these proteins might block the metabolic

pathway and thus lead to the production of new metabolites.

ACKNOWLEDGEMENTS

This work was financially supported by the National Natural Science Foundation of China (Nos. 30960006 and 11275164).

REFERENCES

1. Yu ZL. Introduction to Ion Beam Biotechnology M. New York: Springer Science Media Inc., 2006.
2. Yu ZL. Study on the interaction of low-energy ions with organisms. Surf Coat Technol 2007; 201:8006-13.
3. Ji L, Li YW, Wang CS, Cao GQ, Jia X. Studies on wheat mutants induced by nitrogen ion beam implantation. Yi Chuan Xue Bao 2005; 32:1176-83. (in Chinese)
4. Feng HY, Yu ZL, Chu PK. Ion implantation of organisms. Mat Sci Eng R, 2006, 54:49-120.
5. Gu SB, Li SC, Feng HY, Wu Y, Yu ZL. A novel approach to microbial breeding-low-energy ion implantation. Appl Microbiol Biotechnol 2008; 78:201-9.
6. Ya H, Chen Q, Wang W, Chen W, Qin G, Jiao Z. Gene expression profiles in promoted-growth rice seedlings that germinated from the seeds implanted by low-energy N+ beam. J Radiat Res 2012; 53:558-69.
7. Qian Y, Cheng X, Liu Y, Jiang H, Zhu S, Cheng B. Reactivation of a silenced minimal Mutator transposable element system following low-energy nitrogen ion implantation in maize. Plant Cell Rep 2010; 29:1365-76.
8. Li D, Nie F, Wei L, et al. Screening of high-yielding biocontrol bacterium Bs-916 mutant by ion implantation J. Appl Microbiol Biotechnol 2007; 75:1401-8.
9. Su C, Zhou W, Fan Y, Wang L, Zhao S, Yu Z.Mutation breeding of chitosanase-producing strain Bacillus sp. S65 by low-energy ion implantation. J Ind Microbiol Biotechnol 2006; 33:1037-42.
10. Li XY, Zhang JL, Zhu SW. Improved thermostable α-amylase activity of Bacillus amyloliquefaciens by low-energy ion implantation. Genet Mol Res 2011; 10:2181-9.
11. Xie C, Yao J, Pan R, Wu L, Yu Z. [Mutagenesis of ion beam implantation and identification of two new rifampicin resistance determining sites in rpoB gene in Escherichia coli]. Wei Sheng Wu Xue Bao 2003; 43:732-9. [Article in Chinese]
12. Klein A, Tortora GT, Malowitz R, Greene WH. Hansenula anomala: a new fungal pathogen. Two case reports and a review of the literature. Arch Intern Med 1988; 148: 1210-3.
13. Barnett JA, Payne RW, Yarrow D. Yeasts: Characteristics and identification M. Cambridge, Cambridge University Press, 1983, pp. 306-7.
14. Kurtzman CP. Pichia E.C. Hansen emend. In: Kurtzman CP, Fell JW, eds. The Yeasts, A Taxonomic Study. New York, Elsevier, 1998.
15. Passoth V, Fredlund E, Druvefors UA, Schnürer J. Biotechnology, physiology and genetics of the yeast Pichia anomala. FEMS Yeast Res 2006; 6:3-13.
16. Tao N, Gao Y, Liu Y. Isolation and characterization of a Pichia anomala strain: a promising candidate for bioethanol production. Braz J Microbiol 2011; 42:668-75.
17. K SK, RA, Arumugam P, Berchmans S. Synthesis of gold nanoparticles: an ecofriendly approach using Hansenula anomala. ACS Appl Mater Interfaces 2011; 3:1418-25.
18. Olstorpe M, Borling J, Schnürer J, Passoth V. Pichia anomala yeast improves feed hygiene during storage of moist crimped barley grain under Swedish farm conditions. Anim Feed Sci Technol 2010; 156:47-56.
19. Fan YH, Jin X, Mao PH. Preparation of red component in the secondary metabolites of recombinant Hansenula anomala N6076 and its GC-MS detection. Agric Biotech 2012; 1(4):58-60.
20. Oakley BR, Kirsch DR, Morris NR. A simplified ultrasensitive silver stain for detecting proteins in polyacrylamide gels. Annal Biochem 1980; 105(2):361-3.
21. Knight V, Sanglier JJ, DiTullio D, Braccili S, Bonner P, Waters J, Hughes D, Zhang L. Diversifying microbial natural products for drug discovery. Appl Microbiol Biotech 2003; 62:4462-581.
22. Ro DK, Paradise EM, Ouellet M, et al. Production of the antimalarial drug precursor artemisinic acid in

engineered yeast. Nature 2006; 440:940-3.
23. Hua SS, Beck JJ, Sarreal SB, Gee W. The major volatile compound 2-phenylethanol from the biocontrol yeast, Pichia anomala, inhibits growth and expression of aflatoxin biosynthetic genes of Aspergillus flavus. Mycotoxin Res 2014; 30:71-8.
24. Cao X, Song Q, Wang C, Hou L. Genome shuffling of Hansenula anomala to improve flavour formation of soy sauce. World J Microbiol Biotechnol 2012; 28:1857-62.
25. Qian WD, Cai CL, Mao PH, Jie L, Ma XD, Liang CY. Effects on gene expression of yeast Hansenula anomala by low-energy nitrogen ion implantation. J Chem Pharm Res 2014; 6(7):2311-16.

CORRELATION BETWEEN CLINICAL PATHOLOGY OF LUMINAL B BREAST CANCER AND DETERMINATION OF ESTROGEN RECEPTOR, PROGESTERONE RECEPTOR AND HER2 EXPRESSION COMBINED WITH NUCLEAR MORPHOLOGY

D. YIN[1], YL. WANG[1], YF. WANG[1], L. YANG[1], L. ZHANG[1], C. TANG[2], W. XIE[3] and Y. MA[4]

[1]Oncology Department, The First People's Hospital of Nantong, Nantong, Jiangsu, China; [2]General Surgery Department, The First People's Hospital of Nantong, Nantong, Jiangsu, China; [3]Test Section, The First People's Hospital of Nantong, Nantong, Jiangsu, China; [4]Key Laboratory of Experimental Animal and Safety Evaluation, Zhejiang Academy of Medical Sciences, Hangzhou, China

Received February 27, 2015 – Accepted June 19, 2015

D. Yin and Y Ma are joint first authors and contributed equally to this study

Breast cancer, one of the most common malignant tumors in females, draws little attention because of its untypical symptoms and signs, so the disease is usually confirmed too late, in an advanced stage. Based on the detection of nuclear morphology parameters of luminal B breast cancer, this study explored how pathological features relate to estrogen receptor (ER) and progesterone receptor (PR) expression of human epidermal growth factor receptor-2 (HER2). A quantity of 354 breast cancer specimens with follow-up records from the department of pathology in the First People's Hospital of Nantong and the Tumor Hospital of Nantong were selected as research subjects. Nuclear parameters of specimens stained by hematoxylin and eosin were measured by imaging analysis software. It was found that breast cancer can be divided into four types, luminal B, luminal A, HER2 over-expression and basal-like type based on immunohistochemical results of three antibodies, i.e, ER, PR and HER2. A total of 113 patients (31.8%) were confirmed with luminal B breast cancer, mostly in histological stage II; the difference of nuclear morphology was of statistical significance between ER+/PR+ and ER-/PR- ($P<0.05$), and most ER-/PR- was histologically confirmed as stage III, with lower survival rate than ER+/PR+ ($P<0.05$). Among these four subtypes of breast cancer, luminal B had the lowest brain metastasis rate, while HER2 over-expression subtype was found with the highest rate of lung and pleura metastasis. Besides, luminal B possessed longer disease-free survival (DFS) than basal-like ($P<0.05$) and longer total survival (OS) than HER2 over-expression ($P<0.05$) and basal-like subtypes ($P<0.05$). It can be concluded that detection of ER, PR and HER2 in combination with nuclear morphology is beneficial to evaluate treatment and prognosis of breast cancer.

Breast cancer is one of the most common female malignancies worldwide. It occupies 7% ~10% of the female malignancy occurrence rate in China and tends to occur more among young females, which

Key words: breast cancer, pathological features, nuclear morphology, disease-free survival

Mailing address: Dr Yilang Wang,
Oncology Department,
the First People Hospital, of Nantong,
No.6, Haierxiang North,
Road, Nantong, Jiangsu 226001, China
Tel.: 0513-85200739
e-mail: wangyl@ibhsedu.com

0393-974X (2015)

urges specialists and researchers to increase the study on breast cancer (1). X. Yuntao (2) revealed the pathological mechanism of familial beast cancer and focused on the detection of breast cancer BRCA1, 2 gene mutation, which laid a theoretical basis for the treatment of familial breast cancer. X. Hongqiang and H. Jianrong (3) analyzed the expression of Ki-67, EGFR, HER-2, and P53 in breast cancer tissues and the correlation between the expressions and pathological features of breast cancer, which is of important significance in the diagnosis, treatment and prognosis evaluation of breast cancer. M. Peng and HY. Li reviewed the progress of study on neoadjuvant chemotherapy for breast cancer and gave practical suggestions on the defects of neoadjuvant chemotherapy, which provides new means for breast cancer treatment (4).

In the past years, scholars specialized in oncomolecularbiology have found that tumors with high heterogenicity, have remarkablely different tissue morphology, biological behavior, immune expression and therapeutic reaction (5,6). Therefore, individualized therapies are gradually emerging. However, as study on gene expression deepens, some scholars hold the opinion that some diseases have a specific gene expression spectrum, and molecular typing is closely related to individualized therapy in the mechanism of occurrence and development of tumor. Based on the above stated researches, this study analyzed 354 patients with invasive breast cancer which were divided into four subtypes, measured parameters of nucleus morphology, and discussed the relationship between quantitative analysis of morphology and prognosis, in order to provide references for studies and individualized therapy of luminal B breast cancer in the future.

MATERIALS AND METHODS

Specimens of 354 breast cancer patients who had been treated in the Department of Pathology in the First People's Hospital of Nantong and the Tumor Hospital of Nantong since 2010 and who were with follow-up records were enrolled in this study. The data of all the patients, aged from 25 to 86 years (average 51 years), included age, menstruation condition, tumor size, lymph node conditions and histological stage. All the patients signed an informed consent and this study was approved by the Medical Ethics Committee of the First People's Hospital of Nantong.

Follow-up

The patients in this study were mainly followed-up through telephone and in-hospital medical records, from the day patients received the first pathological diagnosis till 2nd August, 2014 or the day of death. Follow-up included regular re-examination, recurrence and distant metastasis, and recurrence and eventual death were recorded. Recurrence was determined by obvious symptoms and the results of imaging examination and pathological diagnosis.

Tumor tissue wax paraffin section making and HE (hematoxylin-eosin) staining

Firstly, paraffin embedded tumor tissue was sliced into sections (3 μm), followed by HE staining. The detailed procedures were as follows. The sections were placed into a baking chamber and dried at 90°C. Then the sections were dewaxed using xylene twice, for 10 min each time. The sections were then put twice into absolute ethyl alcohol to remove xylene, one min each time. After being soaked in 95% ethyl alcohol for 30 s, sections were taken out and washed in tap water for 2 min. Then they were stained by improved Gill hematoxylin for 5 min. After being rinsed in tap water for 1 min, sections were put into 75% hydrochloric acid alcohol for differentiation for 10 s and the color of tissues developed from blue to red. Then they were put into tap water for 30 min to turn back to blue. They were stained by acidifying eosin-ethyl alcohol solution for 1-2 min, sections were dehydrated with 95% ethyl alcohol twice, for 30 s each time, and then with absolute ethyl alcohol twice, for 30 s each time. After that, sections were transparentized using xylene twice, for 1 min each time. Finally, sections sealed by neutral balsam and cover glass, were observed under the microscope. It was found that, cell nucleus was blue black and endochylema was light red.

Immumohistochemical analysis

Tumor tissues embedded in a paraffin block were sliced into 3.0 μm sections. Then the sections were put into an oven, dried at 60°C for more than 1 h, and stained by PV two-step method. Tissues that showed positive were taken as positive control and PBS was taken for negative control replacing primary antibody. The procedures were as follows: sections were firstly dewaxed and washed in phosphate buffered solution (PBS) (PH7.4) three times, for 3 min each time. The next step was repairing antigen with citrate buffer solution under high temperature and pressure. Dewaxed sections placed on a heat resisting section frame were put into a pressure cooker loaded with 0.01 M (PH6.0) citrate buffer solution and were

boiled and heated until steam came out. Two min later, the pressure cooker was removed from heat source and cooled with water. Sections taken out were put into a wet box and then washed in PBS three times, for 3 min each time. After adding 1 drop or 50 µl 3% H_2O_2, sections were incubated at room temperature for ten minutes. Then sections were washed in PBS times, for 3 min each time. PBS was removed after the tissues were surrounded by oil pike. 50 µl primary antibody was then added to each section and preserved at 4°C overnight. The next day, sections were taken out, rewarmed for 10 min and washed in PBS (three times, for 3 min each time). After PBS was removed, every section was added with 100 µl fresh diaminobenzidine (DAB) for color development for 3 min to 10 min. Positive sections were observed to be brown or red under microscope. After being washed in tap water, sections were redyed by hematoxylin for 3 to 4 min. The color returned to blue after being washed in PBS. Sections were sealed by neutral gum after being dehydrated by ethyl alcohol and transparentized by xylene.

Detection of parameters of cell nucleus

Tumor tissue sections stained by HE were magnified under BA600-4 fully automatic digital scanning microscope and every section was photographed in five views. Image-Pro Plus 6.0 was used to circle 50 tumor nucleuses from each case after measurement scale correction and selection of measurement parameters were completed. Then area, diameter, perimeter, major and minor axis and circular degree of nucleus were measured. After that, measurement data were collected by data collector and preserved.

Result determination

ER and PR expression were considered to be positive when brown particles showed in the nucleus. If the amount of tumor cells with positive nucleus was 1% or over, the case was considered to have positive expression of ER and PR; otherwise, ER and PR expressed negatively. Once cell membrane was found to be clear brown, HER-2 was regarded as positive. Specifically, HER-2 (-) referred to non-dyeing or incomplete and weak staining in cell membrane of less than 10% tumor cells; when more than 10% tumor cells showed incomplete and weak staining in cell membrane, the case was confirmed to have HER-2(+); if more than 10% tumor cells presented incomplete and/or weak and moderate staining, or 10% or less tumor cells performed strong and complete staining, the case was confirmed to have HER-2(++) after redetermination by HER-2 gene amplification; and HER-2(+++) meant more than 10% tumor cells showing strong, complete and even staining, which was also regarded as HER-2 over-expression.

Histological grading of breast cancer

Modified Broom-Richardson histological grading scheme was used, as shown in Table I. Indexes of glandular tube formation scale, nuclear pleomorphism and mitotic count were scored for one to three points. Then breast cancer was histologically graded into level I, II and III according to the sum of the scores. Level I is high differentiation type (3 ~ 5 points); level II is medium differentiation type (6 ~ 7 points); and level III is low differentiation type (8 ~ 9 points).

Statistical analysis

SPSS 19.0 was used in data analysis. Nuclear parameters were presented as mean ± SD. T test was used to analyze average tumor diameter, patients' age and lymph node metastasis of luminal B, luminal A, HER2 over-expression and basal-like subtype breast cancer, while chi-square test (χ^2 test) and Fisher were used to study pathological features and metastasis of liminal B and other types of breast cancer. Also, survival rate was analyzed by Kaplan-Meier and disease-free survival curve and overall survival curve were drawn-up with the help of log-rank detection. If $P<0.05$, the difference was considered as statistically significant.

RESULTS

Results of follow-up

Of the 354 patients (aged from 25 to 86 years) diagnosed with breast cancer, 52 died and 302 survived during 1~65 months (36.3±14.6) of follow-up.

Breast cancer typing

Based on immunohistochemical results, the 354 breast cancer cases were divided into 4 types, i.e., 122 cases (34.5%) of luminal A with ER+ (Fig. 1), PR+ (Fig. 2) and HER2-, 113 cases (31.8%) of luminal B with ER+, PR+ and HER2+, 61 cases (17.2%) of HER2 over-expression with ER-, PR- and HER2+++ (Fig. 3), and 58 cases (16.5%) of basal-like subtype with ER-, PR- and HER2-.

Quantitative parameters of nucleus morphology in breast cancer cells

Assessment results of breast cancer suggested that except for insignificantly different axial ratio and roundness, nucleus area, diameter and perimeter had remarkable differences. Furthermore, the differences of quantitative parameters of nucleus morphology were obvious between cases with ER+/PR+ and

Table I. *Modified Broom-Richardson histological grading.*

Histological grade	Level I	Level II	Level III
Glandular tube formation scale	> 75.4%	10.2% ~ 75.4%	< 10.2%
Nuclear pleomorphism	Small and regular nucleus (8~9 μm)	Large but regular nucleus (10 ~16 μm)	Large, irregular and obvious nucleus (>16 μm)
Mitotic count*	≤ 5	6 ~ 10	≥ 11

** the amount of mitotic figures in 10 high power field (40 ×)*

Table II. *Quantitative comparison of nucleus morphology among breast cancer cells.*

Groups	n	Area	Perimeter	Diameter	Axial ratio	Roundness
Control	20	20.86±3.04*	12.90±1.04*	4.54±0.56*	1.19±0.15	0.99±0.01
luminal A	122	53.60±16.17*	25.54±4.33*	7.89±1.30*	1.29±0.17	1.00±0.01
luminal B	113	60.20±21.60*	27.03±5.12*	8.33±1.43*	1.30±0.47	1.01±0.06
HER2 over-expression	61	83.02±23.90*	31.98±4.55*	9.86±1.39*	1.29±0.17	1.01±0.03
basal-like	58	90.65±46.17*	33.17±6.85*	10.20±2.12*	1.32±0.20	1.02±0.03

(Mean±SD, μm)

Table III. *Immunohistochemical typing and clinically pathological features of 354 breast cancer cases.*

Pathological Parameters in Clinic	Overall Cases (n=354)	Luminal A (n=122)	Luminal B (n=113)	HER 2+++ (n=61)	Basal-like (n=58)
Mean age (year)	51.3±11.7	50.0±11.8	49.9±10.9	53.7±12.2	50.9±11.9
Menstruation					
Pre-menopause	176 (49.7%)	71 (58.2%)	63 (53.4%)	19 (31.1%)	23 (33.3%)
Climacteric	20 (6%)	10 (8.2%)	2 (1.6%)	3 (5.0%)	5 (7.2%)
Post-menopause	158 (44.3%)	41 (35.6%)	48 (45.0%)	39 (63.9%)	30 (59.5%)
Tumor size (cm)	3.3±1.7	3.1±1.4	3.2±1.6	3.7±2.1	3.5±1.8
Positive lymph node (n)					
0	204 (52.6%)	64 (50.7%)	54 (50.4%)	31 (50.8%)	32 (61.4%)
1-3	96 (24.7%)	22 (29.0%)	32 (26.9%)	10 (16.4%)	14 (20.0%)
4-9	32 (15.2%)	25 (13.8%)	16 (16.0%)	11 (18.0%)	10 (14.3%)
≥10	22 (7.5%)	11 (6.5%)	11 (6.7%)	9 (14.8%)	2 (4.3%)
Histological stage					
1	57 (14.7%)	33 (24.0%)	19 (16.0%)	3 (4.9%)	2 (2.9%)
2	172 (44.3%)	78 (56.5%)	64 (53.8%)	17 (27.9%)	13 (18.6%)
3	125 (41.0%)	11 (19.5%)	30 (30.2%)	41 (67.2%)	43 (78.5%)
TNM					
I	53 (13.7%)	22 (16.0%)	15 (12.6%)	5 (8.2%)	11 (15.7%)
II	184 (57.7%)	79 (57.2%)	71 (59.7%)	34 (55.7%)	26 (57.1%)
III	99 (25.5%)	19 (25.3%)	23 (24.4%)	19 (31.1%)	12 (22.9%)
IV	18 (3.1%)	2 (1.5%)	4 (3.3%)	3 (5.0%)	9 (4.3%)
Death cases (n)	76 (19.6%)	15 (10.9%)	21 (17.6%)	18 (29.5%)	22 (31.4%)

Table IV. *Local recurrence and distant metastasis of breast cancer.*

Location of recurrence and metastasis	Luminal B (n=27)	Luminal A (n=19)	HER2 over-expression (n=21)	Basal-like (n=24)
Local and lymphoglandulae supraclaviculares	2(7.4%)	2(10.5%)	3(14.3%)	1(4.2%)
Lung and pleura	8(29.6%)	5(26.3%)	16(76.2%)	12(50.0%)
Bone	10(37.0%)	9(47.4%)	14(66.7%)	11(45.8%)
Liver	4(14.8%)	7(36.8%)	7(33.3%)	2(8.3%)
Brain	2(7.4%)	2(10.5%)	8(38.1%)	4(19.0%)
Stomach	0(0.0%)	0(0.0%)	2(9.5%)	0(0.0%)
Ovary and uterus	1(3.7%)	1(5.3%)	1(4.8%)	0(0.0%)

Table V. *Comparison of DFS and OS of patients with different subtypes of breast cancer.*

Molecular subtypes of breast cancer	Average DFS/ month	Death rate/%
luminal B subtype	43.6	17.6
luminal A subtype	45.8	10.9
HER2 over-expression subtype	34.7	29.5
Basal-like subtype	30.1	31.4

cases with ER-/PR- ($P<0.05$). A basal-like subtype was observed with the greatest parameter values, and luminal A the smallest; and values of luminal B was between subtype of luminal A and HER2 over-expression ($P<0.05$, Table II).

Correlation between breast cancer subtypes and clinically pathological features

As shown in Table III, pathological features were found to vary notably between the four subtypes of breast cancer.

Local recurrence and distant metastasis of breast cancer

In this study, 91 out of 354 cases (23.5%) were detected with local recurrence (on surgery wounds, ipsilateral chest wall and contralateral breast) or distant metastasis. Specifically, 27 cases (22.7%) out of 113 luminal B cases developed recurrence and metastasis, and in basal-like subtype group, luminal A subtype group and HER2 over-expression group, 18 out of 58 cases (34.3%), 19 out of 122 luminal A cases (13.7%), and 21 out of 61 HER2 over-expression cases (34.4%), respectively. Compared to 76.2% (16 cases) metastasis rate of lung and pleura in HER2 over-expression subtype group, luminal A group (5 cases) and luminal B subtype group (8 cases) were observed with much lower metastasis rate ($\chi^2=8.79$, $P<0.05$; $\chi^2=3.27$, $P<0.05$). However, no statistical difference of metastasis rate was observed between HER2 over-expression subtype group and basal-like subtype group (12 cases) ($\chi^2=3.27$, $P>0.05$). Moreover, 2 out of 27 luminal B cases developed brain metastasis, with the lowest rate of 7.4%, which was much lower than the rate in HER2 over-expression subtype group (8 cases) ($\chi^2=5.01$, $P<0.05$). However, no statistical difference was observed between luminal B and luminal A or basal-like subtype ($P>0.05$) (Table IV).

Disease-free survival (DFS), overall survival (OS) and death rate of breast cancer

According to experimental observations and follow-up outcomes, the average value of disease-free survival (DFS) in luminal B was 46.3 months, luminal A was 45.8 months, HER2 over-expression

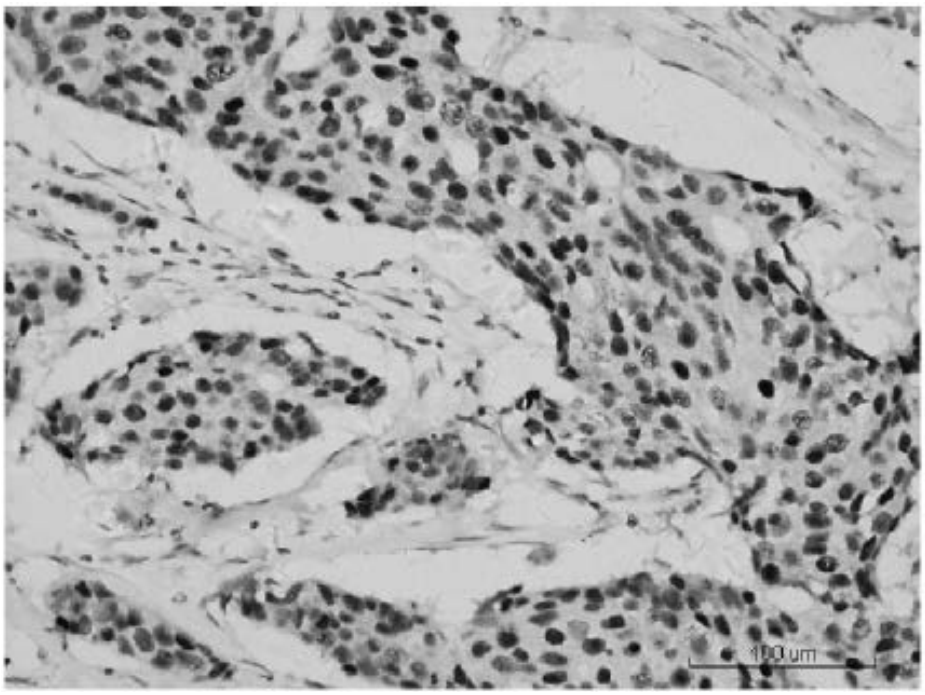

Fig. 1. *ER expression in invasive breast cancer: + (IHC) ×200.*

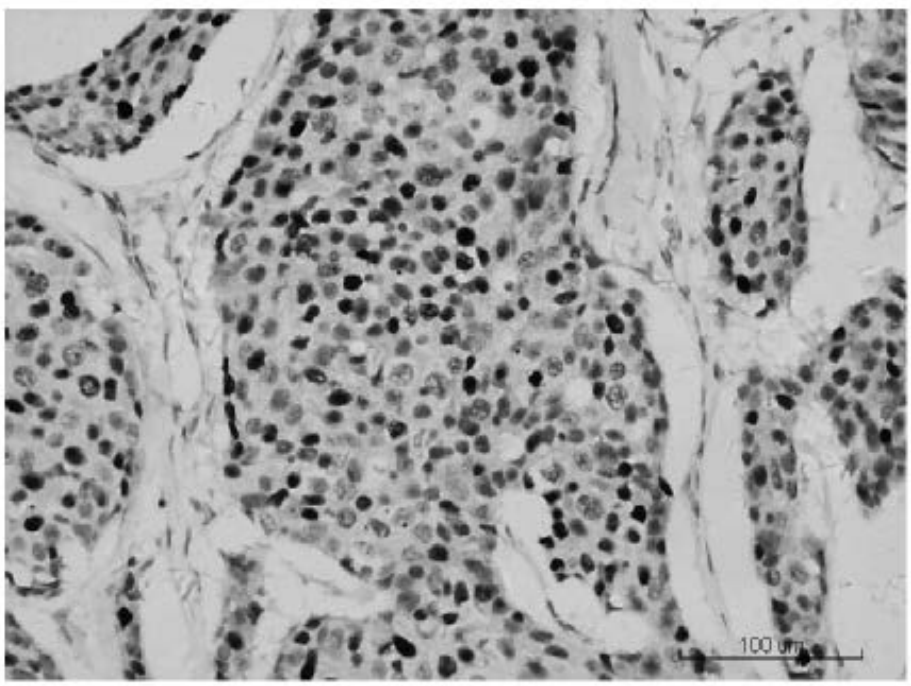

Fig. 2. *PR expression in invasive breast cancer: + (IHC) ×200.*

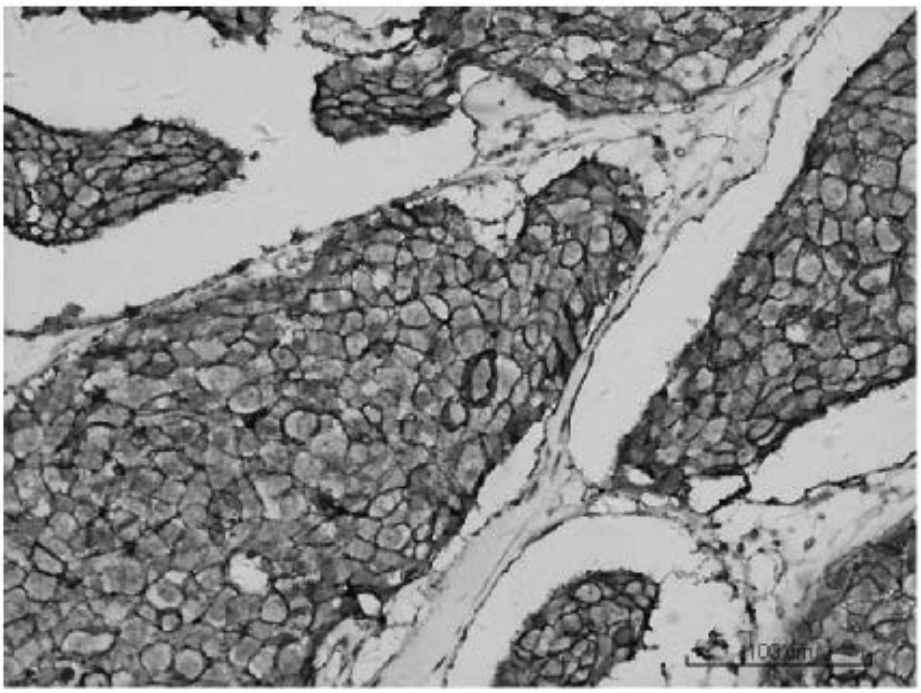

Fig. 3. *HER-2 expression in invasive breast cancer: +++(IHC) ×200*

was 34.7 months and basal-like subtype was 30.1 months. Besides, DFS and overall survival OS in luminal B subtype group was longer than in basal-like subtype group (χ^2 = 10.91, P< 0.05) and HER2 over-expression group (χ^2 = 8.72, P < 0.05), but was not statistically different with that in luminal A subtype (P>0.05).

A total of 76 cases died due to local recurrence or distant metastasis, including 21 luminal B cases (17.6%), 15 luminal A cases (10.9%), 18 HER2 over-expression (29.5%) and 22 basal-like subtype (31.4%), with basal-like subtype having the highest death rate. It was seen that the death rate of luminal B was lower than basal-like subtype (χ^2=4.76 and P<0.05). In addition, luminal B was found with no statistical difference with luminal A and HER2 over-expression (P>0.05) (Table V).

DISCUSSION

Following studies on breast cancer in the past decades (7), histo-morphological typing is considered as the most significant. With the continuing studies on tumor morphology, this aspect is being constantly updated and perfected. Perou et al. (8) proposed to classify breast cancer based on molecular level in 2000. Since then, luminal breast cancer has gradually evolved as the hotspot of clinical and pathological studies on breast cancer because of its targeted therapy and diverse prognosis. To date, accepted molecular types of breast cancer include luminal A, luminal B, HER2 over-expression and basal-like subtype (9). In the latest studies, Geyer et al. (10) stated that, breast cancer with positive ER is the common subtype of invasive breast cancer; breast cancer with high expressed ER gene and PR gene show significant difference in endocrinotherapy, chemotherapy, recurrence risk and prognosis.

To study the characteristics of breast cancer molecular sub-type, Yuan et al. (11) divided 1,280 patients into basal-like subtype (20.9%), HER2 over-expression subtype (23.2%) and luminal subtype (55.9%) on the basis of immunohistochemical results of ER, PR and HER2. Patients with luminal subtype were found to be older, 97.1% of whom were aged over 35 years; they were confirmed at an early stage, and 20.4% were in stage I. In this study, luminal B breast cancer occupied 30.7% (113/354) and histological

stage II dominated, which was in accordance with the literature. Besides luminal B, luminal A accounted for 35.6% (122/354), HER2 over-expression for 15.7% (61/354) and basal-like subtype for 18.0% (58/354). The low proportion of patients with luminal A was thought to be correlated with the subjective selection of patients with follow-up information.

Breast cancer prognosis is always the bottleneck of treatment. In the 46-month follow up of patents with breast cancer, Yuan et al. (11) found that recurrence and metastasis rate of basal-like subtype, HER2 over-expression, luminal subtypes was 25%, 27.9% and 11.7%, respectively. Statistical analysis suggested that, patients with luminal subtype had lower recurrence and metastasis rate than basal-like and HER2 subtypes ($P<0.01$), and no statistical significance of recurrence and metastasis rate was observed between basal-like subtype and HER2 over-expression subtype, but 13.4% of patients with basal-like subtype were detected with lung metastasis ($P=0.017$). In this study, DFS of luminal B, Luminal A, HER2 over-expression and basal-like subtype was 43.6 months, 45.8 months, 34.7 months and 30.1 months, respectively. Compared to basal-like subtype and HER2 over-expression subtype, DFS and OS of luminal B were longer ($\chi^2=10.91$, $P<0.05$; $\chi^2=8.72$ and $P<0.05$); moreover, there was no significant statistical difference in DFS and OS between luminal A and luminal B ($P>0.05$).

Immunohistochemical results of ER, PR, HER2 and Ki-67 are the major immunohistochemical mark for diagnosing luminal breast cancer and also the important basis for determining prognosis and treatment means. Thus standardization detection and correct assessment of ER, PR, HER2 and Ki-67 are of great clinical significance; however, recognized assessment criteria are still lacking. Few ER-/PR+ cases are observed in clinicopathologic examinations, and the expression of ER/PR is requires better specification; for patients with recurrence or metastasis, tests are also required to confirm the expression of ER/PR, to determine any immunophenotype changes. However, there is a lack of evidence-based studies. To date, there is no recognized assessment guide for Ki-67 proliferation index detection in breast cancer. The critical value of Ki-67 proliferation index for distinguishing breast cancer is not unified in studies, and moreover the repeatability of such experiments is difficult. The above are the problems existing in breast cancer treatment of the different subtypes, which require further studies.

Breast cancer is a disease with high heterogeneity at molecular level, that is to say, tumors with the same histological morphology tend to have different changes of molecular genetics (12). We studied 4 molecular sub-types of breast cancer, i.e. luminal A, luminal B, HER2 over-expression and basal-like with no statistical differences of pathological features including age, tumor size, lymph node metastasis and clinical stage. Among the four sub-types, luminal B has poorer prognosis and higher risk of differentiation, compared to luminal A, but performs better in comparison with HER2 over-expression and basal-like subtype. Furthermore, breast cancer without ER and PR expression is observed with greater quantity parameters of nucleus, which is more likely to develop recurrence and metastasis. Therefore, besides expression of hormone receptor and epidermal growth factor receptor, quantitative changes of nucleus morphology are important in breast cancer prognosis, offering vital reference values.

REFERENCES

1. Oh E, Choi Y L, Park T, Lee SY, Nam SJ, Shin YK. A prognostic model for lymphnode-negative breast cancer patients based on the integration of proliferation and immunity. Breast Cancer Res Treat 2012; 132(2):499 -509.
2. Xie YT. Detection and clinical application of gene mutation of familial breast cancer BRCA1, 2. Chin J Prac Surg 2013; 33(3):233-35.
3. Xia HQ, He JR. Expression of Ki-67, EGFR, HER-2 and p53 protein in human breast cancer and their correlation. Chin Clin Oncol 2011; 16(2):139-42.
4. Mou P, Li HY. Advances of neoadjuvant chemotherapy in breast cancer. Chin J Bases Clin Gen Surg 2011; 18(9):1011-16.
5. Gabos Z, Thoms J, Ghosh S, Hanson J, Deschênes J, Sabri S, Abdulkarim B. The association between biological subtype and locoregional recurrence in newly diagnosed breast cancer. Breast Cancer Res Treat 2010; 124(1):187-94.

6. Chen B, Xue MX, Ye CM, Huang ZM, Wang R, Zhao S. Value of different molecular types of breast cancer in prediction of axillary lymph node metastasis. Mod J Integr ChinTrad West Med 2011; 20(009):1100-1.
7. Dabbs DJ, Klein ME, Mohsin SK, Tubbs RR, Shuai Y, Bhargava R. High false-negative rate of HER2 quantitative reverse transcription polymerase chain reaction of the oncotype DX test: an independent quality assurance study. J Clin Oncol 2011; 29(32):4279 -85.
8. Perou CM, Sorlie T, Eisen MB, et al. Molecular portraits of human breast tumors. Nature 2000; 406(6797):747-52.
9. Guiu S, Michiels S, Andre F, et al. Molecular subclasses of breast cancer: how do we define them? The IMPAKT 2012 working group statement. Ann Oncol 2012;23(12):2997-3006.
10. Geyer FC, Rodrigues DN, Weigelt B, et al. Molecular classification of estrogen receptor-positive / luminal breast cancers. Adv Anat Pathol 2012, 19(1):39-53.
11. Yuan ZY, Wang SS, Zhu MQ, Zheng L, Luo WB, Zhou ZM, Guan ZZ. Clinical features and prognosis analysis of different breast cancer molecular subtypes. Chin J Oncol 2008; 30(6):456.
12. Bianchini G, Qi Y, Alvarez RH, et al. Molecular anatomy of breast cancer stroma and its prognostic value in estrogen receptor-positive and negative cancers. Clin Oncol 2010; 28 (28):4316-23.

EFFECT OF SEASONAL CHANGES ON TESTICULAR MORPHOLOGY AND THE EXPRESSION OF CIRCADIAN CLOCK GENES IN JAPANESE WOOD MICE (*APODEMUS SPECIOSUS*)

M. AKIYAMA[1], S. TAKINO[1], Y. SUGANO[1], T. YAMADA[1], A. NAKATA[2], T. MIURA[3], M. FUKUMOTO[4] and H. YAMASHIRO[1]

[1]Faculty of Agriculture, Niigata University, Niigata, Japan; [2]Division of Life Science, Hokkaido Pharmaceutical University School of Pharmacy, Hokkaido, Japan; [3]Graduate School of Health Sciences, Hirosaki University, Aomori, Japan; [4]Institute of Development, Aging and Cancer, Tohoku University, Miyagi, Japan

Received March 17, 2015 – Accepted June 18, 2015

This study aimed to determine the seasonality of reproduction throughout the year in Japanese wood mice (*Apodemus speciosus*). The effect of seasonal changes on testicular morphology and the periodic expression of circadian clock genes in the hypothalamus and testes of male individuals was evaluated. We also examined the morphology of the testes and caudae epididymides of male mice. In addition, RT-PCR analysis was carried out with mRNA extracted from the hypothalamus and testes to evaluate the expression of the circadian clock genes *Clock*, *Bmal1*, *Per1*, and *Cry1*. The complete induction of testicular activity was detected from February to April and from August to October, with testes weight increasing with the completion of spermatogenesis (reproductive season). From May to early June and from November to early January, testicular weight declined, the seminiferous tubules reduced in size, spermatogenesis was arrested, and sperm were not produced (non-reproductive season). From mid-June to July and mid-January, the re-induction of testicular activity for spermatogenesis was observed in the seminiferous tubules (transitional season). Out of the four examined genes, *Cry1* had the highest expression level in both the hypothalamus and testes throughout the year, followed by *Bmal1*, *Per1,* and *Clock*. The expression of *Bmal1* was significantly lower in the hypothalamus and testes during the transitional season compared to the reproductive and non-reproductive seasons. *Cry1* transcript levels were also significantly lower in the hypothalamus and testes during the transitional season compared to the reproductive season. In conclusion, the results indicating changes in testicular morphology revealed annual reproductive, non-reproductive, and transmission periods in Japanese wood mice. When an increase in testicular activity was observed indicating the onset of the reproductive season, the mean day length was approximately 11–13 h. The expression of the circadian clock genes *Bmal1* and *Cry1* in the hypothalamus and testes during the reproductive season was significantly higher than that of the same genes during the transitional season. Consequently, completion of spermatogenesis occurred in the seminiferous tubules of Japanese wood mice testes during the reproductive period.

Key words: Apodemus speciosus, circadian clock gene, season, spermatogenesis, testis

Mailing address: Dr Hideaki Yamashiro,
Laboratory of Animal Reproduction,
Faculty of Agriculture,
Niigata University, 8050 Ikarashi Ninocho Nishiku,
Niigata, 950-2181, Japan
Tel.: +25 262 6596 Fax: +25 262 6596
e-mail: hyamashiro@agr.niigata-u.ac.jp

0393-974X (2015)

The rodent genus *Peromyscus*, the members of which are commonly referred to as deer mice, white-footed mice, or field mice, consists of the most abundant group of native and wild North American mammals (1, 2). However, limited information is available regarding the genetic changes that lead to the behavioural and physiological adaptations of species belonging to this genus in response to the environment, such as photoperiod, seasonal breeding cycles, and circadian period. The reproductive patterns of certain animals in the wild have been extensively documented; hence, *Peromyscus* presents an attractive option for further experimental studies (3, 4). The *Peromyscus* Genetic Stock Centre provides a reliable source of these animals and other related materials to the scientific community (web page; stkctr.biol.sc.edu). Laboratory stocks of both wild-type and genetically variant *Peromyscus* spp. have been used for various studies (5-7). However, even though the wood mice genus *Apodemus* is the most common wild small mammal in Japan, it has not been studied extensively to date. Moreover, to the best of our knowledge, no such mammalian systems, which may be utilized for laboratory-based studies, are available for assessing the effects of wild genetic variation on the reproductive biology, physiology, and endocrinology of this genus.

Many mammals that are seasonal breeders respond to seasonal changes by adjusting their physiology and behaviour in anticipation of seasonal changes (8). The change in day length is the major proximate environmental cue for the accurate seasonal timing of reproduction, while changes in photoperiod drive the development of distinct seasonal reproductive phenotypes (9). These changes may lead to the switching on and off of reproductive functions, including spermatogenesis and oogenesis, during the seasonal breeding cycle. Moreover, a definitive process or regulator of seasonal reproductive cycles has not been identified to date from non-seasonal laboratory strains of mice. A small scale study has been conducted to investigate the seasonality of reproduction during the breeding season and non-breeding season (10), but no detailed analysis has been conducted on the effect of annual seasonal changes on testicular morphology in wild Japanese wood mice (*Apodemus speciosus*).

Circadian rhythms are approximate 24-h biological cycles that function to prepare an organism for daily environmental changes (11). These cycles are controlled by the suprachiasmatic nucleus (SCN) of hypothalamus and subsidiary clock (12-14). Circadian rhythms are driven by the molecular clock, which is a transcriptional:translational feedback mechanism that, in mammals, involves the core clock genes, including *Clock* (*circadian locomotor output cycles kaput*), *Bmal* (*brain and muscle ARNT-like protein 1*), *Period* (*Per1*, *Per2*), and *Cryptochrome* (*Cry1*, *Cry2*) (15, 16). The circadian clock is a universal cellular mechanism that underlies diverse rhythmic functions in organisms, and its molecular mechanism have been well researched (17, 18). The circadian clock is known to influence reproduction in many organisms (19). Most mammals that exhibit a seasonal cycle are able to perceive daily changes in light throughout the year, which influence hormonal signals that regulate reproductive cycles (20, 21). A recent study has shown that prolonged entrainment to light and dark cycles that are slightly longer or shorter than 24 h may result in the altered transcription of the SCN in the hypothalamus, with DNA methylation in the SCN correlating with photoperiodical changes (22). Thus, seasonal photoperiod changes might control circadian gene expression, and, thus, be a key stimulation factor for the adaptation of the reproductive season in wild animals. However, there have been no reports on the influence of seasonal photoperiod changes on the circadian gene expression and associated reproductive physiology of wild Japanese wood mice.

This study aimed to determine the seasonality of reproduction throughout the year for Japanese wood mice. We investigated the effect of seasonal photoperiod changes on testicular morphology, and we evaluated the expression of circadian genes *Clock*, *Bmal1, Per1*, and *Cry1* in the hypothalamus and testes of male individuals.

MATERIALS AND METHODS

Animals

The principles of laboratory animal care were followed during this study, and all procedures were conducted in accordance with the guidelines provided by the Ethics Committee for Care and Use of Laboratory Animals for Research of the Niigata University, Japan. The capture of

wild rodents in the sampling area was permitted by the Niigata City Office.

Sampling of Japanese wood mice was carried out from March 2014 to February 2015, on the Kakuta Mountain in Niigata City, in Niigata Prefecture, Japan. The monthly mean of daylight hours and temperature in this region are shown in Table I. Calendar-based seasons were considered: winter (December to February), spring (March to June), summer (July to August), and autumn (September to November). Individuals of the Japanese wood mice were captured using Sherman-type live traps baited with peanuts (Fig. 1A). Thirty-three Japanese wood male mice were caught during the year (Table II). Captured mice were euthanized by cervical dislocation. The body of each mouse was weighed, and testicular length was measured with a micrometer. The testes and caudae epididymides from mice were fixed in Bouin's solution. To extract total RNA, the testis and hypothalamus were excised in liquid nitrogen and stored at -80°C. Since the captured animals were wild, several variables could not be controlled, even within the same months, such as age, weight, nutritional status; however, some of these variables, such as nutrition, may interfere with the reproductive status of individuals.

Morphological assessment of testes and caudae epididymides

Fixed testes and caudae epididymides were embedded in paraffin, and were then stained using hematoxylin and eosin (HE) according to standard protocols (23). The testes were then briefly dehydrated in a series of different concentrations of alcohol, made transparent by using toluene, embedded in paraffin, and cut into 5-µm-thick sections before staining.

Reverse transcriptase-polymerase chain reaction (RT-PCR) of circadian gene expression

Total RNA was extracted from the hypothalamus and testes of Japanese wood male mice according to

Table I. *Environmental characteristics per month across the year.*

	Mar. 2014	Apr.	May	Jun.	Jul.	Aug.	Sep.	Oct.	Nov.	Dec.	Jan. 2015	Feb.
Mean of day length hours (h)	11.6	13.1	14.1	14.4	14.3	13.3	12.3	11.1	10.1	9.4	9.5	10.5
Mean of day temperature (C°)	6.1	11.1	17.1	22.0	24.9	26.1	21.6	16.0	11.1	3.4	3.1	3.9

Table II. *Body weight of each Japanese wood mouse caught throughout the year.*

Sample No.	Sampling date	Weight (g)	Sample No.	Sampling date	Weight (g)
1	4 Mar. 2014	35.7	18	6 Oct. 2014	44.3
2	3 Apr. 2014	38.4	19	8 Oct.2014	49.2
3	3 Apr. 2014	46.4	20	8 Oct.2014	47.5
4	8 May. 2014	30.6	21	8 Nov. 2014	46.0
5	8 May. 2014	35.0	22	8 Nov. 2014	35.0
6	9 May 2014	31.7	23	8 Dec.2014	41.7
7	2 Jun. 2014	43.8	24	8 Dec.2014	49.6
8	2 Jun. 2014	54.2	25	8 Dec.2014	30.7
9	11 Jun. 2014	44.9	26	7 Jan. 2015	30.3
10	7 Jul. 2014	52.1	27	7 Jan. 2015	26.6
11	7 Jul. 2014	48.0	28	15 Jan. 2015	43.8
12	7 Aug. 2014	49.9	29	16 Jan. 2015	47.0
13	7 Aug. 2014	56.4	30	16 Jan. 2015	36.4
14	2 Sep. 2014	44.9	31	16 Jan. 2015	41.0
15	5 Sep. 2014	50.9	32	4 Feb. 2015	41.4
16	5 Sep. 2014	51.2	33	4 Feb. 2015	43.8
17	5 Sep. 2014	47.5			

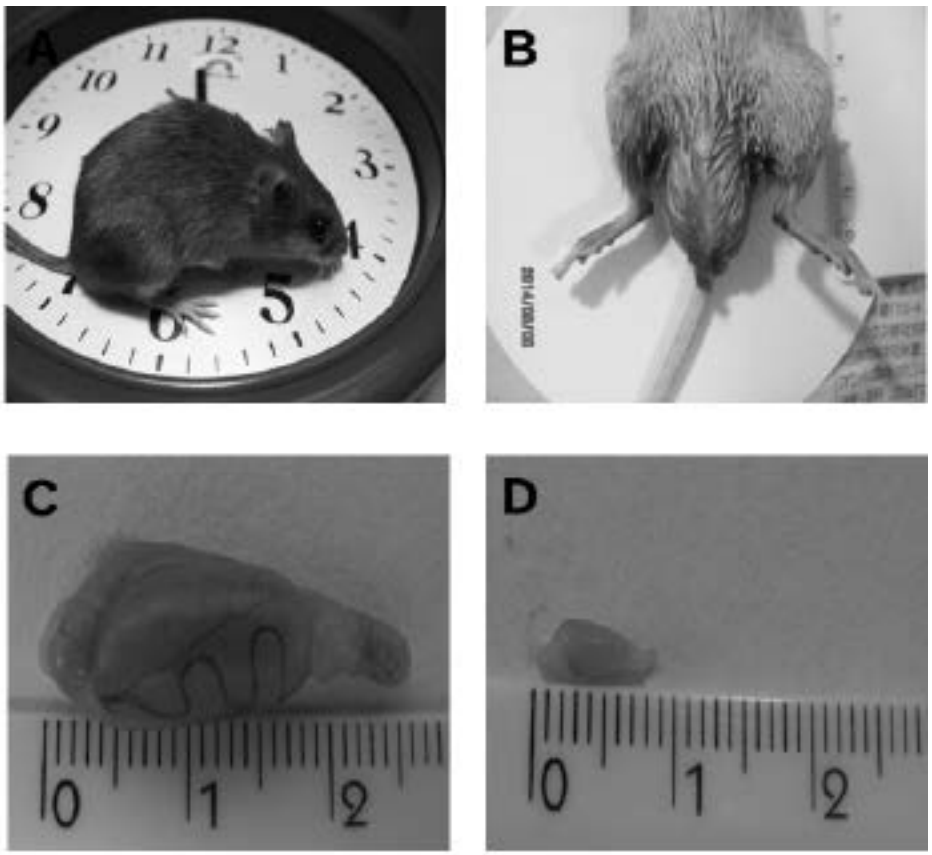

Fig. 1. *Testes of Japanese wood mice in the reproductive and non-reproductive season. **A**) Japanese wood mice, (**B**) descent of testis, (**C**) testis during the reproductive season, (**D**) testis during the non-reproductive season.*

the manufacturer's instructions using RNeasy Mini Kit (Qiagen, Hilden, Germany). All RNA extracts were stored at -80°C until further processing. Reverse transcription (RT) of RNA to generate complementary DNA (cDNA) was performed using the PrimeScript RT-PCR Kit according to the manufacturer's instructions (Takata, Shiga, Japan). Polymerase chain reaction (PCR) was performed using 0.5 μL of Ex Taq Hot Start polymerase (Takara, Shiga). The reaction mixtures contained 5 μL of cDNA, 2 μL of 10 mM dNTP Mixture, 0.5 μL of 10 μM of each primer (GAPDH-F,5′-ACCACAGTCCATGCCATCAC-3′,GAPDH-R, 5′-TCCACCACCCTGTTGCTGTA-3′), (Bmal1-F,5′-GCAGTGCCACTGACTACCAAGA-3′,Bmal1-R, 5′-TCCTGGACATTGCATTGCAT-3′), (Cry1-F,5′-CCCAGGCTTTTCAAGGAATGGAACA-3′,Cry1-R, 5′-TCTCATCATGGTCATCAGACAGAGG-3′), (Per1-F,5′-TTCAAGCTCTCAGGACTCTG-3′,Per1-R, 5′-GGCAGTTTCCTATTGGTTGG-3′), 2 μL of 10 μM of each primer (Clock-F,5′-CCTATCCTACCTTGGCCACACA-3′,Clock-R, 5′-TCCCGTGGAGCAACCTAGAT-3′) (24), 5 μL of 10 × PCR Buffer II, and RNase free water up to 50 μL, and the mixtures were subjected to the following PCR conditions: 45 cycles of 94°C for 30 s, 63°C for 30 s, and 72°C for 60 s, plus a final extension step at 72°C for 5 min. The samples were loaded on a 1% agarose gel.

Statistical analysis

All data were expressed as the mean ± standard deviation (SD). The data presented in Fig. 6B was subjected to one-way analysis of variance (ANOVA) and Fisher protected least significant difference *post hoc* test using STATVIEW (Abacus Concepts Inc., Berkeley, CA). A P value of less than 0.05 indicated a statistical significance.

RESULTS

Body weights and lengths of testes

The body weights of male Japanese wood mice are shown in Table II. The average body weight

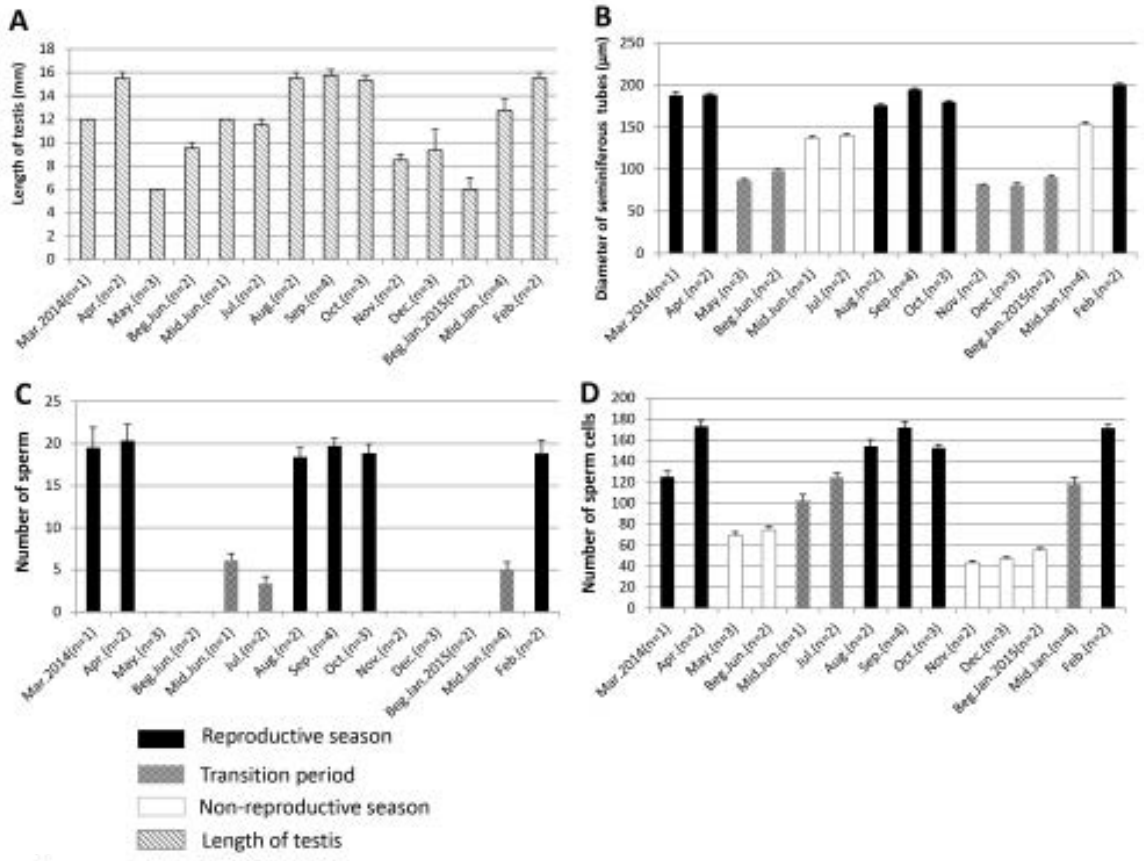

Fig. 2. *Seasonal changes in (**A**) length of testis, (**B**) diameter of seminiferous tubes, (**C**) number of sperm, (**D**) number of spermatogonia, spermatocytes, and spermatids of Japanese wood mice. Values are represented as the mean ± SD. The spermatogonia, spermatocytes, spermatids, and sperm that were counted were randomly chosen from ten seminiferous tubules (reproductive season) with diameters of 170 to 210* μm*, seminiferous tubules (transitional season) with diameters of 120 to 150* μm*, and seminiferous tubules (non-reproductive season) with diameters of 70 to 110* μm*, respectively.*

was 42.9±7.7 g. Fig. 1B shows the descent of testes of mice, while Fig. 1C and D show the differences in size. The seasonal changes affected testicular lengths; testicular length decreased between April (15 mm) and May (6 mm), whereas a gradual increase was observed between the beginning of June (9 mm) and August (15 mm) (Fig. 2A). From August to October, testicular length was maintained between 15 mm and 16 mm, and then decreased to 8 mm in November. From November to the beginning of January, testicular length was maintained between 6 and 9 mm. In mid-January, testicular length was approximately 12 mm, and reached 15 mm in February.

Histology of testes and caudae epididymides

Significant changes to the testes and caudae epidymides associated with seasonal cycles in Japanese wood mice were observed throughout the year (Fig. 2, 3, and 4). Three categories of seminiferous tubes were observed. The average diameter of the first category was approximately 190 mm, with spermatogonia, spermatocytes, spermatids, and sperm being present in the lumen (Fig. 2B, C and D, and Fig. 3A). The second category had an average diameter of 90 mm, with no sperm being detected in the lumen (Fig. 2B and C, and Fig. 3B). The third category had an average diameter of 150 mm, with few spermatogonia, spermatocytes, spermatids, and

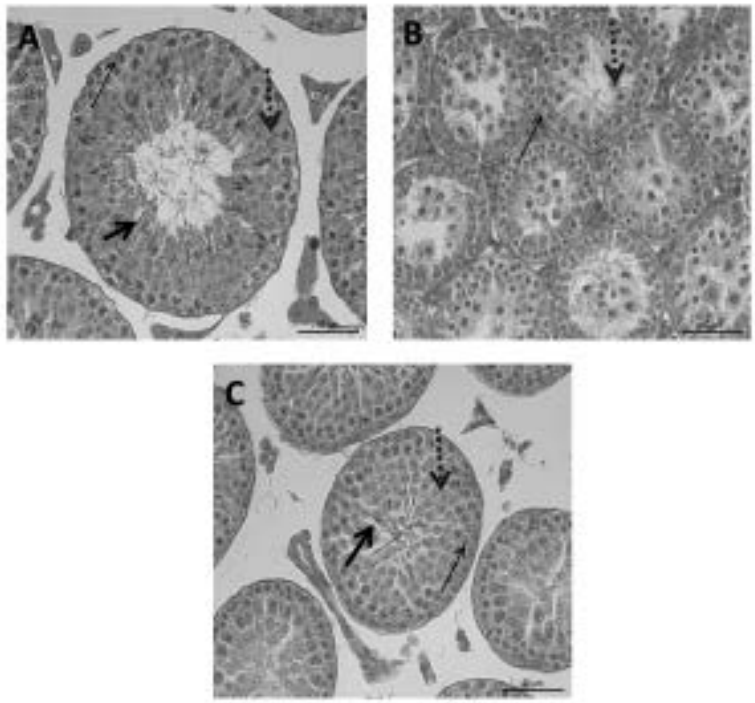

Fig. 3. *Photomicrographs of hematoxylin-eosin-stained sections of Japanese wood mice testes. **A**) Testis from the reproductive season; (**B**) testis from the non-reproductive season; (**C**) testis from the transitional season. 400×, Scale bar = 50 µm ➞Sperm; -----> Spermatocytes and spermatids; ——>Spermatogonia*

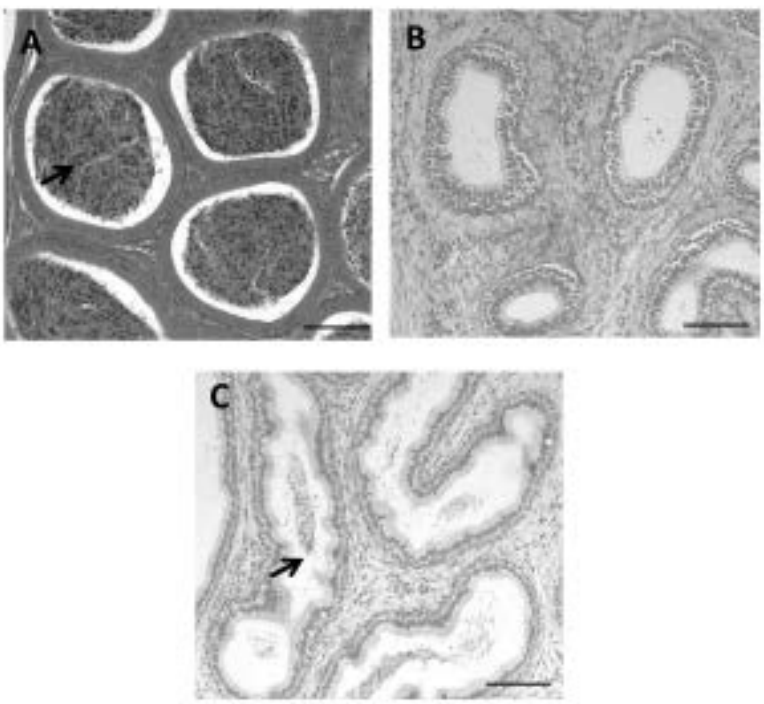

Fig. 4. *Photomicrographs of hematoxylin-eosin-stained sections of Japanese wood mice caudae epididymides. **A**) Caudae epididymides from the reproductive season, (B) caudae epididymides from the non-reproductive season, (C) caudae epididymides from the transitional season. 200×, Scale bar = 100 µm, ➞ Sperm*

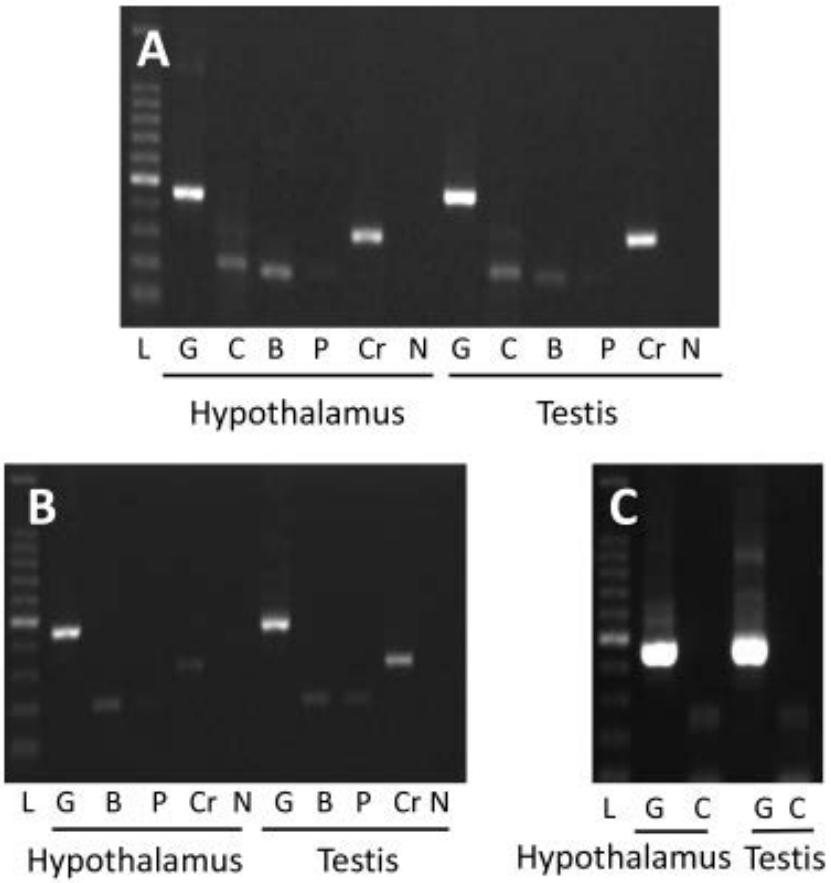

Fig. 5. *RT-PCR analysis of circadian gene expression in the hypothalamus and testis of B6D2F1 mice and Japanese wood mice.* ***A****) Bmal1, Per1, and Cry1 mRNA transcripts in the hypothalamus and testis of B6D2F1 mice.* ***B****) Bmal1, Per1, and Cry1 mRNA transcripts in the hypothalamus and testis of Japanese wood mice.* ***C****) Clock mRNA transcripts in the hypothalamus and testis of Japanese wood mice. GAPDH was amplified as an intrinsic control. L: Ladder, G: GAPDH; C: Clock, B: Bmal1; P: Per1, Cr: Cry1; N: Negative control.*

sperm being observed in the lumen (Fig. 2B–D, and Fig. 3C).

The weights and lengths of the testes were at a maximum from February to April, and August to October (reproductive season). In addition, during these periods, the seminiferous tubules were larger in diameter in comparison with the tubules during the other months, and spermatogonia, spermatocytes, spermatids, and sperm were present in the lumen. Moreover, during the active spermatogenesis season the caudae epididymides were full of sperm (Fig. 4A). From mid-June to July, and during mid-January, the spermatogenic cells consisted of few spermatogonial, spermatocytes, spermatid cells, and a few sperm in both the testes and caudae epididymides (Fig. 4C) (transitional season). From May to the beginning of June, and from November to mid-January, seminiferous tubule diameter was at its smallest, sperm could not be detected, and arrested spermatogenesis was observed in both the testes and caudae epididymides (non-reproductive season) (Fig. 4B). These results clearly indicate that seasonal changes affected the testes and epididymes of Japanese wood mice.

Seasonal circadian clock genes expression in the hypothalamus and testes

The highest year-round expression level in the

hypothalamus and testis (Fig. 5A–C) was obtained for *Cry1*, followed by *Bmal1*, *Per1,* and *Clock* (Fig. 6A). In the hypothalamus, there was no cycle in *Clock* expression. *Bmal1* mRNA transcript levels were lowest in February and increased tendency from April to mid-June. *Per1* expression was high at the beginning of June. The level of *Cry1* transcripts was lowest in February and peaked in October.

In the testes, *Clock* expression was quite low, even in the month with peak expression. Throughout the year, there seemed to be no variation in the expression of *Clock*, *Bmal1*, *Per1*, and *Cry1* in the testes for each month. *Per1* expression in the testes was maintained at a higher level than that of the same gene in the hypothalamus during the year except at the beginning of June.

We determined which circadian clock gene transcripts are expressed in each season (i.e. the reproductive, transitional, and non-reproductive seasons) in the hypothalamus and testes (Fig. 6B). *Clock* and *Per1* expression showed no cycling in either the hypothalamus or testes. The expression of *Bmal1* was significantly lower ($P < 0.05$) in the hypothalamus and testes in the transitional season compared to the reproductive and non-reproductive seasons. *Cry1* transcript levels were also significantly lower ($P < 0.05$) in the hypothalamus and testes in the transitional season compared to the reproductive season.

DISCUSSION

Precise seasonal timing of reproduction is a natural response, with seasonal timing requiring behavioural, neural, hormonal, and genomic plasticity (9). It is important to study seasonal variations in the reproduction of animals, such as mice, to understand their reproductive physiology (10). Such information is vital to understand the mechanisms of spermatogenesis and oogenesis. As part of our experiment, seasonal changes in the reproductive biology of Japanese wood mice were observed across

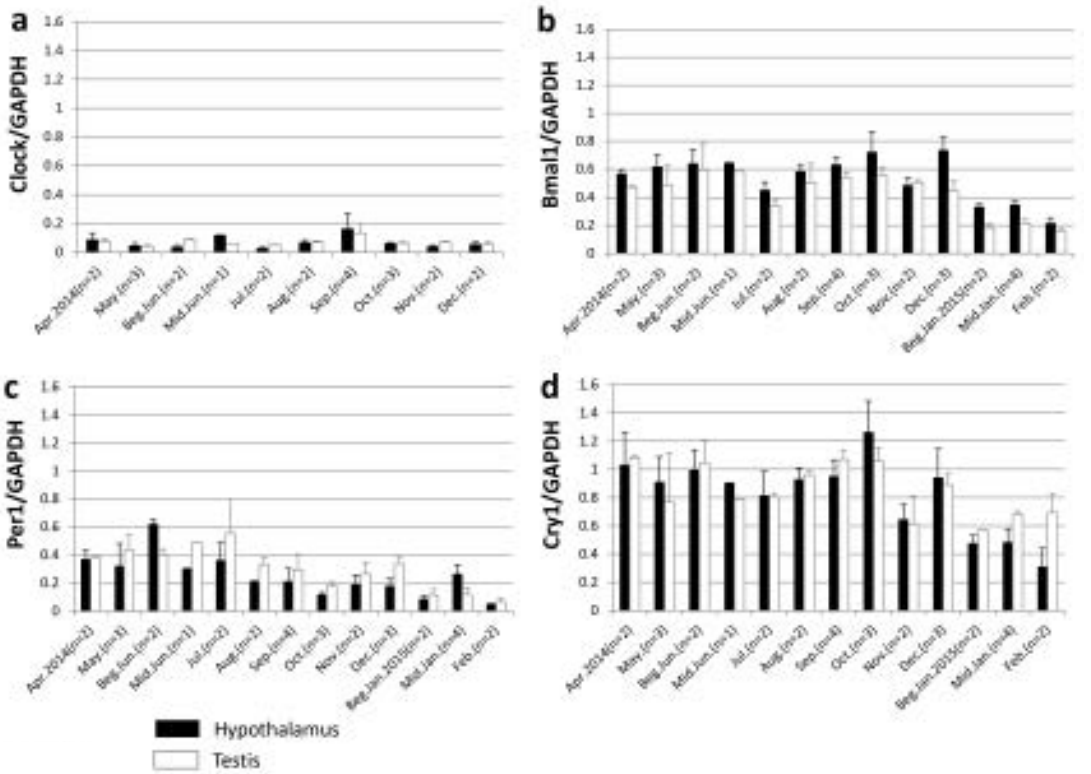

A

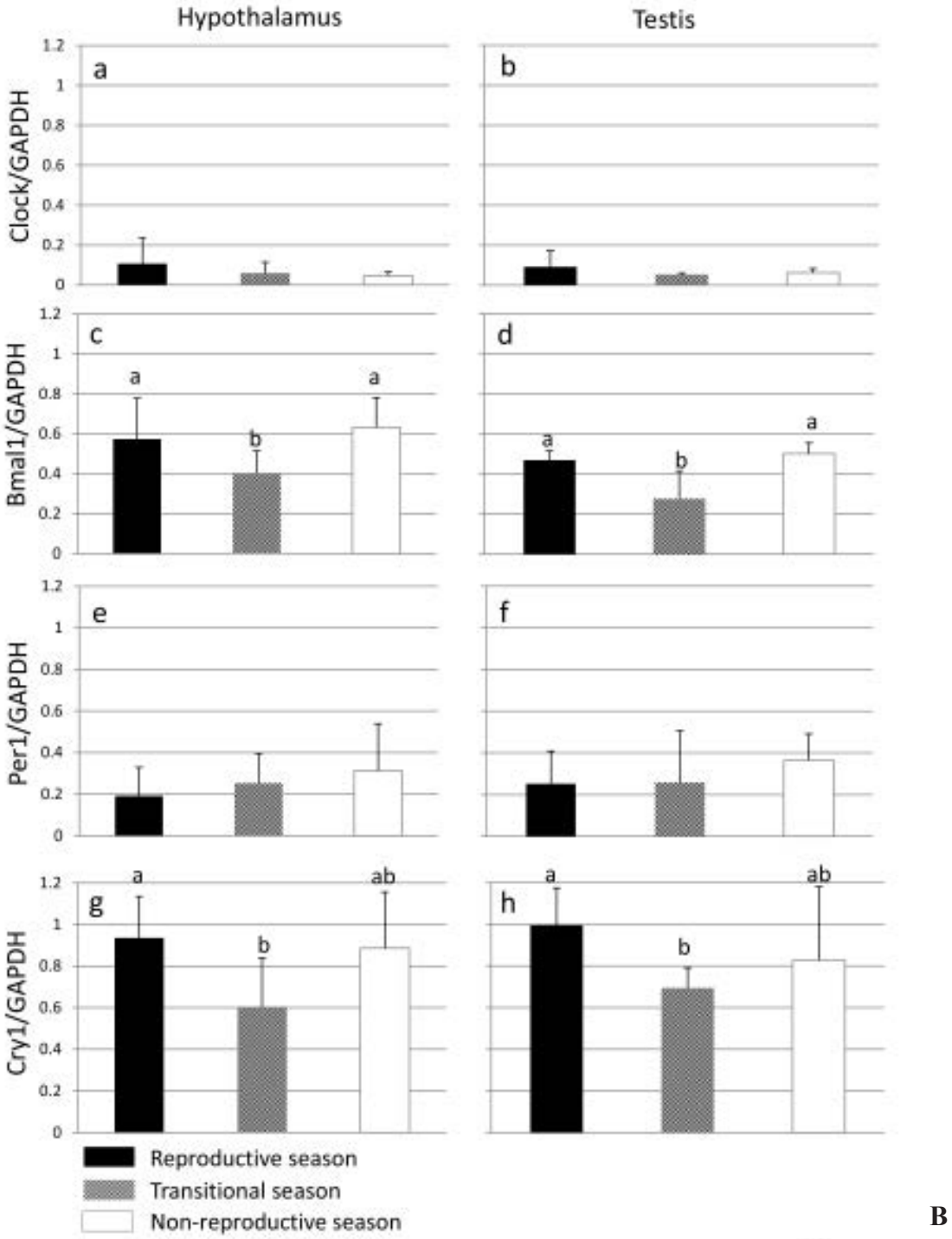

Fig. 6. ***A)*** *RT-PCR analysis of* ***(a)*** *Clock,* ***(b)*** *Bmal1,* ***(c)*** *Per1, and* ***(d)*** *Cry1 mRNA transcripts in the hypothalamus and testis of Japanese wood mice throughout the year. GAPDH was amplified as an intrinsic control. Values are expressed as mean ± SD.* ***B)*** *Seasonal changes based on the RT-PCR analysis of* ***(a, b)*** *Clock,* ***(c, d)*** *Bmal1,* ***(e, f)*** *Per1, and* ***(g, h)*** *Cry1 mRNA transcripts in the hypothalamus and testis of Japanese wood mice. GAPDH was amplified as an intrinsic control. Values are expressed as mean ± SD.* $^{a\text{-}b}$*Different superscripts denote significant differences* ($P < 0.05$).

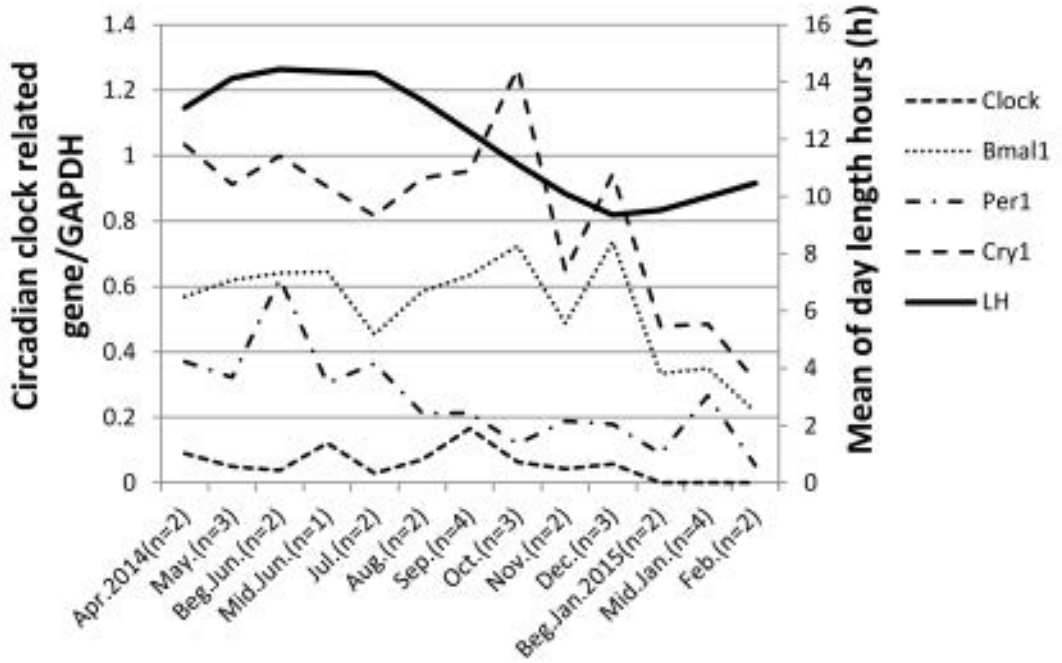

Fig. 7. *The monthly mean of daylight hours in this region merged with the RT-PCR analysis of (**A**) Clock, (**B**) Bmal1, (**C**) Per1, and (C) Cry1 mRNA transcripts in the hypothalamus of Japanese wood mice throughout the year. GAPDH was amplified as an intrinsic control.*

an annual cycle. From February to April and August to October, complete spermatogenesis was observed; these months represent active (reproductive) periods for both the testes and caudae epididymides, with sperm being present in the lumen of the epididymal ducts. From mid-June to July and during mid-January, a small number of spermatozoa were detected in the testes and caudae epididymides, representing the transitional season. From May to early June and from November to early January, spermatogenic cells consisted of only spermatogonial and few spermatocytes in the testes. This period represents the inactive (non-reproductive) season during which spermatogenesis arrest occurs. Our results indicate that changes in testicular morphology may be used to determine the reproductive, non-reproductive, and transmission periods throughout the course of a year in Japanese wood mice. Our results provide baseline information for studies focusing on the manipulation of sperm and the use of this species as a bio-resource. Furthermore, such changes that include the switching on and off of reproductive functions during the annual breeding cycle might be the most striking phenomenon to determine the mechanisms involved in inducing or arresting spermatogenesis.

Circadian rhythms are approximately 24-h biological cycles that prepare an organism for daily environmental changes. These cycles are driven by the molecular clock, with the transcriptional feedback mechanism in mammals involving core clock genes (16). It has been reported that prolonged entrainment to light and dark cycles, which are slightly longer or shorter than 24 h, may alter transcription in the SCN of the hypothalamus, and DNA methylation in the SCN, which correlate with photoperiodical changes (22). Circadian clock genes are present at the light part of the autoregulatory negative-feedback loop in the brain, where PERs heterodimerize with CRYs to inhibit CLOCK:BMAL1, leading to the closure of the autoregulatory negative-feedback loop. In our experiment, both the mRNA levels of *Bmal1* and *Cry1* in the hypothalamus and testes in the reproductive season were significantly higher compared to that of the same genes in the transitional

season. The theatrical-cyclic expression of circadian clock genes was not observed in the hypothalamus and testes of Japanese wood mice in the present study. However, this period overlapped with the active reproductive season of Japanese wood mice. Furthermore, in these seasons, the mean day length ranged between approximately 11 h and 13 h (Fig. 7). There have been no studies on the induction of testicular regression with respect to seasonal circadian rhythms in response to short, intermediate, and long photoperiods. The photoperiod may be an important factor for the regulation of the reproductive system. The SCN hypothalamus becomes active as a result in changes to the photoperiod, and responds to the influence of the gonads. Consequently, testicular and epididymides activity increases. This hypothesis is supported by a hypothalamo-pituitary-testes axis study, which reported gonadotropin releasing hormone synthesis and higher testosterone secretory activity during the reproductive season compared to the non-reproductive season in Japanese wood mice (10).

In contrast, it has been reported that *Clock* and *Per1* expression is restricted to separate and specific developmental stages of spermatogenesis, with the Clock protein being localised in the developing acrosome of round spermatids, while the Per1 protein is expressed in the nucleus of type B spermatogonia and condensing spermatids (25). Our results indicate that *Clock* and *Per1* expression showed no significant cycling in either the hypothalamus or testes throughout the year in Japanese wood mice. Furthermore, clock genes may play non-circadian roles in spermatogenesis, as several studies have also shown no constitutively elevated expression of these genes in the testes or within the seminiferous tubules (26-28).

In conclusion, changes in testicular morphology may be used to indicate the reproductive, non-reproductive, and transmission periods of Japanese wood mice during the course of the year. Increased testicular activity was correlated with mean day lengths of approximately 11–13 h. In addition, the expression of the circadian clock genes *Bmal1* and *Cry1* in the hypothalamus and testes was significantly higher during the reproductive season compared to the transitional season. Consequently, spermatogenesis was completed in the seminiferous tubules of Japanese wood mice testes during this period.

These results indicate that, during the annual reproductive cycle of seasonal breeders, the photoperiod might be the proximate environmental cue for the accurate seasonal timing of reproduction. Consequently, changes to the photoperiod affect the expression of the circadian clock genes *Bmal1* and *Cry1* in the hypothalamus and testes, producing the seasonal reproductive phenotypes of Japanese wood mice.

ACKNOWLEDGEMENTS

This work was partly supported by the Cooperative Research Project Programme of Joint Usage/ Research Center at the Institute of Development, Aging and Cancer, Tohoku University, Japan.

REFERENCES

1. Dewey MJ, Dawson WD. Deer mice: The drosophila of North American mammalogy. Genesis 2001; 29:105-09.
2. Duselis AR, Vrana PB. Assessment and disease comparisons of hybrid developmental defects. Hum Mol Genet 2007; 16:808-19.
3. Johnston PG, Zucker I. Photoperiodic regulation of the testes of adult white-footed mice (*Peromyscus leucopus*). Biol Reprod 1980; 23:859-66.
4. Wallen EP, Turek FW. Photoperiodicity in the male albino laboratory rat. Nature 1981; 289:402-04.
5. Joyner CP, Myrick LC, Crossland JP, Dawson WD. Deer mice as laboratory mice. ILAR J 1998; 39:322-30.
6. Vrana PB, Fossella JA, Matteson P, de Rio T, O'Neill MJ, Tilghman SM. Genetic and epigenetic incompatibilities under hybrid dysgenesis in Permomyscus. Nat Genet 2000; 25:120-24.
7. Shorter KR, Crossland JP, Webb D, Szalai G, Felder MR, Vrana PB. Peromyscus as a mammalian epigenetic model. Genet Res Int 2012; 2012; 179159.
8. Fuentes LB, Caravaca N, Pelzer LE, Scardapane LA, Piezzi RS, Guzman JA. Seasonal variations in the testis and epididymis of vizcacha (*Lagostomus maximus maximus*). Biol Reprod 1991; 45:493-97.

9. Stevenson, TJ, Prendergast, BJ. Reversible DNA methylation regulates seasonal photoperiodic time measurement. Proc Natl Acad Sci USA 2013; 110:16651-56.
10. Kuwahara S, Mizukami T, Omura M, Hagihara M, Iinuma Y, Shimizu Y, Tamada H, Tsukamoto Y, Nishida T, Sasaki F. Seasonal changes in the hypothalamo-pituitary-testes axis of the Japanese wood mouse (*Apodemus speciosus*). Anat Rec 2000; 260:366-72.
11. Larrondo LF, Olivares-Yañez C, Baker CL, Loros JJ, Dunlap JC. Circadian rhythms. Decoupling circadian clock protein turnover from circadian period determination. Science 2015; 347:1257277.
12. Dibner C, Schibler U, Albrecht U. The mammalian circadian timing system: organization and coordination of central and peripheral clocks. Annu Rev Physiol 2010; 72:517-49.
13. Bell-Pedersen D, Cassone VM, Earnest DJ, Golden SS, Hardin PE, Thomas TL, Zoran MJ. Circadian rhythms from multiple oscillators: Lessons from diverse organisms. Nat Rev Genet 2005; 6:544-56.
14. Ko CH, Takahashi JS. Molecular components of the mammalian circadian clock. Hum Mol Genet 2006; 15:R271-77.
15. DeBruyne JP, Weaver DR, Reppert SM. CLOCK and NPAS2 have overlapping roles in the suprachiasmatic circadian clock. Nat Neurosci 2007; 10:543–45.
16. Harfmann BD, Schroder EA, Esser KA. Circadian Rhythms, the Molecular Clock, and Skeletal Muscle. J Biol Rhythms 2015; 30:84–94.
17. Dunlap JC. Molecular bases for circadian clocks. Cell 1999; 96:271-90.
18. Young MW, Kay SA. Time zones: a comparative genetics of circadian clocks. Nat Rev Genet 2001; 2:702-15.
19. Della Ragione F, Comitato R, Angelini F, D'Esposito M, Cardone A. Molecular cloning and characterization of the clock gene period2 in the testis of lizard *Podarcis sicula* and its expression during seasonal reproductive cycle. Gene 2005; 363:105-12.
20. Goldmann BD. The circadian timing system and reproduction in mammals. Steroids 1999; 64:679-85.
21. Turek FW, Swann J, Earnest DJ. Role of circadian system in reproductive phenomena. Recent Prog Horm Res 1984; 40:143-83.
22. Azzi A, Dallmann R, Casserly A, Rehrauer H, Patrignani A, Maier B, Kramer A, Brown SA. Circadian behavior is light-reprogrammed by plastic DNA methylation. Nat Neurosci 2014; 17:377-82.
23. Uematsu E, Takino S, Okajima H, Tong B, Sugiyama T, Yamada T, Niimura S, Yamashiro H. Use of in ovo chorioallantonic membrane engraftment culture testes from neonatal mice. Comp Med 2014; 64:264-69.
24. Duong HA, Robles MS, Knutti D, Weitz CJ. A molecular mechanism for circadian clock negative feedback. Science 2011; 332:1436-39.
25. Alvarez JD, Chen D, Storer E, Sehgal A. Non cyclic and developmental stage-specific expression of circadian clock proteins during murine spermatogenesis. Biol Reprod 2003; 69:81-91.
26. Mazzoccoli G, Francavilla M, Giuliani F, Aucella F, Vinciguerra M, Pazienza V, Piepoli A, Benegiamo G, Liu S, Cai Y. Clock gene expression in mouse kidney and testis: analysis of periodical and dynamical patterns. J Biol Regul Homeost Agents 2012; 26:303-11.
27. Bittman EL, Doherty L, Huang L, Paroskie A. Period gene expression in mouse endocrine tissues. Am J Physiol 2003; 285:561-69.
28. Morse D, Cermakian N, Brancorsini S, Parvinen M, Sassone-Corsi P. No circadian rhythms in testis: Period1 expression is clock independent and developmentally regulated in the mouse. Mol Endocrinol 2003; 17:141-51.

HoxB7 PROMOTES GROWTH AND METASTASIS OF LUNG ADENOCARCINOMA CELLS THROUGH REGULATION OF THE TGF-β/SMAD3 SIGNALING

L. ZHUANG, W-H. LI, K. LI, Y. MAO, C-L. GAO and C. ZHANG

The Second Department of Internal Medicine, The Tumor Hospital of Yunnan Province, Kunming City, Yunnan Province, China

Received April 17, 2015 – Accepted July 2, 2015

HoxB7 is involved in cell migration and metastasis in many malignant tumors. But, the role of HoxB7 in lung adenocarcinoma has not been elucidated. In the present study, we aimed to clarify the function of HoxB7 in the progression of lung adenocarcinoma. The protein expression of HoxB7 was examined by immunohistochemical assay in human lung adenocarcinoma tissues, and lentivirus-mediated HoxB7 shRNA (Lv-shHoxB7) was transfected into lung adenocarcinoma cells to evaluate cell proliferation and invasive potential indicated by MTT and Transwell assays. As a result, the protein expression level of HoxB7 was increased in lung adenocarcinoma tissues compared with the adjacent non-tumor tissues (56.25% *vs* 31.25%, *P*=0.014), and was positively correlated with the lymph node metastasis in patients with lung adenocarcinoma (*P*=0.036). Moreover, knockdown of HoxB7 decreased the proliferation and invasion of lung adenocarcinoma cells followed by decreased expression of TGF-β/SMAD3, vascular endothelial growth factor A (VEGFA) and matrix metalloproteinase-2 (MMP-2). Taken together, our findings demonstrate that increased expression of HoxB7 is associated with tumor metastasis in patients with lung adenocarcinoma and HoxB7 may be implicated in promoting the development of lung adenocarcinoma through activation of the TGF-β/SMAD3 signaling.

Lung adenocarcinoma is the most common type of lung cancer featured for fast progress, high rate of recurrence and metastasis leading to treatment failure and worse prognosis and is a genetic disease developing from a multi-step process (1, 2). Gene mutation and rearrangement occur frequently in tumor tissues and form the molecular genetic basis of malignant transformation and tumor progression (3, 4). Consequently, identification of genes related to tumor growth, invasion and migration is of great importance for diagnosis, targeted therapy and prognosis in patients suffered from lung adenocarcinoma.

HOX genes including four paralogous clusters (HOXA-HOXD) encode many transcriptional factors regulating gene expression, embryonic development and controlling morphogenesis and cell differentiation (5, 6). Reports demonstrating the relationship between HOX genes and diseases including cancer have been addressed in detail (7).

HOXB7 gene, one of HOX family members located on chromosomes 17q, has been shown to participate in many pathological processes including oncogenesis (8). Aberrant expression of HOXB7 is found in the precancerous lesion like Barrett esophagus (BE) (9) and many human

Key words: HoxB7, lung adenocarcinoma, growth, metastasis, TGF-β, SMAD3

Mailing address: Dr Wen-Hui Li,
The Second Department Of Internal Medicine,
The Tumor Hospital Of Yunnan Province,
Kunzhou Road No. 519, Kunming City 650118,
Yunnan province, P.R. China.
Tel.: +86 0871 68185656 Fax: +86 0871 68185656
e-mail: liwenhui1504@163.com

0393-974X (2015)

cancerous diseases such as oral squamous cell carcinoma (10) and oesophageal squamous cell cancer (11). Enforced expression of HOXB7 promotes proliferation and tumorigenic growth of human colorectal cancer cells both *in vivo* and *in vitro* (12). HOXB7 expression could be utilized as an independent predictor indicating poor prognosis verified in many advanced Esophageal Squamous Cell Cancer (ESCC) (13) patients and pancreatic adenocarcinoma patients (4). In addition, HOXB7 is also used to distinguish benign and malignant lesions in patients with biliary strictures (15) and predict the benefit of the anti-estrogen therapy known to render cancer cells resistant to tamoxifen in breast cancer patients (16). Some report that HOXB7 plays a role in the process of DNA double-strand break repair (17), and leads to ionizing radiation as a consequence. Taken together, all of this evidence suggest that high expression of HOXB7 correlates with intensive tumor invasiveness and worse overall survival. Thus, HOXB7 might be a promising target for future biological therapies. However, to our knowledge, there are few investigations clarifying the physiological functions of HOXB7, and few reports regarding its tumor suppressive role. Overexpressed HOXB7 stimulates the self-renewal of hematopoietic stem cells and differentiation of multipotent mesenchymal cells through modulation of proliferative/differentiative program (18, 19). In the present study, to further confirm the function and action mechanisms of HOXB7 in lung adenocarcinoma cells, we detected the expression of HOXB7 in lung adenocarcinoma tissues and indicated that elevated expression of HOXB7 was positively associated with the tumor invasion in lung adenocarcinoma patients, and knockdown of HOXB7 suppressed the growth and metastasis of lung adenocarcinoma cells, suggesting that HOXB7 might be a potential therapeutic target for the treatment of lung cancer.

MATERIALS AND METHODS

The LAC cell line (A549) used in our experiments was purchased from the Institute of Biochemistry and Cell Biology (Shanghai, China). Lentivirus-mediated HOXB7 shRNA (Lv-shHOXB7), negative control vector, and virion-packaging elements were purchased from Genechem (Shanghai, China). Lung adenocarcinoma tissues and the corresponding ANCT were gathered from the tumor hospital of Yunnan province. The tissue microarray of lung adenocarcinoma was made by Shanghai Outdo Biotech Co. Ltd (Shanghai, China). All the antibodies were purchased from Cell Signaling Technologies (Boston, USA). HOXB7 primer was synthesized by ABI (Framingham, USA).

Dulbecco's Modified Eagle medium (DMEM) and fetal bovine serum (FBS) were purchased from Thermo Fisher Scientific Inc. (Waltham, MA,USA); TRIzol Reagent and Lipofectamine 2000 were obtained from Invitrogen (Carlsbad, CA, USA); M-MLV Reverse Transcriptase was purchased from Promega (Madison, WI, USA); SYBR Green Master Mix was obtained from Takara (Otsu, Japan); and the ECL Plus Kit was obtained from GE Healthcare (Piscataway, NJ, USA).

Clinical data

Tissue microarray was prepared for IHC test. Human lung adenocarcinoma tissues and the corresponding ANCT were obtained from biopsies from a total of 48 consecutive lung adenocarcinoma cases admitted in our hospital from January 2012 to December 2014. The baseline characteristics of the patients before neo-adjuvant chemotherapy were summarized. The study was approved by the Medical Ethics Committee of tumor hospital of Yunnan province and written informed consent was obtained from the patients before sample collection. Two pathologists respectively checked all of the cases.

Immunohistochemical assay

Tissue microarray sections were processed for IHC analysis of HOXB7 protein as follows. Immunohistochemical examinations were carried out on 3-mm thick sections. For anti-HOXB7 immunohistochemistry, unmasking was performed with 10 mM sodium citrate buffer, pH 6.0, at 90°C for 30 min. Sections were incubated in 0.03% hydrogen peroxide for 10 min at room temperature, to remove endogenous peroxidase activity, and then in blocking serum [0.04% bovine serum albumin, A2153, (Sigma-Aldrich, Shanghai, China) and 0.5% normal goat serum X0907, (Dako Corporation, Carpinteria, CA, USA), in PBS] for 30 min at room temperature. Anti-HOXB7 antibody was used at a dilution of 1:200. The antibody was incubated overnight at 4°C. Sections were then washed three times for 5 min in PBS. Non-specific staining was blocked with 0.5% casein and 5% normal serum for 30 min at room temperature.

Quantification of protein expression

The expression of HOXB7 was semiquantitatively evaluated as the total immunostaining scores, calculated

as the product of a proportion score and an intensity score. The proportion and intensity of the staining was judged by two observers. The proportion score is defined as: 0, none; 1, ≤10%; 2, 10% to ≥25%; 3, >25% to 50%; 4, >50%, and the intensity score is: 0, no staining; 1, weak; 2, intermediate; 3, strong. HOXB7 expression was categorized into two groups: negative expression and positive expression.

Cell culture and transfection

Lung adenocarcinoma cells were cultured in DMEM medium supplemented with 10% heat-inactivated FBS, 100U/ml of penicillin, and 100 μg/ml of streptomycin. Cells in this medium were placed in a humidified atmosphere containing 5% CO_2 at 37°C. Cells were subcultured at a 1:5 dilution in medium containing 300μg/ml G418. LAC cells were transfected with recombinant experimental virus or control virus at the optimal MOI (multiplicity of infection) of 50, and cultured at 37°C and 5% CO2 for 4 h. The Lv-shHOXB7 vector-transfected clone and the negative control vector-transfected cells were named as Lv-shHOXB7 group and NC group, and lung adenocarcinoma cells non-transfected were as CON group.

Quantitative Real-time PCR

To quantitatively determine the mRNA expression level of HOXB7 in lung adenocarcinoma cells, Real-time PCR was performed. Total RNA was extracted for each clone using TRIzol according to the manufacturer's protocol. Reverse transcription was carried out using M-MLV and cDNA amplification was performed using the SYBR Green Master Mix kit according to the manufacturer's guidelines. The HOXB7 gene was amplified using a specific oligonucleotide primer and the GAPDH gene was used as an endogenous control.

Western blot assay

Lung adenocarcinoma cells were harvested and extracted using lysis buffer (Tris-HCl, SDS, mercaptoethanol, and glycerol). Cell extracts were boiled for 5 min in loading buffer, and then an equal amount of cell extracts was separated on 15% SDS-PAGE gels. Separated protein bands were transferred onto polyvinylidene fluoride (PVDF) membranes, which were subsequently blocked in 5% skim milk powder. Primary antibodies against HOXB7, TGFβ, SMAD3, VEGFA and MMP-2 were diluted according to the manufacturer's instructions and incubated overnight at 4°C. Subsequently, horseradish peroxidase-linked secondary antibodies were added at a dilution of 1:1000 and incubated at room temperature for 2 h. The relative protein levels in different cell lines were normalized to the concentration of GAPDH.

Cell proliferation assay

Cell proliferation was analyzed using the MTT assay. Briefly, cells transfected with Lv-shHOXB7 virus were incubated in 96-well-plates at a density of 1×10^5 cells per well with DMEM medium supplemented with 10% FBS. Cells were treated with 20 μl of MTT dye at 0, 24 h, 48 h, 72 h, and subsequently incubated with 150 μl of DMSO for 5 min. The color reaction was measured at 570 nm using an Enzyme Immunoassay Analyzer (Bio-Rad, Hercules, CA, USA). The proliferation activity was calculated for each clone.

Transwell invasion assay

Transwell filters were coated with Matrigel (3.9 mg/ml; 60–80 ml) on the upper surface of a polycarbonate membrane (diameter, 6.5 mm; pore size, 8 mm). After incubating at 37°C for 30 min, the Matrigel solidified and served as the extracellular matrix for analysis of tumor cell invasion. Harvested cells (1×10^5) in 100 ml of serum-free DMEM were added into the upper compartment of the chamber. A total of 200 ml of conditioned medium derived from NIH3T3 cells was used as a source of chemoattractant, which was placed in the bottom compartment of the chamber. After 24 h of incubation at 37°C with 5% CO_2, the medium was removed from the upper chamber. The non-invaded cells on the upper side of the chamber were scraped off with a cotton swab. Cells that had migrated from the Matrigel into the pores of the inserted filter were fixed with 100% methanol, stained with hematoxylin, then mounted and dried at 80°C for 30 min.

Statistical analysis

SPSS 20.0 was used for the statistical analysis. Kruskal-Wallis H test and *Chi*-square test were used to analyse the expression rate in all groups. One-way analysis of variance (ANOVA) was used to analyze the differences between groups. The LSD method of multiple comparisons was used when the probability for ANOVA was statistically significant. Statistical significance was set at $P < 0.05$.

RESULTS

Expression of HOXB7 in lung adenocarcinoma tissues

The protein expression of HOXB7 was estimated by IHC staining in lung adenocarcinoma tissues. According to the HOXB7 immuno-reactive intensity, the positive expression of HOXB7 was markedly increased in lung adenocarcinoma tissues compared with that in ANCT (P=0.014) (Fig. 1, Table I).

Table I. *Expression of HoxB7 in lung adenocarcinoma tissues.*

Target	Group	Total	N				Positive rate (%)	χ^2	*P*
			-	+	++	+++			
HoxB7	LAC	48	21	14	10	3	56.25		
	ANCT	48	33	9	4	2	31.25	6.022	0.014

LAC: lung adenocarcinoma; ANCT: adjacent non-cancerous tissues.

Table II. *Correlation between HoxB7 expression and clinicopathologic factors in LAC.*

Variables	Cases (n)	HoxB7 expression		*P* value
		-	+	
Total	48	21	27	
Age (years)				
≥60	29	12	17	
<60	19	9	10	0.686
Sex				
Male	35	17	18	
Female	13	4	9	0.274
Tumor size (cm)				
≥5	37	17	20	
<5	11	4	7	0.578
Degree of differentiation				
Well/Moderately	13	5	8	
Poorly	35	16	19	0.656
TNM stage				
I+II	21	12	9	
III+IV	27	9	18	0.103
Lymph node metastasis				
Negative	26	15	11	
Positive	22	6	16	0.036

Association between HOXB7 expression and clinicopathologic characteristics

The association between HOXB7 expression and clinical and pathologic factors was analyzed. As indicated in Table II, elevated expression of HOXB7 was closely correlated with lymph node metastases in lung adenocarcinoma (P=0.036, but there was no significant link between HOXB7 expression and other factors including age, gender, histology and tumour size, degree of differentiation and TNM stage in lung adenocarcinoma (P>0.05, respectively).

Effect of HOXB7 knockdown on the expression of TGFβ and SMAD3

After Lv-shHOXB7 was transfected into lung adenocarcinoma cell line (A549) for 24 h, the mRNA expression levels of HOXB7, TGFβ and SMAD3 (Fig. 2A-C) and their protein expression levels (Fig. 2D) were examined by Real-time PCR and Western blot assays, demonstrating a decreased expression of HOXB7, TGFβ1 and SMAD3 in Lv-shHOXB7 group compared with the NC and CON groups in lung adenocarcinoma cells (**P < 0.01).

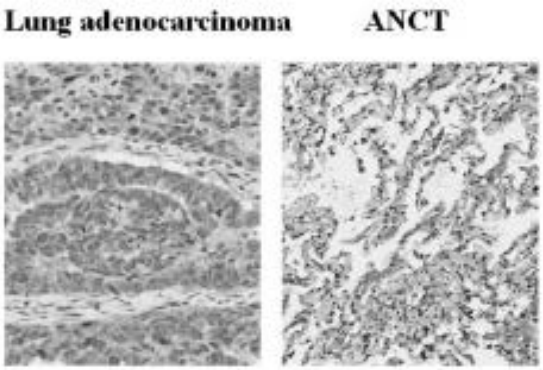

Fig. 1. *Expression of HOXB7 in lung adenocarcinoma tissues (×200). The expression of HOXB7 protein was examined by IHC staining. Positive expression of HOXB7 protein was found increased in lung adenocarcinoma tissues compared to that in ANCT.*

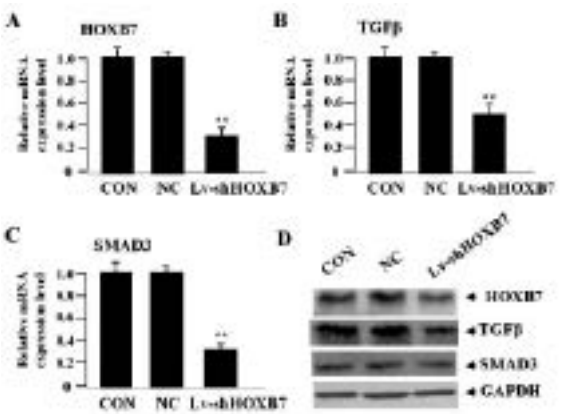

Fig. 2. *Effect of HOXB7 knockdown on TGFβ and SMAD3 expression.* ***A-C****) The mRNA expression of HOXB7, TGFβ and SMAD3, shown by Real-time PCR assay, was reduced in Lv-shHOXB7 group compared with the NC and CON groups (**P<0.01).* ***D****) The protein expression of HOXB7, TGFβ1 and SMAD3, indicated by Western blot assay, was downregulated Lv-shHOXB7 group compared with the NC and CON groups.*

The effect of HOXB7 knockdown on cell proliferation and cell invasion

To verify the effect of HOXB7 knockdown on cell proliferation, we determined cell proliferative activities by MTT assay. It was found that knockdown of HOXB7 reduced the proliferative activities of lung adenocarcinoma cells in a time-dependent manner compared to the NC and CON groups (**$P < 0.01$) (Fig. 3A). The mRNA expression level of VEGFA, indicated by Real-time PCR assay (Fig. 3B), was significantly decreased in the Lv-shHOXB7 group compared with the NC and CON groups (**$P < 0.01$).

To assess the effect of HOXB7 knockdown on cell invasion, the Transwell assay was carried out. The invasive activity of lung adenocarcinoma cells was defined by the ability of tumor cells to invade a matrix barrier containing laminin and type IV collagen (Fig. 4A). It was found that the invasive potential of lung adenocarcinoma cells was decreased in Lv-shHOXB7 group compared to the NC and CON groups (**$P < 0.01$) (Fig .4B). The mRNA expression level of MMP-2, detected by Real-time PCR assay (Fig. 4C), was found significantly decreased in the Lv-shHOXB7 group compared with the NC and CON groups (**$P < 0.01$).

DISCUSSION

Many previous studies have shown that HOXB7 might play key roles in the process of tumor formation and progression, including transformation, proliferation, angiogenesis, invasion and metastasis, through diverse mechanisms. HOXB7 can repress the expression of tumor suppressor gene death-associated protein kinase 1 (DAPK1), which in turn contributes to leukemogenesis, such as Chronic Lymphocytic Leukemia (CLL) (20), and triggers oral carcinogenesis by increasing tumor cell proliferation (21). In the present study, we examined the expression of HOXB7 in lung adenocarcinoma tissues, indicating that HOXB7 was up-regulated in lung adenocarcinoma tissues compared with the ANCT, and was positively correlated with lymph node metastasis of the tumor, suggesting that intracellular accumulation of HOXB7 might be involved in the tumorigenesis of lung adenocarcinoma.

Transduction of HOXB7 into breast carcinoma cell line gives rise to the generation of bFGF promoting cell proliferation and reducing growth factor dependence (22). HOXB7 protein increases the intracellular accumulation and secretion of basic fibroblast growth factor, known as a potent angiogenic and mitogenic factor in ovarian

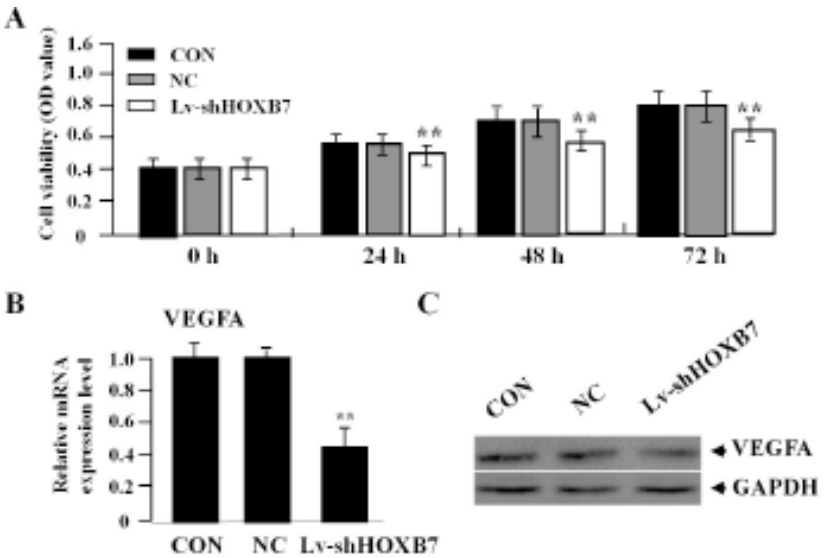

Fig. 3. *Effect of HOXB7 knockdown on cell proliferation.* ***A)*** *We evaluated the growth of lung adenocarcinoma cells by MTT assay. Knockdown of HOXB7 significantly attenuated cell proliferative activities of lung adenocarcinoma cells in a time dependent manner compared with the NC and CON groups (**P<0.01). B,* ***C)*** *The expression of VEGFA, indicated by Real-time PCR and western blotting, was downregulated in Lv-shHOXB7 group compared with the NC and CON groups (**P<0.01).*

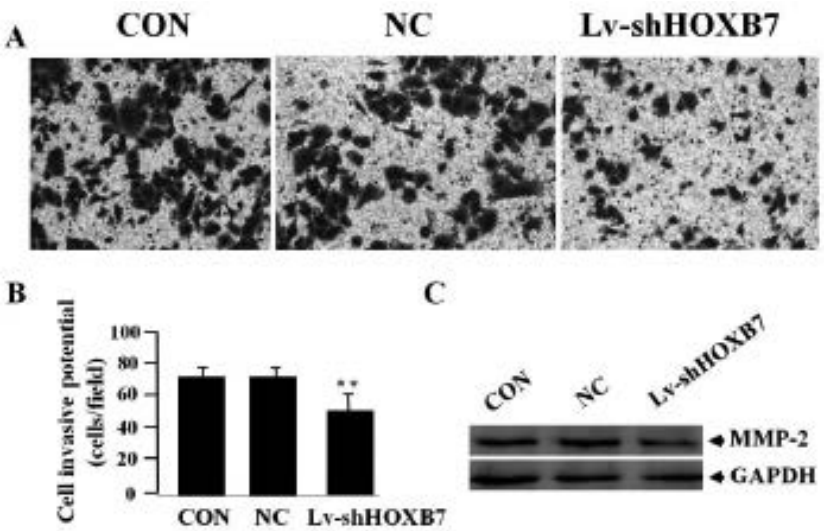

Fig. 4. *Effect of HOXB7 knockdown on cell invasion.* ***A)*** *The invasive potential was determined by Transwell assay on the basis of the ability of lung adenocarcinoma cells to invade a matrix barrier containing laminin and type IV collagen.* ***B)*** *The invasive potential of lung adenocarcinoma cells was weakened in Lv-shHOXB7 group compared with the NC and CON groups (**P<0.01).(****C)*** *The protein expression of MMP-2, indicated by western blotting, was downregulated in Lv-shHOXB7 group compared with the NC and CON groups.*

carcinomas (23), and upregulates the expression of pro-angiogenic factors such as VEGFA, FGF2, MMP2, WNT5a and platelet-derived growth factor alpha chain (PDGFA) in myeloma (24), enhancing their invasiveness. In colorectal cancer (CRC) cells, HOXB7 promotes the transition of G0/G1 to S-phase, concomitantly upregulates the expression of cyclinD1 and downregulates that of p27Kip1 (12). HOXB7 boosts breast cancer progression by activating TGF-β/SMAD3 signaling pathway and lung metastasis by tumor-associated macrophage (TAM) recruitment and an M2 tumor-promoting phenotype acquisition (25). However, knockdown of HOXB7 induces cell cycle arrest and apoptosis in pancreatic ductal adenocarcinomas (PDAC) through increased expression of pro-apoptotic proteins, including BAX and BAD, and decreased expression of anti-apoptotic proteins such as Bcl-2 (26). In the present study, it was found that knockdown of HOXB7 could inhibit tumor proliferation and invasion and remarkably downregulate the expression of TGFβ, SMAD3, VEGFA and MMP-2, suggesting that HOBX7 might prompt the development of lung adenocarcinoma through TGFβ1/SMAD3 signaling.

On the other hand, HOXB7 can be the regulating target of gene, such as taurine-upregulated gene 1 (TUG1), in human non-small cell lung cancer (27) and micro-RNA, like microRNA-196b (miR-196b), in cervical cancer (28), exhibiting its coordinating involvement in the progression of cancer. Furthermore, combination of HOXB7 with other marker genes have shown great detective potential with high specificity and sensitivity in early diagnosis of a variety of cancers such as cholangiocarcinoma (29) and epithelial ovarian carcinoma (30).

Hence, we have reasons to believe that HOXB7 could be a valuable and universal biomarker tightly linked to the clinical prognosis and survival status of lung adenocarcinoma patients, and HOXB7 may be implicated in promoting the development of lung adenocarcinoma through activation of the TGF-β/SMAD3 signaling.

ACKNOWLEDGEMENTS

This study was supported by Social Development Plan of Science and Technology Basic Application Research of self-financing project (No. 2010ZC131).

REFERENCES

1. Goldstraw P, Ball D, Jett JR, Le Chevalier T, Lim E, Nicholson AG, Shepherd FA. Non-small-cell lung cancer. Lancet 2011; 378:1727-40.
2. Tsim S, O'Dowd CA, Milroy R, Davidson S. Staging of non-small cell lung cancer (NSCLC): A review. Respir Med 2010; 104:1767-74.
3. Moran C. Importance of molecular features of non-small cell lung cancer for choice of treatment. Am J Pathol 2011; 178:1940-48.
4. Lam KC, Mok TS. Targeted therapy: An evolving world of lung cancer. Respirology 2011; 16:13-21.
5. Garcia-Fernandez J. The genesis and evolution of homeobox gene clusters. Nat Rev Genet 2005; 6:881-92.
6. Mark M, Rijli FM, Chambon P. Homeobox genes in embryogenesis and pathogenesis. Pediatr Res 1997; 42:421-29.
7. Bhatlekar S, Fields JZ, Boman BM. HOX genes and their role in the development of human cancers. J Mol Med (Berl) 2014; 92:811-23.
8. Zhang R, Zheng S, Du Y, Wang Y, Zang W, Zhao G. Levels of HOXB7 and miR-337 in pancreatic ductal adenocarcinoma patients. Diagn Pathol 2014; 9:61.
9. di Pietro M, Lao-Sirieix P, Boyle S, et al. Evidence for a functional role of epigenetically regulated midcluster HOXB genes in the development of Barrett esophagus. Proc Natl Acad Sci U S A 2012; 109:9077-82.
10. Bitu CC, Carrera M, Lopes MA, Kowalski LP, Soares FA, Coletta RD. HOXB7 expression is a prognostic factor for oral squamous cell carcinoma. Histopathology 2012; 60:662-65.
11. Xie X, Zhang SS, Wen J, et al. Prognostic value of HOXB7 mRNA expression in human oesophageal squamous cell cancer. Biomarkers 2013; 18:297-303.
12. Liao WT1, Jiang D, Yuan J, et al. HOXB7 as a prognostic factor and mediator of colorectal cancer progression. Clin Cancer Res 2011; 17:3569-78.
13. Long QY, Zhou J, Zhang XL, Cao JH. HOXB7 predicts poor clinical outcome in patients with advanced esophageal squamous cell cancer. Asian Pac J Cancer Prev 2014; 15:1563-6.
14. Nguyen Kovochich A, Arensman M, Lay AR, Rao

NP, Donahue T, Li X, French SW, Dawson DW. HOXB7 promotes invasion and predicts survival in pancreatic adenocarcinoma. Cancer 2013; 119:529-39.
15. Nischalke HD, Schmitz V, Luda C, et al. Detection of IGF2BP3, HOXB7 and NEK2 mRNA expression in brush cytology specimens as a new diagnostic tool in patients with biliary strictures. PLoS One 2012; 7:e42141.
16. Jin K, Kong X, Shah T, et al. The HOXB7 protein renders breast cancer cells resistant to tamoxifen through activation of the EGFR pathway. Proc Natl Acad Sci USA 2012; 109:2736-41.
17. Rubin E, Wu X, Zhu T, et al. A role for the HOXB7 homeodomain protein in DNA repair. Cancer Res 2007; 67:1527-35.
18. Carè A1, Valtieri M, Mattia G, et al. Enforced expression of HOXB7 promotes hematopoietic stem cell proliferation and myeloid-restricted progenitor differentiation. Oncogene 1999; 18:1993-2001.
19. Boström K, Tintut Y, Kao SC, Stanford WP, Demer LL. HOXB7 overexpression promotes differentiation of C3H10T1/2 cells to smooth muscle cells. J Cell Biochem 2000; 78:210-21.
20. Raval A, Tanner SM, Byrd JC, et al. Downregulation of death-associated protein kinase 1 (DAPK1) in chronic lymphocytic leukemia. Cell 2007; 129:879-90.
21. De Souza Setubal Destro MF, Bitu CC, Zecchin KG, Graner E, Lopes MA, Kowalski LP, Coletta RD. Overexpression of HOXB7 homeobox gene in oral cancer induces cellular proliferation and is associated with poor prognosis. Int J Oncol 2010; 36:141-49.
22. Caré A, Silvani A, Meccia E, Mattia G, Peschle C, Colombo MP. Transduction of the SkBr3 breast carcinoma cell line with the *HOXB7* gene induces bFGF expression, increases cell proliferation and reduces growth factor dependence. Oncogene 1988; 16:3285-89.
23. Naora H, Yang YQ, Montz FJ, Seidman JD, Kurman RJ, Roden RB. A serologically identified tumor antigen encoded by a homeobox gene promotes growth of ovarian epithelial cells. Proc Natl Acad Sci U S A 2001; 98:4060-65.
24. Caré A, Silvani A, Meccia E,et al. HOXB7 constitutively activates basic fibroblast growth factor in melanomas. Mol Cell Biol 1996; 16:4842-51.
25. Liu S, Jin K, Hui Y, et al. HOXB7 promotes malignant progression by activating the TGF-β signaling pathway. Cancer Res 2015; 75:709-19.
26. Chile T1, Fortes MA, Corrêa-Giannella ML, et al. HOXB7 mRNA is overexpressed in pancreatic ductal adenocarcinomas and its knockdown induces cell cycle arrest and apoptosis. BMC Cancer 2013; 13:451.
27. Zhang EB, Yin DD, Sun M, et al. P53-regulated long non-coding RNA TUG1 affects cell proliferation in human non-small cell lung cancer, partly through epigenetically regulating HOXB7 expression. Cell Death Dis 2014; 5:e1243.
28. How C, Hui AB, Alajez NM, et al. MicroRNA-196b regulates the homeobox B7-vascular endothelial growth factor axis in cervical cancer. PLoS One 2013; 8:e67846.
29. Kraiklang R, Pairojkul C, Khuntikeo N, Imtawil K, Wongkham S, Wongkham C. A novel predictive equation for potential diagnosis of cholangiocarcinoma. PLoS One 2014; 9:e89337.
30. Piura B1, Piura E. Autoantibodies to tumor-associated antigens in epithelial ovarian carcinoma. J Oncol 2009; 2009:581939.

REPAIR EFFECTS OF UMBILICAL CORD MESENCHYMAL STEM CELLS ON PODOCYTE DAMAGE OF IgA NEPHROPATHY

D.W. ZHANG, H. QIU, Y.M. MEI, H. FU and H.G. ZHENG

Department of Nephrology, General Hospital of Shenyang Military Area, Shenyang, China

Received March 21, 2015 – Accepted July 17, 2015

This study aimed to explore the influence of umbilical cord mesenchymal stem cells (UMSC) on stem cell homing and glomerular mesangial cell (GMC) after intravenous injection performed on mice tails with IgA nephropathy (IgAN) and its possible mechanism, which provide a new way and theoretical basis for the application of stem cell transplantation (SCT) in kidney disease treatment. Specific pathogen free (SPF) male Kunming mice were randomly divided into groups. A complex method applying bovine serum albumin (BSA) gavage, hypodermic injection of CCl_4 and lipopolysaccharide (LPS) was used for building IgAN mice model. In addition, vascular endothelial growth factor (VEGF), connective tissue growth factor (CTGF) and cluster of differentiation (CD) 44 were observed by Masson staining and detected with immunohistochemistry (IHC) to confirm homing and location of mesenchymal stem cells (MSCs). Moreover, Western Blot was used for detecting VEGF and CTGF so as to explore the possible mechanism of applying UMSC in treating IgAN. Masson staining indicated that fibrosis degree of MSCs in treatment group was significantly lower than in negative control group after stem cell treatment. Routine urine test explained that proteinuria in treatment group were (7.15±0.31), (4.87±0.22), (2.95±0.16) g/24 h and (12.00±1.38) g/24 h in model group ($P<0.05$). MSCs were observed to be located in glomerulus and renal interstitium by IHC detection of CD44 and IHC qualitative observation of VEGF and CTGF had different positive expressions in three groups. Furthermore, different expressions of VEGF and CTGF were observed quantitatively by Western Blot. Fibrosis degree of renal tissue relieves, hematuresis and proteinuria eases and IgAN symptoms obviously improve after UMSC treatment, which hints that the treatment of HUMSC has protective effect on IgAN mice model.

Chronic kidney disease (CKD) is a general term for the majority of kidney diseases. Its incidence ranges from 11% to 12% and increases year by year. IgA nephropathy (IgAN), an important factor causing CKD, refers to primary glomerular disease accompanied with or accompanied without other immune globulin (Ig) depositing in glomerular mesangial area dominated by IgA or IgA deposition, which is one of the most common types in chronic glomerulonephritis (CGN). About 25% of patients develop end stage renal disease (ESRD) within 5-25 years after being confirmed as IgAN (1).

To date, this disease does not benefit from satisfying treatment and is still orientated towards non-specific therapy, such as glucocorticoid (GCS), cyclophosphamide, Angiotensin Converting Enzyme Inhibitor (ACEI). Therefore, the development of new treatment inhibiting IgA deposition, relieving renal interstitial fibrosis and reducing hematuria proteinuria and renal function is an urgent issue (2).

Key words: IgA nephropathy, mice, human umbilical cord mesenchymal stem cells, CD44, immunofluorescence

Mailing address: Dr Hongguang Zheng,
Department of Nephrology,
General Hospital of Shenyang, Military Area, No. 83,
Wenhua Road of Shenhe,
District, Shenyang, China
Tel.: 0371-65528998 Fax: 0371-65528998
e-mail: zhgsyyy@163.com

0393-974X (2015)

In recent years, study results have suggested that the transplant of mesenchymal stem cells (MSCs) is likely to be a potential method in treating kidney disease. So far, stem cells transplantation (SCT) has been widely applied in treating autoimmune disease (AID), hematological system diseases, myocardial infarction neurological diseases and congenital immunodeficiency disease, and has made great achievements.

MSCs, a cell with multi-directional differentiation potential, self-renewal and high multiplication capacity, can differentiate into a variety of tissues and cells under suitable micro-environment and its biological function lies in renewing aging and damaged cells to ensure normal structure and function of the body. Bone marrow stem cells (BMSCs) are able to be divided into hematopoietic stem cell (HSC) and MSC. Currently, research findings display that MSCs with potential of differentiating to kidney parenchymal cell participate in regeneration and repair of kidney after injury and ease the fibrosis degree of kidney while also protecting it and improving hematuresis, proteinuria and renal function (3). MSCs derived from bone marrow are characterized by hard material collection, easy concurrent infection and little content in human bone marrow. Its quantity, proliferation and differentiation ability decrease significantly with age, which limits widespread use of MSCs to a large extent. MSCs and umbilical cord are both originated from mesoblast in embryonic development period. Many scholars have successfully separated and acquired similar cells by different methods through Wharton's Jelly umbilical cord. Recent studies have shown that umbilical cord containing MSCs (1-3) is able to improve clinical application of MSCs compared to adult bone marrow.

The cluster of differentiation (CD44) as an adhesive factor of mediating cell and matrix is the integration of membrane and glycoprotein in molecular form and CD44 with the molecular weight of 90×10^3 is closely related to cell homing. Vascular endothelial growth factor (VEGF), a mitogen of vascular endothelial cell with specificity, is an important angiogenesis factor which has vital biological functions such as increasing the permeability of blood vessels, promoting the proliferation of endothelial cells and accelerating angiogenesis. In the physiological state, the expression of VEGF can be detected in renal tissues and VEGF also plays a regulating role in the process of kidney development (4).

Connective tissue growth factor (CTGF) with chemotaxis for fibroblast is effective in promoting mitosis and at the same time boosting cell proliferation, migration and differentiation. Lately, many studies have further discovered that CTGF is linked to occurrence and development of numerous tissue and organ fibroses in blood vessels, skin, heart, kidney, pancreas, lung and liver. It plays an important role in glomerulus and renal interstitial fibrosis, especially in obviously increased expression of various hyperplasia and sclerosis diseases i.e. IgAN, focal segmental glomerulosclerosis (FSGS) (5).

This study aimed to explore the influence of IgAN model mice on MSCs homing and cytokine after transplanting MSCs.

MATERIALS AND METHODS

Experimental animals

Sixty specific pathogen free (SPF) normal Kunming mice ranging in weight from 25 to 40 g, offered by the animal center in Liaoning Medical University, were divided into control group, model group and HUMSC treatment group.

Main reagents and instruments

Carbon tetrachloride (CCl4, Chemical Reagent Factory, Tianjin, China; batch number: 20100527); HUC-MSCs (MSC Bank of Heze Biological Technology Co., Ltd, Beijing, China; batch number: 11011201); goat anti-rat IgA antibody (Bioss Biological Technology Co., Ltd, Beijing, China; batch number: BA0911); human anti-rabbit CTGF primary antibody (Bioss Biological Technology Co., Ltd, Beijing, China; batch number: bs00105R); human anti-rabbit VEGF primary antibody (Bioss Biological Technology Co., Ltd, Beijing, China; batch number: BA0820); CD44 primary antibody (Bioss Biological Technology Co., Ltd, Beijing, China; batch number: BA0954); bovine serum albumin (Hongjiecheng Biological Technology Co., Ltd, Beijing, China); lipopolysaccharide (Hongjiecheng Biological Technology Co., Ltd, Beijing, China).

Modeling method and treatment

Based on literature data, reformed method applying lipopolysaccharide bovine serum albumin (LPSBSA) + LPS + carbon tetrachloride (CTC) was adopted to build IgAN mice model (6). The detailed procedures were as

follows: mice were gavaged with 400mg/kg BSA every other day for 6 weeks, CCl_4 hypodermic injection with 1/3 liver cirrhosis inducing dosage and concentration of 0.3 ml/100 g (volume ratio of soybean oil and CCl_4 5:1) was performed for 9 weeks, 0.05 mg LPS was injected on caudal vein in the 6th and 8th week respectively. Control group conducted normal diet and life without any intervention. Treatment group was injected 0.5 ml HUMSC suspension (5×10^5) on caudal vein after model was detected as renal interstitial fibrosis model in the end of the 14th week. Finally, control group and model group were injected normal saline (NS) with equal quantity.

Methods of injecting MSCs: before puncture, tails of mice were infiltrated in warm water (45°C-50°C) for half a minute and wiped with alcohol repeatedly, then they were punctured with a small needle and slowly injected with 0.5 ml HUS-MSCs cell suspension; local pressing was performed to stop bleeding after pulling out the needle. Mice were kept warm after the operation and given a sugar/salt solution to drink.

Detection of biochemical criterion

Venous blood in model group was collected at the end of the 14th week after 24 h modeling for detection of urine protein quantitation, urea nitrogen (BUN) and serum creatinine (SCr) with full-automatic biochemical analyzer. Blood was also collected from the normal control group at the same time. To ensure concise experimental data and representative indexes, SCr and BUN were tested in the 7th, 21st and 56th day (7) after the experiment in order to confirm the changes of renal function. On the 0, 7th, 21st and 56th day after operation, mice in each group were put into metabolism cage to collect 24 h urine and supernatant was taken after centrifuging for 3 min (3000 r/min) and saved separately at -80°C. Twenty-four h urine protein quantitation was then performed using coomassie brilliant blue (CBB) method. Lastly, the specimen was delivered to biochemistry checkout room in the first affiliated hospital of medical university for detection.

Kidney tissues (VEGF, CTGF, CD44) in IgAN mice with immunohistochemistry IHC staining

After building models successfully, 5 model mice randomly selected were sacrificed on the 7th, 21st and 56th day of stem cell transplantation for tissue samples, and all specimens were embedded with paraffin, fixed, and sliced in the thickness of 4 μm with immunohistochemical SP0023 method.

The detection of VEGF and CTGF protein with Western Blot

As to the extraction of total protein in tissues, BAC protein quantification method, SDS-PAGE Vertical Gel Electrophoresis and CBB gel staining were applied.

Pathological analysis of kidney

The kidney tissues obtained were immerged in 10% neutral formalin and fixed for 48 h. It was then available to conventional pathological and immunological examination after gradient dehydration with alcohol, hyaline, waxdip and paraffin embedding.

Steps of Masson staining

Masson stained kidney tissue slices were put under a200x optical microscope and 15 glomerulus in each specimen were counted at random; IPP full-automatic image analysis system was used for marking glomerular mesangial area, calculating square meters and measuring capillary cluster area and finally working out the percentage of glomerular mesangial area in whole capillary cluster.

In reference to the domestic and foreign universal five level method (0~4+), results were graded into following levels: ± (visible under high magnification microscope while invisible under low magnification microscope); + (visible under high magnification microscope while nearly visible under low magnification microscope); ++ (clearly visible under high magnification microscope while visible under low magnification microscope); +++ (extremely visible under high magnification while clearly visible under low magnification microscope); ++++ (dazzling under high magnification).

Statistical analysis

SPSS l7.0 software was used for statistical processing on all data, and measurement data was expressed as mean ± SD. Factorial designed analysis of variance was applied in comparing data in multiple groups and comparison between any two groups was performed by independent-samples *t*-test. Product moment correlation coefficient was available in carrying out relevant analysis. The inspection standard was P=0.05.

RESULTS

Clinical index

Table I shows 24 h urine protein quantity of HUMSC in control group. A total of 25 and 15 mice were found with microscopic hematuria and gross hematuria respectively. After HUMSC treatment, hematuresis basically disappeared in the 56th day in treatment group and gross hematuria and microscopic hematuria still existed in mice in model group. BUN and SCr level in treatment group applying HUMSC were clearly lower than in control group, and the difference was of statistical significance (P<0.05).

Table I. *24-h proteinuria in different periods (g/24h).*

Time / group	Control group	Model group	Treatment group
Zero day of treatment	2.95±0.16	12.81±0.96	12.81±0.96
7th day of treatment	2.81±0.24	11.99±1.17[1*]	7.15±0.31
21st day of treatment	2.89±0.15	11.76±1.46[2*]	4.87±0.22
56th day of treatment	2.83±0.22[3*]	11.45±1.81[4*]	2.95±0.16[5*]

**: comparison of model group and treatment group on the 7th day of treatment (t=8.9, P<0.01); *: comparison of model group and treatment group on the 21st day of treatment (t=10.416, P<0.05); *: comparison of control group and treatment group on the 56th day of treatment (t=-1.002, P>0.05); *: comparison of model group and treatment group in the 56th day of treatment (t=10.466, P<0.05); *; comparison of proteinuria in control group and model group in the 56th day of treatment (t=-29.43, P<0.01).*

Table II. *Correlation of HUMSC and VEGF, CTGF protein expression in mice with IgAN.*

Groups	VEGF protein		r	P	CTGF protein		r	P
	+	-			+	-		
Model group	1	14	0.566	<0.01	12	3	-0.471	<0.01
Treatment group	9	6			5	10		

Table III. *VEGF content in different periods (μg/μl).*

Groups/time	7th day of treatment	21st day of treatment	56th day of treatment
Control group	0.83±0.023	0.87±0.066	0.84±0.045
Model group	0.19±0.0791	0.21±0.0182	0.18±0.0463
Treatment group	1.03±0.047	1.29±0.014	0.85±0.019

**: expresses model group compared with treatment group, t=-20.364, P<0.05, 7th day of treatment; *: model group compared with treatment group, t=-107.217, P<0.01, 21st day of treatment; *: comparison between model group and treatment group, t=-30.148, P<0.05, 56th day of treatment.*

Table IV. *Percentage of glomerular mesangial area in whole capillary cluster area.*

Groups/time	Zero day of treatment	The 7th day of treatment	The 21st day of treatment	The 56th day of treatment
Control group	0.16±0.012	0.16±0.007	0.17±0.017	0.16±0.015
Model group	0.31±0.004	0.31±0.007*	0.31±0.004*	0.32±0.007*
Treatment group	0.32±0.007	0.26±0.015▲	0.19±0.016▲	0.16±0.014▲

**: comparison of model group and treatment group (P<0.05); ▲: comparison of treatment group in different periods (P<0.05).*

Correlation of HUMSC and VEGF, CTGF protein expression in IgAN

Table II displays Spearman correlation analysis. HUMSC is positively correlated with VEGF protein expression in IgAN (r=0.566, P<0.01), and negatively related to CTGF protein expression in IgAN (r=-0.471, P<0.01).

Locating expression of CD44 after applying HUMSC treatment

CD44, an adhesive factor of mediating cell and matrix and cells, is the integration of membrane and glycoprotein in molecular form, in which CD44 with

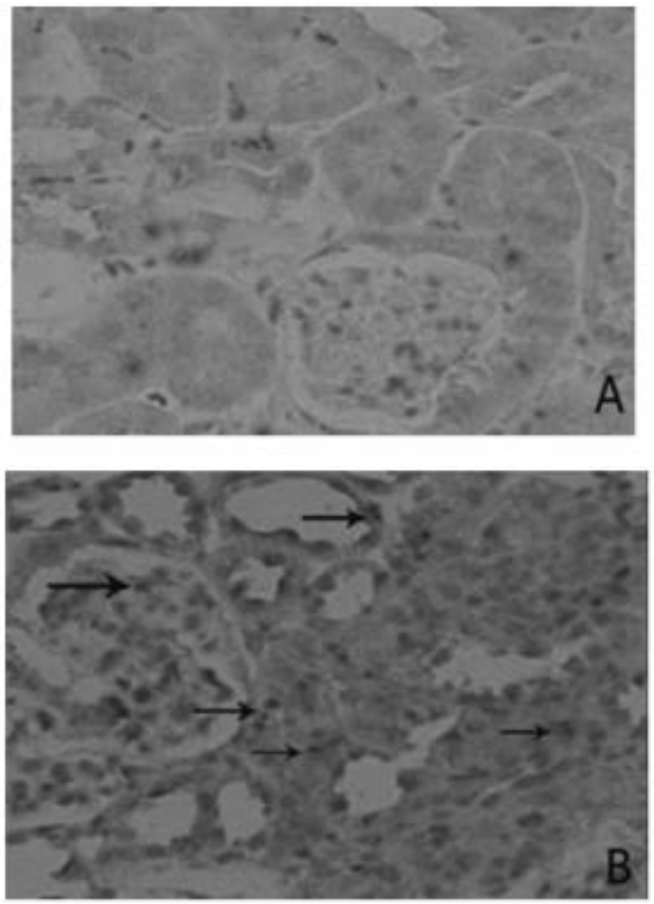

Fig. 1. A*) The 7th day in control group.* **B***) The 7th day in treatment group. CD44+ cells are distributed in glomerulus and renal interstitium on the 7th day of treatment, and the direction of arrow signifies positive expression presented as claybank particles.*

the molecular weight of 90×10^3 is closely related to cell homing. We studied expression of CD44 in the 7th day of stem cell treatment, and Fig. 1 shows the expression of CD44 positive protein in treatment group. The upper picture in Fig. 1 is normal group and lower picture displays the 7th day of control group. From the figures we can see that CD44, together with cells distributed in glomerulus and renal interstitium in the 7th day of treatment and the areas where arrows point, were observed with positive expression (yellow granular). CD44 in treatment group expressed in cytoplasm presenting claybank particles, while few CD44 expressions existed in control group.

Expression quantity of VEGF protein in IgAN model mice

Expression quantity of VEGF in IgAN mice is shown in Fig. 2 and Table III. Fig. 2 expresses the detection with Western Blot, A is the control group in the 7th day of treatment, B, D and F are the model group in the 7th, 21st and 56th day and C, E and G are the treatment group in the 7th, 21st and 56th day of treatment respectively. *T* test performed on two independent samples indicated that three groups had different expressions in different periods. The difference between model group and control group in different periods was significant ($P<0.05$). Expression of VEGF in treatment group in the 21st day reached highest and it was close to normal in control group on the 56th day of treatment.

Expression quantity of CTGF protein in IgAN model mice

Expression quantity of CTGF in IgAN mice is

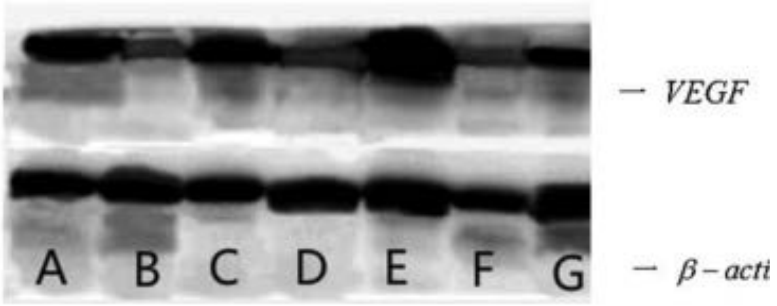

Fig. 2. *Expression of VEGF in three groups in different periods.*

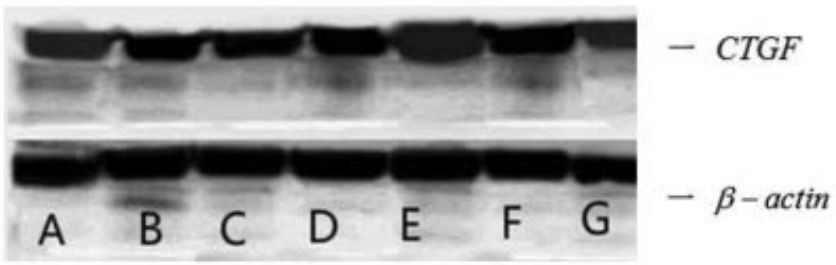

Fig. 3. E*xpression of CTGF in three groups in different periods.*

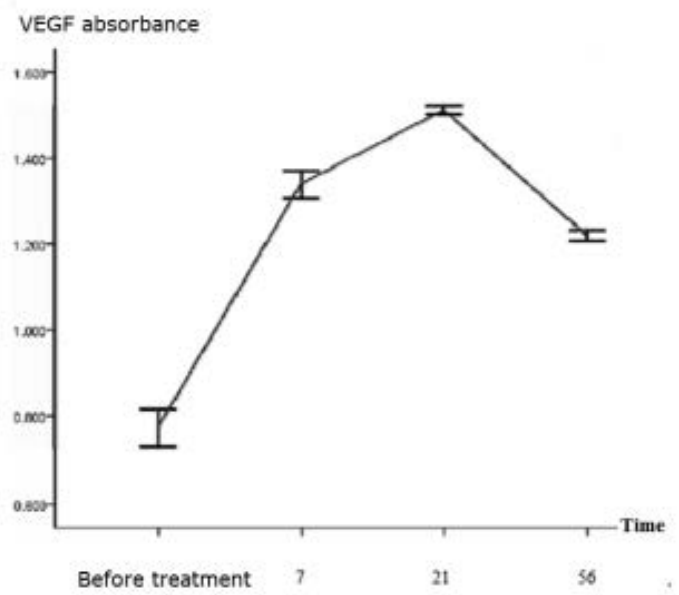

Fig. 4. *VEGF linear trend chart before and after stem cell transplantation.*

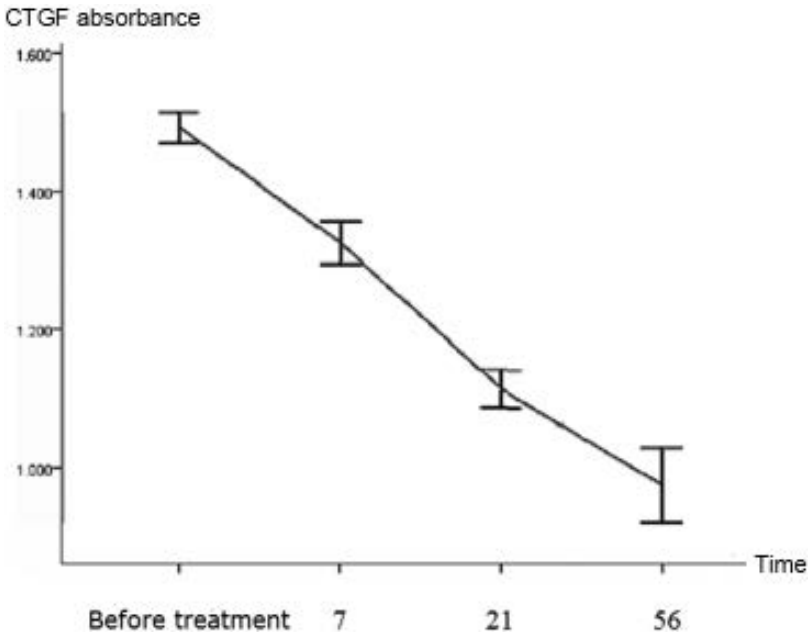

Fig. 5. *CTGF linear trend chart of stem cell transplantation in different periods.*

shown in Fig. 3. According to Western Blot detection shown in the figure, A is the control group in the 7th day of treatment, B, D, F are the 7th, 21st, 56th day of model group respectively and C, E, G are the 7th, 21st and 56th day of treatment group respectively. *T*-test performed on two independent samples explained that three groups had different expressions in different periods. The difference of model group and control group in different periods were significant ($P<0.05$), expression of CTGF in treatment group tended to decrease and it was close to the normal control group in the 56th day of treatment.

Correlation of VEGF, CTGF protein and HUMSC treatment

After HUMSC treatment, VEGF protein and HUMSC treatment presented a linear upward trend as shown in Fig. 4, while CTGF protein and HUMSC treatment were supposed to present a downward trend, as shown in Fig. 5.

Observation of fibrosis of model mice with Masson staining

Nephridial tissue of mice in model group had fibrosis in different degrees and there was no obvious fibrosis in control group and treatment group (Table IV). Control group had weak fibrosis degree, model group had severe fibrosis degree and fibrosis degree in treatment group approached control group.

DISCUSSION

HUMSC and IgAN

HUMSC with totipotency and pluripotency is capable of differentiating, developing and forming any part of tissues and organs of the body (12) at the same time homing injured part selectively no matter what kind of tissue (8). Of HUMSC, CD44 is a type of transmembrane glycoprotein (TP) and CD44 with a molecular weight of 90,000 kd is closely related to cell homing action.

Stem cells are planted in damaged glomerular area when a certain quantity of MSCs are injected and those cells will stimulate kidney stem cells or progenitor cells by secreting cytokines and humoral factors such as VEGF, hepatocyte growth factor (HGF) and insulin-like growth factor (IGF) and build a suitable microenvironment to differentiate it to damaged kidney tissues and cells. Besides secreting these factors, microvesicles (MVs) of MSCs have the ability of stimulating existing damaged renal tubular cell proliferation potential by transferring mRNA (9). MSCs secrete MVs, repairing injured renal tubule in the form of paracrine. Meanwhile, MSCs play a

significant role in occurrence and regeneration of vascular and endothelial repair according to studies (10). This discovery supports that MSCs are likely to be planted in kidney and take part in repair and regeneration of kidney tissues.

After HUMSC treatment, homing effect of MSCs was proved through detection of CD44 expression in kidney tissues. Hematuresis in IgAN model mice decreased and the comparison of proteinuria in treatment group and model group in the 21st and 56th day of treatment showed $P<0.05$ which concluded that HUMSC treatment was able to lower proteinuria level. In comparison to each renal function, Scr and urea nitrogen level in treatment group and model group in the 21st and 56th day of treatment indicated $P<0.05$, proving that HUMSC treatment could improve renal function. As to VEGF and CTGF expression, comparison of positive expression rates in treatment group and model group both suggested $P<0.05$, verifying that HUMSC treatment was capable of regulating expression levels of two proteins.

VEGF and IgAN

VEGF, a mitogen of vascular endothelial cells with specificity, is a highly conservative homodimer glycoprotein 19 and dimer is made up of single strand with two molecular weights of 24 kDa and disulfide bond. VEGF resolves inactive monomer and removes N 2 glycosyl without affecting biological reaction, but may play a role in cell secretion (11). At least 5 kinds of protein forms are produced due to different cut modes of mRNA, including VEGF 121, VEGF 145, VEGF 165, VEGF 185 and VEGF 206, in which VEGF 121, VEGF 145 and VEGF 165 are soluble proteins in secreting type, characterized by promoting vascular endothelial cell proliferation and division, neoangiogenesis, collateral circulation, and increasing vascular permeability. Located in chromosome 6p21.3, the VEGF gene is composed of 8 exons and 7 introns and comes in different sub-types according to the exon in which VEGF 121, VEGF 165 and VEGF 189 are expressed in humans (12). In our study, mice model had seriously damaged kidney tissue and structure and previous kidney function deterioration but after the use of HUMSC, VEGF expression of model mice increased, new capillaries were born and clinical indexes obviously improved, so we speculated that VEGF was the vital kidney protecting factor.

IHC and Western Blot results indicated that positive expression rate and expression level in control group, model group and treatment group were different at diverse stages. VEGF protein expression quantity in model group varied in the 7th, 21st and 56th day of treatment compared with treatment group ($P<0.05$), while increased VEGF expression existed in all groups. Measurement of biochemical criterion in treatment group in different periods varied compared to the other two groups. In accordance with this, we worked out that increased VEGF protein expression in IgAN model mice might decrease hematuresis and proteinuria level and recover renal function. Hence, it was inferred that the application of HUMSC was effective in up-regulating VEGF protein expression level and increasing angiogenesis by promoting damaged glomerulus so as to achieve the purpose in treating IgAN.

Renal interstitial fibrosis occurring after IgAN aggravates renal injury. On account of this, we studied changes of CTGF expression. CTGF, a secreting peptide containing 349 amino acids with higher cysteine content (molecular weight: 34~38 KD) has influence on promoting cell proliferation, migration, differentiation and cell apoptosis. Lately many studies have further discovered that CTGF is connected to occurrence and development of numerous tissue and organ fibrosis, including blood vessel, skin, heart, kidney, pancreas, lung and liver. Human CTGF gene located in 6q23.1 is an early response gene (13) in normal circumstances. CTGF is able to exist in glomerular epithelium, renal interstitium, smooth muscle and other tissues (14).

In kidney tissues of mice with IgAN in this study, glomerulus, renal interstitium and basement membrane were all damaged to different degrees and had severe fibrosis, which seriously damaged kidney function. Mice alleviated fibrosis degree under light microscope and improved clinical symptoms after using MSCs for treatment. Expression of CTGF in treatment group detected with IHC and Western Blot was lower than in model group. The detection of biochemical criterion, such as proteinuria, Scr and urea nitrogen all showed $P<0.05$ compared with model group before and after treatment. In view of this, it was summarized that decreased expression level of CTGF was capable of relieving fibrosis of

IgAN thus reaching the goal of lowering hematuresis, proteinuria, Scr and urea nitrogen level so as to treat IgAN.

This study discovered that HUMSC was positively connected to expression of VEGF protein in damaged kidney and negatively related to CTGF protein. After the treatment of HUMSC, IgAN mice had increased VEGF protein expression, decreased CTGF protein expression and obviously improved clinical symptoms. HUMSC was likely to have some sort of regulatory mechanism to them, therefore, we made the following deductions: 1): some literature reported that HUMSC could secrete VEGF protein (15) thus we thought that HUMSC was able to regulate the expression of VEGF protein in kidney damage with IgAN by two ways of secreting VEGF protein and regulating VEGF expression level; 2): HUMSC was considered to be able to lower expression level of CTGF protein of damaged kidney with IgAN.

In conclusion, increased VEGF expression and decreased CTGF expression are both involved in the regeneration and repair of kidney tissue and improve a series of clinical IgAN symptoms. Furthermore, HUMSC plays a significant role in treating IgAN model mice, relieves degrees of glomerulus and interstitial fibrosis and hematuresis and proteinuria and IgAN symptoms improve after HUMSC treatment. Therefore, we confirm that HUMSC treatment has a protective effect on IgAN mice model.

REFERENCES

1. Huang DL, Yi ZW. Application of stem cell transplantation in kidney diseases. Chin J Contem Pediat 2012; 14(2):154-61.
2. Wang ZQ, Zhou D, Zhang MM. Changes of VEGF expression after applying human umbilical cord mesenchymal stem cells in treating IgA nephropathy model mice. Chi Med Engin 2012; 20(4):126-7.
3. Zhang RF, Wu JY, Yao JF, Zhang Y, Li ZQ, Zhou DP. Sources of mesenchyma stem cells. J Clin Rehab Tiss Engin Res 2007; 11(15):2968-70.
4. Ortiz LA, Gambelli F, McBride C, Gaupp D, Baddoo M, Kaminski N, Phinney DG. Mesenchymal stem cell engraftment in lung is enhanced in response to bleomycin exposure and ameliorates its fibrotic effects. Proc Natl Acad Sci USA 2010; 100(14):8407-11.
5. Yu WL, Zeng D, Yuan KH, Li Q, Cheng B. Connective tissue growth factor and fibrosis. J of Clinical Rehabilitative Tissue Engineering Research 2007; 11(23):4610-4613.
6. Devine SM, Bartholomew AM, Mahmud N, et al. Mesenchymal stem cells are capable of homing to the bone marrow of non-human primates following systemic infusion. Exp Hematol 2010; 29(2):244-55.
7. Ermert L, Ermert M, Goppelt-Struebe M, et al. Cyclooxygenase isoenzyme localization and MRNA expression in rat lungs. Am J Respir Cell Mol Biol 2010; 18(4):479-88.
8. Engsh K, Ryan JM, Tobin L, Murphy MJ, Barry FP, Mahon BP. Cell contact, prostaglandin E(2) and transforming growth factor β1 play non-redundant roles in human mesenchymal stem cell induction of cd4+cd2 (high) forkhead box P3+ regulatory *t* cells. Clin Exp Immunol 2009; 156(1):149-60.
9. Hirotsugu Iwatani, Enyu Imai. Kidney repair using stem cells: myth or reality as a therapeutic option? Thor Crit Appr 2010; 23 (02):143-6.
10. Bruno S, Grange C, Deregibus MC, et al. Mesenchymal stem cell-derived microvesicles protect against acute tubular injury. J Am Soc Nephrol 2009; 20:1053-67.
11. Sun DX, Wang ZQ, Zhou D. Influence of transplantation of human umbilical cord mesenchymal stem cell on renal function of mice with IgA nephropathy. Shan Med J 2012; 52(26):36-8.
12. Meisel R, Zibert A, Laryea M, Göbel U, Däubener W, Dilloo D. Human bone marrow stromal cells inhibit allogeneic t-cell responses by indoleamine 2, 3-dioxygenase-mediated tryptophan degradation. Blood 2009; 103(12):4619-21.
13. Yokoo T, Ohashi T. Gene Delivery using human cord blood-derived CD34+cells into inflamed glomeruli in NOD/SCID mice. Kidney Int 2009; 64(1):102-9.
14. Obara T, Mizopuchi S, Shimozuru Y, Sato T, Hotta O. The complex of immunoglobulin A and uromodulin as a diagnostic marker for immunoglobulin A nephropathy. Clin Exp Nephrol 2012; 33(2):145-52.
15. Togel F, Westenfelder C, Zhang P, Hu Z. VEGF is a mediator of the renoprotective effects of multipotent marrow stromal cells in acute kidney injury. J Cell Mol Med 2009; 13(8B):2109-14.

EFFECT OF INDOMETHACIN AND ITS COMPLEXES ON REPRODUCTIVE PERFORMANCE AND OXIDATIVE STRESS IN TESTIS AND STOMACH OF MALE ALBINO RATS WITH REFERENCE TO THEIR CHEMICAL CHARACTERIZATIONS

S.M. EL-MEGHARBEL[1,2], R.Z. HAMZA[3], M.S. REFAT[1,4], M.A. AL-OMAR[5] and A.M. NAGLAH[5,6]

[1]Department of Chemistry, Faculty of Science, Taif University, Taif, Saudi Arabia; [2]Department of Chemistry, Faculty of Science, Zagazig University, Zagazig, Egypt; [3]Department of Zoology, Faculty of Science, Zagazig University, Zagazig, Egypt; [4]Department of Chemistry, Faculty of Science, Port Said University, Port Said, Egypt; [5]Department of Pharmaceutical Chemistry, College of Pharmacy, King Saud University, Riyadh, Saudi Arabia; [6]Peptide Chemistry Department, Chemical Industries Research Division, National Research Centre, Dokki, Cairo, Egypt

Received March 10, 2015 – Accepted July 3, 2015

Four new complexes of Hg (II), Pb (II), Sn (II) and Bi (III) with indomethacin drug ligand (IMC) were synthesized and characterized by using infrared, electronic, ^{1}H-NMR spectral, thermogravimetric and conductivity measurements. The IMC was found to act as bidentate chelating agent. IMC complexes coordinate through the oxygen of the carboxyl group. The molar ratio chelation is 1:2 (M^{2+}:IMC) with general formula [M (IMC) $_2$], nH_2O for Hg (II), Pb(II) and Sn(II), but 1:3 for Bi(III) ions. Antibacterial screening of these heavy metal complexes against *Escherichia coli* (Gram−ve), *Bacillus subtilis* (Gram +ve) and anti-fungi (*Asperagillus oryzae*, *Asperagillus niger*, *Asperagillus Flavus*) were investigated. In the present study, we found evidence suggesting that Bi^{+3}/IMC possesses the capacity to protect the stomach, sperm, testes, cellular ATP, cellular NAD, INSL3, PGD2, PGE2 and antioxidant enzymes from deleterious actions of IMC.

Indomethacin (IMC) is a non-steroidal anti-inflammatory drug (NSAID). Preparation and characterization of magnetite nanoparticles loaded with IMC suitable for magnetic drug targeting was studied (1). Three medical IMC complexes were prepared by complexing agents, β-cyclodextrin hydroxyethyl-β-, and hydroxypropyl-β-cyclodextrin (2). The interaction between IMC anions and heavy metal ions, such as cadmium, zinc and copper (II) ions, was studied in aqueous solution by polarographic techniques (3). Five complexes were prepared with β-cyclodextrin and the insoluble, non-steroidal, anti-inflammatory drug IMC (4). The complexes were found to contain drug, water and ammonia in several unique combinations. It was theorized that the complexes were tri-molecular in nature and their formation was controlled by a hydrophobic: hydrophilic balance created within the β-cyclodextrin ring cavity prior to complex formation.

Key words: indomethacin, heavy metal ions, spectroscopic, thermal, antioxidant enzymes

Mailing address: Dr. Reham Zakaria Hamza,
Department of Zoology,
Faculty of Science,
Zagazig University,
Zagazig 44519, Egypt
Tel.: +20 1211371215
e-mail: dr_reham_z@yahoo.com

0393-974X (2015)

Each complex was characterized by differential spectroscopic and thermo gravimetric techniques. $[Ru_2(dNSAID)_4Cl]$ and $[Ru_2(dNSAID)_4(H_2O)2]$ PF_6 complexes, where dNSAID = deprotonated carboxylate from the NSAIDs, ibuprofen, Hibp, aspirin, naproxen, and IMC, respectively, were prepared and characterized by optical spectroscopic methods (5). All of the compounds exhibited mixed valent Ru_2 (II, III) cores where metal–metal bonds are stabilized by four drug-carboxylate bridging ligands in paddlewheel type structures. The complexes $[Me_2$ (Indo) SnOSn (Indo) $Me_2]_2$, and Bu_2 (Indo) SnOSn (Indo) $Bu_2]_2$, where Indo is indomethacin, were prepared and structurally characterized by means of ^{119}Sn Mossbauer, vibrational, and NMR (^{1}H and ^{13}C) spectroscopy (6). The crystal structures of the complexes $[Me_2$ (Indo) SnOSn (Indo) $Me_2]_2.2C_4H_8O_2$ were determined by X-ray crystallography. Each structure is centro-symmetric and features a central rhombus Sn_2O_2 unit with two additional tin atoms linked at the O atoms. A discrete variational-Xa (DV-Xa) method was applied to elucidate the formation of C–O–Si bridging bonds, produced when a silanol group of SiO_2 comes close enough to react with a carboxyl group of IMC (7) . A decrease in the coordination number (CN) of oxygen atoms per silicon atom at the SiO_2 surface increased the net charge (NC) of the silanolic hydrogen atom and decreased the bond overlap population (BOP) between the silanolic oxygen and hydrogen atoms. These changes favored the formation and stabilization of C–O–Si bridging bonds with simultaneous dehydration. The computational results agreed well with our previous experimental study of a ground indomethacin–SiO_2 mixture to obtain a better solid dispersion of the drug. For continuity, in this study we employed the coordination mode of IMC complexes with Hg (II), Pb (II), Sn (II) and Bi (III) heavy metal ions. The solid products were isolated and characterized by elemental analysis CHN, infrared spectra, molar conductance, ^{1}H-NMR and thermal analyses. The effect of IMC and its complexes on reproductive performance and oxidative stress in the testis and stomach of male albino rats were investigated.

MATERIALS AND METHODS

All chemicals used in the study were of the purest laboratory grade (Merck) and indomethacin (IMC) was purchased from Egyptian International Pharmaceutical Industrial Company (EIPI-Co.). Carbon, hydrogen and nitrogen contents were determined by using a Perkin–Elmer CHN 2400. The metal content was found gravimetrically by converting the compounds into their corresponding oxides. Infrared spectra were recorded on Bruker FT-IR Spectrophotometer (4000–400 cm^{-1}) in KBr pellets. The UV–vis spectra was studied in the DMF solvent with concentration ($1x10^{-3}$ M) for the IMC complexes by the help of Jenway 6405 Spectrophotometer with 1 cm quartz cell, in the range 800–200 nm. Molar conductivities of freshly prepared $1x10^{-3}$ mol/dm^{-3} DMF solutions were measured using Jenway 4010 conductivity meter. Thermogravimetric analyses (TG/DTG) were carried out in a dynamic nitrogen atmosphere (30 ml/min) with a heating rate of 10C/min using a Schimadzu TGA-50H thermal analyzer.

Synthesis of IMC complexes

IMC (0.716 g, 2.0 mmol) was added to 30 ml methanol and titrated against aqueous ammonium hydroxide (5%) to adjust pH at 9.00, then 10 ml aqueous solution of (0.271 g, 1 mmol) of $HgCl_2$ was added with continuous stirring, after that the mixture was warmed to approx. 60°C and then neutralized. Immediately, the pale white precipitate settled down and was filtered off, washed several times by minimum amounts of hot methanol and dried under vacuum over anhydrous $CaCl_2$.

Preparation of Pb (II) and Sn (II) complexes followed essentially the same procedure as preparation of Hg (II), but the weight of Pb $(OAc)_2$ and $SnCl_2.2H_2O$ were (0.361 g, 1 mmol) and (0.256 g, 0.5 mmol), respectively. The pH was adjusted at 9 and 8.23, respectively.

Bismuth (III) complex was prepared by mixing equal volumes (30 ml) of IMC (3 mmol) with $BiCl_3$ (0.315 g, 1mmol). The mixture was neutralized by titration with NH_4OH to adjust pH at 8.77 and then heated on a water bath at 60°C with constant stirring for about 45 min. A white solid complex was precipitated and its amount increased with increasing the time of heating. The obtained precipitate was separated, washed several times with hot water and then dried in a vacuum over anhydrous $CaCl_2$ and re-crystallization occured using a mixture of water and methanol (1:1).

Antibacterial and anti-fungal investigation

From previous studies, according to Gupta et al. (8), the hole-well method was applied. The investigated isolates of bacteria were seeded in tubes with nutrient broth (NB). The seeded NB (1 cm^3) was homogenized in the tubes with 9 cm^3 of melted (45°C) nutrient agar (NA). The homogeneous suspensions were poured into Petri dishes. The holes (diameter 4 mm) were made in the cool medium. After cooling in these holes, 2×10^{-3}dm3 of the

investigated compounds were applied using a micropipette. After incubation for 24 h in a thermostat at 25–27°C, the inhibition (sterile) zone diameters (including disc) were measured and expressed in mm. An inhibition zone diameter over 7 mm indicates that the tested compound is active against the bacteria under investigation. The antibacterial activities of the investigated compounds were tested against *Escherichia coli* (Gram−ve), *Bacillus subtilis* (Gram +ve) and anti-fungal (*Asperagillus oryzae, Asperagillus niger, Asperagillus Flavus*).

Experimental animals

Sixty healthy adult male albino rats of the Wistar strain (*Rattus norvegicus*) with proven fertility, 4–5 months of age and weighing 150–180 g, were supplied from the Animal Breeding House of the Medical Research Institute (MRI), Cairo University, Egypt. The animal experimental work was carried out in accordance with the Code of Ethics of the World Medical Association (Declaration of Helsinki) for experiments (EU Directive 2010/63/EU). The animals were maintained at the animal care facility in the Zoology Department, Faculty of Science, Zagazig University in plastic cages under controlled temperature (23±2°C), 12 h light/dark cycle and 50±5% relative humidity. Rats were acclimatized to the laboratory environment for two weeks prior to the start of experiments and then 10 rats were placed into each cage. The present study was undertaken to assess the effects of single or multiple-dose administration of IMC and its complexes in normal treated rats.

Treatment schedule (each group comprised 10 rats): In order to optimize drug absorption, all animals were starved overnight prior to IMC exposure and its complexes. All the animals were allowed free access to food and water 1 h after administration of IMC and its complexes.

Preparation of IMC and IMC complex solutions

The test compounds used were indomethacin (IMC), Hg^{+2}-IMC, Pb^{+2}-IMC, Sn^{+2}-IMC and Bi^{+3}-IMC.

IMC was first dissolved in dimethylsulphoxide (90 mg IMC in 400 µl) and neutralized with 1 N sodium hydroxide and brought to the final concentration with 3% BSA enriched Krebs-Henseleit solution (9).

The 1st group animals received 1 ml of isotonic solution by gastric tube daily for 3 days, and served as the control group.

The 2nd IMC-treated group of animals received 60 mg/kg Indomethacin (10), Indomethacin prepared as previously described (11) through a metal stomach tube, daily for 3 consecutive days.

The 3rd Hg^{+2}/IMC-treated group of animals received Hg^{+2}/IMC (60mg/kg) daily for 3 successive days by using a metallic stomach tube.

The 4th Pb^{+2}/IMC-treated group of animals received Pb^{+2}/IMC (60mg/kg) daily for 3 successive days by using a metallic stomach tube.

The 5th Sn^{+2}/IMC-treated group of animals were given Sn^{+2}/IMC (60mg/kg) for 3 successive days by using a metallic stomach tube.

The 6th Bi^{+3}/IMC-treated group of animals were given Bi^{+3}/IMC (60 mg/kg) daily as mentioned above for 3 successive days.

The rats included in the groups that were given IMC and its complexes were weighed daily and administered doses were adjusted based on the recorded body weights.

Six hours after the last administration of the IMC and IMC complexes, blood samples were collected from the retro-orbital vein. Individual blood was drawn by orbital puncture (from eye plexus) using microhematocrit capillary tubes into dry tubes from 10 rats in each group, serum was harvested from blood without Ethelenediamine tetraacetic acid (EDTA) and their testis and stomach tissues were excised after sacrificing the animals according to the Declaration of Helsinki ethics. Blood samples were centrifuged at 3000 rpm for 10 min for the separation of sera. The serum samples obtained were transferred into Eppendorf tubes and were criopreserved at -80°C. Part of the testis tissue (left testis) was transferred into 10% buffered formalin for histopathological examination while the right testis were used in tissue homogenate preparation.

Antioxidant assay

Measurements were taken of Superoxide dismutase (SOD), Malondialdhyde (MDA), catalase and reduced glutathione in stomach and testis homogenates.

Preparation of tissue homogenates

The remaining tissues of testis and stomach were used for the analysis of oxidative stress parameters. They were washed with saline and distilled water for the removal of blood, and later the fatty parts were removed and blotted over a piece of filter paper. Prior to dissection, tissue was perfused with a 50 mM (sodium phosphate buffer saline (100 mM Na_2HPO_4/NaH_2PO_4) (pH 7.4) in an iced medium containing 0.16 mg / ml heparin or containing 0.1 mM ethylene di amine tetra acetic acid (EDTA) to remove any red blood cells and clots. Then tissues were homogenized in 5–10 ml cold buffer per gram tissue and centrifuged at 5000 r.p.m for ½ hour. The resulting supernatant was transferred into Eppendorf tubes, and criopreserved at -80°C until used for various biochemical assays (12).

Catalase (CAT) activity was determined by biodiagnostic kit method (Biodiagnositc Company, Dokki, Giza, Egypt), according to the method of Habig, et al. (13). Superoxide dismutase (SOD) activity was determined by biodiagnostic kit (Biodiagnositc Company,

Dokki, Giza, Egypt), according to the method of Aebi et al. (14). Glutathione reduced (GSH) activity was determined by biodiagnostic kit (Biodiagnositc Company, Dokki, Giza, Egypt), according to the method of Nishikimi et al. (15). Malondialdehyde (MDA) was determined by using Biodiagnostic kit (Biodiagnostic Company, Dokki, Giza, Egypt), according to the method of Ohkawa et al. (16).

Biochemical assay

Inhibin B was assayed in the culture media of the TEXAS using a commercial Enzyme-linked immunosorbent Assay (ELISA) kit (DSL-10-84100 Active, Beckman Coulter, Villepinte, France) according to the manufacturer's instructions. Each sample was diluted 2-fold in sample diluent solution prior to reactions. The intra- and inter-assay coefficients of variation for serum samples were ≤5.6 and 7.6%, respectively. Control testis explants produced an average of 0.19+0.15 ng/ml/explant inhibin B after 24 h of culture, and 0.33+0.09 ng/ml/explant after 48 h.

Cellular Adenosine triphosphosphate (ATP) content was determined by using an ATPLite™ luminescence ATP detection assay system (PerkinElmer Life Science, Boston, MA).

Testosterone determination

Serum samples of the treated male rats were used for estimating testosterone concentration using radioimmunoassay (RIA) method. After incubation, the liquid contents in the tubes were withdrawn and the bound radioactivity was determined using a gamma counter according to the method described by Shalaby et al. (17).

Semen characteristics (Sperm quantity and quality)

The right caudal epididymis was used for sperm motility and left caudal epididymis was used for sperm counts and morphology. Right caudal epididymis was first weighed, placed in a Petri dish. An appropriate dilution (1:20) was made with physiological saline (0.9% NaCl). Caudal epididymis was nicked in few sites with a scalpel blade and kept at 37°C to release the spermatozoa from the tubules. The sperm suspension was examined within 5 min after their isolation from epididymis. The counting of both motile and immotile sperm was carried out at 40 magnification. The calculated results were finally expressed as percent motility. Left caudal epididymis was weighed, diluted at 1:20 with physiological saline (0.9% NaCl) solution in a petri dish and minced with a scalpel blade in the mid-to-distal region. The suspension was kept at 37°C for 5 min for the dispersion of sperm into the medium. Sperm suspension was pipated very gently 20 times and placed in a hemocytometer and the total number of the sperm head counted at 40 magnification. Each sample was counted twice and the mean value was taken for the calculation.

Histopathological examination

Testes of the treated rats were taken and fixed in formalin solution 10%. The fixed specimens were then trimmed, washed and dehydrated in ascending grades of alcohol. These specimens were cleared in xylene, embedded in paraffin, sectioned at 4–6 ml thickness and stained with Hematoxylen and Eosin (H&E) and then examined microscopically according to Lillie (18).

Statistical analysis

Data were collected, arranged and reported as mean ± standard error of mean (S.E.M) of nine groups (each group was considered as one experimental unit), summarized and then analyzed using the computer program SPSS/ version 15.0. The statistical method was one way analyses of variance ANOVA (F-test), and if significant differences between means were found, Duncan's multiple range test (the significant level was defined as $P < 0.05$) was used according to Snedecor et al. (19) to estimate the effect of different treated groups.

RESULTS

The elemental analysis (CHN) agreed quite well with the speculated structure of the solid IMC complexes (Table I). The elemental analysis data of the IMC complexes indicate that the 1:2 (metal: ligand) stoichiometry with Hg (II), Pb (II) and Sn (II) while 1:3 (Metal: ligand) stoichiometry with Bi (III).

Molar conductivities

The molar conductivity values for IMC complexes were measured in DMF at room temperature and located in the range of non-electrolytes for all IMC complexes (20) Table II. The interpretation concerning decreasing of conductivity values back to the deprotonation of carboxylic group for the IMC ligand. This assumption proves that free ligand acts in a bidentate fashion via carboxylic group.

Infrared spectra

The essential infrared data are summarized in Tables II and III and Fig. 1. IMC exhibited a very strong absorption band at 1700 cm^{-1} due to the stretching vibration of ν(C=O) of free ketonic of the carboxylic group. This group is shifted or disappeared

Table I. *Elemental analysis and physical data for IMC complexes.*

Complexes	Mwt.	Color	Content (found) calculated				A (Scm^2mol^{-1})
			% C	% H	% N	%M	
$[Hg (IMC)_2].6H_2O$ ($I,C_{38}H_{42}N_2O_{14}Cl_2Hg$)	1020	Pale white	44.70 (44.82)	4.11 (4.18)	2.74 (2.64)	19.70 (19.98)	5
$[Pb (IMC)_2].6H_2O$ ($II,C_{38}H_{42}N_2O_{14}Cl_2Pb$)	1027	Yellowish white	44.40 (44.32)	4.04 (4.17)	2.97 (2.69)	20.15 (20.23)	11.5
$[Sn(IMC)_2].6H_2O$ (III, $C_{38}H_{42}N_2O_{14}Cl_2Sn$)	940	Yellowish white	48.51 (48.70)	4.74 (4.36)	2.98 (3.12)	2.651 (12.32)	9.5
$[Bi (IMC)_3] .3H_2O$ (IV, $C_{57}H_{51}N_3O_{15}Cl_3Bi$)	1333	White	55.16 (51.41)	3.82 (3.76)	3.15 (3.42)	15.70 (15.93)	12

Table II. *IR Frequencies (cm^{-1}) of IMC and its metal complexes.*

Assignments	**IMC**	I	II	III	IV
ν(OH); H_2O	3450	3431	3435	3348	3430
ν_{as}(CH)	3120, 2985	2928	2928	2926	2926
ν_s(CH)	2890	2356	2356	2362	2362
ν(COOH)	1700	-	-	-	-
$\nu_{as}(COO^-)$	1595	1590	1591,1548	1597,1527	1590
δ(CH)	1490, 1450, 1415	1472	1471	1474	1470,1400
$\nu_s(COO^-)$	1360,1350	1371,1316	1365,1320	1364,1319	1362,1319
ν_{as}(CC)	1300	1224	1227	1226	1225
ν(CN)	1260, 1240, 1077	1153,1077,1028	1146,1077, 1029	1146,1079,1024	1080
ν_s(CC)	933	923	918	919	922
δ(CC)	770	753, 652	753,666	712,674	749
ν(M–O)	-	530, 480	480	554,479	524

in the spectra of its complexes. Interestingly, there are two bands which appeared in the range of 1527–1599 cm^{-1} and corresponded to ν_{as} (COO−) and the other band is exhibited within the range of 1316–1365 cm^{-1} assigned to ν_s(COO−). Accordingly, the antisymmetric and symmetric stretching, vibration modes [ν_{as} (COO−), and ν_s (COO−)] of the COO− group, and the structure of our complexes could be elucidated (21). The direction of the frequency shift of the ν_{as} (COO−) and the ν_s (COO−) bonds in respect to those of the free ion depends on the coordination mode of the COO− group with the metal ion. Nakamoto and McCarthy (22) have established that if the coordination is monodentate (structure I) the ν_{as} (COO−) and ν_s (COO−) will be shifted to higher and lower frequencies, respectively. Whereas, if the coordination is chelating bidentate (structure II) or bridging bidentate (structure III) both ν_{as}(COO−) and ν_s(COO−) frequencies will change in the same direction because the bond orders of both C=O bonds would change by the same amount. Based on these facts and comparison the ν_{as}(COO−) and ν_s(COO−) frequencies of the IMC complexes by the ν_{as}(COO−) and ν_s(COO−) frequencies of sodium carboxylate (23), as shown in Table III, it can be hypothesized that all the prepared complexes are chelating bidentate structure. The stretching broadband vibration of OH− group ν(O–H) occurred as expected (24) at the range 3400 cm^{-1}. The angular deformation motions of the coordinated water in the hydrated IMC can be classified into four types of vibrations: δ_b(bend), δ_r(rock), δ_t(twist) and δ_w(wag).

Table III. *Asymmetric and symmetric stretching vibrations of the carboxylate group.*

Compound	$\nu_{as}(COO^-)$	$\nu_s(COO^-)$	$\nu = \nu_{as}(COO^-) - \nu_s(COO^-)$	Bonding mode
IMC	1595	1338	257	Bidentate
I	1591	1355	236	Bidentate
II	1591	1365	226	Bidentate
III	1590	1364	226	Bidentate
IV	1590	1362	228	Bidentate

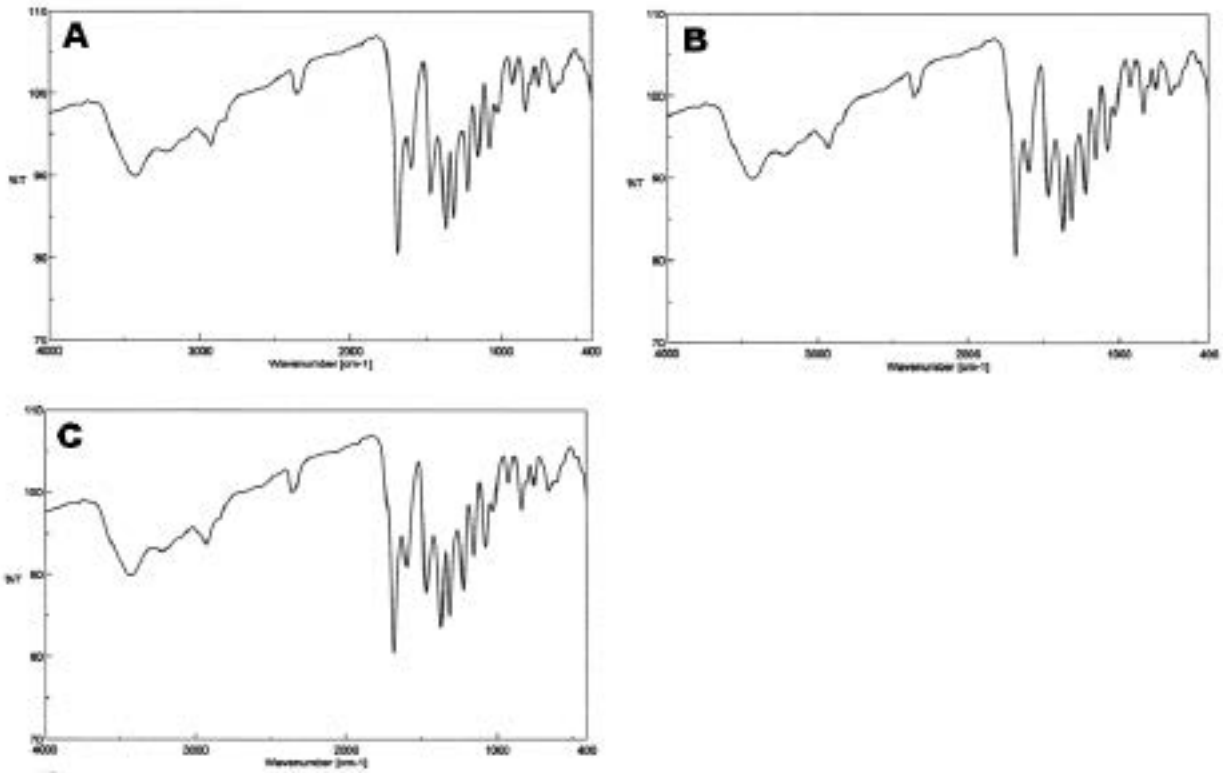

Fig. 1. *Infrared spectra of: (**A**) Hg(II)-IMC, (**B**) Pb(II)-IMC and (**C**) Sn(II)-IMC complexes.*

It should be mentioned here that these assignments for both the bond stretches and angular deformation of the coordinated water molecules fall in the frequency regions reported for related complexes (22). The weak or medium intensity observed in the wave number range (479-554 cm^{-1}) can be assigned to ν(M-O) vibration of IMC chelates.

Electronic absorption spectra

The spectra of IMC complexes in DMF are shown in Fig. 2. There are two detected absorption bands at around 235 NM and 279 nm assigned to π-π* and *n*-π* intraligand transitions, respectively. The first band is probably due to an π-π* of the alkyl group as well as aromatic rings, but the other band is due to presence of COOH and C=O groups (25). After complexation, they are shifted to *ca*. 15 nm and 25 nm, for π-π* and n-π* respectively, confirming the complexation of metal ions via carboxylic group. Also complexes having a band at range 360 nm may be assigned to the ligand to metal charge transfer (26).

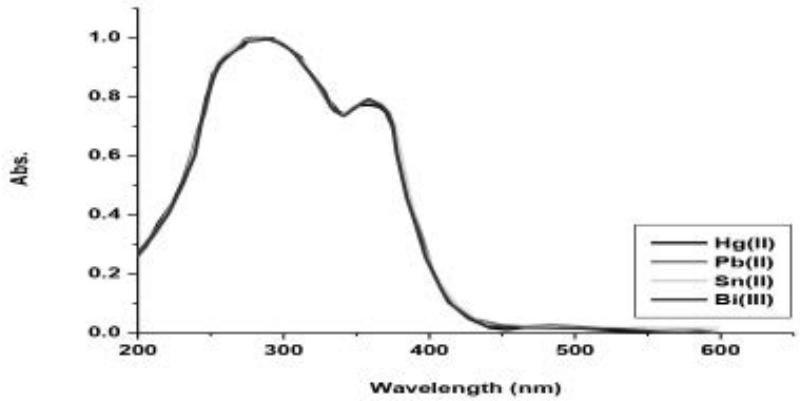

Fig. 2. *Electronic spectra of Hg(II), Pb(II), Sn(II) and Bi(III)-IMC complexes.*

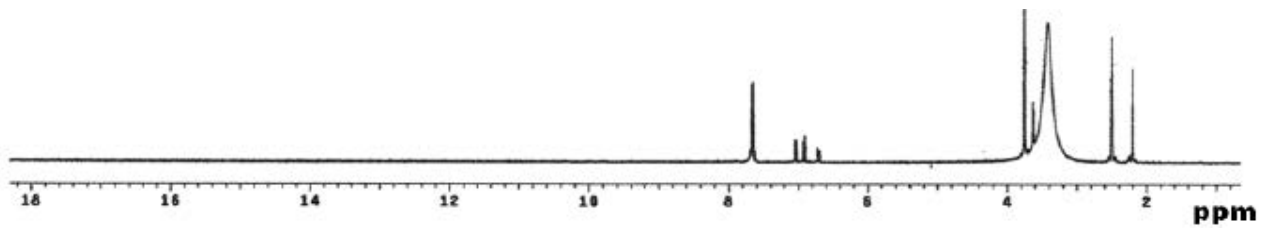

Fig. 3. *^{1}H-NMR spectrum of Hg(II)-IMC complex.*

^{1}HNMR spectra

The proton NMR spectrum of the formed Hg(II) was obtained using DMF as a solvent and is shown in Figs. 3 and 4. The proton NMR spectra for the [Hg $(IMC)_2$].6H_2O show the expected seven signals described for the free IMC around 2.20 ppm, 2.49 ppm, 2.50 ppm (CH_3), 3.75 ppm (CH_2), 6.72 ppm, 7.00 ppm and 7.69 ppm (proton of aromatic ring). These signals are observed at nearly the same frequencies recorded for free IMC and indicated that the magnetic environment associated with these protons has not changed significantly with coordination (2). The proton NMR spectrum for [Hg $(IMC)_2$] 6H_2O show a singlet at 3.41 and 3.75 ppm. This singlet is not observed in the free ligand spectrum and can be assigned due to protons of H_2O molecules, supporting the complex formula. The singlet due to the proton of carboxylic acid group observed in the spectrum of the free ligand is not observed in the complex spectrum. The disappearance of this proton comes into agreement with the coordination through the carboxylic group of IMC. This conclusion supports the suggestion that Indomethacine deprotonated during the reaction with Hg (II) and is consistent with the data previously obtained from the infrared spectrum.

Thermal analysis

The TGA curves for the IMC metal complexes were carried out within a temperature that ranged from 50 to 1000°C. The calculated mass losses were estimated based on the TG data and agree quite well with the molecular formula of the suggested complexes (Table IV). The decomposition stages, temperature ranges, maximum decomposition peaks DTG_{max}, the percentage losses in mass, and the

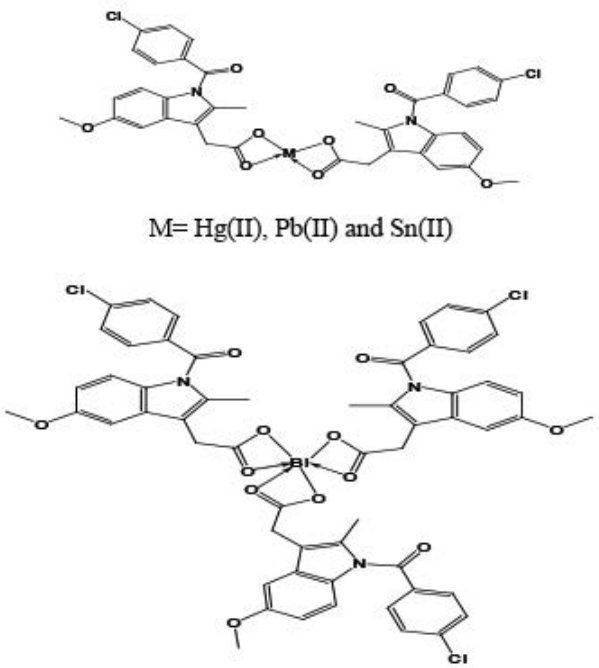

Fig. 4. *Suggested structure of Hg(II), Pb(II), Sn(II) and Bi(III)-IMC complexes.*

assignments of decomposition moieties are given in Table III, which deduced the data reported below.

The thermal decomposition of the mercury complex with the general formula [Hg $(IMC)_2$].$6H_2O$ is thermally decomposed in a successive four decomposition steps. The first estimated mass loss of (obs. = 9.95%) within the temperature range 50–116 °C may be attributed to the loss of ($6H_2O$) molecules of mass loss of (calc. = 10.58 %). The second step which occurs within the temperature range116–200°C with a mass loss (obs. = 38.35%, calc. = 38.72%) is reasonably accounted for the decomposition of $C_{15}H_{20}N_2O_6Cl_2$ (Organic moiety). The third step which occurs at a maximum temperature of 450 °C with a mass loss (obs. = 19.70%, calc. = 19.70%) is reasonably accounted for the evaporation of Hg as vapor. The final decomposition stage which occurs within the temperature range 500–1000°C may be attributed to the loss of $C_{12}H_{10}O_2$ (Organic moiety) with leaving 2C as the residue of decomposition. Thermal degradation of the Pb (II) complex occurs mainly in five degradation stages. The first estimated mass loss of (obs. = 3.42%) within the temperature range 50–162°C may be attributed to the loss of ($2H_2O$) molecules of mass loss of (calc. = 3.50%). The second step occurs within the temperature range 162–270°C with a mass loss (obs. = 31.60%, calc. = 31.15%) and reasonably accounts for the decomposition of $4H_2O$ + $C_6H_{12}N_2O$ (organic moiety). The third step occurs at a maximum temperature of 470°C with a mass loss (obs.= 29.04%, calc. = 29.30%) and reasonably accounts for the loss of C_6H_6O (Organic moiety). The fourth decomposition stage occurs within the temperature range 270–700°C and may be attributed to the loss of $C_6H_4O_6Cl$ (Organic moiety) with a mass loss (obs. = 18.60%, calc. = 18.69%). The final decomposition stage which occurs within the temperature range 700–1000°C may be attributed to the loss of C_6H_4OCl (Organic moiety) with leaving 4C as the residue of decomposition. The Sn(II) complex of IMC gives four main stages of decomposition pattern. The first estimated mass loss of (obs. = 3.75%) within the temperature range 50–170°C may be attributed to the loss of ($2H_2O$) molecules of mass loss of (calc. = 3.82%). The second step which occurs within the temperature range170–250°C with a mass loss (obs. = 24.00%, calc. = 24.06%) is reasonably accounts for the decomposition of $4H_2O$ +$C_7H_{10}N_2O_2$ (Organic moiety). The third step which occurs at a maximum temperature of 470°C with a mass loss (obs. = 18.52%, calc. = 18.19%) is reasonably accounted for by the decomposition of $C_4H_{10}O_3Cl_2$ (Organic moiety) as vapor. The final decomposition stage occurs within the temperature range 660–1000°C and may be attributed to the loss of $C_2H_{10}O_2$ (Organic moiety) with leaving (SnO+25C) as the residue of decomposition. The Bi(III) complex of IMC gives three main stages of decomposition pattern. The first stage, within the temperature range of 50–380°C, represents the loss of three uncoordinated water molecules of mass loss of (obs. = 4.37%, calc. = 4.05%). The second stage (380–724°C) is assigned to the loss of 3HCl+0.5NO+$7H_2$ (obs. = 10.60%, calc. = 10.39%). The final decomposition stage (866–1000°C) is assigned to the loss of $1.5NO_2$+$3.5O_2$+$0.5N_2$+$14H_2$ (obs. = 16.53%, calc. = 16.74%). Then, leaving (BiO1. 5+ residual carbon atoms) as final residue. Finally on the basis of the

Table IV. *Thermal data of IMC complexes.*

Compound	DTG_{max} (°C)	Weight loss (%)		Assignments
		Calc.	Found	
I	116	10.58	9.95	$6H_2O$
	180	38.72	38.35	$C_{15}H_{20}N_2O_6Cl_2$(Organic moiety)
	450	19.70	19.70	Hg
	600	28.82	28.60	$C_{12}H_{10}O_2$(Organic moiety) 2C (Residue)
II	162	3.50	3.42	$2H_2O$
	270	31.15	31.60	$4H_2O+C_6H_{12}N_2O$(Organic moiety)
	470	**29.30**	**29.04**	**Pb+C_6H_6O (Organic moiety)**
	695	**18.69**	**18.60**	**$C_6H_4O_6Cl$ (Organic moiety)**
	900	**12.46**	**11.97**	**C_6H_4OCl (Organic moiety) 4C (Reesidue)**
III	**170**	**3.82**	**3.75**	**$2H_2O$**
	245	**24.06**	**24.00**	**$4H_2O+C_7H_{10}N_2O_2$(Organic moiety)**
	470	**18.19**	**18.52**	**$C_4H_{10}O_3C_{l2}$(Organic moiety)**
	660	**7.02**	**7.41**	**$C_2H_{10}O_2$ (Organic moiety) SnO +25C (Residue)**
IV	**380**	**4.05**	**4.37**	**$3H_2O$**
	724	**10.39**	**10.60**	**$3HCl+0.5NO+7H_2$**
	866	**16.74**	**16.53**	**$1.5NO_2+3.5O_2+0.5N_2+14H_2$ $BiO_{1.5}$ +57C(Residue)**

above studies, the suggested structures of the IMC are be represented in Fig. 4.

Antimicrobial activity

In Table V, the biological activities were increased in the following order: Hg^{+2}/IMC = Sn^{+2}/IMC (2–3.30 cm) > Pb^{+2}/IMC =Bi^{+3}/IMC (1.70–3.00 cm) against the five kinds of bacterial and fungi, *Escherichia coli* (Gram, –ve), *Bacillus subtilis* (Gram, +ve) and antifungal (*Asperagillus oryzae, Asperagillus niger, Asperagillus Flavus*) inhibitory zones. The high sensitivity of the IMC complexes was attributed to hyper-conjugation of the coordinated aromatic Lewis bases, which increases the net electron density on the coordinated metal ion and consequently the higher antimicrobial activity (27).

Effect of SOD on testis and stomach homogenates

The data presented in Table VI indicate that treatment of normal rats with IMC afforded a significant decrease in SOD value in testis homogenate compared to the control group, but this decrease was less intense compared to other groups treated with IMC and its complexes with Hg^{+2}, Pb^{+2} and Sn^{+2} as they showed highly significant decrease in SOD compared to the control group. However, complexation between IMC and Bi^{+3} highly ameliorated SOD value and showed non-significant changes compared to a normal control group. Table VI showed that SOD in stomach homogenates was decreased significantly in all groups treated with IMC and its complexes when compared with the normal control group except the group treated with Bi^{+3} with IMC which showed no significant decrease in SOD compared to a normal control group.

Effect of CAT on testis and stomach homogenates

Treatment of normal rats with IMC elicited a significant decrease in CAT value in testis homogenates compared with the normal control

Table V. *Antimicrobial data of IMC complexes.*

Complexes	Diameter of inhibition zone (cm)				
	E.Coli	***B.subtilis***	***Asperagillus oryzae***	***Asperagillus niger***	***Asperagillus Flavus***
Control	**0**	**0**	**0**	**0**	**0**
I	**2**	**1.7**	**0**	**3.3**	**2**
II	1.7	1.5	1.5	3	1.5
III	2	1.7	0	3.3	2
IV	1.7	1.5	1.5	3	1.5

Table VI. *Effect of **IMC** and its complexes on antioxidant assay (SOD (U/g), MDA(nmol/ml), CAT (U/g) and Reduced glutathione (U/g) in stomach and testis homogenates.*

Item	Cont	**IMC**	Hg^{+2}/ **IMC**	Pb^{+2}/ **IMC**	Sn^{+2}/ **IMC**	Bi^{+3}/ **IMC**
SOD in Testis homogenates	85.32 ± 0.87^{ab}	80.61 ± 1.52^{c}	24.14 ± 2.98^{d}	12.82 ± 0.91^{e}	14.14 ± 0.35^{f}	84.92 ± 1.59^{b}
MDA in Testis homogenates	1.74 ± 0.10^{e}	2.35 ± 0.26^{d}	8.50 ± 0.66^{b}	12.81 ± 0.12^{a}	3.30 ± 0.25^{c}	1.78 ± 0.38^{e}
CAT in Testis homogenates	$8.68\pm0.^{01b}$	2.87 ± 0.02^{d}	1.52 ± 0.01^{e}	1.23 ± 0.01^{e}	7.42 ± 0.02^{c}	9.24 ± 0.03^{a}
Reduced glutathione in Testis homogenates	26.11 ± 0.75^{a}	24.12 ± 0.48^{b}	9.99 ± 0.58^{c}	1.30 ± 0.94^{e}	4.01 ± 0.82^{d}	26.03 ± 1.56^{a}
SOD in Stomach homogenates	65.20 ± 0.23^{ab}	51.30 ± 2.51^{c}	35.65 ± 3.25^{e}	23.52 ± 2.63^{f}	40.32 ± 2.11^{d}	61.87 ± 2.98^{b}
MDA in Stomach homogenates	3.20 ± 0.12^{ef}	5.32 ± 0.62^{c}	8.10 ± 1.32^{ab}	7.98 ± 1.01^{b}	4.20 ± 0.75^{d}	3.00 ± 0.32^{f}
CAT in Stomach homogenates	7.65 ± 0.63^{ab}	6.50 ± 0.65^{d}	4.20 ± 0.98^{e}	3.65 ± 0.55^{f}	6.99 ± 0.87^{cd}	7.20 ± 0.68^{b}
Reduced glutathione in Stomach homogenates	30.63 ± 2.21^{a}	25.63 ± 2.01^{d}	24.21 ± 2.52^{e}	21.52 ± 1.95^{f}	27.42 ± 3.36^{c}	28.52 ± 1.20^{b}

Means within the same column in each category carrying different litters are significant at ($P \leq 0.05$) using Duncan's multiple range tests, where the highest mean value has symbol (a) and decreasing in value were assigned alphabetically.

group, as shown in Table VI, but the groups treated with IMC complexes with Hg^{+2}, Pb^{+2} and Sn^{+2} were much decreased in CAT in testis homogenates compared to the normal control group but Bi^{+3}/IMC complex showed the highest value in CAT activity and increased significantly compared to the normal control group. As shown in Table VI, it is obvious that treatment of normal rats with IMC complexes with Bi^{+3} elicited non-significant changes in CAT activity in stomach homogenates when compared with the control group. However, other groups treated with IMC and its complexes with Hg^{+2}, Pb^{+2} and Sn^{+2} showed a significant decrease in CAT activity, but the least value in decreasing CAT was Sn^{+2} with the IMC treated group as the decrease had a less intense effect.

Table VII. *Effect of IMC and its complexes on Inhibin enzyme (ng/ml) activity after (48 hours) in male rats.*

Item	Cont	**IMC**	Hg^{+2}/ **IMC**	Pb^{+2}/ **IMC**	Sn^{+2}/ **IMC**	Bi^{+3}/ **IMC**
Inhibin B	0.33 ± 0.09^{a}	0.25 ± 0.09^{d}	0.26 ± 0.00^{cd}	0.20 ± 0.07^{f}	0.22 ± 0.02^{ef}	0.31 ± 0.03^{b}

Means within the same column in each category carrying different litters are significant at ($P \leq 0.05$) using Duncan's multiple range tests, where the highest mean value has symbol (a) and decreasing in value were assigned alphabetically

Table VIII. *Effect of IMC and its complexes on ATP (%)activity in male rats.*

Item	Cont	**IMC**	Hg^{+2}/ **IMC**	Pb^{+2}/ **IMC**	Sn^{+2}/ **IMC**	Bi^{+3}/ **IMC**
Cellular ATP (%)	110.22 ± 4.20^{a}	75.22 ± 4.20^{c}	60.20 ± 3.10^{d}	45.20 ± 3.56^{f}	50.20 ± 4.10^{e}	95.85 ± 2.31^{b}

Means within the same column in each category carrying different litters are significant at ($P \leq 0.05$) using Duncan's multiple range tests, where the highest mean value has symbol (a) and decreasing in value were assigned alphabetically.

Table IX. *Effect of IMC and its complexes on Testosterone hormone (μIU/ml) activity in male rats.*

Item	Cont	**IMC**	Hg^{+2}/ **IMC**	Pb^{+2}/ **IMC**	Sn^{+2}/ **IMC**	Bi^{+3}/ **IMC**
Testosterone hormone	3.24 ± 0.0^{8a}b	1.68 ± 0.07^{d}	1.18 ± 0.05^{e}	1.05 ± 0.05^{f}	2.20 ± 0.15^{c}	3.16 ± 0.05^{b}

Means within the same column in each category carrying different litters are significant at ($P \leq 0.05$) using Duncan's multiple range tests, where the highest mean value has symbol (a) and decreasing in value were assigned alphabetically.

Table X. *Effect of IMC and its complexes on semen characteristics in male rats.*

Item	Cont	**IMC**	Hg^{+2}/ **IMC**	Pb^{+2}/ **IMC**	Sn^{+2}/ **IMC**	Bi^{+3}/ **IMC**
Total count$X10^{6}$	78.05 ± 3.52^{b}	65.52 ± 3.01^{c}	60.52 ± 2.25^{d}	20.42 ± 2.05^{e}	60.54 ± 2.02^{d}	85.92 ± 5.96^{a}
Motility%	70.25 ± 3.25^{a}	45.12 ± 2.25^{b}	35.63 ± 2.45^{c}	25.32 ± 3.11^{e}	30.24 ± 3.11^{d}	70.11 ± 4.31^{a}
Abnormal forms%	30.20 ± 1.53^{ef}	45.53 ± 4.32^{d}	55.26 ± 3.21^{c}	58.25 ± 3.21^{bc}	60.20 ± 3.50^{a}	29.52 ± 2.30^{f}
Viability% after 1/2 h	75.20 ± 3.25^{ab}	55.20 ± 3.52^{c}	45.21 ± 2.20^{d}	35.20 ± 1.20^{e}	30.25 ± 2.13^{f}	74.52 ± 3.24^{b}

Means within the same column in each category carrying different litters are significant at ($P \leq 0.05$) using Duncan's multiple range tests, where the highest mean value has symbol (a) and decreasing in value were assigned alphabetically.

Effect of GSH on testis and stomach homogenates

Then data presented in Table VI indicate that Bi^{+3} complex with IMC afforded non-significant changes either by a decrease or increase in GSH in testis homogenates when compared to the normal control group, while other groups treated with IMC and its other complexes showed a significant decrease in GSH compared with the control group, but less decrease was noticed in the IMC treated group.

GSH value in stomach homogenates was significantly reduced in all groups treated with IMC complexes when compared to a normal control group, but the effect was less intense in groups treated with Sn^{+2} and Bi^{+3}/IMC complex-treated groups.

Effect of MDA on testis and stomach homogenates

Table VI shows that IMC afforded a highly significant increase in MDA in testis homogenates in groups treated with Hg^{+2} and Pb^{+2}/IMC complexes as compared to the normal control group, and there were also significant decreases in other treated groups, but with less intense effect while the Bi^{+3}/IMC-treated group showed no significant increase in MDA compared to a normal control group.

With regard to the activity of MDA in stomach homogenates, there were slightly significant increases in MDA activity in the IMC treated groups and its complexes except the Bi^{+3}/IMC-treated group which showed no significant increase in MDA

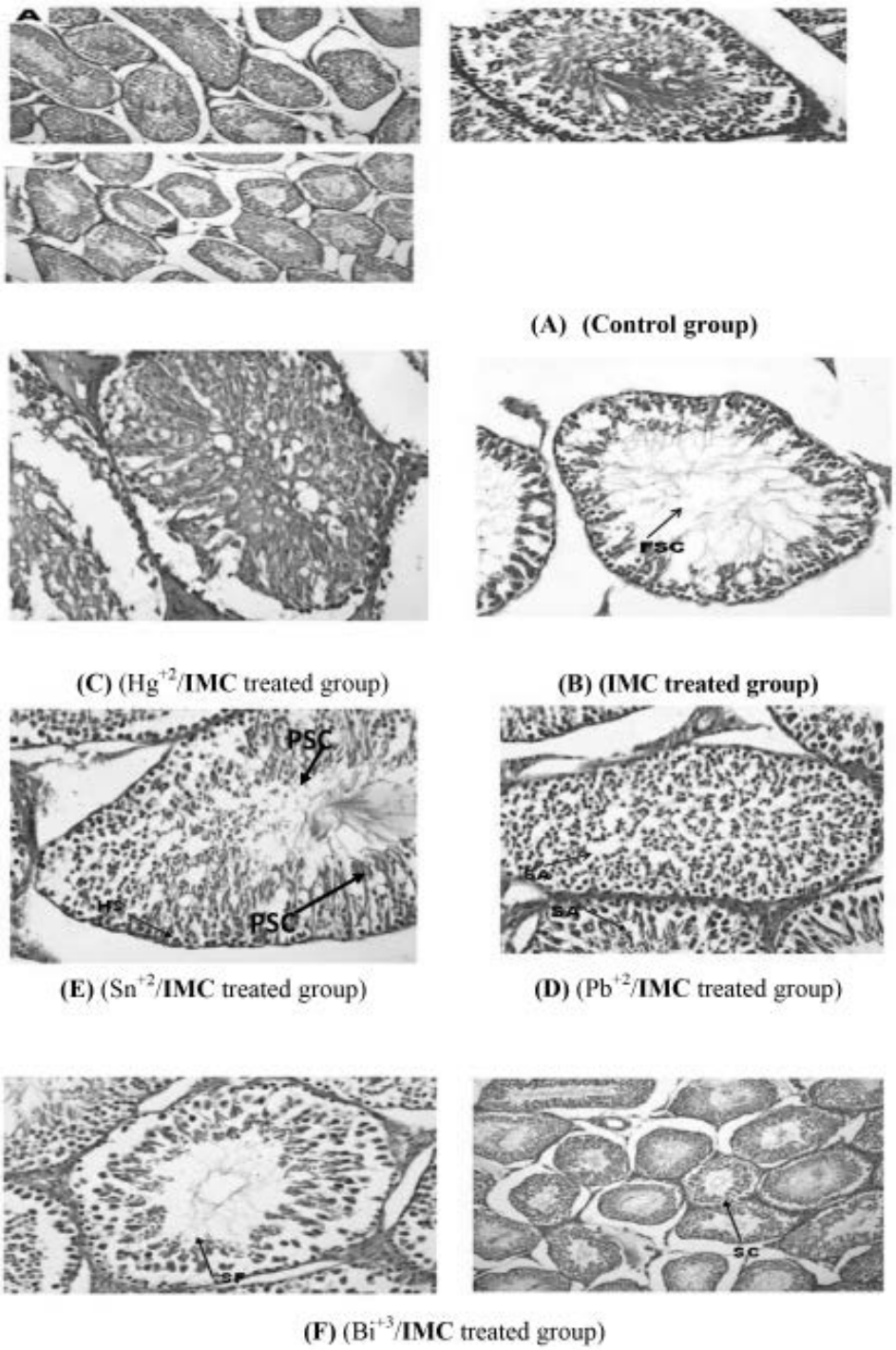

Fig. 5. ***A)*** *Cross-section of rat testis of group (1) (control group) treated with isotonic solution showing seminiferous tubule lined by layers of spermatogenic cells up to sperm formation and surrounded by a thin basement membrane (H and E x 200) (SF: sperm formation).* ***B)*** *Cross-section of rat testis of group (2) treated with (IMC-treated group) showing seminifeous tubules lined by few layers of spermetrogenic cells and few sperms (hypospermatogenesis) (H and E x 200) (FSC: Few spermatogenic cells, HS: hypospermatogenesis).* ***C)*** *Cross-section of rat testis of group (3) treated with (Hg^{+2}/IMC treated group) showing seminferous tubules filled by primary spermatogonia only, with no sperm formation (spermatogenic*

arrest) (H and E x 200) (PSC: Primary spermatogenic cells). ***D****) Cross-section of rat testis of group (4) treated with (Pb^{+2}/IMC treated group) showing seminiferous tubules filled by spermatogenic cells up to spermatid only, with no sperm formation (spermatogenic arrest) (HandE x 200) (SA: spermatogenic arrest).* ***E****) Cross-section of rat testis of group (5) treated with (Sn^{+2}/IMC-treated group) (60 mg/kg) respectively for 3 successive days showing semineferous tubule lined by few layers of spermatogenic cells and few sperms (hypospermatogenesis) (H&EX200) (HS: Hypospermatogenesis).* ***F****) Cross-section of rat testis of group (6) (Bi^{+3}/IMC-treated group) (60 mg/kg) treated respectively for 3 successive days showing seminiferous tubules lined by several layers of spermatogenic cells up to sperm formation but surrounded by mild edematous stroma (H and E x 200) (SF: sperm formation, SC: speromatogenic cells).*

activity compared to the normal control group.

Effect on Inhibin B enzyme activity

Table VII indicates that treatment of normal rats with IMC and its complexes (Hg^{+2}, Pb^{+2}, Sn^{+2}) afforded significant decrease in inhibin B enzyme when compared with the normal control group, but the Bi^{+3}/IMC complex afforded non-significant decrease in inhibin B when compared with the normal control group.

Effect on Cellular ATP activity

There was a reduction in ATP activity in both the IMC-treated group and IMC/complexes-treated groups when compared with the normal control group as shown in Table VIII, but the Bi^{+3}/IMC-treated group afforded statically less significant decrease in ATP level when compared with the normal control group.

Effect on testosterone hormone

Treatment of normal rats with Bi^{+3}/ IMC complex elicited a non-significant decrease in testosterone hormone when compared with the normal control group, while other groups treated with IMC and its complexes (Hg^{+2}, Pb^{+2} and Sn^{+2}) showed a significant decrease in testosterone hormone when compared with the normal control group as shown in Table IX.

Effect on semen characteristics

Table X indicates elevation in total count of sperm in the group treated with Bi^{+3}/IMC when compared with the normal control group, while the IMC-treated group, Sn^{+2}/ IMC and Hg^{+2}/IMC, showed significant decrease in total count in sperm, but the Pb^{+2}/IMC treated group showed the least count of semen when compared with control group and other treated groups. Table X shows that there were non-significant changes in sperm motility in the group treated with Bi^{+3}/IMC complex compared with the normal control group while other treated groups elicited a significant decrease in sperm motility when compared with the normal control group, but the lowest percentage was in the Pb^{+2}/IMC-treated group compared to the other treated groups. Table X shows that the highest percentage of abnormal forms of sperm were in the Sn^{+2}/IMC complex-treated group followed by the Pb^{+2}/IMC complex-treated group when compared with the normal control group and other treated groups with IMC and its complexes. The lowest percentage of abnormal forms were shown in the normal control group, followed by the Bi^{+3}/IMC-treated group. It was shown that the group treated with Bi^{+3}/IMC complex elicited a non-significant decrease in viability of sperm after 30 min when compared with the normal control group, while other treated groups showed a significant decrease in viability of sperm compared with the normal control group, but the lowest percentage of viability was shown in the Sn^{+2}/IMC-treated group when compared with the control group and other treated groups, as shown in Table X.

Histopathological effects

Control group. Microscopically, seminiferous tubules were seen lined by layers of spermatogenic cells up to sperm formation and surrounded by a thin basement membrane (Fig. 5A).

IMC-treated group. Microscopically, seminiferous tubules were shown, lined with a few layers of spermatogenic cells and few sperm (hypospermatogenesis) (Fig. 5B).

Hg^{+2}/IMC-treated group. Microscopically, testis showed seminiferous tubules filled by primary spermatogonia only,with no sperm formation (spermatogenic arrest) (Fig. 5C).

Pb^{+2}/IMC-treated group. Microscopically, showed seminiferous tubules filled with spermatogenic cells up to spermatid only, with no sperm formation (spermatogenic arrest) (Fig. 5D).

Sn^{+2}/IMC-treated group. Microscopically, showed seminiferous tubule lined with a few layers of spermatogenic cells and few sperm (Hypospermatogenesis) (Fig. 5E).

Bi^{+3}/IMC-treated group. Microscopically, showed seminiferous tubules lined by several layers of spermatogenic cells up to sperm formation, but surrounded by mild edematous stroma (Fig. 5F).

DISCUSSION

Effect of SOD on testis and stomach homogenates

Superoxide dismutases are enzymes that catalyze the dismutation of superoxide (O^{2-}) into oxygen and hydrogen peroxide. Thus, they are an important antioxidant defense in nearly all cells exposed to oxygen and oxidative stress resulting in the accumulation of lipid peroxidation products in different organs of rats. Reactive oxygen species (ROS) and its metabolites are the subject of intense research because of their active role in cellular physiology and pathogenesis of a number of diseases. ROS also lead to oxidative damage (28). Inflammatory reactions induced by IMC are a significant source of ROS in the gastric tissue. ROS, e.g., hydrogen peroxide (H_2O_2) and the superoxide radical (O_2), play a causative role in cancer, gastric injury, atherosclerosis, neurodegeneration and arthritis through various processes, including the generation of ROS, inhibition of prostaglandin synthesis, infiltration of polymorphonuclear leukocytes, induction of apoptosis and initiation of lipid peroxidation. Lipid peroxidation is the process of oxidative degradation of polyunsaturated fatty acids. The occurrence of degraded polyunsaturated fatty acids in biological membranes causes impaired membrane fluidity and inactivation of several membrane-bound enzymes (29) which may be the reason for the unsuccessful role of IMC complexes with Hg^{+2}, Pb^{+2} and Sn^{+2} in alleviating the toxicity of these free radicals and thus decreasing SOD activity. Accordingly, the group treated with Bi^{+3}/IMC had success to a great extent in reducing these free radicals and capturing them, thus increasing the antioxidant capacity by increasing SOD activity.

Effect of CAT on testis and stomach homogenates

Nonsteroidal anti-inflammatory drugs (NSAIDs) are widely used in the treatment of pain, fever and inflammation. However, these drugs have some side effects, especially in the gastrointestinal tract. Recently, reactive oxygen species (ROS) have also been shown to play a critical role in the gastric ulceration process. The role of ROS in the development of acute experimental gastric lesions induced by stress, ethanol and NSAIDs is well known (30). The IMC-treated group significantly reduced CAT activity compared to control group, but the Bi^{+3}/IMC complex succeeded in improving antioxidant activities by increasing CAT activity with no significant changes compared to the normal control group.

Effect of GSH on testis and stomach homogenates

Recent studies have also shown that ROS contents such as superoxide, hydroxyl radicals (OH^-) and singlet oxygen, reduced the occurrence of some diseases (31). ROS damage membrane proteins by causing lipid peroxidation in membranes by attacking unsaturated fatty acids (31). The damage to membrane proteins decreases the membrane permeability, the activities of enzymes and receptors and the activation of cells. Bi^{+3}/IMC complex may chelate free radicals, thus increasing GSH activity.

Effect of MDA on testis and stomach homogenates

Recent studies have suggested that IMC performs pro-oxidant activity and initiates lipid peroxidation by generating ROS which is the cause of increasing MDA level in testis tissues and the damge we noticed in testis tissues, also interfering with the mucosal cell endogenous antioxidant-systems. Krishnendu et al. (29) reported that IMC administration produces H_2O_2, which acts as a mediator to inhibit metalloproteinase (MMP)-2 gene transcription and decrease MMP-2 activity at the synthesis and secretion levels in acute gastric ulcers (29). The presence of O_2 may be considered a reason for occurrence of gastric damage and other tissue damage. Thus, much attention has recently been focused on oxygen-derived free radicals. Oxygen-handling cells contain antioxidant enzymes that can protect them against oxidative

stress. The enzymatic and non-enzymatic antioxidant defenses include superoxide dismutase, glutathione peroxidase, catalase, glutathione reductase (32). These antioxidants also play an important role in the prevention of gastric damage in addition to our proven Bi^{+3}/IMC complex, which achieved a great role in the prevention of oxidative stress induced by IMC alone and retrieving the antioxidant enzymes to their normal value or with non-significant decrease or increase compared to the normal control group.

Bismuth accumulation in the gastric mucus during the evolution of mucosal injury may play an important role in the gastroprotective effect of bismuth subsalicylate against indomethacin injury and we are in agrement with Koo et al., (36) who reported that IMC (60 mg/kg) significantly thinned the mucus gel layer consistent with a weakened gastric mucosal barrier to acid. Bismuth partially reversed this effect of IMC. The mechanism underlying the gastroprotective effect of the bismuth compounds, however, is poorly understood. Since bismuth salts have no effect on acid secretion but act on coating over the lining of peptic ulcers, their effects are thought to be mostly on gastric defensive mechanisms. Bismuth preferentially coats ulcers in patients after taking colloidal bismuth and this greatly supported our results. Our results seem to be conceivable with those of Lee (35) which indicated that bismuth is considered to provide a protective layer and we believe that bismuth has a great role in reducing the MDA level, thus protecting gastric mucosa and testis tissues.

Effect on Inhibin B enzyme activity

The only hormone that remained almost totally unaffected by a direct exposure to mild analgesics like IMC was the Sertoli cell product, inhibin B. In similar conditions, inhibin B production was unaffected by the exposure to phthalates (33) which is contrary to our results, as Inhibin B was effected after exposure to IMC and its novel complexes. Although PGE2 and PGI2 are synthesized by Sertoli cells in adult rats, before this work their presence in adult human Sertoli cells has never been explored, and nothing is known about their link, if any, with Sertoli cell products. Inhibin B secretion by rat Sertoli cells is regulated by the inflammatory mediator interleukin (IL)-1b. IL-1b induces COX-2 in various tissues, including Leydig cells in infertile men (34); therefore, the Pb^{+2}/IMC, Hg^{+2}/IMC and Sn^{+2}/IMC inhibition of inhibin B production may be a consequence of a putative link between the PG system and inhibin B production by Sertoli cells. However, this suggestion is speculative at this stage. We report the first evidence that direct exposure to mild analgesics can result in several endocrine disturbances, causing an unbalance in the hormonal activity of the adult testis in short-term culture. The present *in vitro* results highlight the risks associated with the abusive use of mild analgesics, alone or with some metal complexes, for the testicular endocrine system in men, but the high ameliorative effect was in Bi^{+3}/IMC and we will carry out further study on novel metal complexes with IMC to ameliorate this risk effect.

Effect on cellular ATP activity

As a consecutive result of lipid peroxidation occurrence due to IMC and its complexes with Hg^{+2}, Pb^{+2} and Sn^{+2}, the expected result was the reduction of both cellular ATP in these treated groups, but there significant increment was observed in the group treated with Bi^{+3}/IMC complex which also succeeded to a great extent in the reduction of SOD and thus improvement of ATP activity.

Effect on testosterone hormone

The testosterone hormone level decrease induced by mild analgesics appeared to be unrelated to PG production. Indeed, although indomethacin treatments and its complexes were associated with major anti-PG effects, only Pb^{+2}/IMC significantly inhibited testosterone production, as shown in Table IX.

Effect on semen characteristics

The administration of IMC brought about a marked alteration in the number of spermatogenic elements and spermatozoa that was also observed (1) with different doses and exposure time from the present study. Sperm motility is an important functional measurement to predict sperm fertilizing capacity. Any negative impact on motility would seriously affect fertilizing ability. In the present study, the marked inhibition of sperm motility in the groups treated with IMC and their complexes (Hg^{+2}, Sn^{+2} and Pb^{+2}) may be because of low levels of ATP

content (28) which was increased in the Bi^{+3}/IMC-treated group as a result of increasing ATP content. Sperm motility may be affected by altering enzymatic activities of the oxidation phosphorolytic process. An oxidative phosphorolytic process is required for ATP production, a source of energy for the forward movement of spermatozoa (29). The full ATP pool is crucial for normal spermatozoa movement and a slight deprivation of ATP leads to reduction in motility, which may cause infertility. Sperm count is considered to be one of the important factors that affect fertility (29). Suppression of gonadotrophins might have caused a decrease in sperm density in testes (1). Also, IMC has a direct effect on Sertoli cell function, which appears to be involved in the control of spermiation, and when disturbed causes epithelial disorganization and subsequent tubular atrophy (29). The negative fertility test may be attributed to lack of forward progression and reduction in density of spermatozoa and altered biochemical milieu of the caudal epididymis as shown in Hg^{+2}, Pb^{+2} and Sn^{+2}/IMC complexes. The present study considers the first study that used these novel metal complexes with IMC against the side effects of IMC. Thus, our results, recommending the use of Bi^{+3}/IMC as it ameliorates to a high extent the possible side effects of indomethacin, are greatly in support of and reinforcthe study by Tanaka et al. (34) who indicated that bismuth compounds prevent gastric injury from the short-term administration of nonsteroidal anti-inflammatory drugs.

Histopathological effect

Of great importance in the present study, is that Bi^{+3}/IMC possesses the capacity to protect the sperm, testes and enzymes from deleterious actions of IMC with the appearance of mild edema. Bi^{+3}/IMC increased ($P < 0.05$) the levels of testosterone, relative testes and epididymis weight, and alleviated the negative effects of IMC. These results were confirmed by our biochemical findings, which showed high improvement in testis tissue antioxidant parameters which is very similar to a normal control group and not like other IMC complexes which showed some injury in testis tissues.

ACKNOWLEDGEMENTS

The authors would like to extend their sincere appreciation to Zagazig University for supporting this scientific research and to the Deanship of Scientific Research at King Saud University for its funding of this research through the Research Group no: RG-1436-015.

REFERENCES

1. Hédoux A, Paccou L, Guinet Y, Willart JF, Descamps M. Using the low-frequency Raman spectroscopy to analyze the crystallization of amorphous indomethacin. Eur J Pharm Sci 2009; 38:156-64.
2. Jambhekar S, Casella R, Maher T. The physicochemical characteristics and bioavailability of indomethacin from β-cyclodextrin, hydroxyethyl-β-cyclodextrin, and hydroxypropyl-β-cyclodextrin complexes. Int J Pharm 2004; 270:149-66.
3. Fini A, Cavallari C, Rabasco Alvarez A M, Rodriguez ML. Diclofenac salts, part 6: Release from lipid microspheres. J Pharm Sci 2011; 100:3482-94.
4. Casella R, Williams DA, Jambhekar SS. Solid-state β-cyclodextrin complexes containing indomethacin, ammonia and water. Int J Pharm 1998; 165:1-14.
5. Kovala-Demertzi D, Theodorou A, Demertzis MA, Rilptopoulou CP, Terzis A. Palladium(II) complexes of 2-acetylpyridine N(4)- methyl, N(4)-ethyl and N(4)-phenyl-thiosemicarbazones. Crystal structure of chloro(2-acetylpyridine N(4)-methylthiosemicarbazato) Palladium(II). J Inorg Biochem 1996; 65:151-57.
6. Morzyk-Ociepa B, Rozycka-Sokolowska E. Structures and spectroscopic studies of indolecarboxylic acids. Part III. Diamminetetrakis-μ-(O,O'-indole-3-carboxylate) dicopper(II). J Mol Struct 2006; 784:69-77.
7. Galani A, Kovala-Demertzi D, Kourkoumelis N, et al. Organotin adducts of indomethacin: synthesis, crystal structures and spectral characterization of the first organotin complexes of indomethacin. Polyhedron 2004; 23:2021-30.
8. Gupta R, Saxena RK, Chatarvedi P, Virdi JS. Chitinase production by *Streptomyces viridificans*: its potential in fungal cell wall lysis.J App Bacteriol 1995; 78:378-83.
9. Mion F, Cuber JC, Minaire Y, Chayvialle JA. Short term effects of indomethacin on rat small intestinal

permeability. Role of eicosanoids and platelet activating factor. Gut 1994; 35:490-95.
10. Tanaka S, Guth P, Paulsen H, Kaunitz JD. Gastroprotective effect of ranitidine bismuth citrate is associated with increased mucous bismuth concentration in rats. Gut 1996; 39:164-71.
11. Paget S, Parnes R. Evaluation of drug activities and pharmacometrics. Ed. Laurance and Bacharach. Vol1. Academic Press. New York (1964).
12. Scherners S. The blood morphology of laboratory animals. Blackwell Scientific Publication (3rd Ed); Sci 72:363-68(1967).
13. Habig W, Pabast M, Jakoby WJ. Glutathione S-transferases. The first enzymatic step in mercapturic acid formation. Biol Chem 1974; 249:7130-39.
14. Aebi H. Catalase in vitro. Methods Enzymol 1984; 105:121-26.
15. Nishikimi M, Roa NA, Yogi K. Measurement of superoxide dismutase. Biochem Biophys Res Commun 1972; 46(2):849-54.
16. Ohkawa H, Ohishi W, Yagi K. Assay for lipid peroxides in animal tissues by thiobarbituric acid reaction. Anal Biochem 1979; 95(2):351-58.
17. Shalaby MA, El-Zorbaa HY, Ziada RM. Reproductive toxicity of methomylinsecticide in male rats and protective effect of folic acid. Food Chemical Toxicol 2010; 48(11):3221-26.
18. Lillie RD. "Histopathological Technique and Practical Histochemistry", 3rd ed., Published by the Blakistar Division of McGraw-Hill Book Co., York, Toronto, London, (1965).
19. Snedecor GW, Cochran WG, Statistical Methods (8th Ed), Ames Iowa State University, (1982).
20. Geary WJ. The use of conductivity measurements in organic solvents for the characterization of coordination compounds. Coord Chem Rev 1971; 7: 81-122.
21. Mesubi MA. An infrared study of zinc, cadmium and lead salts of some fatty acids. J Mol Struct 1982; 81:61-71.
22. Nakamato K, McCarthy PJ. "Spectroscopy and Structure of Metal Chelate Compounds", John Wiley, New York, p. 268(1968).
23. Goto R, Takenaka T. Quantitative determination of marine toxins associated with diarrhetic shellfish poisoning by liquid chromatography coupled with mass spectrometry. Bull Chem Soc Jpn 1963; 84:392-99.
24. Gelfand LS, Iaconianni FJ, Pytlewski LL, Speca AN, Mikulski CM, Karayannis NM. Nicotinic and isonicotinic acid n-oxide interactions with 3d metal perchlorates. J Inorg Nuc Chem 1980; 42:377-85.
25. Fasman GD, "Handbook of Biochemistry and Molecular Biology, Nucleic Acids", I, CRC Press, pp.65–215 (1975).
26. Cotton FA, Wilkinson CW. Advanced Inorganic Chemistry, 3th ed., Interscience Publisher, New York, (1972).
27. Osowole AA, Woods JAO, Fagade OE, Odunola OA. Physicochemical properties of some nickel(II) 3-chloro ¢-ketoamines and their adducts with 2,2-bipyridyl and 1,10-phenanthroline. Bioscience Res Commun 2002; 14:531-35.
28. Messarah M, Saoudi M, Boumendjel A, Boulakoud MS, El-Feki A. Oxidative stress induced by thyroid dysfunction in rat erythrocytes and heart. Environ Toxicol Pharm 2011; 31:33-41.
29. Krishnendu G, Parag K, Aditi B, Russel JR, Snehasikta S. Hydrogen peroxide-mediated downregulation of matrix metalloprotease-2 in indomethacin-induced acutre gastric ulceration is blocked by melatonin and other antioxidants. Free Radical Bio Med 2006; 41:911-25.
30. Das D, Bandyopadhyay D, Bhattacharjee M, Banerjee RK. Hydroxyl radical is the major causative factor in stress-induced gastric ulceration. Free Radical Bio Med 1997; 23:8-18.
31. Ames BN, Shigenaga MK, Hagen TM. Oxidants, antioxidants, and the degenerative diseases of aging. P Natl acad sci 1993; 90:7915-22.
32. Hamza RZ, El-Shenawy NS, Ismail HA. Protective effects of blackberry and quercetin on sodium fluoride-induced oxidative stress and histological changes in the hepatic, renal, testis and brain tissue of male rat. J Basic Clin Physiol Pharm 2015; 26(3):237-51.
33. Ferlin A, Pepe A, Gianesello L, et al. Mutations in the Insulin-Like Factor 3 Receptor Are Associated With Osteoporosis. J Bone Miner Res 2008; 23:683- 93.
34. Tanaka S, Guth PH, Carry OR, Kaunitz JD. Cytoprotective effect of bismuth subsalicylate in indomethacin-treated rats is associated with

enhanced mucus bismuth concentration. Aliment Pharm Therap 1997; 11:605-12.
35. Lee SP. A potential mechanism of action of colloidal bismuth subcitrate: diffusion barrier to hydrochloric acid. Scand. Gast 1982; 17:17-21.
36. Koo J, Ho J, Lam SK, Wong J, Ong GB. Selective coating of gastric ulcer tripotassium dicitrato-bismuthate in the rat. Gast 1982; 82:864-70.

CAPACITIVE COUPLING ELECTRIC FIELDS IN THE TREATMENT OF VERTEBRAL COMPRESSION FRACTURES

A. PIAZZOLLA[1], G. SOLARINO[1], D. BIZZOCA[1], N. GAROFALO[1], F. DICUONZO[2], S. SETTI[3] and B. MORETTI[1]

[1]Department of Basic Medical Sciences, Neuroscience and Sense Organs, Orthopedic Clinic, School of Medicine, University of Bari "Aldo Moro", Azienda Ospedaliero-Universitaria Policlinico, Bari, Italy; [2]Department of Basic Medical Sciences, Neuroscience and Sense Organs, Neuroradiology Section, School of Medicine, University of Bari "Aldo Moro", Azienda Ospedaliero-Universitaria Policlinico, Bari, Italy; [3]IGEA SpA - Clinical Biophysics, Carpi (Mo), Italy

Received February 1, 2015 – Accepted May 26, 2015

Positive effects of Capacitive Coupling Electric Field (CCEF) stimulation are described for several orthopedic indications such as the healing of recent fractures, non-unions and spinal fusion, due to the capacity to involve the up-regulation of osteopromotive factors. *In vitro* studies on MC3T3-E1 bone cells showed that CCEF acts opening the plasma membrane voltage gated calcium channels, thus increasing the cytosolic calcium concentration and the phospholipase A2 (PLA2) activity. Cytosolic calcium activates the calmodulin pathway, thus resulting in an up-regulated expression of osteogenic genes, such as transforming growth factor-β superfamily genes (TGF-β1, -β2 -β3, bone morphogenetic protein-2 and -4), fibroblast growth factor (FGF)-2, osteocalcin (BGP) and alkaline phosphatase (ALP). PLA2 acts increasing the synthesis of Prostaglandin E2 (PGE2), which promotes osteogenesis by raising the cellular L-ascorbic acid uptake through the membrane carrier sodium vitamin C transporter-2 (SVCT-2). *In vivo*, Brighton et al. in a castration-induced osteoporosis animal model, demonstrated that CCEF was able to restore bone mass/unit volume in the rat vertebral body. To investigate the role of CCEF stimulation in vertebral bone marrow edema (VBME) its percentage was assessed in 24 patients with 25 acute vertebral compression fractures (VCFs) conservatively treated with CCEF (group A) or without CCEF (group B) using serial MR imaging follow-up at 0, 30, 60, 90 days. Pain and quality of life were assessed by visual analog scale (VAS) and Oswestry Low Back Disability Index (ODI) in the same periods. At 90 day follow-up the complete resolution of VBME was found only in group A (p=0.0001). A significant improvement of VAS (p=0.007) and ODI (p=0.002) was also observed in group A. This preliminary observational study shows that patients treated with CCEF stimulation present an improvement of clinical symptoms with faster fracture healing and a complete VBME resolution.

Key words: capacitively coupling electric fields, vertebral compression fractures, vertebral bone marrow edema, magnetic resonance imaging, spine, osteoporosis

Mailing address: Andrea Piazzolla, M.D.,
Department of Basic Medical Sciences,
Neuroscience and Sense Organs,
Orthopedic Clinic, School of Medicine,
University of Bari "Aldo Moro",
Azienda Ospedaliero-Universitaria Policlinico,
Piazza Giulio Cesare 11, 70100 Bari, Italy
Tel.: +39 0805592720
e-mail: dott.piazzolla@gmail.com

0393-974X (2015)

Vertebral compression fractures (VCFs) are the most common type of osteoporotic fractures, with an estimated annual incidence of 700,000 in the USA (1) and 1.4 million in Europe (2). The annual incidence of VCFs is 10.7 per 1,000 women and 5.7 per 1,000 men (3). The prevalence of these fractures increases with age, reaching 40% by age 80 (4).

The presence of vertebral bone marrow edema (VBME) on magnetic resonance imaging (MRI) is a marker of acute/subacute VCFs or incomplete fracture healing (3, 5). VBME is presumably the result of micro fractures within the medullar bone and resultant hemorrhage (5).

Acute VCFs have an important impact on the patient's health status; they may cause: back pain (3, 5), reduced range of motion (6), slower gait (7) and impaired pulmonary function (7, 8).

There is currently no consensus as to the best conservative management of the acute painful vertebral compression fracture, and little published work on the subject. Traditional management has concentrated on analgesia, rest with physical support such as a brace or corset, and subsequent gradual mobilization within the limits of pain. The use of a corset should no longer be advocated, as it immobilizes the spine, thereby aggravating bone loss and wasting of the muscles around the spine. A balance has to be found between relieving pain sufficiently to allow rapid remobilization, but avoiding the potential adverse effects of strong analgesics such as opiates and opioids, to which elderly people are particularly susceptible (3). A first period of bed rest is followed by gradual mobilization with hyperextension brace (3, 7, 8), that can be progressively dismissed when the radiologic or MRI consolidation (i.e. VBME resolution) of the fracture is assessed (9). Elderly patients often need more bed rest (3) because of the slow VBME resolution. This predisposes them to several comorbidities such as venous thrombosis, pulmonary embolism, pressure ulcers, pulmonary and urinary tract infections (3). In literature, it is also reported that bone mineral density decreases by 0.25% to 1% per week in patients who are on bed rest (3, 10). Thus, the search for a noninvasive tool to manage acute VCFs is gaining increasing importance.

Capacitively coupling electric field (CCEF) is a non-invasive type of biophysical stimulation approved by US FDA to treat spinal fusions (11). In clinical trials, Brighton et al. and Impagliazzo et al. described the role of CCEF in the treatment of recalcitrant non-union healing (12-13). Goodwin et al. reported that CCEF stimulation enhances lumbar fusion in instrumented vertebral arthrodesis (14). Rossini et al. underlined that CCEF stimulation reduces chronic pain and discontinues the use of NSAIDs in patients with osteoporotic VCFs (11).

None of previous studies investigated the role of CCEF stimulation in VBME resolution. The primary end-point of this study was to evaluate the effect of CCEF on the VBME resolution using an MRI study follow-up. The secondary end-points were to evaluate CCEF impact on pain relief (VAS for pain) and quality of life (Oswestry Low Back Disability Index). For these purposes, patients with acute VCFs treated with CCEF were compared, in a perspective study, to patients who did not receive biophysical stimulation.

MATERIALS AND METHODS

Between January 2013 and January 2014, 96 patients (20 male, 76 female), with 100 thoracic or lumbar fresh spinal fractures type A1 according to AOSpine Thoracolumbar Spine Injury Classification System (15) were treated in our Institute. According to inclusions and exclusion criteria, 72 patients (15 male, 57 female), with 75 thoracic or lumbar fresh spinal fractures were excluded (posterior vertebral wall rupture on CT (n=15), preexisting pathology liable to alter the study results (n=14), obesity (BMI>30 n=15), degenerative scoliosis (n=24), contraindications to MRI (n=4)) while 24 patients (5 male, 19 female) with 25 fractures were selected and included in this prospective observational study. Mean specialist referral time was 3 days after back pain onset (range, 0-10).

Inclusion criteria were: maximum 10 days post-trauma interval; pain at the fracture level; presence of VBME on MRI, in no more than two vertebrae.

Exclusion criteria were: neurologic lesion; posterior vertebral wall rupture on CT; preexisting pathology liable to alter the study results — i.e. previous vertebroplasty on the affected vertebra; bone tuberculosis or other spine infections; pregnancy; obesity; scoliosis; or any contraindications to MRI.

Ethical clearance was obtained from our center's clinical research ethics (code ECCEFAVCF), as per 1964 Declaration of Helsinki, and all patients gave informed consent before enrollment in the study.

All the patients were informed of the potential risks and benefits associated with CCEF stimulation, then each patient autonomously decided to adhere to the study group protocol (with CCEF stimulation) or the control group protocol (without CCEF stimulation).

The patients were therefore divided into two groups: group A and group B. Group A patients (n=12) received antiresorptive therapy (75 mg risedronate tablet weekly + supplemental calcium carbonate with 1000 mg of elemental calcium daily; Vitamin D (≤500 IU daily) given only if the serum 25-hydroxyvitamin D concentration at the time of screening was below 16 ng per milliliter or 40 nmol per liter), CCEF stimulation (Osteospine®, IGEA SpA, Carpi, Italy) and C35 hyperextension brace for three months with bed rest in the first 20 days. Group-B (n=12) received antiresorptive therapy (75 mg risedronate tablet weekly + supplemental calcium carbonate with 1000 mg of elemental calcium daily; Vitamin D (≤500 IU daily) given only if the serum 25-hydroxyvitamin D concentration at the time of screening was below 16 ng per milliliter or 40 nmol per liter) and C35 hyperextension brace for three months with bed rest in the first 20 days.

In both groups, during the bed rest period, a physical support such as a brace or corset, was used to allow a little mobilization, e.g., for hygienic cleansing.

Group-A patients were instructed to use CCEF device 8h/day for 90 days. The portable generator supply a density current of 25 μA/cm^2 in the region of interest. The electric signal consists of electrical pulses of 12.5 Hz with a duty cycle of 50%. The active part of the electric pulse consists of a sinusoidal wave of 60 kHz, with an amplitude adjusted by a microprocessor according to the impedance of the patient's body. The microprocessor allowed us to monitor the patient's compliance with the biophysical treatment in hours. The adhesive electrode pads are made of a layer of highly conductive material and were placed paraspinally on the skin, at the level of the VBME.

MRI study was performed at 0 (T0), 30 (T1), 60 (T2) and 90 (T3) days using 1.5-T MRI system (Signa 1.5T SYS GEMSOW General Electronic, Wisconsin, USA). Sagittal T1-weighted spin-echo imaging (TR, 357.0 msec; TE, 15.0 msec; slice thickness, 13.0 mm; FOV, 300 x 300 mm; matrix size, 380 x 224) and fat-suppressed T2-weighted spin-echo imaging (TR, 4500.0 msec; TE 46.4 msec; slice thickness, 13.0 mm; FOV, 400x400 mm; 380 x 224) were performed along the left pedicle, the spinous process and the right pedicle.

A neuroradiologist and two orthopedists, with more than 10 years of experience, analyzed the signal intensity (SI) of these three MRI slices. VBME was quantified by applying the method of Piazzolla et al. (17): using DICOM software (Weasis Medical Viewer, Atlassian), two regions of interest (ROIs), the fractured vertebral body and the VBME zone, were identified manually in T2 fat-sat sequences, taking care not to contain the cortex.

The area in mm^2 of both ROIs and their ratio, expressed in percentage, were calculated. VBME was defined as the mean of the ratios calculated in the three MRI slices.

At 0 (T_0), 30 (T_1), 60 (T_2) and 90(T_3) days each patient underwent clinical evaluation using the Visual Analogue Scale (VAS) for pain and the Oswestry Disability Index (ODI) (18).

The CCEF device internal clock enabled the patient's compliance to be monitored according to the formula (1):

$$ADHERENCE = \frac{\text{Recorded hours of treatment}}{\text{Expected hours of treatment}} \text{x } 100 \qquad (1)$$

Previous clinical trials on CCEF stimulation were analyzed to identify the minimum adherence request. In the study by Goodwin et al. patients were required to use CCEF stimulation 24 hours per day, but an average time of 15.7 hours per day was recorded. Rossini et al. asked the patients to use the CCEF device at least 10 hours per day and an average time of 8.6 hours per day was recorded in the stimulated group. Therefore, we considered compliant patients with adherence ≥ 80%.

In order to evaluate VBME reduction independently of patient's compliance, the edema reduction corrected for the hours of treatment (ΔE) was calculated, as follows:

$$\Delta E = \frac{\text{Baseline VBME} - \text{90 days VBME}}{\text{Hours of treatment}} \ (\text{mm}^2/\text{h}) \ (2)$$

Statistical analysis was performed using SPSS® 11.0 software (SPSS Inc., Chicago, IL, USA). Unpaired *t*-test after ANOVA was used to compare the VBME, VAS and ODI values between the two groups at 0 (T0), 30 (T1), 60 (T2) and 90 (T3) days 0. Paired *t*-test was used to compare within the same group the VBME, VAS and ODI values at follow-ups versus baseline. A p value of less than 0.05 was considered significant.

RESULTS

Twelve patients (13 VCFs) followed the group-A protocol, while twelve patients (12 VCFs) adhered to the group-B protocol. Two patients in group A and two patients in group B were lost at T_1 (30 days) follow-up (two patients in group B died and two patients in group-A suspended the CCEF stimulation after 20 and 25 days for other and independent health problems with subsequent hospitalization).

We therefore compared 10 treated vertebrae with 11 untreated vertebrae; fracture site was T9 (n=1),

Table I. *General data of the study.*

Patient	Age	Gender	Fracture site	Specialist referral (Days after pain onset)	Height (cm)	Weight (kg)	Smocking status
				Group A			
A1a	27	F	T12	0	164	55	YES
A1b	27	F	L1	0	164	55	YES
A2	75	F	L1	8	161	65	NO
A3	48	F	T9	0	166	67	NO
A4	71	F	T10	0	152	54	YES
A5	73	F	T12	0	157	66	NO
A6	61	F	L1	0	163	71	YES
A7	68	F	L1	0	160	62	NO
A8	78	F	T10	0	166	60	NO
A9	62	F	L3	7	171	75	YES
				Group B			
B1	53	M	T12	0	175	71	YES
B2	54	F	T12	7	168	65	YES
B3	57	M	T12	0	180	82	YES
B4	65	M	L1	0	174	75	NO
B5	69	F	L5	3	166	58	NO
B6	71	F	T12	2	148	53	NO
B7	73	F	L1	6	159	62	NO
B8	68	F	L3	7	153	51	YES
B9	72	F	L1	0	156	60	NO
B10	69	F	L1	9	162	66	YES
B11	87	F	L1	0	159	50	NO

VBME: Vertebral Bone Marrow Edema; VAS: Visual Analogue Scale; ODI: Oswestry Disability Index; Fu: Follow-up.

T10 (n=2), T12 (n=6), L1 (n=9), L3 (n=2), or L5 (n=1) (Table I).

A power analysis was performed using data recently published by Piazzolla A. et al, (17) that describe a reduction of VBME of about 22% at 60 days of follow-up. Our hypothesis is that when the patients are treated with CCEF, the percentage of VBME reduction can rise up to 40%. If a difference is considered between treated and non-treated patients of 18%, with a superiority margin of 8% and a standard deviation of 9%, as reported in literature, our estimation of the sample size at 80% power and 5% alpha, is of 10 fractures per group.

A good compliance (adherence= 90%) in CCEF stimulation was recorded (Table II).

Table II summarizes also the MRI study main data, while Fig. 1 shows the VBME resolution at each follow-up in both groups.

Figs. 2 and 3 show VBME quantification in a group-A patient (clinical case A3, Fig. 2) and in a group-B patient (Clinical Case B1, Fig. 3).

MRI evaluation showed a comparable VBME

Table II. *MRI study and compliance data: group A and group B.*

Group A									Group B				
	VBME (%)				COMPLIANCE					VBME (%)			
	0	30	60	90	R hours	E hours	Adh	ΔE (mm^2/h)		0	30	60	90
A1a	72.2	40.2	0	0	413	480	86%	1	B1	87	81.6	55.7	48.6
A1b	77.5	49.6	0	0	413	480	86%	1.2	B2	86.8	75.6	62.7	41.6
A2	89.6	54.2	26.4	0	716	720	99%	1.7	B3	89.9	84.2	65.3	59.4
A3	74.7	44.8	8.2	1.4	812	720	100%	0.8	B4	92.3	86.5	72	65.6
A4	83.6	54.9	21.9	6	731	720	100%	1.9	B5	84	72.3	55.8	29.4
A5	85	47.2	27.7	4.3	597	720	83%	1.8	B6	79	75.5	69.9	41.9
A6	80.2	41.6	25.2	7.2	584	720	81%	1.4	B7	87.9	78.3	65.8	43.3
A7	81.4	60.9	24.6	9.6	577	720	80%	1.25	B8	85.7	76.8	42.5	39.3
A8	90.2	58.9	23.7	2	608	720	84.5%	1.2	B9	85.4	75	58	48
A9	89.3	60.3	24.7	0	656	720	91%	1.3	B10	61	56.6	32.5	19.4
									B11	74.5	53.2	48.6	43.4
Mean	**82.4 %**	**51.3 %**	**18.2 %**	**3 %**	**655.3**	**672**	**90%**	**1**	**Mean**	**84 %**	**76 %**	**58 %**	**43 %**
SD	**0.064**	**0.07**	**0.11**	**0.03**	**168.2**	**101.2**	**0.08**	**0.35**	**SD**	**0.09**	**0.9**	**0.12**	**0.14**
CI 95%	**±0.04**	**±0.05**	**±0.07**	**±0.02**	**±104**	**±62.7**	**±0.06**	**±0.2**	**CI 95%**	**±0.06**	**±0.06**	**±0.07**	**±0.09**

VBME: Vertebral Bone Marrow Edema; 0: Baseline; 30: thirty days follow-up; 60: sixty days follow-up; 90:ninety days follow-up; R hours: recorded hours of treatment; E hours: expected hours; Adh: Adherence to therapy; ΔE: edema reduction corrected for treatment hours.

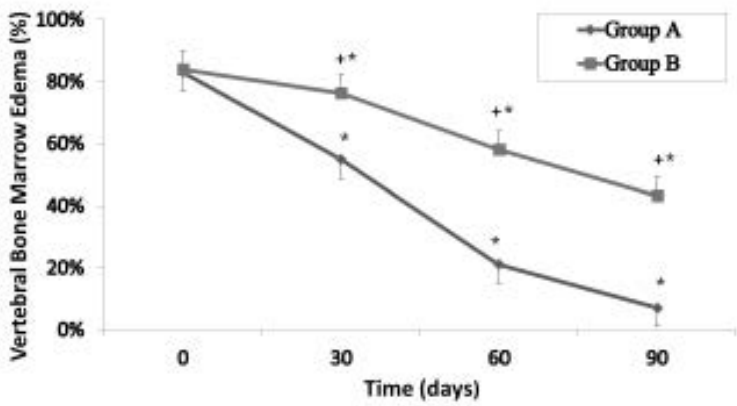

Fig. 1. *The mean VBME value reduction is significantly different in the stimulated group (group-A). The error bars are represented only in one direction for clarity of representation. +p<0.05, p values refer to a comparison between groups at each follow-up visit (unpaired t-test). *p<0.05, p values refer to the difference between each follow-up versus baseline (paired t-test).*

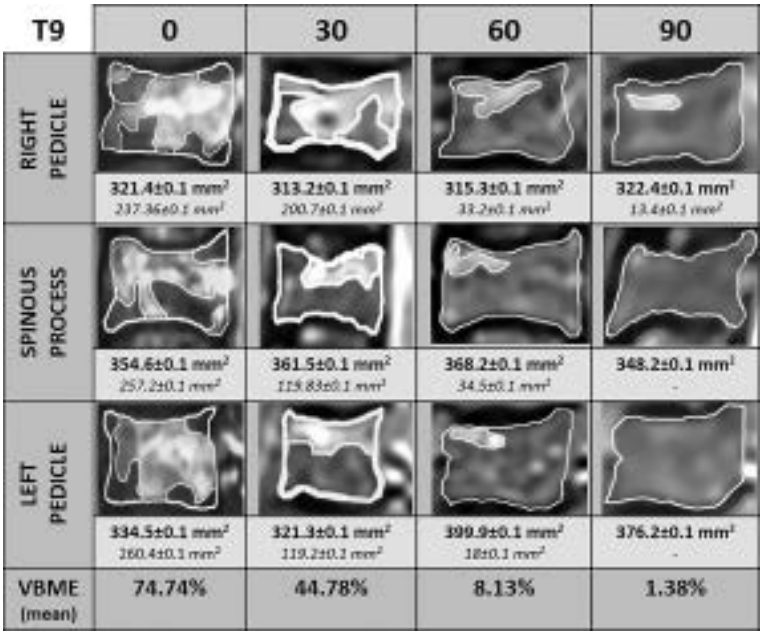

Fig. 2. *Clinical case A5 VBME mean values at baseline and at follow-up MRIs. The patient, a 49-year-old woman with T9 acute VCF, was compliant (Adherence=100%) in CCEF therapy. T9 area is reported in bold, VBME area in italics.*

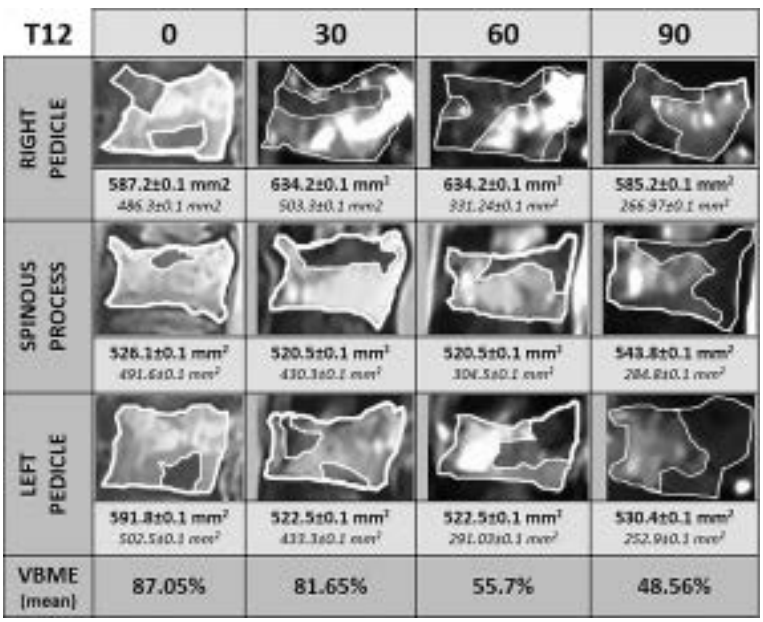

Fig. 3. *Clinical case B1 VBME values at baseline and at follow-up MRIs. The patient, a 53-year-old man with T12 acute VCF, did not receive CCEF stimulation. T12 area is reported in bold, VBME area in italic.*

Table III. *Comparison between groups.*

Time	VBME			
	Group A (Mean±SD)	**Group B (Mean±SD)**	***p* value**	**CI (95%)**
Baseline	0.83±0.06	0.84± 0.09	0.758*	-0.06/0.08
30 days Fu	0.55±0.13	0.76±0.08	0.0002	0.11/0.31
60 days Fu	0.24±0.14	0.58±0.13	0.0001	0.21/0.48
90 days Fu	0.07±0.137	0.43±0.14	0.0001	0.22/0.5

*VBME: Vertebral Bone Marrow Edema; Fu: Follow-up. * Non-significant p-value*

Table IV. *VBME, VAS and ODI P values for differences between each follow-up versus baseline (Paired t test).*

Time	Group A			Group B		
	VBME	VAS	ODI	VBME	VAS	ODI
30 days Fu	< 0.05	< 0.05	< 0.05	0.000153	0.08*	0.122015*
60 days Fu	< 0.05	< 0.05	< 0.05	< 0.05	<0.05	<0.05
90 days Fu	< 0.05	< 0.05	< 0.005	< 0.05	<0.05	< 0.05

*Group A and Group B. VBME: Vertebral Bone Marrow Edema; VAS: Visual Analogue Scale; ODI: Oswestry Disability Index; Fu: Follow-up. *Non-significant p-value*

mean in both groups at baseline (p=0.78). A significant difference in VBME mean follow-up values between the two groups was recorded at each follow-up (p<0.05; Table III).

In 4 stimulated VCFs out of 10 we found a complete VBME resolution at 90 days MRI, whereas in group-B VBME resolution was never found at 90 days MRI (Table II).

P values for differences between each follow-up VBME, VAS and ODI values versus baseline (paired *t*-test) are shown in Table IV.

In group A, a halving of VBME resolution time was recorded, thus group A VBME mean at 30 days follow-up was comparable with group VBME B mean at 60 days follow-up in unpaired student's *t*-test (p=0.75). In group-A a faster pain reduction was recorded than in B group; group-A 30-day follow-up mean VAS was comparable to group-B 90-day follow-up mean VAS in unpaired student's *t*-test (p=0.73). Furthermore, in group-A an early improvement of ODI score was recorded; group-A 30-day follow-up mean ODI was comparable to group-B 90-day follow-up mean VAS in unpaired student's *t*-test (p=0.8).

The mean VAS and ODI scores were comparable in groups A and B at baseline (VAS, p=0.7; ODI p=0.98, respectively). A statistically significant difference of these scores between groups was observed at 30 days (VAS, p=0.007; ODI, p=0.0077), 60 days (VAS, p=0.0002; ODI, p=0.007) and 90-day follow-up examinations (VAS, p=0.0003; ODI, p=0.002) (Table V, Fig. 4, Fig. 5).

Table V. *Comparison between the two groups: VAS (left) and ODI (right).*

Time	VAS				ODI			
	Group A (Mean±SD)	Group B (Mean±SD)	*p* value	CI (95%)	Group A (Mean±SD)	Group B (Mean±SD)	*p* value	CI (95%)
Baseline	7.27± 1.4	7.48±1.4	0.74*	-1.08/1.5	0.65±0.06	0.65±0.1	0.987*	-0.08/0.09
30 days Fu	4.8±1.5	6.8±1.5	0.007	0.61/3.4	0.49±0.1	0.615±0.76	0.0077	0.04/0.21
60 days Fu	2.5±1.5	5.5±1.2	0.0002	1.7/4.36	0.28±0.1	0.48±0.12	0.007	0.05/0.26
90 days Fu	1.6±1.6	5.03±1.3	0.0003	1.85/4.96	0.17±0.05	0.32±0.097	0.0021	0.06/0.24

*VAS: Visual Analogue Scale; ODI: Oswestry Disability Index; Fu: follow-up. *Non-significant p-value*

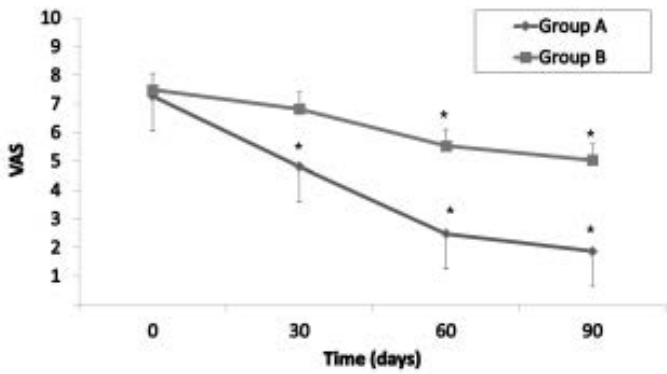

Fig. 4. *The mean VAS for pain scores at baseline and at follow-ups indicate a significant difference between groups. The error bars are represented only in one direction for clarity of representation. +p<0.05, p values refer to a comparison between groups at each follow-up visit (unpaired t-test). *p<0.05, p values refer to the difference between each follow-up versus baseline (paired t-test).*

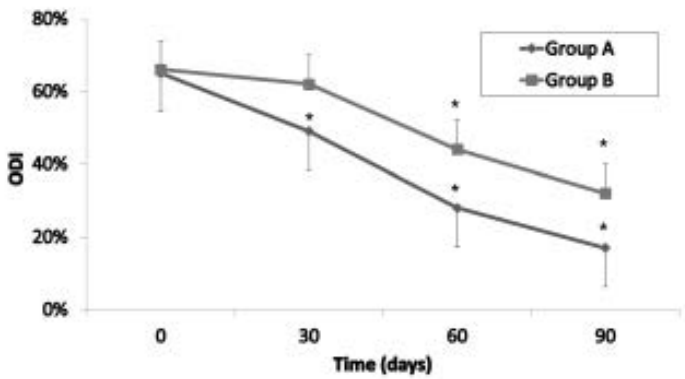

Fig. 5. *The mean ODI scores at baseline and at follow-ups indicate a significant difference between groups. The error bars are represented only in one direction for clarity of representation. +p<0.05, p values refer to a comparison between groups at each follow-up visit (unpaired t-test). *p<0.05, p values refer to the difference between each follow-up versus baseline (paired t-test).*

DISCUSSION

VBME is an MRI marker of acute/subacute VCFs; its persistence, on MRI follow-ups, depicts an incomplete fracture healing (3, 5). Conservative management of VCFs with bed rest and functional bracing may, especially in elderly patients, take several months to reach fracture healing.

We hypothesized that biophysical stimulation with CCEF could enhance the VCFs healing, by expediting VBME resolution time. *In vitro* studies on MC3T3-E1bone cells showed that CCEF acts by opening the plasma membrane Voltage Gated Calcium Channels, thus increasing the cytosolic calcium concentration and the Phospholipase A2 (PLA2) activity (20). Cytosolic calcium activates the calmodulin pathway, thus resulting in an up-regulated expression of osteogenic genes, such as Transforming Growth Factor-β superfamily genes (TGF-β1, -β2 -β3, BMP-2 and -4), Fibroblast Growth Factor (FGF)-2, osteocalcin (BGP) and alkaline phosphatase (ALP) (21-22). PLA2 acts by increasing the synthesis of Prostaglandin E2 (PGE2), which promotes osteogenesis by raising the cellular L-ascorbic acid uptake through the membrane carrier Sodium Vitamin C Transporter-2 (SVCT-2) (23).

Positive effects of CCEF stimulation on fracture healing in animal models have been reported by different authors. Brighton et al. in a castration-induced osteoporosis animal model demonstrated that CCEF was able to restore bone mass/unit volume in the rat vertebral body (24). Gan et al., using a rabbit posterolateral intertransverse spinal fusion model, reported a greater percentage of bilateral and unilateral fusion in the CCEF-stimulated group in contrast to the control group (25).

CCEF stimulation is currently used in the treatment of recalcitrant non-union healing (12-13), as an adjunct in the treatment of vertebral fusions (14) and in patients with osteoporotic VCFs to reduce chronic pain NSAID assumption (11).

In the current study no negative side-effects were observed during the use of the capacitive stimulation. A VBME significant reduction at three months MRI follow-up was found only in compliant group-A patients. This datum confirms that, as stated in previous studies (11, 14), compliance plays a central role in capacitive stimulation effectiveness. This can be explained by considering that the gene expression changes caused by CCEF need some time to be achieved. We hypothesized that CCEF stimulation should be performed at least 8 hours per day for 90 days to achieve the expected results.

In group-A, significant difference of VAS and ODI scores was recorded; this shows CCEF stimulation provides a symptomatic improvement, depending on the complete VBME resolution. At 30-day follow-up a significant improvement of mean VAS and ODI scores was observed only in group-A in paired *t* test ($p<0.05$).

The lack of randomization is a limitation of this study, but all clinical and MRI evaluations were carried out by physicians unaware whether the patient belonged to group-A or B. The small population size was exceeded by excluding from statistical analysis non-compliant group-A patients.

In this study, CCEF stimulation proved clinically and MRI effective in treating A1 thoraco-lumbar spinal fractures at 3-month follow-up. Patients treated with capacitive stimulation present an improvement of clinical symptoms depending on a faster fracture healing, documented by the VBME values recorded at MRI follow-ups. CCEF stimulation can be used as an adjunct to conservative treatment of VCFs, for expediting the fracture healing and thus shortening the patient's recovery.

REFERENCES

1. Riggs BL, Melton LJ 3rd. The worldwide problem of osteoporosis: insights afforded by epidemiology. Bone 1995; 17(5 S):505S-511S.
2. Felsenberg D, Silman AJ, Lunt M, et al. Incidence of vertebral fracture in Europe: results from the European Prospective Osteoporosis Study (EPOS). J Bone Miner Res 2002; 17(4):716-24.
3. Alexandru D, So W. Evaluation and management of vertebral compression fractures. Perm J 2012; 16(4):46–51.
4. Lindsay R, Silverman SL, Cooper C, et al. Risk of new vertebral fracture in the year following a fracture. JAMA 2001; 285(3):320-23.
5. Voormolen MHJ, van Rooij WJ, van der Graaf Y, Lohle PNM, Lampmann LEH, Juttmann JR, Sluzewski M. Bone marrow edema in osteoporotic

vertebral compression fractures after percutaneous vertebroplasty and relation with clinical outcome. AJNR Am J Neuroradiol 2006; 27:983-88.
6. Ettinger B, Black DM, Nevitt MC, et al. Contribution of vertebral deformities to chronic back pain and disability. J Bone Miner Res 1992; 7(4):449-56.
7. Mazanec DJ, et al. Vertebral compression fractures: Manage aggressively to prevent sequelae. Cleveland Clinic J Med 2003; 70(2):147-56.
8. Lentle BC1, Brown JP, Khan A, et al. Recognizing and reporting vertebral fractures: reducing the risk of future osteoporotic fractures. Can Assoc Radiol J 2007; 58(1):27-36.
9. Do HM. Magnetic resonance imaging in the evaluation of patients for percutaneous vertebroplasty. Top Magn Reson Imaging 2000; 11:235-44.
10. Leblanc AD, Schneider VS, Evans HJ, Engelbretson DA, Krebs JM. Bone mineral loss and recovery after 17 weeks of bed rest. J Bone Miner Res 1990; 5(8):843-50.
11. Rossini M, Viapiana O, Gatti D, De Terlizzi F, Adami S. Capacitively coupled electric field for pain relief in patients with vertebral fractures and chronic pain. Clin Orthop Relat Res 2010; 468:735-40.
12. Brighton CT, Pollack SR. Treatment of recalcitrant non-union with a capacitively coupled electrical field: a preliminary report. J Bone Joint Surg Am 1985; 67:577-85.
13. Impagliazzo A, Mattei A, Spurio Pompili GF, Setti S, Cadossi R. Treatment of ununited fractures with capacitively coupled electric field. J Orthopaed Traumatol 2006; 7:16-22.
14. Goodwin CB, Brighton CT, Guyer RD, et al. A double-blind study of capacitively coupled electrical stimulation as an adjunct to lumbar spine fusions. Spine 1999; 24:1349-57.
15. Vaccaro AR, Oner C, Kepler CK, et al. AOSpine thoracolumbar spine injury classification system fracture description, neurological status, and key modifiers. Spine 2013; 38(23):2028-37.
16. Baker LL, Goodman SB, Perkash I, et al. Benign versus pathologic compression fractures of vertebral bodies: assessment with conventional spin-echo, chemical-shift, and STIR MR imaging. Radiology 1996; 199:541-49.
17. Piazzolla A, Solarino G, Lamartina C, et al. Vertebral Bone Marrow Edema (VBME) in conservatively treated acute Vertebral Compression Fractures (VCFs): Evolution and Clinical Correlations. Spine 2015. (Epub ahead of print).
18. Fairbank JC, Couper J, Davies JB. The Oswestry low back pain disability questionnaire. Physiotherapy 1980; 66:271-73.
19. Dansie DM, Luetmer PH, Lane JI, et al. MRI findings after successful vertebroplasty. AJNR Am J Neuroradiol 2005; 26:1595-600.
20. Brighton CT, Wang W Seldes R Zhang G, Pollack SR. Signal transduction in coupled electrical field. J Bone Joint Surg Am 2001; 83-A(10):1514-23.
21. Zhuang H, Wang W, Seldes RM, Tahernia AD, Fan H, Brighton CT. Electrical stimulation induces the level of TGF-beta1 mRNA in osteoblastic cells by a mechanism involving calcium/calmodulin pathway. Biochem Biophys Res Commun 1997; 237:225-29.
22. Clark CC, Wang W, Brighton CT. Up-regulation of expression of selected genes in human bone cells with specific capacitively coupled electric fields. J Orthopedic Res J Orthop Res 2014; 32(7):894-903.
23. X Wu, L-H Zeng, T Taniguchi, Q-M Xie Activation of PKA and phosphorylation of sodium-dependent vitamin C transporter 2 by prostaglandin E2 promote osteoblast-like differentiation in MC3T3-E1 cells. Cell Death Diff 2007; 14(10):1792-801
24. Brighton CT, Luessenhop CP, Pollack SR, Steinberg DR, Petrik ME, Kaplan FS. Treatment of castration-induced osteoporosis by a capacitive coupled electrical signal in the rat vertebrae. J Bone Joint Surg Am 1989; 71(2):228-36.
25. Gan J, Glazer P. Electrical stimulation therapies for spinal fusions: current concepts. Eur Spine J 2006; 15(9):1301-11.

HYALURONIC ACID: THE USE OF ITS PRECURSOR IN SKIN BIO-STIMULATION

A. AVANTAGGIATO[1], M. MARTINELLI[2], A. PALMIERI[2], M. PASCALI[3], G. BERTUZZI[4] and F. CARINCI[1]

[1]Department of Morphology, Surgery and Experimental Medicine, University of Ferrara, Ferrara, Italy; [2]Department of Experimental, Diagnostic and Specialty Medicine, University of Bologna, Bologna, Italy; [3]Plastic Surgeon, Rome, Italy; [4]Department of Systems Medicine, University of Tor Vergata, Rome, Italy

Received March 6, 2015 – Accepted May 8, 2015

Bio-stimulation is an injective therapy aimed to boost the anabolic functions of dermal fibroblasts to obtain skin improvement. It can be achieved with multiple intradermal injections (0.05–0.1 ml each) of a solution of 400 mg (3 ml) of injectable glucosamine sulphate, plus 5.623 mg (3 ml) of polideoxyribonucleotide, 1 ml of lidocaine and 0.5–1 ml of sodium bicarbonate, to repeat every 7, 14, 21, and 28 days. The administration of glucosamine sulphate to skin fibroblasts is believed to lead to its incorporation in glycosaminoglycans, and thereby to the stimulation of extracellular matrix synthesis, whereas polideoxyribonucleotide possesses anti-inflammatory and regenerative capability. This study aims to elucidate the *in-vitro* effects of this treatment by studying what happens to several genes related to connective tissue integrity. Human dermal fibroblasts were seeded in a culture medium enriched with either two drugs alone or combined: glucosamine sulphate and/or polideoxyribonucleotide. After the end of the exposure time of 24 h, 48 h, and 72 h, the cells were trypsinized and lysed for RNA extraction. Reverse transcription to cDNA was performed directly from cultured cell lysate. Finally, the cDNA was amplified by real-time PCR and a panel of genes involved in dermal integrity was tested. Gene expression of Hyaluronan synthase 1 (HAS1), Elastine (ELN), Insulin like growth factor 1 (IGF1), Growth differentiation factor 6 (GDF6) and of a series of catabolic enzymes, such as Metalloproteases (MMP) 2, 3 and 13, the neutrophyl expressed Elastase (ELANE) and the Hyaluronidase 1 (HYAL1) were tested after 24, 48 and 72 hours of exposure to glucosamine sulphate and polideoxyribonucleotide alone or combined. All the tested genes but one were up-regulated. A negative synergism on several enzymes (particularly appreciable for Insulin-like growth factor 1 and metalloprotease 13) was observed when the two drugs were delivered together. Glucosamine sulphate acts not only as building block in the biosynthesis of glycosaminoglycan chains, but also as a booster of hyaluronan synthase 1. The association of glucosamine sulphate and polideoxyribonucleotide, used in bio-stimulation therapy protocol, has a negative synergism on catabolic genes in dermal fibroblast cultures. The present observations produce further insight into the effects of glucosamine sulphate in the biosynthesis of glycosaminoglycan chains.

Key words: glucosamine sulphate, polideoxyribonucleotide, extracellular matrix, hyaluronic acid

Mailing address: Martinelli Marcella, Ph.D.
Dept. of Experimental,
Diagnostic and Specialty Medicine,
University of Bologna, Via Belmeloro 8,
40126 Bologna, Italy
Tel.: +39 051 2094106 Fax: +39 051 2094110
e-mail: marcella.martinelli@unibo.it

0393-974X (2015)

DISCLOSURE: ALL AUTHORS REPORT NO CONFLICTS OF INTEREST RELEVANT TO THIS ARTICLE.

The progressive atrophy process is the main factor in determining facial aging (1) and this combines perfectly with both the phenotypic manifestations of aging (2) and the histological findings (3).

The first years of the 2000s were dominated by studies on collagen, the major structural protein of the connective tissue (4), which is present in the dermis as fibrillar component of the extra cellular matrix (ECM). In this regard, it has been shown that fibroblasts do not lie inert in the ECM, but connect their cytoskeleton to the collagen fibers to create a three-dimensional network that realizes the consistency of the dermal connective (5). In this view, the glycosaminoglycans of the matrix were progressively studied because the space among cellular and fibrillar components of the connective tissue is embedded by these molecules and by the water they can hold.

In clinical use, the lower immunogenicity of hyaluronic acid (HA) compared to collagen gave rise to its progressive substitution in volume restoration as filler (after cross-linking to reduce its hyaluronidases sensitivity) and in anti-aging therapies, such as the bio-revitalization (where HA is often mixed to aminoacids and vitamins), or bio-stimulation (where HA is virtually absent). These treatments are directed to skin improvement through intra-dermal injection of different drugs in order to promote ECM optimization with regard to its non-fibrillar component (6). HA is a polymer of dimeric units of *N*-acetyl-glucosamine and glucuronic acid synthesized by HA synthase on the inner surface of plasma membrane, and then secreted in the extracellular space (7).

Glucosamine can be extracted and stabilized by chemical modification and is used as a drug for the treatment of osteoarthritis (OA) in Europe, to promote cartilage and joint health, and it is sold over the counter as a dietary supplement in the USA (8).

The administration of glucosamine sulphate (Gluc) to skin fibroblasts is believed to lead to its incorporation in glycosaminoglycans, and thereby to the stimulation of ECM synthesis as a building block without direct use of HA. The advantages are the more physiological approach in order to respect the homeostatic mechanisms of cell biology and the cost that is less expensive for injective glucosamine than for an HA-containing product. The limit is that HA synthesis occurs inside the cells, thus healthy fibroblasts are required, consequently, the potential of bio-stimulation (BS) is better in younger and less photo-damaged skins.

The term BS indicates stimulation of the anabolic functions of dermal fibroblasts such as replication, protein synthesis and production of ECM. It can be achieved with multiple intra-dermal injections (0.05–0.1 ml each) of a solution of 400 mg (3 ml) of injectable Gluc, plus 5.623 mg (3 ml) of PDRN, 1 ml of lidocaine and 0.5–1 ml of sodium bicarbonate, to repeat every 7, 14, 21 and 28 days (9). The second component of this protocol is PDRN, a mixture of deoxyribonucleotide polymers with chain lengths ranging from 50 bp to 2,000 bp obtained from trout sperm by an extraction process. PDRN acts through stimulation of the A2A purinic receptors. Adenosine is a purine nucleoside that is released from a variety of cells in response to several types of stress. It has been suggested that adenosine regulates inflammation via interaction with one or more of its 4 known receptors (A1, A2A, A2B, and A3). Stimulation of adenosine A2 and A3 receptors has been shown to alter the cytokine network by decreasing inflammatory cytokine secretion by macrophages *in vitro* (10).

In a previous paper (6), the effects of this therapy was discussed by analyzing through RT-PCR several genes of cultured human dermal fibroblasts. Those genes are involved in dermal integrity. The aim of the present research is to observe these effects over time, not only after 24 hours but also at 48 and 72 hours after cell stimulation.

MATERIALS AND METHODS

Primary human dermal fibroblast cell (HFb) culture

Fragments of dermal tissue of healthy volunteers were collected during surgery. The pieces were transferred to 75 cm^2 culture flasks containing DMEM medium (Sigma-Aldrich, Inc., St. Louis, Mo, USA) supplemented with 20% fetal calf serum and antibiotics, i.e. penicillin 100 U/ml and streptomycin 100 μg/ml (Sigma-Aldrich, Inc., St. Louis, Mo, USA). Cells were incubated in a humidified atmosphere of 5% CO_2 at 37°C. Medium was changed the next day and twice a week thereafter. After 15 days, the pieces of dermal tissue were removed from the culture flasks. Cells were harvested after additional 24 h of incubation.

Cell cultures

Human dermal fibroblasts at the second passage were

Table I. *Primer sequences for SYBR® Green assay.*

Gene symbol	Gene name	Primer sequence (5'>3')
HAS1	Homo sapiens hyaluronan synthase 1	F-CTCGGAGATTCGGTGGACTA R-CGCTGATGCAGGATACACAG
ELN	Homo sapiens elastin	F- CTAAATACGGTGCTGCTGGC R- CATGGGATGGGGTTACAAAG
IGF1	Homo sapiens insulin-like growth factor 1	F-GCGCAATGGAATAAAGTCCT R-ACAGCGCCAGGTAGAAGAGA
GDF6	Homo sapiens growth differentiation factor 6	F-CCCCACGAGTACATGCTGTC R-GAGCATGGACACATCAAACAA
MMP2	Homo sapiens matrix metalloprotease 2	F- TACGATGGAGGCGCTAATGG R- CGCATGGTCTCGATGGTATT
MMP3	Homo sapiens matrix metalloprotease 3	F-TTTCCCAAGCAAATAGCTGAA R-AGTTCCCTTGAGTGTGACTCG
MMP13	Homo sapiens matrix metalloprotease 13	F-AGTTCGGCCACTCCTTAGGT R-TGGTAATGGCATCAAGGGAT
ELANE	Homo sapiens elastase, neutrophil expressed	F- CTACGACCCCGTAAACTTGCT R- CCTCACGAGAGTGCAGACGTT
HYAL1	Homo sapiens hyaluronoglucosaminidase 1	F-ACAGATGTATGTGCAACACCG R-AAGGGCCCCAGTGTAGTGTC
TFRC	Homo sapiens transferrin receptor protein 1	F-CGCTGGTCAGTTCGTGATTA R-GCATTCCCGAAATCTGTTGT

seeded in a culture medium enriched with either two drugs alone or combined: glucosamine sulphate 400 mg (Dona, Rottafarm, Milan, Italy) and polideoxyribonucleotide 5.625 mg (Placentex Integro, Mastelli, Sanremo, Italy). A set of untreated cells was used as control. The cells were maintained in a humidified atmosphere of 5% CO_2 at 37°C. After the end of the exposure time of 24 h, 48 h, and 72 h., respectively, cells were trypsinized and lysed for RNA extraction.

RNA processing and real-time PCR

Reverse transcription to cDNA was performed directly from cultured cell lysate using the TaqMan Gene Expression Cells-to-Ct Kit (Ambion Inc., Austin, TX, USA), following the manufacturer's instructions. Briefly, cultured cells were lysed with lysis buffer and RNA released in this solution. Cell lysate was reverse-transcribed to cDNA using the RT Enzyme Mix and appropriate RT buffer (Ambion Inc., Austin, TX, USA).

Finally, the cDNA was amplified by real-time PCR. The amplification was performed by using Power SYBR® Green PCR Master Mix (Applied Biosystems, Foster City, CA, USA), and the specific assay was designed for the investigated genes (Table I). SYBR assay reactions were performed in a 20 µl volume using ABI PRISM 7500 (Applied Biosystems, Foster City, CA, USA). Each reaction contained 10 µl 2X Power SYBR® Green PCR Master Mix (Applied Biosystems, Foster City, CA, USA), 400 nM concentration of each primer and cDNA. All experiments included non-template controls to exclude contamination of reagents. PCR was performed with two biological replicates.

Expression was quantified using real-time PCR. The gene expression levels were normalized to the expression of the housekeeping gene Homo sapiens transferrin receptor protein 1 (TFRC). Quantification was carried out with the delta/delta calculation method. Forward and reverse primers for the selected genes were designed using primer express software (Applied Biosystems, Foster City, CA, USA), and were: Hyaluronic synthase 1 (HAS1) and Elastine (ELN), two proteins involved in connective tissue structure, Insulin like growth factor 1 (IGF1) and Growth differentiation factor 6 (GDF6), two enzymes involved in metabolic regulation and a series of catabolic enzymes as the Metalloproteases (MMP) 2, 3 and 13, the Neutrophyl expressed Elastase (ELANE) and

the Hyaluronidase 1 (HYAL1) after 24, 48 and 72 hours of exposure to Gluc and PDRN alone or combined.

RESULTS

Gene expression of HAS1, ELN, IGF1, GDF6 and of a series of catabolic enzymes, such as MMP2, MMP3 and MMP13, ELANE and HYAL1, were tested after 24, 48 and 72 hours of exposure to Gluc and PDRN alone or combined. All the tested genes but one (IGF1) were up-regulated (Fig. 1). A lesser activation of HAS1 could be observed when PDRN alone was added to culture medium (Fig. 2). Association of PDRN and Gluc acted not only as building block in the biosynthesis of glycosaminoglycan chains, but acted as a booster of HAS1 (Fig. 3). A negative synergism on several enzymes (particularly appreciable for IGF1 and MMP13) was observed when the two drugs were delivered together (Fig. 3).

DISCUSSION

Bio-stimulation is an injective therapy aimed to boost the anabolic functions of dermal fibroblasts to obtain a skin improvement. It can be achieved with multiple intradermal injections of a solution of Glucosamine sulphate (Gluc), plus polideoxyribonucleotide (PDRN). The administration of Gluc to skin fibroblasts is believed to lead to its incorporation in glycosaminoglycans, and thereby to the stimulation of extracellular matrix synthesis, whereas PDRN possesses anti-inflammatory and regenerative capability. This research is aimed to elucidate the *in-vitro* effects of this treatment by studying what happens to several genes related to connective tissue integrity.

HAS1 gene expression is enhanced in Gluc cultured fibroblasts.

HAS1 gene expression was enhanced after Gluc supplementation to cultured fibroblasts (Fig.1). The activation was increasing after 24, 48 and 72 hours. This behavior supports the idea that Gluc is not only important as building block in the biosynthesis of glycosaminoglycan chains, but can act as a booster for HA synthesis and for other cellular products.

Some Authors (11) demonstrated that addition

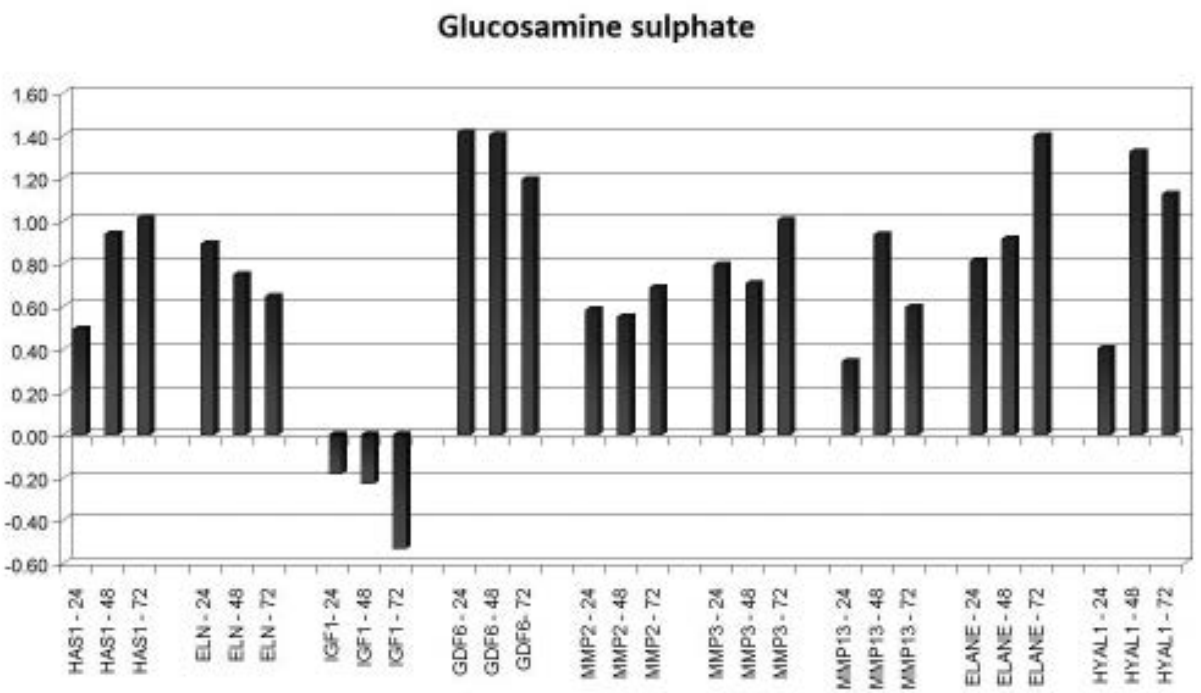

Fig. 1. *Gene activation after administration of glucosamine sulphate; all the tested genes were up regulated except insulin like growth factor 1.*

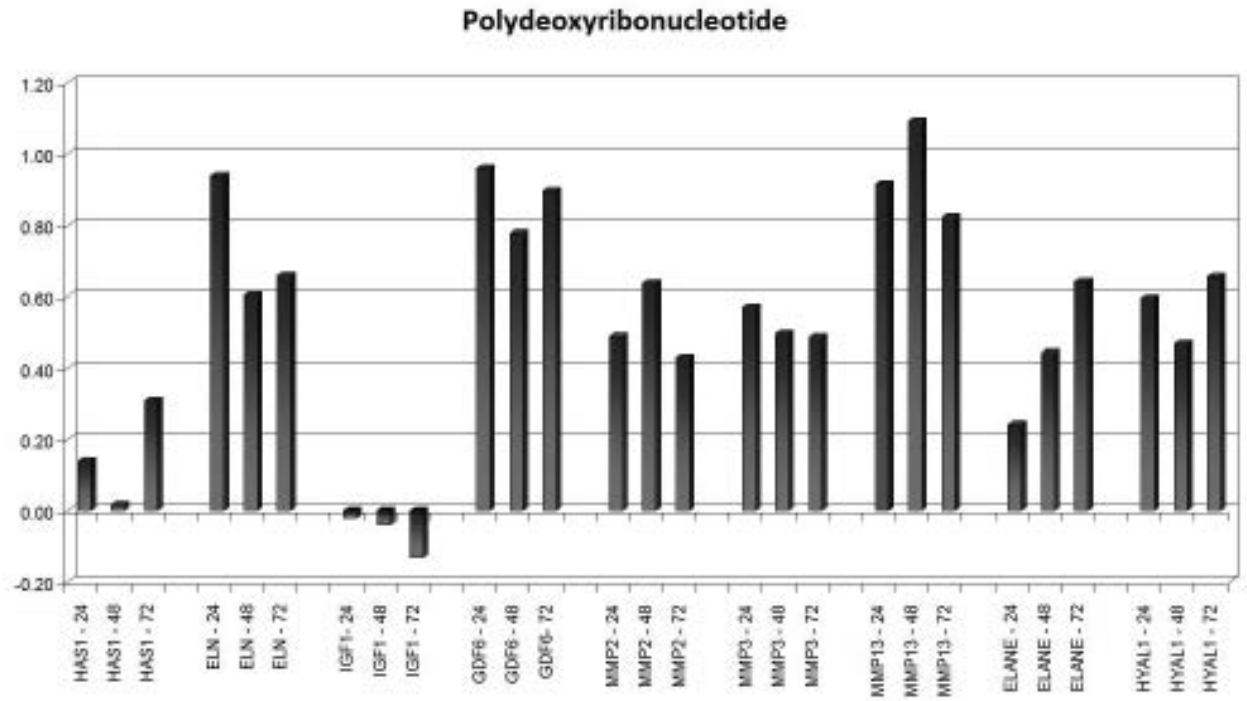

Fig. 2. *Polideoxyribonucleotides are usually associated to Gluc in the bio stimulation protocol. A lower activation can be observed of hyaluronan synthase 1 when polideoxyribonucleotide alone is added to the culture medium.*

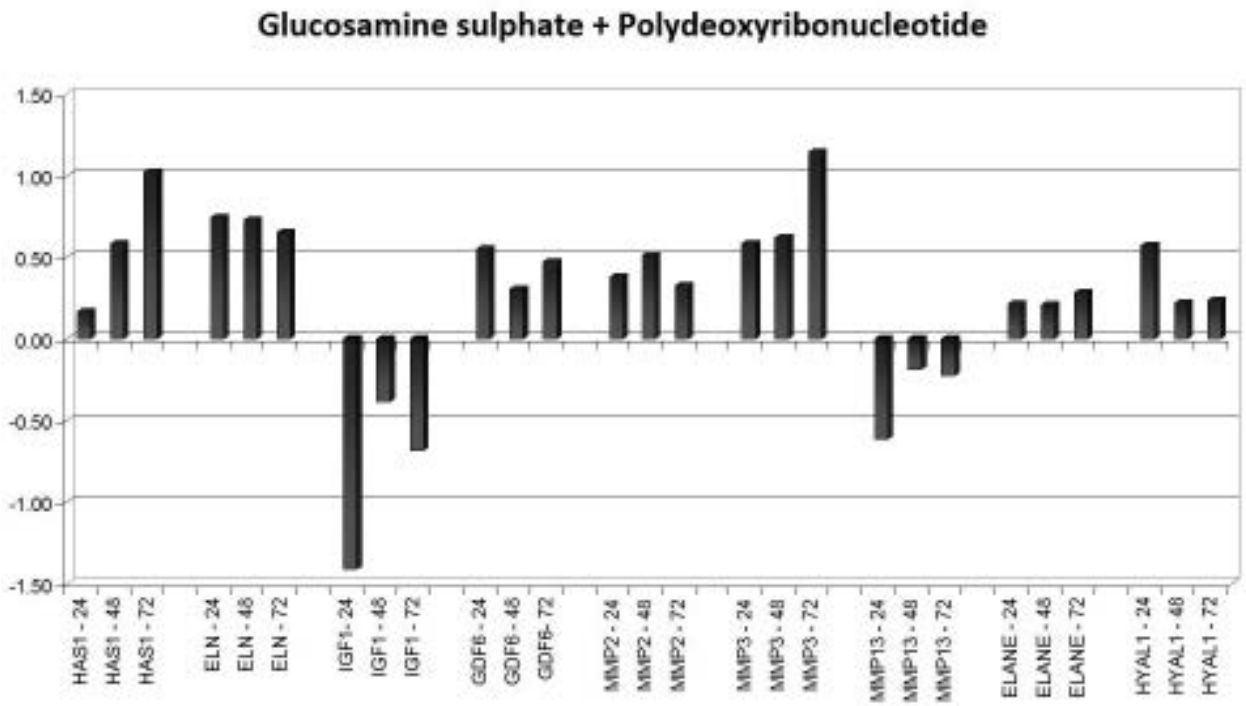

Fig. 3. *Effect of the association of the two substances with a negative synergism on several enzymes, particularly appreciable for insulin like growth factor 1 and metalloprotease 13.*

of glucosamine hydrocloride or glucose did not significantly alter HAS gene expression on cultured chondrocytes. Since they inferred that the registered increased amount of HA in the culture medium might be explained by the fact that addition of glucosamine hydrocloride simply implements the building blocks that are required for the HA synthesis.

In the present study, instead, an activation of HAS1 gene was demonstrated but the increasing effect over time was obtained by using injectable Gluc, and thus a different molecule. This drug has shown efficacy and safety in clinical trials in knee osteoarthritis (OA) when orally administered at a dose of 1,500 mg once a day. In addition to the clinical data, its use is supported by a distinct pharmacologic profile and well-described pharmacokinetics (12).

Gluc produces anabolic and catabolic gene activation.

Gluc has been studied in OA where it has been demonstrated to reduce prostaglandin E2 production, to interfere with nuclear factor kappa B DNA binding in chondrocytes and synovial cells, and to be associated with decreased expression of interleukin-1b. Long-term oral administration of Gluc reduces the destruction of cartilage and the up-regulation of MMP-3 mRNA in a model of spontaneous OA. It was suggested that since glucosamine inhibits both anabolic and catabolic genes, the therapeutic effects might be due to anti-catabolic rather than to anabolic activities (13). The present study on human dermal fibroblasts confirms what was previously described in chondrocytes, demonstrating an enhancement in both anabolic and catabolic gene activation. Chondrocyte and fibroblast can share some mechanisms associated to senescence. Several factors (cell apoptosis, oxidative stress, decreased responsiveness to growth factors, telomere erosion, glycation of ECM macromolecules) contribute to the modification of ECM production in a quantitative and qualitative manner and, as a consequence, this may lead to decreased tissue repair (14).

In a recent paper (15), the Authors studied whether the concentration of HA in several bio-revitalizing medical devices could represent a significant factor in eliciting the gene encoding for some components of the ECM. Among these, the elastine (ELN) encoding gene displayed a progressively (at 24, 48 and 72 h) more relevant activation using a medical device with a low HA concentration (6.2 mg/ml) but enriched by aminoacids and vitamins. Instead, the product containing a higher (20 mg/ml) HA concentration exhibited a slow and poor ELN gene activation. In contrast, the neutrophil expressed elastase (ELANE) gene was more activated by the products displaying the highest HA concentrations (13 and 20 mg/ml). Noticeably, in the presented experiments Gluc produces activation both of ELN and ELANE genes, thus we hypothesize that this can be due to the progressive transformation of Gluc in HA. Because of the decrease of Gluc and of the consequent increase of HA over time, the gene activation of ELN decreases while ELANE expression increases. This can be a further element supporting the view that the added Gluc really becomes HA.

PDRN enhances the tested genes in lesser amount compared to Gluc

Here the role of PDRN (Fig. 2) was studied. All the tested genes but one were enhanced, the main difference is that HAS1 is virtually unaffected, whereas all the catabolic genes were activated. A possible explanation is an enhancement in cellular metabolism. Further researches are needed to better understand whether it is the cause or consequence of cellular replication.

It is known that PDRN acts as mitogen for fibroblasts, endothelial cells, and pre-adipocytes, working with different growth factors. PDRN is used in plastic and dermatologic surgery for its regenerative properties in ischemic skin flaps and its role has been demonstrated in the clinical improvement after local sub-dermal administration, focusing on its anti-inflammatory and positive regenerative effects (16).

PDRN treatment significantly ameliorated clinical signs of arthritis, improved histologic damage, reduced the cartilage expression and circulating levels of high mobility group box chromosomal protein 1, tumor necrosis factor beta, and interleukin-6 and -10 expression. The concomitant administration of a PDRN antagonist ablated the PDRN-induced protective effect in experimental arthritis. PDRN reduced cytokine production from stimulated human chondrocytes (10).

A recent study confirmed the positive effects of PDRN on the survival of random pattern skin flaps

in rats. The underlying mechanism is likely related to the activation of the PDRN-adenosine A2A receptor-VEGF pathway (17).

Gluc and PDRN exhibit negative synergism on many connective tissue-related genes

In a previous study (18), it was demonstrated that MMP13 and IGF1 gene expression in fibroblast cultures are strongly inhibited after 24 h of incubation with the association of Gluc and PDRN, whereas Gluc and PDRN alone produced a modest inhibition of IGF1 and activation of MMP13. Moreover, ELANE gene was highly over-expressed after incubation with Gluc, less over-expressed with PDRN, but there was a negative synergistic effect with the association that could be useful to reduce ELANE activation given by Gluc alone. The present series of experiments was carried out after 24, 48 and 72 hours of exposure to Gluc and PDRN together, and the negative synergism on all the studied catabolic genes including ELANE was confirmed (Fig. 3).

The relationship between IGF1 and TGF beta has been studied in OA where an increased cartilage inorganic phosphate generation occurs in response to TGF beta and is normally antagonized by IGF1 (19). GDF6 is related to TGF beta super-family and its activation is less pronounced when Gluc is associated to PDRN, and this is further antagonized by the negative synergism observed for IGF1 in the present research.

Bio-stimulation is a therapy aimed to improve the skin appearance by means of cell activation. In this context, the tested drugs seem to produce a tissue repair effect with a further advantage when they are administered simultaneously. In fact, Gluc and PDRN given together produced a negative synergism on all the tested catabolic genes. This can be relevant in anti-aging therapies where the cellular metabolism can be slow and fibroblasts are less represented than in young patients. Thus, it is important to preserve all the components of the extracellular matrix. Moreover, Gluc acts not only as building block in the biosynthesis of glycosaminoglycan chains, but as a booster of HAS1 and this is a further explanation of the hydration improvement observed after the injections.

REFERENCES

1. Coleman SR and Grover R. The anatomy of the aging face: volume loss and changes in 3-dimensional topography. Aesthet Surg J 2006; 26:S4-9.
2. Lambros V. Observations on periorbital and midface aging. Plast Reconstr Surg 2007; 120: 1367-76; discussion 77.
3. Fisher GJ, Varani J, Voorhees JJ. Looking older: fibroblast collapse and therapeutic implications. Arch Dermatol 2008; 144:666-72.
4. Varani J, Perone P, Fligiel SE, Fisher GJ, Voorhees JJ. Inhibition of type I procollagen production in photodamage: correlation between presence of high molecular weight collagen fragments and reduced procollagen synthesis. J Invest Dermatol 2002; 119:122-9.
5. Chen CS, Mrksich M, Huang S, Whitesides GM, Ingber DE. Geometric control of cell life and death. Science 1997; 276:1425-8.
6. Avantaggiato A, Palmieri A, Carinci F, Pasin M, Bertuzzi GL. Biostimulation and biorevitalization: effects on human skin fibroblasts. Ann Oral Maxillofacial Surg 2013; 1:11.
7. Laurent TC, Laurent UB, Fraser JR. The structure and function of hyaluronan: An overview. Immunol Cell Biol 1996; 74:A1-7.
8. Henrotin Y, Mobasheri A, Marty M. Is there any scientific evidence for the use of glucosamine in the management of human osteoarthritis? Arthritis Res Ther 2012; 14: 201.
9. Bertuzzi G. Medicina anti-aging. Editor Academia Universa Press 2010: 188-90.
10. Bitto A, Polito F, Irrera N, et al. Polydeoxyribonucleotide reduces cytokine production and the severity of collagen-induced arthritis by stimulation of adenosine A((2)A) receptor. Arthritis Rheum 2011; 63:3364-71.
11. Uitterlinden EJ, Koevoet JL, Verkoelen CF, Bierma-Zeinstra SM, Jahr H, Weinans H, Verhaar JA, van Osch GJ. Glucosamine increases hyaluronic acid production in human osteoarthritic synovium explants. BMC Musculoskelet Disord 2008; 9:120.
12. Rovati LC, Girolami F, Persiani S. Crystalline glucosamine sulfate in the management of knee osteoarthritis: efficacy, safety, and pharmacokinetic properties. Ther Adv Musculoskelet Dis 2012; 4:167-80.
13. Reginster JY, Neuprez A, Lecart MP, Sarlet N,

Bruyere O. Role of glucosamine in the treatment for osteoarthritis. Rheumatol Int 2012; 32:2959-67.
14. Henrotin Y, Chevalier X, Herrero-Beaumont G, et al., Participants at the Hohenheim Consensus Conference in August 2011. Physiological effects of oral glucosamine on joint health: current status and consensus on future research priorities. BMC Res Notes 2013; 6:115.
15. Avantaggiato A, Girardi A, Palmieri A, Pascali M, Carinci F. Comparison among bio-revitalizing injective products: a study on skin fibroblast cultures. Rejuvenation Res 2015; 18:270-6.
16. Laino L, Suetti S, Sperduti I. Polydeoxyribonucleotide dermal infiltration in male genital lichen sclerosus: adjuvant effects during topical therapy. Dermatol Res Pract 2013; 2013:654079.
17. Chung KI, Kim HK, Kim WS, Bae TH. The effects of polydeoxyribonucleotide on the survival of random pattern skin flaps in rats. Arch Plast Surg 2013; 40:181-6.
18. Avantaggiato A, Palmieri A, Carinci F, Trapella G, Sollazzo V, Lauritano D. Effects of glucosamine and nucleotide association on fibroblast: extracellular matrix gene expression. Int J Immunopathol Pharmacol 2014; 27:689-93.
19. Johnson K, Farley D, Hu SI, Terkeltaub R. One of two chondrocyte-expressed isoforms of cartilage intermediate-layer protein functions as an insulin-like growth factor 1 antagonist. Arthritis Rheum 2003; 48:1302-14.

PAPILLARY THYROID CANCER IS CHARACTERIZED BY ALTERED EXPRESSION OF GENES INVOLVED IN THE SUMOYLATION PROCESS

C. TUCCILLI[1], E. BALDINI[1], S. SORRENTI[2], C. DI GIOIA[3], D. BOSCO[3], V. ASCOLI[3], C. MIAN[4], S. BAROLLO[4], R. RENDINA[1], C. COCCARO[1], M. PEPE[1], A. CATANIA[2], M. BONONI[5], F. TARTAGLIA[2], E. DE ANTONI[2], M. D'ARMIENTO[1] and S. ULISSE[1]

[1]Department of Experimental Medicine, "Sapienza" University of Rome, Italy; [2]Department of Surgical Sciences, "Sapienza" University of Rome, Italy; [3]Department of Radiology,Oncology and Pathological Anatomy, "Sapienza" University of Rome, Italy; [4]Department of Medicine, University of Padua, Italy; [5]Department of Surgery "Pietro Valdoni", "Sapienza" University of Rome, Italy

The first two authors contributed equally to the work

Received April 9, 2015 - Accepted June 19, 2015

Small Ubiquitin–like MOdifier (SUMO) proteins are small protein modifiers capable of regulating cellular localization and function of target proteins. Over the last few years, a relevant role has been demonstrated for sumoylation in the modulation of important cellular processes, including gene transcription, DNA repair, cell-cycle regulation and apoptosis. Components of the sumoylation machinery have been found deregulated in different human cancers, and are thought to significantly affect cancer cell progression. In the present study we sought to analyze the expression of all the components of the sumoylation machinery in a case study comprising 77 papillary thyroid cancers (PTC) and normal matched tissues. In particular, we evaluated the expression of the SENP1 to SENP8 (SENtrin-specific proteases), SAE1 (SUMO1 activating enzyme subunit 1), UBA2 (UBiquitin-like modifier activating enzyme 2), UBC9 (UBiquitin conjugating enzyme 9), RanBP2 (RAN binding protein 2), MSMCE2 (Non-SMC element 2), CBX4 (ChromoBoX homolog 4), PIAS1 to PIAS4 (protein inhibitor of activated STAT), ZMIZ1 (zinc finger, MIZ-type containing 1) and ZMIZ2 (Zinc finger, MIZ-type containing 2) by means of quantitative RT-PCR. In most of the PTC examined we observed a significant alteration in the mRNAs of SENP8, ZMIZ1, SAE1, PIAS1 and PIAS2. These tended to be reduced in about 50 to 66% of cases, and unchanged or increased in the remaining ones. Univariate and Kaplan-Mayer analyses documented the lack of association between the expression of the above 5 genes and clinicopathological parameters. Only SAE1 was significantly higher in female PTC tissues, in respect to male PTC tissues (p=0.021), and SENP8 was significantly lower in TNM stages III-V, with respect to stages I-II (p=0.047). In conclusion, we demonstrated that the expression of SENP8, SAE1, PIAS1, PIAS2 and ZMIZ1 is deregulated in the majority of PTC tissues, likely contributing to the PTC phenotype. However, differently from other human cancers, their mRNA level does not represent a prognostic biomarker in PTC patients.

Key words: thyroid cancer, prognosis, sumoylation, SENP, SAE1, UBA2. UBC9, RanBP2, MSMCE2, CBX4, PIAS, ZMIZ

Mailing address: Prof. Salvatore Ulisse,
Department of Experimental Medicine,
"Sapienza" University of Rome,
Viale Regina Elena, 324
00161-Rome, Italy.
Tel.: +39 0649972607 Fax: +39 0649972606
e-mail: salvatore.ulisse@uniroma1.it

0393-974X (2015)

Small Ubiquitin–related MOdifier (SUMO), ubiquitously expressed proteins of about 10 kDa, are reversible protein modifiers including SUMO1, 2, 3 and 4. Following sumoylation, target proteins can alter their cellular localization because of changes in their interactions with other proteins (1). The first step in sumoylation is the activation of SUMO proteins by SUMO-specific isopeptidases (SENPs, SENtrin-specific Proteases). Eight different SENP proteins have been identified in human cells (SENP1 to SENP8). Activated SUMOs interact with the E1 activating enzyme, composed by SAE1 and UBA2 proteins, which forms a thioester bond between SUMO and UBA2. SUMO is then transferred to the E2 conjugating enzyme UBC9, and from this to target proteins. This reaction is catalyzed by different SUMO E3 ligases, which include the PIAS protein family (PIAS1 to 4), ZMIZ1, ZMIZ2,CBX4, MSMCE2 and RanBP2. Finally, SUMO can be removed from target proteins by SENPs (1). Experimental evidence demonstrated that sumoylation affects important cellular processes such as cell-cycle regulation, proliferation and apoptosis (1). Not surprisingly, the sumoylation pathway is deregulated in different human cancers where it is thought to significantly affect cancer development and progression (2). To date, however, no information regarding the expression of the components of the sumoylation machinery has been reported in differentiated thyroid cancer (DTC). The latter represents the most common endocrine malignancy with an increasing incidence over the last decades (3, 4). DTC comprise two main histological entities, the follicular thyroid carcinoma (FTC) and the more common papillary thyroid carcinoma (PTC). Relevant molecular alterations encountered in DTC progression comprise gene rearrangements of tyrosine kinase receptors, such as the RET/PTC (REarranged in Transformation/Papillary Thyroid Carcinoma) and NTRK1 (neurotrophic tyrosine kinase receptor, type 1), activating point mutations of RAS, BRAF, PI3K (Phosphatidyl-Inositol 3-Kinase) or the oncogenic fusion protein PAX8-PPARg, as well as inactivating mutations of the tumor suppressor genes PTEN and TP53 (5). The prognosis of DTC patients is usually favorable, but about 20% of them face disease recurrence and/or DTC-related deaths (6). At present, the stratification and prognosis of DTC patients count only on clinicopathological variables, which, however, are capable of providing only a rough prediction of the disease outcome (7). Similarly, they fail to predict the risk of cancer recurrence. Therefore, the identification of new prognostic biomarkers able to testify tumor aggressiveness is required (8, 9).

We here analyzed the expression of the components of the sumoylation machinery in a case study of 77 PTC, and evaluated their association with clinicopathological parameters, including disease recurrence and disease-free intervals.

MATERIALS AND METHODS

Tissue samples, histology and patient staging

The case study included 77 consecutive patients; papillary thyroid cancer (PTC) and normal matched tissues were obtained from surgical specimens of 18 males and 59 females (age range 11-83 yrs, median 47 yrs) who underwent total thyroidectomy for PTC in the Department of Surgical Sciences, “Sapienza” University of Rome (n=20), or in the Department of Medical and Surgical Sciences, University of Padua, Italy (n=57). All patients gave their written informed consent. For three underage patients the written informed consent was obtained from their parents. The study was approved by the Policlinico Umberto I hospital ethics committee (Ref. 2615). Tissue samples were collected, frozen in liquid nitrogen and stored at −80°C. Of the 77 PTC patients, 68 exhibited the classical, 8 the follicular, and 1 the tall cell variant. Two different histopathologists made the histological diagnoses independently according to the World Health Organization classification (10). At the time of surgery, lymph node metastases were found in 36 patients. Following TNM staging, 47 patients were identified as being at stage I, 1 at stage II, 22 at stage III and 7 at stage IV. Forty to fifty days after surgery all patients underwent radioiodine therapy, and the subsequent whole body scan (WBS) showed the absence of metastases. Patients then started thyroid hormone replacement therapy. To ascertain their disease-free condition, 4 to 5 months later all the patients underwent neck ultrasound and serum Tg measurement. Recurrences were diagnosed by fine-needle aspiration (FNA) cytology, ^{131}I WBS or histological analysis following surgical resection of the lesion. The follow-up (median 64 months, range 8-133 months) was available for 75 patients (18 males and 57 females with a median age of 45 yrs), 48 of whom were at TNM stage I-II and the remaining 27 at stage III-IV. The lower limit of times-to-recurrence started at 6 months. During the

follow-up 19 recurrences were recorded, 16 being cervical lymph nodes, diagnosed by FNA cytology, and 3 lung metastases, diagnosed by WBS.

Determination of $BRAF^{V600E}$ mutation

Genomic DNA was extracted from the frozen tissues using the DNeasy Blood and Tissues kit according to the manufacturer's protocol. The BRAF status of exon 15 was assessed by both direct sequencing and mutant allele-specific PCR amplification for the T to A substitution at nucleotide 1799 (V600E), using the procedure previously described (11).

Extraction and analysis of mRNA

The thyroid tissues were homogenized in Isol-RNA Lysis Reagent™ (Eppendorf, Milan, Italy) with ultra-turrax, and total RNA was extracted as previously described (12). The first cDNA strand was synthesized from 5 µg of RNA with M-MLV reverse transcriptase and anchored oligo(dT)23 primers (Sigma-Aldrich, Milan, Italy). Parallel controls for DNA contamination were carried out omitting the reverse transcriptase. The templates obtained were used for quantitative PCR amplifications of the different components of the sumoylation machinery and housekeeping genes employing the LightCycler instrument (Roche Diagnostics, Mannheim, Germany), the SYBR Premix Ex Taq II (TliRNase H Plus) (Takara, Otsu, Shiga, Japan) and specific primers listed in Table I. Amplicon specificities were checked by automated DNA sequencing (Primm, San Raffaele Biomedical Science Park, Milan, Italy), evaluation of melting temperatures, and/or electrophoresis on 2% agarose gel containing ethidium bromide. Standard curves for all genes were achieved with five-fold dilutions of cDNA from mixed human thyroid tissues. Calculation of data was performed by the Relative Expression Software Tool (REST 2009) using a normalization factor (NF) computed as the geometric media of three reference genes (GAPDH, RPL13A and SDHA), as previously described (13). The fold change of gene expression for each tumor sample was referred to its normal counterpart. Fold variations between 0.8 and 1.2 were considered unchanged.

Statistical analysis

The non-parametric Mann Whitney test was used to calculate the statistical significance of differences in the expression levels of the considered components of the sumoylation machinery, comparing their mRNA levels

Table I. *Sequences of the primers used in qRT-PCR for the target and reference genes.*

Gene	Primer sequence	Gene	Primer sequence
SAE1	F: 5'-CGACACCAAGAGAGCAAAAC-3' R: 5'-CTCCAGGGCTTCTTTAACAGG-3'	**PIAS4**	F: 5'- AGACCATTGGGGTAAAGCAC-3' R: 5'- CATCTTCACCAGCGGACAG-3'
UBA2	F: 5'- CAAGCAGATGACTTCCTCCAG-3' R: 5'- CTTTTGGCAGCATCTTCAGC-3'	**SENP1**	F: 5'- TTGGAGTGGTTCATGTCGTC-3' R: 5'- AAAATGTGTGGTGGGTTTGG-3'
UBC9	F: 5'- AAAGGGACTCCGTGGGAAG -3' R: 5'- CGGGTGAAATAATGGTGGTTC -3'	**SENP2**	F: 5'- CAGAGTCCTGCCTTCCTTTG-3' R: 5'- CAGCCTGTTCCTGAGGTTTC-3'
RanBP2	F: 5'- TCCTCTGAAACTATGGACAAACC-3' R: 5'- TTACTGGAAGCCAAGTCTGC-3'	**SENP3**	F: 5'- ACCTGGTCATGGACACAGTC-3' R: 5'- TGGATGGGGATTAGCAGTAGC-3'
NSMCE2	F: 5'- GCCTGTATCAACTCTGGTATGG-3' R: 5'- AGTTGCCGATCCAATGTAGC-3'	**SENP5**	F: 5'- AACAGTCAGAAAGCCTCTCCAG-3' R: 5'- GGAACCAAACTGCCATACTTC-3'
CBX4	F: 5'- GTGAAATGGAGAGGCTGGTC-3' R: 5'- ACGACGGGCAAAGGTAGG-3'	**SENP6**	F: 5'- TTCCTCGCTGATGACAACTG-3' R: 5'- GACAACATTTGACCGAGAAGG-3'
ZMIZ1	F: 5'- TGAAGTGCCCCATCACATTC-3' R: 5'- CCAGCAGAGCGGTTTTATTG-3'	**SENP7**	F: 5'- TTCTTTCCCTGCTGGTGTTG-3' R: 5'- AACCGCTACTTTGCTTCTGC-3'
ZMIZ2	F: 5'- CTCAAGCCCAACCTCAACTC-3' R: 5'- GAAGGTCAGCCGCAACTC-3'	**SENP8**	F: 5'- TGTACTGGAAAGGGATGTCG-3' R: 5'- ACGGGGTCCATCTTGTACTG-3'
PIAS1	F: 5'- ACCTGGGTTTGTCCTGTCTG-3' R: 5'- ATCTCATCGGTGCCCAAG-3'	**GAPDH**	F: 5'-ATCATCAGCAATGCCTCCTG-3' R: 5'-GGCCATCCACAGTCTTCTG-3'
PIAS2	F: 5'- GAAACACAAAGCAGCCCAAC-3' R: 5'- ATCAACCGAAGTCACACTGG-3'	**RPL13A**	F: 5'-ACCGTGCGAGGTATGCTG-3' R: 5'-TAGGCTTCAGACGCACGAC-3'
PIAS3	F: 5'- GACAAGAAGGCTCCCTATGAATC-3' R: 5'- AAACCTCAGATGCCTCCTTC-3'	**SDHA**	F: 5'-GCATAAGAACATCGGAACTGC-3' R: 5'-GGTCGAACGTCTTCAGGTG-3'

GAPDH, glyceraldehyde-3-phosphate dehydrogenase; RPL13A, ribosomal protein L13a; SDHA, succinate dehydrogenase complex, subunit A.

between PTC tissues, and in wild type versus BRAF-mutated BRAF PTC samples. In addition, the association of the deregulated expression of components of the sumoylation machinery with gender, histology, lymph node metastasis, TNM stage or recurrences was evaluated by the Mann Whitney test. The correlation analysis between mRNA levels and age was performed using the Rho Spearman test. The impact of gene expression on the disease-free interval (DFI) was assessed by means of Kaplan-Meier analysis combined with Mantel-Cox log-rank. For the Kaplan-Meier analysis, PTCs were divided into three groups based on increased, unchanged or decreased gene expression. All statistical analyses were carried out using version 8.0 of the Stata software (Stata Corporation 2003, College Station, Tx). Results were considered significantly different if p values were lower than 0.05.

RESULTS

Normal human thyroid tissues express, at the mRNA level, all the molecular players involved in the sumoylation pathway (data not shown). In order to evaluate major alterations in the expression of these genes, we first analyzed a pool of cDNA obtained from 20 PTC tissues compared to a pool of cDNA from 20 normal matched tissues, by means of quantitative RT-PCR experiments. The results demonstrated a significant deregulation of SENP8, SAE1, PIAS1, PIAS2 and ZMIZ1 (data not shown). The expression of these genes was then analyzed in the single cDNAs from papillary thyroid cancer (PTC) and normal matched tissues (Table II). The data obtained showed that SENP8 mRNA level was altered in 64 out of 77 PTC tissues (83.1%, up-regulated in 14 and down-regulated in 50), that of SAE1 in 54 (70.1%, up-regulated in 15 and down-regulated in 39), that of PIAS1 in 64 (83.1%, up-regulated in 13 and down-regulated in 51), that of PIAS2 in 64 (83.1%, up-regulated in 14 and down-regulated in 50), and that of ZMIZ1 in 57 (74%, up-regulated in 17 and down-regulated in 40). Overall, a tendency to underexpression emerged, ranging from 50.6% (SAE1) to 66.2% (PIAS1) of the PTC tissues (Table II). Thereafter, we performed a univariate statistical analysis in which the mRNA levels of SENP8, SAE1, PIAS1, PIAS2 and ZMIZ1 were compared to gender, age, tumor histology, presence/absence of BRAF mutations, tumor size, lymph node metastasis, TNM stage and recurrences (Table III). No association was found between the expression of the above 5 genes and BRAF status or the clinicopathological parameters. The only exceptions were represented by SENP8, significantly lower in TNM stages III-IV compared to stages I-II (p=0.047), and SAE1, significantly higher in female PTC tissues compared to male PTC tissues (p=0.021) (Table III). Moreover, Kaplan-Meier analyses demonstrated the lack of correlation between any alteration of these mRNAs and disease free interval (Fig. 1).

Table II. *Fold changes of mRNA levels of SENP8, ZMIZ1, SAE1, PIAS1 and PIAS2 in 77 PTC tissues compared to their normal matched tissues.*

	SENP8	ZMIZ1	SAE1	PIAS1	PIAS2
N° of cases with unchanged expression	13/77	20/77	23/77	13/77	13/77
***Fold* change Median (Range)**	0.952 (0.861 - 1.112)	1.004 (0.807 - 1.186)	0.967 (0.816 - 1.161)	0.911 (0.812 - 1.164)	0.960 (0.804 - 1.108)
N° of cases with decreased expression	50/77	40/77	39/77	51/77	50/77
***Fold* change Median (Range)**	0.519 (0.000 - 0.791)	0.528 (0.052 - 0.763)	0.557 (0.052 - 0.786)	0.530 (0.082 - 0.797)	0.500 (0.100 - 0.960)
P value	**<0.0001**	**<0.0001**	**<0.0001**	**<0.0001**	**<0.0001**
N° of cases with increased expression	14/77	17/77	15/77	13/77	14/77
***Fold* change Median (Range)**	1.602 (1.235 - 5.659)	1.795 (1.286 - 4.168)	1.498 (1.208 - 10.381)	1.686 (1.200 -20.504)	1.7135 (1.247 - 6.274)
P value	**<0.0001**	**<0.0001**	**<0.0001**	**<0.0001**	**<0.0001**

For each gene, the median fold change is reported along with the range of the fold change shown in brackets.

Table III. *Univariate statistical analysis of the expression of the different components of the sumoylation machinery and clinicopathological parameters in 77 PTC patients.*

	SENP8	*p* value	ZMIZ1	*p* value	SAE1	*p* value	PIAS1	*p* value	PIAS2	*p* value
Gender										
Male (n=18)	0.595 (0.000-1.969)	0.241	0.552 (0.112-2.633)	0.186	0.645 (0.115-1.251)	**0.021**	0.594 (0.132-2.228)	0.838	0.617 (0.100-4.387)	0.196
Female (n=59)	0.681 (0.077-5.659)		0.763 (0.052-4.168)		0.836 (0.052-10.381)		0.629 (0.082-20.504)		0.662 (0.148-6.274)	
Age (Range 11-83 yr)										
Correlation coefficient	-0.175	0.130	-0.194	0.091	-0.096	0.408	-0.132	0.252	-0.077	0.506
Histology										
Classic variant (n=68)	0.681	0.155	0.785	0.210	0.820	0.067	0.633	0.414	0.652	0.568
	(0.000-5.659)		(0.235-4.135)		(0.276-6.953)		(0.082-20.504)		(0.100-6.274)	
Other variants (n=9)	0.612		0.666		0.610		0.576		0.659	
	(0.077-0.936)		(0.025-1.718)		(0.052-1.151)		(0.202-3.331)		(0.148-1.900)	
BRAF										
Wild Type (n=38)	0.731	0.209	0.832	0.795	0.833	0.350	0.663	0.835	0.747	0.122
	(0.000-5.659)		(0.052-4.135)		(0.052-10.381)		(0.082-1.701)		(0.100-6.274)	
V600E (n=38)	0.633		0.726		0.742		0.568		0.612	
	(0.070-2.749)		(0.185-4.168)		(0.379-1.721)		(0.283-20.504)		(0.262-2.074)	
Tumor size										
T1-2 (n=29)	0.764	0.346	0.807	0.427	0.872	0.175	0.742	0.087	0.807	0.110
	(0.000-5.659)		(0.052-4.135)		(0.052-6.953)		(0.082-3.331)		(0.100-6.274)	
T3-4 (n=48)	0.633		0.741		0.776		0.586		0.625	
	(0.065-1.986)		(0.185-4.168)		(0.337-10.381)		(0.132-20.504)		(0.237-3.955)	
Lymph node metastasis										
No (n=41)	0.620	0.242	0.741	0.799	0.768	0.327	0.568	0.286	0.628	0.752
	(0.000-3.628)		(0.052-2.544)		(0.052-2.836)		(0.082-3.331)		(0.100-3.955)	
Yes (n=36)	0.693		0.770		0.830		0.652		0.662	
	(0.065-5.659)		(0.233-4.168)		(0.365-10.381)		(0.132-20.504)		(0.237-6.274)	
TNM Stage										
I-II (n=48)	0.740	**0.047**	0.832	0.308	0.811	0.355	0.711	0.059	0.640	0.418
	(0.000-5.659)		(0.052-4.135)		(0.052-10.381)		(0.082-20.504)		(0.100-6.274)	
III-IV (n=29)	0.595		0.711		0.710		0.531		0.707	
	(0.065-1.847)		(0.185-4.168)		(0.398-1.498)		(0.132-1.317)		(0.237-4.387)	
Recurrences										
No (n=56)	0.681	0.322	0.785	0.184	0.820	0.639	0.681	0.099	0.652	0.361
	(0.000-5.659)		(0.052-4.168)		(0.052-6.953)		(0.082-20.504)		(0.100-6.274)	
Yes (n=19)	0.581		0.658		0.691		0.566		0.598	
	(0.065-1.986)		(0.233-2.827)		(0.337-10.381)		(0.132-1.479)		(0.237-3.955)	

For each gene, the median fold change is reported along with the range of the fold change shown in brackets.

DISCUSSION

Over the last decade, considerable experimental evidence clearly indicated that protein sumoylation could have an important role in tumorigenesis (2, 14). In fact, sumoylation has been demonstrated to be involved in the maintenance of genomic integrity and DNA damage repair, gene transcription, nuclear-cytoplasmic transport, functions of mitochondrial, endoplasmic reticulum and plasma membrane proteins, affecting important cellular processes such as cell-cycle progression, proliferation and apoptosis (2, 14). Several components of the sumoylation pathway, including UBC9, SENP1 and PIAS1, have been found deregulated in different cancer tissues (2). In particular, up-regulation of UBC9 was shown to occur in multiple myeloma and ovarian, lung and cervical cancers (2, 15, 16). On the contrary, lower UBC9 expression was observed in metastatic breast, lung and prostate cancer (15). In addition, in breast

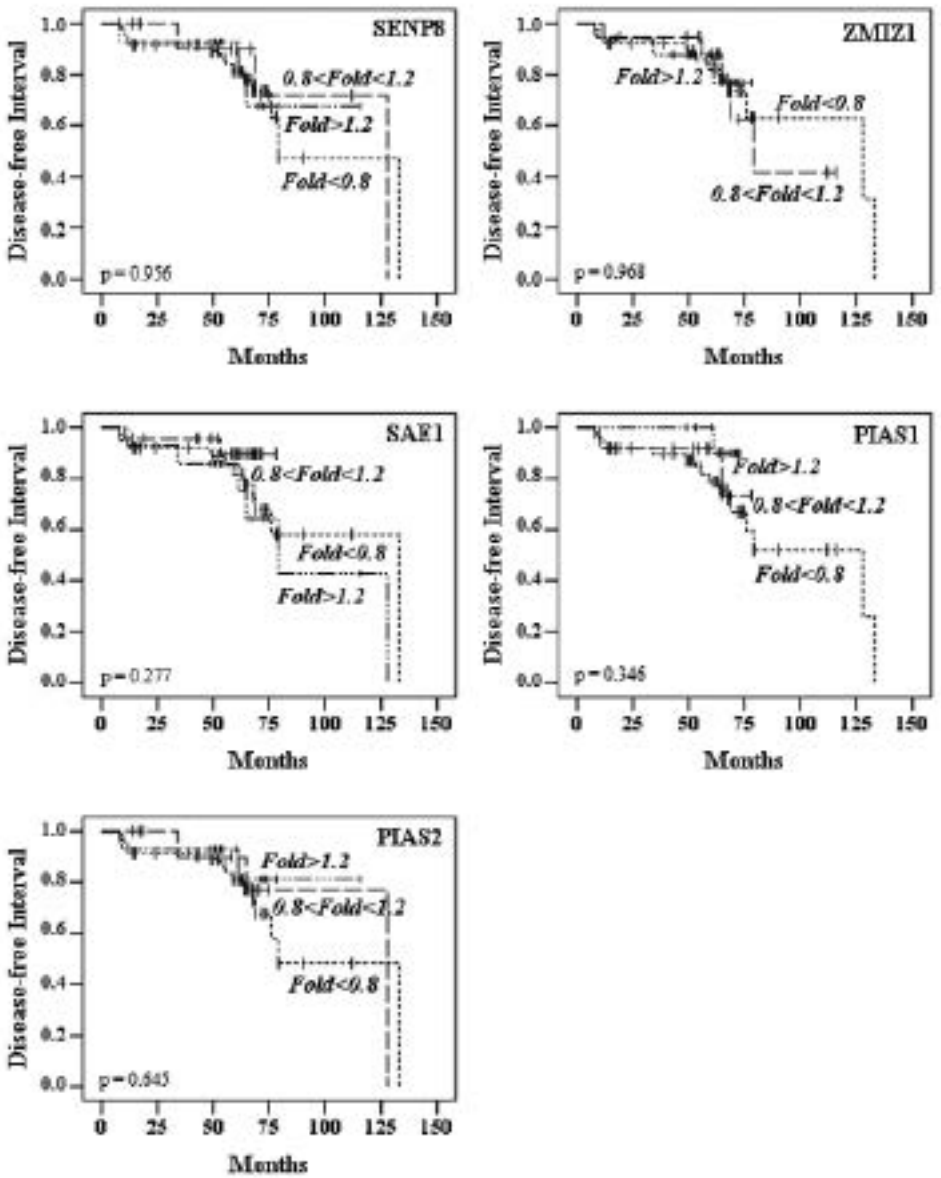

Fig. 1. *Kaplan-Meier analyses demonstrating the lack of correlation between SENP8, SAE1, PIAS1, PIAS2 and ZMIZ1 mRNAs and disease-free interval in papillary thyroid cancer patients. Kaplan-Meier analysis combined with Mantel-Cox log-rank test was performed as described in the Materials and Methods section. PTC patients were divided into three groups based on increased, unchanged or decreased gene expression.*

cancer the association of UBC9 polymorphisms with tumor grade was observed, and in multiple myeloma PIAS1 was found overexpressed and correlated with a poor outcome (17). Regarding thyroid neoplasms, to the best of our knowledge only one report described the overexpression of SENP1 in oncocytic adenomas compared to normal thyroid tissues (18). In the present study, we showed that at least five of the twenty genes of the sumoylation machinery analyzed were deregulated in papillary thyroid cancer (PTC) compared to normal matched tissues. These include SENP8 and SAE1, both involved in SUMO activation, and the E3 ligases ZMIZ1, PIAS1 and PIAS2. In particular, all five genes were down-regulated in a high proportion of the PTC tissues analyzed (about 60%), while in the remaining cases were either up-regulated (approx. 20%) or unchanged (approx. 20%). Since

the $BRAF^{V600E}$ mutation represents the most frequent genetic alteration encountered in PTC tissues, we sought to verify whether it could be responsible for the observed changes in the mRNA levels of SENP8, SAE1, ZMIZ1, PIAS1 and PIAS2. The results clearly demonstrate that this is not the case.

The findings here reported could contribute to clarifying the molecular mechanisms underlying PTC progression. For example, RET/PTC oncoproteins, constitutively active tyrosine kinases found in about 6 to 10% of PTC, phosphorylate and activate the transcription factor STAT1 (signal transducer and activator of transcription 1). As PIAS1 has been shown to strongly repress RET/PTC-induced transcriptional activity of STAT1, it may be speculated that the reduced expression of PIAS1 here reported may reinforce RET/PTC-induced STAT1 activation (19). Moreover, some PTC exhibit the oncogene RET/PTC1, generated by CCDC6-RET fusions, whose effect on CCDC6 activity is not yet known. CCDC6 is a protein ubiquitously expressed, thought to function as a tumor suppressor and recently identified as a repressor of CREB1-dependent transcription. Sumoylation has emerged as an important mechanism in CCDC6 transcriptional control, constraining most of the protein in the cytosol and affecting its functional interaction with CREB1 (20).

A further example of possible involvement of sumoylation in thyroid tumors is represented by the ERK (extracellular signal-regulated kinase) MAPK (mitogen-activated protein kinase) cascade, initiated by cell-surface-receptor tyrosine kinases and essential in cellular proliferation, differentiation, and survival. Its inappropriate activation is a common feature in human cancers. In particular, ERK pathway was found to be downregulated by MEK (MAPK-ERK kinase) sumoylation, which inhibits MEK-induced ERK phosphorylation by disrupting MEK-ERK docking (21). Activating mutations of RAS, often observed in PTC, were shown to abrogate MEK sumoylation by impairing the specific SUMO-E3 ligase function of MEKK1 (22). Thus, oncogenic RAS can trigger the ERK pathway directly via the effector Raf, but also through inhibition of MEK sumoylation.

The tumor suppressor gene p53, of which loss-of-function mutations are held responsible for the transition from the well-differentiated to the poorly differentiated and anaplastic thyroid cancers (1, 22, 23), is also worthy of mention. Using a yeast two-hybrid screening strategy with a common tumour-derived p53 mutant as bait, UBC9 and PIAS1 were identified as mutant p53-interacting partners, and PIAS1 was shown to be involved in the sumoylation of p53 (22, 23). However, recent data on p53 and PIAS1 have been conflicting because one study reported that PIAS proteins exert a strong repressive effect on p53-dependent transactivation, while another study showed that PIAS1 increased the steady-state levels and the half-life of p53 enhancing p53-mediated gene expression in a variety of cell lines (23). According to the latter, the reduced expression of PIAS1 here reported could be detrimental to p53 functions in thyroid cancer cells.

As mentioned above, previous findings suggested a prognostic value for components of the sumoylation machinery in different types of human cancers. Thus, in the present study we attempted to correlate the expression of SENP8, SAE1, ZMIZ1, PIAS1 and PIAS2 with clinicopathological variables such as gender, age, tumor size and histology, lymph node metastasis, TNM stage and recurrences. Univariate analyses documented the lack of association between the mRNA levels of all 5 genes analyzed and the clinicopathological parameters.The only exceptions were represented by SENP8, significantly lower in TNM stages III-IV compared to stages I-II, and SAE1, significantly higher in female PTC tissues compared to male PTC tissues. The clinical implications of these observations remain, however, to be elucidated. In addition, Kaplan-Meier and multivariate analyses confirmed that deregulated expression of SENP8, SAE1, ZMIZ1, PIAS1 and PIAS2 is not a prognostic biomarker for PTC patients.

Further studies are needed to confirm these data in post-transcriptional level, that is to evaluate quantitative changes of proteins contributing to the sumoylation process as well as of their targets, especially those involved in the progression of thyroid cancer as STAT1 and p53.

In conclusion, our data demonstrate that the expression of SENP8, SAE1, ZMIZ1, PIAS1 and PIAS2 was deregulated in the majority of PTC tissues analysed, likely contributing to tumor progression. However, differently from other human cancers, the expression of these genes fail to predict the risk of recurrence in PTC patients.

REFERENCES

1. Geiss-Friedlander R, Melchior F. Concept in sumoylation: a decade on. Nat Rev Mol Cell Biol 2007; 8:947-56.
2. Betterman K, Benesch M, Weis S, Haybaeck J. SUMOylation in carcinogenesis. Cancer Lett 2012; 316:113-25.
3. Davies L, Welch HG. Increasing incidence of thyroid cancer in the United States, 1973-2002. Jama 2006; 295:2164-67.
4. Kinder BK. Well differentiated thyroid cancer. Curr Opin Oncol 2003; 15:71-77.
5. The cancer Genome Atlas Research Network. Integrated genomic characterization of papillary thyroid carcinoma. Cell 2014; 159:676-90.
6. Gospodarowicz MK, Henson DE, Hutter RVP, O'Sullivan B, Sobin LH, Wittekind Ch (eds). Prognostic factors in cancer. 2nd ed. New York: Wiley-Liss, 2001.
7. Castagna MG, Maino F, Cipri C, Belardini V, Theodoropoulou A, Cevenini G, Pacini F. Delayed risk stratification, to include the response to initial treatment (surgery and radioiodine ablation), has better outcome predictivity in differentiated thyroid cancer patients. Eur J Endocrinol 2011; 165:441-46.
8. Handkiewicz-Junak D, Czarniecka A, Jarząb B.Molecular prognostic markers in papillary thyroid cancer: current status and future directions. Mol Cell Endocrinol 2010; 322:8-28.
9. Baldini E, Sorrenti S, D'Armiento E, Di Matteo FM, Catania A, Ulisse S. The urokinase plasminogen activating system in thyroid cancer: clinical implications. G Chir 2012; 33:305-10.
10. Hedinger C, Williams ED, Sobin LH. The WHO histological classification of thyroid tumors: a commentary on the second edition. Cancer 1989; 63:908-11.
11. Barollo S, Pennelli G, Vianello F, et al. BRAF in primary and recurrent papillary thyroid cancer: the relationship with (131)I and 2-[(18)F]fluoro-2-deoxy-D-glucose uptake ability. Eur J Endocrinol 2010; 163:659-63.
12. Chomczynsky P, Sacchi P. Single step method of RNA isolation by guanidinium thiocyanate-phenol-chloroform extraction. Anal Biochem 1987; 62:156-9.
13. Ulisse S, Baldini E, Sorrenti S, et al. High expression of the urokinase plasminogen activator and its cognate receptor associates with advanced stages and reduced disease-free interval in papillary thyroid carcinoma. J Clin Endocrinol Metab 2011; 96:504-8.
14. Lee SL, Choi HJ, Baek SH. Sumoylation and its contribution to cancer. In: SUMO regulation of cellular processes. V.G. Wilson. Ed. Springer, London, 2009; pp253-72.
15. Moschos SJ, Jukic DM, Athanassiou C, et al. Expression analysis of Ubc9, the single small ubiquitin-like modifier (SUMO) E2 conjugating enzyme, in normal and malignant tissues. Hum Pathol 2010; 41:1286-98.
16. Mo YY, Moschos SJ. Targeting Ubc9 for cancer therapy. Expert Opin Ther Targets 2005; 9:1203-16.
17. Driscoll JJ, Pelluru D, Lefkimmiatis K, et al. The sumoylation pathway is deregulated in multiple myeloma and is associated with adverse patient outcome. Blood 2010; 115:2827-34.
18. Jacques C, Baris O, Prunier-Mirebeau D, et al. Two-step differential expression analysis reveals a new set of genes involved in thyroid oncocytic tumors. J Clin Endocrinol Metab 2005; 90:2314-20.
19. Hwang ES, Kim DW, Hwang JH, et al. Regulation of "signal transducer and activator of transcription" (STAT1) and STAT1-dependent genes by RET/PTC (rearranged in transformation/papillary thyroid cancer) oncogenic tyrosine kinases.
20. Luise C, Merolla F, Leone V, Paladino S, Sarnataro D, Fusco A, Celetti A. Identification of sumoylation sites in CCDC6, the first identified RET partner gene in papillary thyroid carcinoma, uncovers a mode of regulating CCDC6 function on CREB1 transcriptional activity. PLoS One 2012; 7:e49298.
21. Kubota Y, O'Grady P, Saito H, Takekawa M. Oncogenic Ras abrogates MEK SUMOylation that suppresses the ERK pathway and cell transformation. Nat Cell Biol 2011; 13:282-91.
22. Kahyo T, Nishida T, Yasuda H. Involvement of PIAS1 in the sumoylation of tumor suppressor p53. Mol Cell 2001; 8:713-8.
23. Schmidt D, Müller S. Members of the PIAS family act as SUMO ligases for c-Jun and p53 and repress p53 activity. Proc Natl Acad Sci USA 2002; 99:2872-7.

CD133 EXPRESSION COULD BE A PREDICTIVE MARKER OF PERIODONTAL REGENERATION

G. LUCARINI[1], A. ZIZZI[2], L. FERRANTE[3], A.B. D'ANGELO[4], C. RUBINI[2] and S.D. ASPRIELLO[5]

[1]Department of Clinic and Molecular Sciences, Histology, Polytechnic University of Marche, Torrette, Ancona; [2]Department of Biomedical Sciences and Public Health, Section of Pathologic Anatomy and Histopathology, Polytechnic University of Marche, Torrette, Ancona; [3]Department of Clinical Medicine and Applied Biotechnologies, Unit of Medical Statistics, Polytechnic University of the Marche, Torrette, Ancona; [4]Dental Clinic Private Practice, Ancona, Italy; [5]Dental Clinic Private Practice, Pesaro, Italy

The first two authors contributed equally to this work

Received November 11, 2014 – Accepted June 23, 2015

Periodontal regeneration needs formation of new connective tissue at the root surface, involving periodontal fibre development and angiogenesis. CD133 or prominin-1, is an important regulator of apoptosis, proliferation and angiogenesis. CD133 positive cells seem to be influenced in number and distribution by periodontal inflammatory changes. Studies showed different clinical and radiographic outcomes achieved with the used of Demineralized Freeze-Dried Bone Allografts (DFDBA) for periodontal intrabony defects treatment. Our aim was to investigate the relationship between CD133 expression in gingival biopsies before periodontal treatment and periodontal tissue response in the same site at 12 months post-surgery. We selected fifty-six patients with at least one intrabony defect with clinical attachment level (CAL) ≥ 6 mm and needing periodontal regeneration. A gingival biopsy for each patient was obtained for CD133 immunostaining. Clinical and radiographical parameters were taken at baseline and 12 months post-surgery. We found a positive correlation between gingival CD133 expression and CAL gain achieved by use of DFDBA and measured 12 months post-surgery. Our results suggest that gingival CD133 expression could be a predictive marker of favourable periodontal healing. The CAL gain after periodontal regeneration seems to be related with a native gingival regenerative capacity.

Periodontal regeneration needs formation of new connective tissue at the root surface, involving periodontal fibre development and angiogenesis. Unfortunately, at present, current periodontal procedures allow only a partial regeneration (1, 2).

Demineralized Freeze-Dried Bone Allograft (DFDBA) is a successfully used bone substitute with potential osteoinductive properties (3-6). The reasons for its success are in: i) the capacity to prevent soft tissue collapse in the defect sites; ii) the growth of differentiation factors or bone morphogenic protein presence; iii) the mesenchymal

Key words: stem cells, periodontitis, periodontal regeneration, DFDBA, CD133

Mailing address: Dr. Guendalina Lucarini,
Dipartimento di Scienze Cliniche e Molecolari,
Università Politecnica delle Marche,
Via Tronto 10/a,
60126 Torrette (Ancona), Italy
Tel./Fax: +390712206073
e-mail: guendalina.lucarini@univpm.it

0393-974X (2015)

DISCLOSURE: ALL AUTHORS REPORT NO CONFLICTS OF INTEREST RELEVANT TO THIS ARTICLE.

cell migration, attachment, osteogenesis and stimulus of the microenvironment to produce new bone (7-8). Some authors showed different radiographic and clinical outcomes in the management of periodontal intrabony defects after DFDBA treatment (2, 9, 10).

More than 20 years ago Melcher found that stem cells may reside in the periodontal tissues, although it was not then clear whether cementoblasts, alveolar bone cells and ligament fibroblasts were originated from a single progenitor or stem cells (11).

CD133 or prominin-1, a 115-kDa pentaspan transmembrane protein, is a highly expressed gene that was proposed initially as primitive hematopoetic stem and endothelial progenitor cell (EPCs) marker (12). Prominin-1 is also an important regulator of apoptosis, proliferation and angiogenesis by virtue of its ability to interact with VEGF (13)**.** CD133+ cells exhibit stem cell features by their ability to self-renew and regenerate, demonstrating a great functional regenerative capacity, although the biological function of Prominin-1 is not well understood (14).

Li X et al. found that moderate to severe chronic periodontitis was associated with an increased level of circulating endothelial progenitor CD34-/CD133+/KDR+ cells (15). In our preview study we found the presence of CD133+ cells in gingival tissues and suggested that involvement of CD133, VEGF and CD44 expression in periodontal disease may predict a greater regeneration capacity of gingival tissue (16).

The aim of the present study was to investigate whether the preoperative gingival CD133 expression has favorable effects on postoperative periodontal healing. In particular, it was hypothesized whether the gingival CD133 expression at baseline level (before periodontal surgery) could be correlated with the outcome of periodontal regeneration 12 months post-surgery.

MATERIALS AND METHODS

Study design

Subjects diagnosed with generalized chronic periodontitis (17) were selected from the patient pool of a private dental clinic in Pesaro, Italy. The research was conducted in full accordance with ethical principles, including the Declaration of Helsinki, and each participant gave a written consent according to the above mentioned principles to participate in the study.

The criteria for inclusion of patients in this study were: individuals who were non-smokers, free from systemic complications, and with no history of allergies; no use of antibiotics, corticosteroids or nonsteroidal anti-inflammatory drugs within the 6 months prior to treatment; no treatment for periodontitis during the previous 2 years; radiographic and clinical evidence of one defect with a probing depth (PD) $\geq$ 6 mm, clinical attachment level (CAL) $\geq$ 6 mm, osseous defect depth estimated from radiographic evaluation as $\geq$ 3 mm, and two or three osseous walls without extending into a furcation area.

All subjects received initial therapy including oral hygiene instruction, full-mouth scaling and root planing, utilizing 40mg/ml of articainhydroclorid (alpha caina Dentsply), with 1:100,000 adrenalina, and occlusal adjustment when indicated. Re-evaluations were accomplished 2 months after initial therapy to determine patient response to the therapy and to confirm the need for periodontal surgery. When adequate plaque control, judged by <10 using the O'Leary plaque index (18), was demonstrated. Finally, fifty-six patients (34 females and 22 males; aged range from 48 to 62 years) participated in this study and initiated surgical therapy.

Clinical and rradiographic measurements

On the day of the surgical procedure, baseline clinical and radiograph measurements were recorded by the same examiner (S.D.A.) and were repeated after 12 months. The differences between the 12-month and baseline values of the PD, CAL, CEJ-BD (distance from cementoenamel junction to the base of the defect) and AC-BD (distance from alveolar crest to the base of defect) indicated the PD reduction, the CAL gain, the amount of the Hard Tissue Fill (HTF) within the osseous defect and the Bone Defect Resolution (BDR), respectively (19).

Surgical procedures and gingival biopsies

Each patient was instructed to rinse with 0.2% chlorhexidine gluconate (Curasept, Curaden heath care Srl, Saronno, Varese, Italy) for 2 min prior to the surgical procedure which was carried out using routine local anesthetics (2% arthycaine with epinephrine 1:100,000). Sulcular incisions were made for all teeth. Mucoperiosteal flaps were then raised on the buccal and lingual/palatal parts of the teeth. The flaps included all affected teeth in the quadrant, taking care to preserve as much of the gingival connective tissue as possible. A vertical release incision extending into the alveolar mucosa was placed only when necessary for proper access to the defect, and the coronal portion of the gingiva was removed (3 mm x 3 mm) for the histo-pathologic diagnosis and immunohistochemical analysis. Then, the remaining

epithelium and the granulation tissues from the inner surface of the flaps were carefully removed. Thorough soft tissue debridement and root planing were accomplished with hand instruments, ultrasonic instruments, rotating diamond stones, and finishing burs. The surgical area was rinsed with copious amounts of 0.9% NaCl irrigation, then once hemostasis had been achieved, 24% EDTA pH 6.7 (Prefgel, Straumann Biologic Division, Waltham, MA, USA) was applied to the root surface with a cotton pellet for 2 min to remove the smear layer, detoxify the root surface, and expose collagen fibrils. The surgical area was then thoroughly irrigated with sterile saline solution. The graft DFDBA (MTF, Musculoskeletal Transplant Foundation, Edison, NJ, USA), previously reconstituted with sterile saline solution in a sterile dappen dish, was gently packed into the defects to fill the most coronal levels of the defect walls using an amalgam condenser.

After grafting, great care was taken to obtain complete closure of the interdental soft tissues above the treated defects in all the patients: flaps were repositioned slightly coronally to obtain a complete primary interproximal closure as possible. The flaps were stitched with a 6-0 polyammide (MONOMYD MM-2620; Butterfly Italia, Milan, Italy) using modified vertical mattress and single detached stitching suturing as necessary, damp gauze pressure was applied for 3 min. Patients were treated with Ceftibuten 400 (Isocef, Recordati Industria Chimica e Farmaceutica SpA, Milano, Italy) mg/daily for 6 days and Piroxicam (CICLADOL, Rottapharm SpA, Monza, Italy) 20 mg/daily for 10 days. Patients rinsed with 0.20% chlorhexidine gluconate mouthrinse (Corsodyl, GlaxoSmithKline, Verona, Italy) twice daily for the first 2 weeks following surgery, and were instructed not to brush or floss for 10 days in the areas where surgery had been performed. Sutures were removed when the flap and root-soft tissue interface was stable, usually after 10 days. Moreover, gentle brushing on buccal and lingual surfaces with a soft toothbrush was recommended. Supragingival professional tooth cleaning was performed weekly for the first 6 weeks post-surgery. Thereafter, each patient was reinstructed in proper oral hygiene measures including sulcular and interproximal brushing and were recalled once a month up to 12 months post-surgery for oral hygiene reinforcement and prophylaxis.

Immunohistochemistry

Tissue samples were fixed in 10% formalin for 24 h at room temperature, embedded in paraffin blocks to obtain 4-6 μm thick paraffin tissue sections. Morphologic analysis was performed on tissue sections stained with conventional hematoxylin and eosin. All lesions were histologically diagnosed as generalized and chronic periodontitis. Immunostaining was performed on positively-charged slides. After heat drying, sections were dewaxed in xylene and rehydrated through a graded series of ethanol. To better unmask antigenic sites, a Dako Target Retrieval solution (DakoCytomation, Carpinteria, CA, USA) pH 6.0 was applied, at 750 KW for 20 min. Endogenous peroxidase activity was quenched incubating the sections in 3% (v/v) hydrogen peroxide for 7 min at room temperature. Tissue sections were then incubated with the monoclonal antibody anti-CD133 (clone AC133; Miltenyi Biotec, Auburn, CA, USA) for 1 h at room temperature. The reaction was visualized using the streptavidin-biotin-peroxidase technique (Dako-Envision Plus/HRP peroxidase kit; DakoCytomation, Carpinteria, CA, USA). Sections were incubated with 3,3-diaminobenzidine (0.05 diaminobenzidine in 0.05M Tris buffer, pH 7.6 and 0.01% hydrogen peroxide; Sigma–Aldrich, Milan, Italy) and counterstained with Mayer's haematoxylin (Bio-Optica SpA, Milano, Italy). Foetal kidney tissue was prepared for immunohistochemistry as positive control as detailed above. Negative controls were performed by substituting the primary antibody with non-immune serum.

The counts were performed by two investigators simultaneously (CR and AZ), using a double-headed light microscope (Nikon, Düsseldorf, Germany). Both examiners had to agree on the count of the positive cells. CD133 positive cells were counted at 400x magnification from at least 1,000 cells in the more representative fields, and their number was expressed as a percentage of positive cells in respect to total cells counted.

Immunostained slides were scanned with APERIO ScanScope digital system (Nikon, Düsseldorf, Germany) and representative images were recorded with ImageScope software (Nikon, Düsseldorf, Germany) at the original magnification of 10x and 20x.

We compared CD133+ cell values with clinical and radiographic variables of periodontal regeneration (PD reduction, CALgain, HTF and BDR).

Statistical analysis

Statistical analyses were performed using R statistical software (20).

Spearman's correlation test was used to analyze the association between CD133 expressions in gingival biopsies, and clinical and radiographic variables at baseline.

A multiple linear regression analysis was used to estimate the changes of clinical and radiographic variables (PD reduction, CAL gain, HTF and BDR) at 12 month post periodontal intrabony treatment as linear function of CD133 expressions in gingival biopsies, and their corresponding values at baseline. Significance was set at $p<0.05$.

Table I. *Spearman's correlation test between CD133 expression in gingival biopsies and clinical and radiographic parameters at baseline.*

	CD133 in epithelial cells	CD133 in endothelial cells	CD133 in dermal cells
PD baseline	- 0.509**	- 0.537**	- 0.511**
CAL baseline	- 0.066	0.018	0.035
CEJ-BD baseline	- 0.363*	- 0.418**	- 0.387**
AC-BD baseline	- 0.250	- 0.278	- 0.272
CD133 in epithelial cells	-	0.938***	0.927***
CD133 in endothelial cells	0.938***	-	0.940***
CD133 in dermal cells	0.927***	0.940***	-

The values represent the Spearman's rank correlation coefficients
** (0.05<p<0.1); **(0.001<p<0.05); ***(p<0.001)*

Table II. *Analysis of variance (ANOVA).*

Response: CAL gain					
	Df	Sum Sq	Mean Sq	F value	p
CD133 in dermal cells	1	16.0974	16.0974	193.5089	<0.001
CAL baseline	1	0.0015	0.0015	0.0181	0.894 (NS)
Residuals	25	2.0797	0.0832		
Response: PD reduction					
	Df	Sum Sq	Mean Sq	F value	p
CD133 in dermal cells	1	1.5694	1.5694	4.9671	0.0351
PD baseline	1	0.0583	0.0583	0.1844	0.6713 (NS)
Residuals	25	7.8991	0.3160		
Response: HTF					
	Df	Sum Sq	Mean Sq	F value	p
CD133 in dermal cells	1	0.0661	0.0661	0.2029	0.6563
CEJ-BD baseline	1	0.0283	0.0283	0.0867	0.7708 (NS)
Residuals	25	8.1467	0.32587		
Response: BDR					
	Df	Sum Sq	Mean Sq	F value	p
CD133 in dermal cells	1	0.1176	0.1176	0.4587	0.5044
AC-BD baseline	1	0.1545	0.1545	0.6029	0.4448 (NS)
Residuals	25	6.4065	0.25626		

Table III. *Regression analysis.*

Response: CAL gain				
	Estimate	Std. Error	t value	p
Intercept	-3.85560	0.51392	-7.502	<0.001
CD133 in dermal cells	0.18518	0.01306	14.181	<0.001
$R^2 = 0.886$				

CAL: Clinical Attachment Level

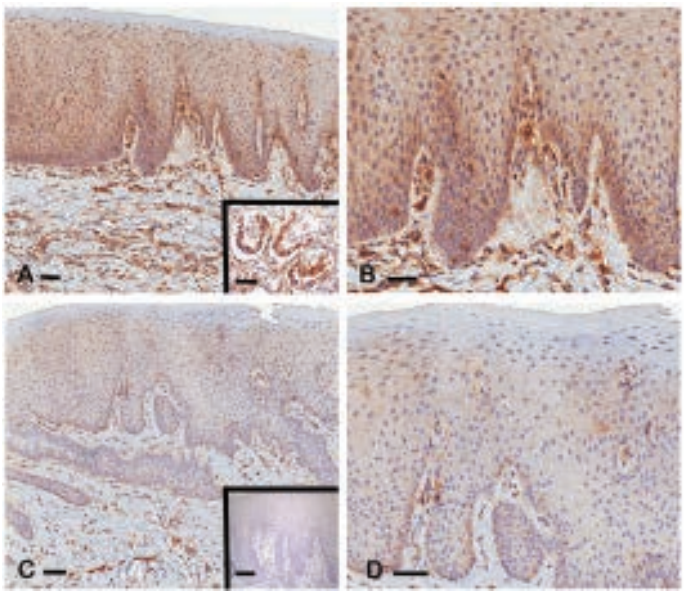

Fig. 1. *CD133 immunostaining in gingival sites before surgery: (**A, B**) High gingival CD133 expression in a patient with 5-mm CAL gain, measured at 12 month post-surgery; inset: Foetal kidney tissue as positive control. (**C, D**) Low gingival CD133 expression in a subject with 3-mm CAL gain measured at 12 month post-surgery; inset: negative control. (Immunoperoxidase, bars: 20μm).*

RESULTS

Table I shows the association between CD133 expression, and clinical and radiographic parameters at baseline. CD133 immunostaining was observed in epithelial cells (57.32±10.5), dermal cells, i.e. lymphocytes and fibroblasts (39.14±4.17) and endothelial cells (20.71±4.48) of gingival biopsies, before treatment for periodontal regeneration with DFDBA.

We found a strong positive association ($p<0.001$) between CD133 expression in epithelial, endothelial and dermal cells and radiographic parameters at baseline in each patient (Table I).

The CD133 expression was negatively associated with PD baseline, and with CEJ-BD baseline only in endothelial and dermal cells. CAL and AC-BD baseline values were never related to the gingival CD133 expression.

Taking into account the strong correlation observed (Table I), we only considered dermal CD133 values for antibody expression as explicative variable in the subsequent regression analysis. As shown in Table II, PD reduction, HTF and BDR were not significantly related with dermal CD133 expression and baseline values. On the contrary CAL gain was significantly associated with dermal CD133 expression (Fig. 1), but it was not influenced by its baseline value. Linear regression showed that CAL gain was positively and significantly related to CD133 expression in gingival biopsies (Table III). The determination coefficient, $R2 = 0.886$, pointed out that CD133 expression explained 88.6% of the CAL gain variability.

DISCUSSION

Periodontal regeneration events involve recruitment of progenitor cells, which can subsequently differentiate into the three cell populations of periodontium (21, 23). In healthy and diseased periodontal ligament, cells were identified mainly as putative stem cells (24) and during the periodontal ligament healing, an increased number of progenitor cells in the paravascular area occurs (25).

The high expression of CD133 in gingival biopsies, especially effective in younger people, seems to predict a greater regeneration capacity of periodontal tissue (16). In our study the strong

association found between CD133+ epithelial, dermal and endothelial cells suggested that CD133 marker was uniformly and proportionately expressed at the different level of the gingival tissues.

Our data show that gingival CD133 expression seems to be negatively related to PD baseline measurements, and moderately to CEJ-BD baseline values.

Furthermore, we found a positive correlation between gingival CD133 expression at baseline and CAL gain achieved 12 months-post-surgery using DFDBA for the treatment of intrabony defects.

This finding seems to indicate that high CD133 expression in gingiva could be a favourable prognostic marker of CAL gain achievable in the intrabony defects management with bone substitute. Moreover, it seems to suggest the involvement of CD133+ gingival cells in the periodontal regeneration/wound healing and that CAL gain, after periodontal regeneration, could be related with a native gingival regenerative capacity.

The success of regeneration strategies was influenced by our ability to repopulate periodontal lesions by cells able to promote regeneration (23, 26, 27). Several studies in animals and humans suggested the effective contribution of EPCs to re-endothelialization and neo-vascularization (28). Tissue regeneration closely depends on the vascular supply and deficient healing situations are frequently associated with poor blood perfusion. Adini et al. showed that CD133 expression influences vascular endothelial growth factor (VEGF) that regulates angiogenesis and apoptosis, two crucial cellular processes in healing. CD133 is an important regulator of apoptosis, proliferation and angiogenesis by virtue of its ability to interact with VEGF, stabilize it, and increase VEGF binding to its receptors, probably via potentiation of VEGF dimer formation (13). Preininger et al. (29) found an increased callus formation, vessel formation and higher bone mineral density of callus tissue after the CD133+ cell transplantation.

In future, clinical CD133+ cell-based therapy and tissue-engineering may be useful for restoring periodontal tissue defects.

REFERENCES

1. Zohar R, Tenenbaum HC. How predictable are periodontal regenerative procedures? J Can Dent Assoc 2005; 71:675-80.
2. Laurell L, Gottlow J, Zybutz M, Persson R. Treatment of intrabony defects by different surgical procedures. A literature review. J Periodontol 1998; 69:303-13.
3. De Leonardis D, Garg AK, Pedrazzoli V, Pecora GE. Clinical evaluation of the treatment of class II furcation involvements with bioabsorbable barriers alone or associated with demineralized freeze-dried bone allografts. J Periodontol 1999; 70:8-12.
4. De Biase P, Campanacci DA, Beltrami G, Scoccianti G, Ciampalini L, Pecchioli O, Capanna R. Scaffolds combined with stem cells and growth factors in healing of pseudotumoral lesions of bone. Int J Immunopathol Pharmacol 2011; 24:11-15.
5. Bowers G, Felton F, Middleton C, et al. Histologic comparison of regeneration in human intrabony defects when osteogenin is combined with demineralized freeze-dried bone allograft and with purified bovine collagen. J Periodontol 1991; 62:690-702.
6. Piemontese M, Aspriello SD, Rubini C, Ferrante L, Procaccini M. Treatment of periodontal intrabony defects with demineralized freeze-dried bone allograft in combination with platelet-rich plasma: a comparative clinical trial. J Periodontol 2008; 79:802-10.
7. Yukna RA, Vastardis S. Comparative evaluation of decalcified and non-decalcified freeze-dried bone allografts in rhesus monkeys. Histologic findings. J Periodontol 2005; 76:57-65.
8. Schwartz Z, Sommers A, Mellonig JT. Addition of human recombinant bone morphogenetic protein-2 to inactive commercial human demineralized freeze-dried bone allograft makes an effective composite bone inductive implant material. J Periodontol 1998; 69:1337-45.
9. Hoidal MJ, Grimard BA, Mills MP, Schoolfield JD, Mellonig JT, Mealey BL. Clinical evaluation of demineralised freeze dried bone allograft with and without enamel matrix derivative for the treatment of periodontal osseous defects in humans. J Periodontol 2008; 79:2273-80.
10. Fucini S, Quintero G, Gher ME, Black BS, Richardson AC. Small versus large particles of DFDBA in human intrabony periodontal defects. J

Periodontol 1993; 64:844-47.
11. Melcher AH. Cells of periodontium: their role in the healing of wounds. Ann R Coll Surg Engl 1985; 67:130-31.
12. Calloni R, Cordero EA, Henriques JA, Bonatto D. Reviewing and updating the major molecular markers for stem cells. Stem Cells Dev 2013; 22:1455-76.
13. Adini A, Adini I, Ghosh K, Benny O, Pravda E, Hu R, Luyindula D, D'Amato RJ. The stem cell marker prominin-1/CD133 interacts with vascular endothelial growth factor and potentiates its action. Angiogenesis 2013; 16:405-16.
14. Shmelkov SV, St.Clair R, Lyden D, Rafii S. Molecules in focus AC133/CD133/Prominin-1. Int J Biochem Cell Biol 2005; 37:715-19.
15. Li X, Tse HF, Yiu KH, Jia N, Chen H, Li LS, Jin S. Increased levels of circulating endothelial progenitor cells in subjects with moderate to severe chronic periodontitis. J Clin Periodontol 2009; 36: 933-39.
16. Lucarini G, Zizzi A, Aspriello SD, et al. Involvement of vascular endothelial growth factor, CD44 and CD133 in periodontal disease and diabetes: an immunohistochemical study. J Clin Periodontol 2009; 36:3-10.
17. Armitage GC. Development of a classification system for periodontal diseases and conditions. Ann Periodontol 1999; 4:1-6.
18. O'leary TJ, Drake RB, Naylor JE. The plaque control record. J Periodontol 1972; 43:38.
19. Aspriello SD, Ferrante L, Rubini C, Piemontese M. Comparative study of DFDBA in combination with enamel matrix derivative versus DFDBA alone for treatment of periodontal intrabony defects at 12 months post-surgery. Clin Oral Invest 2011; 15:225-32.
20. R Development Core Team. R: A language and environment for statistical computing. R Foundation for Statistical Computing 2011, Vienna, Austria. ISBN 3-900051-07-0, URL http://www.R-project.org.
21. Fu X, Li F. Mesenchymal stem cells and skin wound repair and regeneration: possibilities and questions. Cell Tissue Res 2009; 335:317-21.
22. Wu Y, Chen L, Scott PG, Tredget EE. Mesenchymal stem cell enhance wound healing through differentiation and angiogenesis. Stem Cells 2007; 25:2648-59.
23. Bartold PM, Shi S, Gonthos S. Stem cells and periodontal regeneration. Periodontol 2000 2006; 40:164-72.
24. Chen SC, Marino V, Gronthos S, Bartold PM. Location of putative stem cells in human periodontal ligament. J Periodont Res 2006; 41:547-53.
25. Walker CG, Ito Y, Dangaria S, Luan X, Diekwisch TG. RANKL, osteopontin, and osteoclast homeostasis in a hyperocclusion mouse model. Eur J Oral Sci 2008; 116:312-18.
26. Aspriello SD, Zizzi A, Lucarini G, Rubini C, Faloia E, Boscaro M, Tirabassi G, Piemontese M. Vascular endothelial growth factor and microvessel density in periodontitis tissues of systemically healthy and type 1 and 2 diabetic patients: a comparative immunohistochemical study. J Periodontol 2009; 80:1783-89.
27. Aspriello SD, Zizzi A, Spazzafumo L, Rubini C, Lorenzi T, Marzioni D, Bullon P, Piemontese M. Effects of enamel matrix derivative on vascular endothelial growth factor expression and microvessel density in gingival tissues of periodontal pocket: a comparative study. J Periodontol 2011; 82:606-12.
28. Erl W, Weber PC. Endothelial progenitor cells: mobilization, differentiation, and homing. Arterioscler Thromb Vasc Biol 2003; 23:1185-89.
29. Preininger B, Duda G, Gerigk H, et al. CD133: enhancement of bone healing by local transplantation of peripheral blood cells in a biologically delayed rat osteotomy model. Plos One 2013; 8:e52650.

LETTER TO THE EDITOR

INHIBITORY ACTION OF $CoCl_2$-INDUCED MCF-7 CELL HYPOXIA MODEL OF BREAST CANCER AND ITS INFLUENCE ON VASCULAR ENDOTHELIAL GROWTH FACTOR

M. ZHANG[1], R. MA[2] and Q. LI[1]

[1]Department of Breast and Thyroid Surgery, Shandong Provincial Qianfoshan Hospital, Shandong University, Jinan, China; [2]Department of Breast Surgery, QiLu Hospital of Shandong University, Jinan, China

Received, March 27 2015 – Accepted May 12, 2015

Breast cancer, a malignant tumor frequently occurring in females, is traditionally treated with excision. In the search for a new treatment, we analyzed the influence of $CoCl_2$ on MCF-7 cell proliferation of breast cancer and tumor angiogenesis factor and discussed the results. Having applied $CoCl_2$ as chemical hypoxia-induced agent, *in-vitro* MCF-7 cell hypoxia model of breast cancer was established, after which methyl thiazolyl tetrazolium (MTT) staining was performed in detecting inhibitory action of $CoCl_2$ to proliferation of MCF-7 cells cultured in-vitro, and inverted phase contrast microscope was adopted to observe morphological changes of MCF-7 cell in hypoxia model. Furthermore, reverse transcription-polymerase chain reaction (RT-PCR) was made to determine how $CoCl_2$ influences mRNA expression changes of hypoxia inducible factor-1α (HIF-1α), chemokine receptor-4 (CXCR4) and vascular endothelial growth factor (VEGF) in MCF-7 cells. Western blot was designed to study and record data on the influence of $CoCl_2$ on protein expression changes of HIF-1α, CXCR4 and VEGF. As a result, $CoCl_2$ was proved to control MCF-7 cell proliferation and increase expression of HIF-1α, CXCR4 and VEGF.

Worldwide, breast cancer is one of the most common female malignancies, and in China the occurrence rate is 7% ~10%, with an increasing trend in younger females. For this reason, more specialists and scholars are concentrating on the study of breast cancer (1). Xie (2) revealed the pathological mechanism of familial breast cancer and focused on the detection of breast cancer BRCA1, 2 gene mutation, which laid a theoretical basis of therapy. Xia and He (3) analyzed expression of Ki-67, EGFR, HER-2, and P53 in breast cancer tissues and the relationship between the expressions and pathological features, reaching significant results in clinical diagnosis, therapy and prognosis evaluation of breast cancer. Mou and Li (4) discussed the research progress of neoadjuvant chemotherapy for breast cancer and report practical suggestions on defects of neoadjuvant chemotherapy, which blazed a new trail for breast cancer treatment.

It has been reported in recent studies that hypoxia inducible factor-1α (HIF-1α), chemokine receptor-4 (CXCR4) and vascular endothelial growth factor (VEGF) have positive influence on breast cancer recovery. However, few studies paid attention to regulation of HIF-1α, CXCR4 and VEGF on tumor angiogenesis of breast cancer with the condition of

Key words: breast cancer, hypoxia, inducing factor, $CoCl_2$

Mailing address: Dr Qing Li,
Department of Breast and Thyroid Surgery, Shandong Provincial Qianfoshan Hospital,
Shandong University,
No. 16766, Jingshi Road,
Jinan, 250014, China
e-mail: lqqfsyy@163.com

0393-974X (2015)

hypoxia when they studied oxygen homeostasis of micro-environment for breast tumor (5). For this reason, we studied MCF-7 cells of breast cancer, and built an *in-vitro* tumor hypoxia model on the basis of $CoCl_2$ that was regarded as the hypoxia-inducing agent. After observing the influence of $CoCl_2$ on MCF-7 cell proliferation, we further analyzed $CoCl_2$ inducement to regulation of MCF-7 cells on tumor angiogenesis factor.

MATERIALS AND METHODS

According to cell concentration required by experiment design, MCF-7 cell strains (Cell bank of Chinese Academy of Science, Shanghai, China) in logarithmic growth stage with sound conditions were selected and implanted in culture bottles that were placed in an incubator. When cells had complete even adherence growth, Dulbecco Modified Eagle Medium (DMEM) solution (Gibco, CA, U.S.A) in different concentrations was added; for $CoCl_2$ (Gibco, CA, U.S.A) group, the concentration was respectively 50, 100, 150 and 200 μmol/L, while the control group took equivalent PBS. At different time periods, cell morphology of MCF-7 treated with $CoCl_2$ was observed under inverted phase contrast microscope; inhibitory action of $CoCl_2$ to MCF-7 was determined by MTT; mRNA expression changes of HIF-1α (Santa Cruz Biotech, Inc., Texas, U.S.A), CXCR4 (Santa Cruz Biotech) and VEGF (Santa Cruz Biotech) in MCF-7 cells induced by $CoCl_2$ were detected via RT-PCR; and protein expression of HIF-1α, CXCR4 and VEGF was tested by Western blot (Western blot electrophoresis kit, Bio-tech Inc., Shanghai, China).

Statistical analysis

SPSS19.0 was adopted to analyze experimental data that were presented as mean ± SD, and one-way ANOVA was performed in inter-group comparison. $P<0.05$ differences were regarded as statistically significant; $P<0.01$, differences were considered to have remarkably statistical significance.

RESULTS

Observation on morphological changes of cells processed with $CoCl_2$ under inverted phase contrast microscope

Under inverted phase contrast microscope, cell amount increased in the group with 50, 100 and 150 μmol/L $CoCl_2$ after 12 and 24 h culture. As shown in Fig. 1, most cells maintained complete morphology without any obvious change after 12 h; but 48 h later, cell metabolin accumulated and plasmatorrhexis occurred in some cells (Fig. 2).

MTT-based test on $CoCl_2$ inhibitory action on MCF-7 cell proliferation of breast cancer

At different time periods, $CoCl_2$ with different concentrations (50, 100, 150 and 200 μmol/L) functioned on MCF-7 cell proliferation in a diverse way, and $CoCl_2$ did not have the same control on cell proliferation. It could be noticed that inhibitory action of $CoCl_2$ to MCF-7 cell proliferation depended on timing and concentration (Table I).

RT-PCR-based determination of mRNA expression of HIF-1α, CXCR4 and VEGF in MCF-7 Cells induced by $CoCl_2$

With 24-hour processing of MCF-7 cells with $CoCl_2$ (50, 100, 150 and 200 μmol/L), mRNA expression of HIF-1α was not detected to have any change of average relative gradient. But when $CoCl_2$ concentration reached 50, 100 and 150 μmol/L, mRNA expression of CXCR4 and VEGF tended to increase as shown in Table II.

Western blot-based determination of protein expression of HIF-1α, CXCR4 and VEGF in MCF-7 cells induced by $CoCl_2$

MCF-7 cells of breast cancer were treated with $CoCl_2$ (50, 100, 150 and 200 μmol/L) and after 24 h, protein expression of HIF-1α, CXCR4 and VEGF was found to increase (Table III).

DISCUSSION

Hypoxia is a key pathological situation, and its relationship with tumor has been the focus of many studies in recent years. In human tumors, many areas witness 5 mmHg-below partial pressure of oxygen, while 90% of solid tumor is detected with hypoxia areas that mainly occur on tumor growth edges or tumors with more than 1~2 mm diameter (6, 7). Based on existing literature, hypoxia or anoxia is quite common in breast cancer, which changes oxygen homeostasis of tumor micro-environment; mutation rate rises due to selective production of malignant cell morphology; and gene expression related to angiogenesis and tumor invasion is enhanced,

Table I. *MMT-based Test of $CoCl_2$'s Influence on MCF-7 Cell Proliferation (A570.)*

	12h	24h	48h
PBS	1.890±0.023	1.679±0.033	1.331±0.053
50 μmol/L $CoCl_2$	1.672±0.019*	1.089±0.024*	0.951±0.031*
100 μmol/L $CoCl_2$	1.454±0.02*	0.783±0.02*	0.545±0.024*
150 μmol/L $CoCl_2$	1.235±0.021*	0.635±1.018*	0.377±0.023*
200 μmol/L $CoCl_2$	1.086±0.017*	0.371±0.015*	0.264±0.028*

** P<0.05 (mean±SD, n=3)*

Table II. *Comparison of mRNA and β-actin expression gradient of HIF-1α, CXCR4 and VEGF among groups.*

Groups	HIF-1α/β-actin	CXCR4/β-actin	VEGF/β-actin
Control	0.67±0.04	0.41±0.03	0.47±0.01
50 μmol/L $CoC1_2$	0.79±0.02	0.43±0.01	0.52±0.04
100 μmol/L $CoC1_2$	0.81±0.07	0.62±0.06*	0.67±0.02
150 μmol/L $CoC1_2$	0.83±0.04	0.87±0.07*	0.85±0.01
200 μmol/L $CoC1_2$	0.80±0.02	0.76±0.02*	0.69±0.03

** P<0.05; v P<0.01. (mean±SD, n=3)*

Table III. *Protein expression of HIF-1α, CXCR4 and VEGF.*

Groups	HIF-1α/β-actin	CXCR4/β-actin	VEGF/β-actin
Control	1.02±0.10	1.00±0.10	1.00±0.10
50 μmol/L$CoC1_2$	2.73±0.09*	1.75±0.09*	1.45±0.11*
100 μmol/L$CoC1_2$	4.81±0.07*	2.77±0.10*	2.67±0.10*
150 μmol/L$CoC1_2$	8.17±0.14*	7.12±0.14*	5.35±0.17*
200 μmol/L$CoC1_2$	6.89±0.11*	5.12±0.08*	5.65±0.09*

** P<0.05 (mean±SD, n=3)*

resulting in a worsening of the patient's condition. It can therefore be concluded that as a vital factor of tumor prognosis, hypoxia acts significantly in angiogenesis, invasion and metastasis of malignant tumors.

Hypoxia inducible factor (HIF-1) is a nuclear factor commonly seen in mammals and human bodies with high expression, which contains HIF-1α and HIF-1β in the form of heterodimer. HIF-1 transcriptional activity is decided by HIF-1α which is regulated by oxygen concentration of tumor micro-environment (8, 9), thus HIF-1α is regarded as the "master switch of hypoxia gene expression". More precisely, HIF-1α functions on regulating downstream gene expression, oxygen transportation in micro-environment and adaptive ability of cell to hypoxia, and inducing hypoxia actions to initiate targeted gene transcription. In recent years, more studies have focused on hypoxia inducible factor (10, 11); but while they studied oxygen homeostasis of micro-environment for breast tumor, less attention was paid to HIF-1α, CXCR4 and VEGF which regulate tumor angiogenesis of breast cancer in the condition of hypoxia.

HIF-1α, CXCR4 and VEGF are important biological markers stimulating tumor angiogenesis and inducing tumor invasion, and their increased expression is in a dose-dependent relation with $CoCl_2$ induction found in the present study. It is hypothesized that hypoxia enhances tumor invasion

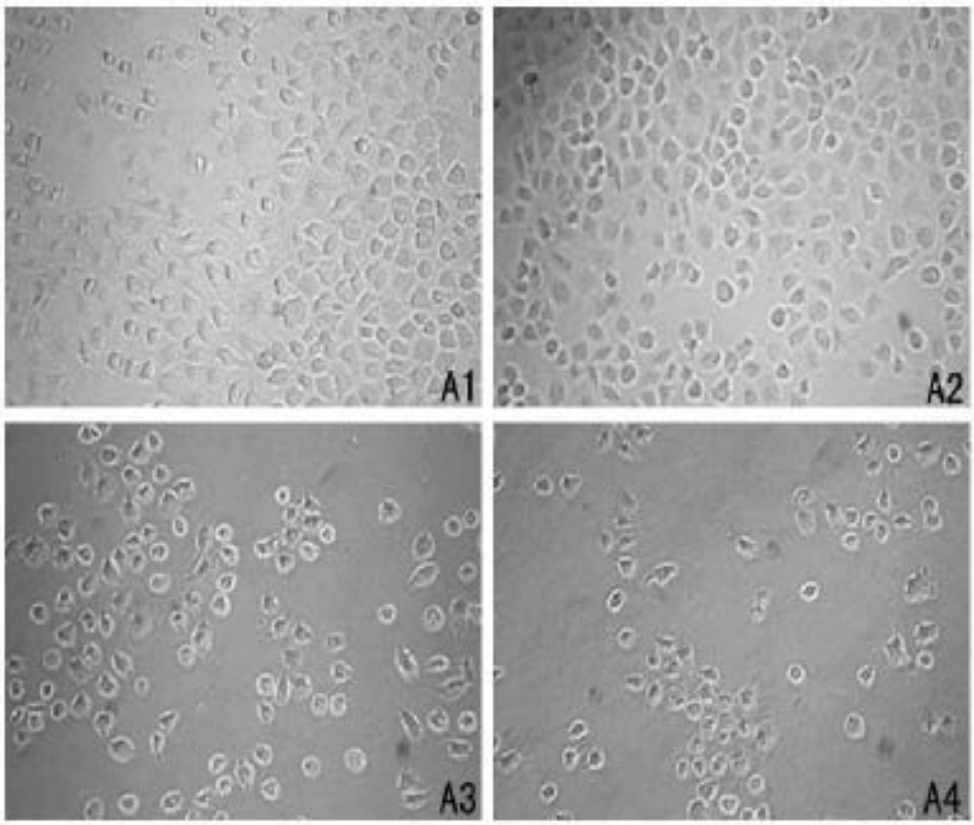

Fig. 1. *Morphological changes (×100) of MCF-7 cell after 12-h processing with different $CoCl_2$ concentrations (A1, A2, A3 and A4 with 50, 100, 150 and 200μmol/L $CoCl_2$, respectively).*

and metastasis ability by inducing an increase in their expression, which will be the subject requiring further confirmation and discussion in future studies. However, in the literature, reports in this field are rare. Dunn et al. (12) discovered that HIF-lα was able to strongly induce chemokine receptor-4(CXCR4) and its ligand SDF-1 expression in breast cancer tissues or cells, playing a vital role in directional migration of tumor cells. A mass of CXCR4 existing in human breast cancer tumor tends to migrate to the part that can produce considerable cytokine SDF-1, for instance, lung and bone marrow. Interaction of CXCR4 and SDF-1 plays a key role in invasion and metastasis of tumor cells (5), activating VEGF up-regulation, thus being involved in the angiogenesis, which provides material basis for further growth and metastasis of tumor and promotes cell invasion. Some Authors have suggested that HIF-1 has a central link effect on regulating VEGF in signal transduction pathway when lack of oxygen not only increased the mRNA stability of VEGF, but also increased VEGF transcriptional activity (13), thereby promoting angiogenesis.

Therefore, this study simulated *in-vitro* hypoxia environment for MCF-7 cell strains of human breast cancer. Having applied $CoCl_2$ to induce hypoxia, RT-PCR and Western blot were performed in testing mRNA and protein expression of HIF-1α, CXCR4 and VEGF. While RT-PCR did not reveal any mRNA expression change of HIF-1α, notable increase of expression of CXCR4 and VEGF was determined; and the difference between $CoCl_2$ group and the control group was statistically significant, $P<0.05$. As for protein expression, its improvement was

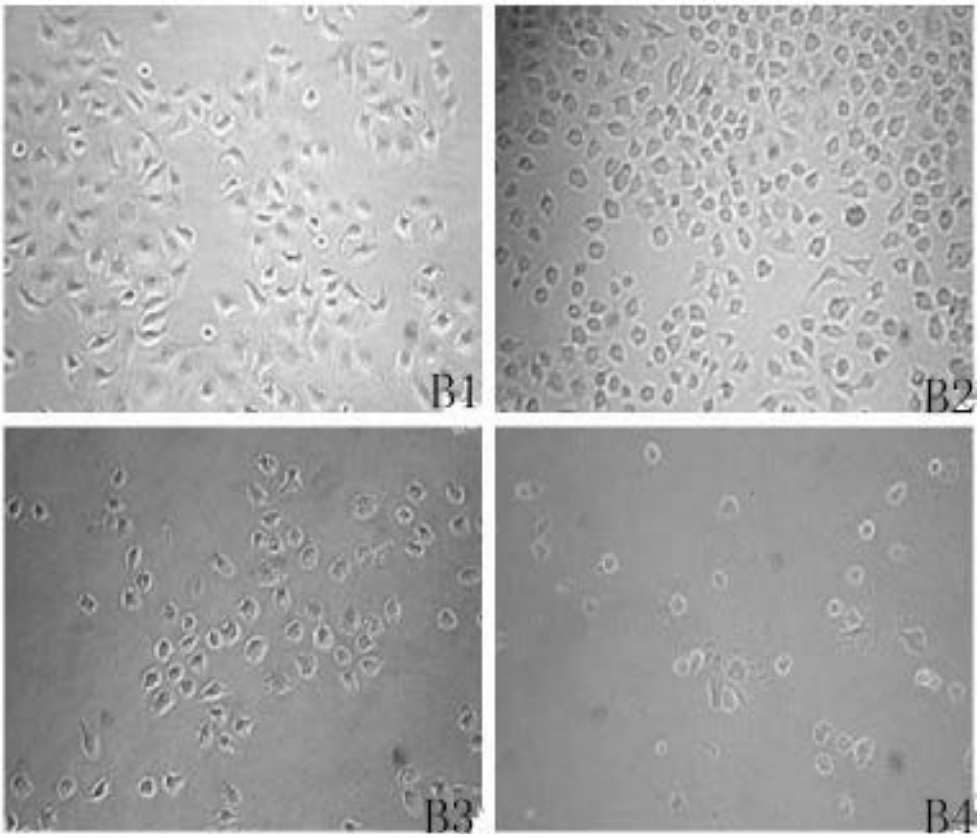

Fig. 2. *Morphological changes (×100) of MCF-7 cell after 48-h processing with different $CoCl_2$ concentrations (B1, B2, B3 and B4 with 50, 100, 150 and 200μmol/L $CoCl_2$, respectively).*

detected by Western blot when $CoCl_2$ completed its inducement to MCF-7 cells. To be specific, protein expression of HIF-1α increased remarkably when $CoCl_2$ concentration rose, causing average relative gradient with respective value of 1±0.061 (0 μmol/L), 2.73±0.15 (50μmol/L), 4.81±0.42 (100μmol/L), 8.17±0.52 (150μmol/L), and 6.89±0.38 (200μmol/L), which resulted in 1±0.12, 1.75± 0.18, 2.77±0.620, 7.12±0.34 and 5.12±0.18 in CXCR4. The comparison between the control group and $CoCl_2$ group showed a difference with $P<0.05$. Furthermore, protein expression of VEGF also increased with various average relative gradients, i.e. 1±0.01, 1.45±0.071, 2.67±0.17, 5.35±0.150 and 5.65±0.15; but no difference was demonstrated between the control group and $CoCl_2$ group ($P>0.05$).

On the basis of the statements above, $CoCl_2$ is able to activate oxidative stress reaction, and cell cytotoxicity and apoptosis; $CoCl_2$ promotes HIF-1α over-expression depending on concentration and timing, and improves CXCR4 and VEGF expression, which is likely to induce tumor angiogenesis and advance tumor invasion and metastasis. Moreover, it is possible that hypoxia is regulated by HIF-1α, CXCR4 and VEGF.

ACKNOWLEDGEMENTS

This study was funded by the following: Natural Science Funds of Shandong Province Project: Mutation and Expression of Parathyroid Carcinoma Susceptibility Gene HRPT2, MEN1, CyclinD1 and RET, Project Number: ZR2012HL04; and Science and Technology Development Plan of

Shandong Province Project: Clinical Application of Selective ALND of CN+Breast Cancer Patients Project Number: 2012YD18062.

REFERENCES

1. Nishibe T, Dardik A, Kondo Y, et al. Expression and localization of vascular endothelial growth factor in normal abdominal aorta and abdominal aortic aneurysm. J Int Union Angiol 2010; 29(3):260-65.
2. Xie YT. Brca1, 2 gene mutation determinations of familial breast cancer and its clinical application. Chin J of Pract Surg 2013; 33(3):233-35.
3. Xia HQ, He JR. Expression of Ki-67, EGFR, HER-2 and p53 protein in human breast cancer and their correlation. Chinese Clinical Oncology 2011; 16(2):139-42.
4. Mou P, Li YH. Advances of neoadjuvant chemotherapy in breast cancer. Chin J of Bases and Clin in General Surg 2011; 18(9):1011-16.
5. Teicher BA, Fricker SP. CXCL12 (SDF-1)/ CXCR4 pathway in cancer. Clin Cancer Res 2010; 16(11):2927-31.
6. Tsutsui S, Matsuyama A, Yamamoto M, Hideya T, Oshiro Y, Ishida T, Maehare Y. The Akt expression correlates with the VEGF-A and -C expression as well as the microvessel and lymphatic vessel density in breast cancer. Oncol Rep 2010; 23(3):621-30.
7. Zhang Z, Wu J, Liang B, Huangfu CS. Correlation between Hypoxia Inducible Factor (HIF-1α) and epithelium-mesenchyma transform of ductal carcinoma with invasive breast cancer. Shandong Med J 2012; 52(3):90-92.
8. Xiong ZW, Cao L, Hu HX, Li W, Zhang HD, Xun FH. Expression of snail and VEGF gene in invasive ductal carcinoma of breast. Chin J of Bases and Clin in General Surg 2011; 18(11):1194-99.
9. Liu CM, Li Y, Lin MH, Wang CX, Wang J. Expression of VEGF and the correlation with ER and PR in breast cancer. Modern Oncol 2012; 20(3):527-29.
10. Dong X, Wang YS, Dou GR, et al. Influence of Dll4 via HIF-1α-VEGF signaling on the angiogenesis of choroidal neovascularization under hypoxic conditions. PLoS One 2011; 6(4):e18481.
11. Chen H, Zhou BJ, Zhao WM, Li JM, Zhang JK. Expression and significance of HIF-1α, CAIX, VEGF and Galectin-3 in basal-like breast cancer. Chin J of Clin and Exper Pathol 2012; 28(7):803-5.
12. Dunn LK, Mohammad KS, Fournier PG, et al. Hypoxia and TGF-β drive breast cancer bone metastases through parallel signaling pathways in tumor cells and the bone microenvironment. PLoS One 2009; (9):e6896.
13. Liu LX, Lu H. Stabilization of vascular endothelial growth factor mRNA by hypoxia-inducible factor. Biochem Biophys Res Commun 2002; 291(4):908-14.

LETTER TO THE EDITOR

TRANSPLANTATION OF HYPERTHERMIC PRECONDITIONING OLFACTORY ENSHEATHING CELLS COMBINED WITH NEURAL STEM CELLS IN THE TREATMENT OF CENTRAL NERVE INJURY

SG. GUO, CJ. WANG, YX. WANG and CQ. QU

Department of Neurology, Shandong Provincial Hospital Affiliated to ShandongUniversity, Jinan, China

Received March 11, 2015 – Accepted May 21, 2015

This study aims to observe the effect of the transplantation of hyperthermic preconditioning (HPC) olfactory ensheathing cells (OECs) at 40°C combined with neural stem cells (NSCs) in the treatment of spinal cord injury (SCI), based on the OECs and NSCs taken from the olfactory bulbs and cerebral cortex of newborn rats. Forty-two female Sprague Dawley (SD) rats were randomly divided into: control group, NSCs+OECs without HPC group and NSCs+HPC OECs group. Firstly, hemisected spinal cord injury model was established; the motor function recovery of the right lower limb of the rats was compared by Basso-Beatie-Bresnahan rating (BBB rating), climbing score and running time on a rotating platform during the whole experiment. At one day, two weeks and four weeks after transplantation, two rats were randomly selected from each group for section preparation. Hematoxylin and eosin (HE) staining was performed on the sections to observe and analyze the pathological changes of the spinal cord tissue, and bromodeoxyuridine (BrdU) labeling was used to observe the distribution of transplanted cells. The results demonstrated that, BBB score of the rats that were treated by transplantation of NSCs combined with HPC OCEs was distinctly improved; a rapid increase of BBB score was found two weeks after transplantation, while BBB score had slightly increased six weeks later. BBB score of the control group and the NSCs+OECs without HPC group was found with a slight increase, especially in the control group. BBB score of NSCs+HPC OECs was significantly higher than in the control group and the NSCs+OECs without HPC group at the 2nd, 4th, 6th, 8th and 12th week after treatment ($P<0.05$). Climbing tests and detection of running time after 4 weeks and 6 weeks demonstrated that, the recovery of limb function of the NSCs+HPC OECs group was better than the other groups ($P<0.05$). HE staining results of NSCs+HPC OECs indicated that, cells of the spinal cord were neatly arranged, close to normal. BrdU labeling results revealed that, transplanted cells were found in injury tissue, indicating that they were involved in the spinal cord repair. This study proves that, the effect of NSCs combined with HPC OECs in the treatment of SCI is better than NSCs combined with OECs without HPC, and the ratio of NSCs differentiating to neuron after inducing HPC OECs supernate is higher than that after inducing OECs supernate without HPC.

A wealth of literature has reported that olfactory ensheathing cells (OECs) and neural stem cells (NSCs) are the ideal cells for treating SCI. Duan et al. (1) found that OECs could induce NSCs to differentiate to neuron at a high ratio; OECs transplanted into an injured spinal cord can promote

Key words: HP, OECs, NSCs, cell transplantation, spinal cord injury

Mailing address: Dr Chuanqiang Qu,
Department of Neurology,
Shandong Provincial Hospital
Affiliated to Shandong University,
No.324, Jingwu Road, Huaiyin
District, Jinan, Shandong 250021, China
e-mail: qcq@ibhsedu.com

0393-974X (2015)

axonal regeneration, thus accelerating the recovery of functions. Duan Zhaoxia et al. (2) discussed the change of expression of neurotrophic factors in the process of nerve injury and repair after OECs were transplanted into rats with injured spinal cord and found that behavioral score increased as the injury time prolonged, but no motor function recovery was found in the hind legs. Also, compared to the control group, spinal cord tissue tended to have significantly increased expression of neurotrophic factors after transplantation of OECs, which hinted that OECs could improve the pathological form of injured spinal cord tissue to some extent and promote the expression of multiple neurotrophic factors within spinal cord tissue. Moreover, many studies (3-5) have demonstrated that, transplanted stem cells could shift, differentiate to neuron and secrete neurotrophin to promote the recovery of nerve tissue, thereby improving the functions of nerves. Preconditioning can simulate a local sublethal environment. HPC cells can better tolerate the subsequent lethal environment. It has been reported that heat treatment can strengthen the capacity of nerve cells from rats with secondary forebrain ischemia, with spinal cord ischemia and injury, to protect the neurological function of rats (6). It has also been reported that, heat treatment can not only increase the hypoxia-inducible factor-1α (HIF-1α), heat shock proteins (HSPs), heme oxygenase-1 (HP-1) and nerve adenosine receptors, but can also cause the up-regulation of polymer saliva acidification, thereby improving the biological activity of cells. Previous experiments have found that, the differentiation ratio of neurons greatly increased when OEC supernatant was pretreated at 40°C. This study treated spinal cord injury by transplantation of HPC OECs combined with NSCs, in order to explore a new method for treating SCI and lay an experimental bases for its application in treating SCI.

MATERIALS AND METHODS

Experimental animals and grouping

Forty two healthy female Sprague Dawley (SD) rats with weight ranging from 200 to 220g were selected and divided into a control group (group A, 14), a group treated by transplantation of NSCs and OECs without HPC (group B, 14) and a group treated by transplantation of NSCs and HPC OECs (group C, 14). The handling of the animals in the experiment conformed to the standard of animal ethics.

Immunocytochemical staining

NGFR p75 staining for OECs was done using cells grown in cover glass which were washed three times in 0.1 M PBS for 3 min each time. They were then fixed in 95 % ethyl alcohol for 30 min, washed in 0.1 MPBS four times for 3 min each time. The cells were then incubated in 3% H_2O_2 for 10 min to remove endogenous peroxidase, then washed in 0.1 MPBS three times for 3 min each time. The cells were incubated in rabbit anti-rat NGFR p 75 as primary antibody, at a concentration of 1:100. A blank control group with PBS as primary antibody was set up at 4°C. The cells were washed in 0.1 MPBS three times for 3 min each time and then incubated in goat anti-rabbit IgG at 37°C for 15 min, washed in 0.1 MPBS three times for 3 min each time. After dripping streptavidin liquid labeled by horseradish peroxidase they were incubated in the liquid at 37°C for 15 min, then washed by 0.1 MPBS three times for 3 min each time. The color of the liquid was developed by DAB in the dark for 3 min, then they were rinsed in tap water for 3 min. They were dehydrated in 75% ethyl alcohol once, 95 % ethyl alcohol twice, absolute ethyl alcohol three times for 1 min each time, then washed in xylene three times for 1 min each time. They were the dried and mounted with gum for observation and photographing under microscope.

Nestin staining for NSCs was done using spheres in cover glass which were washed three times in 0.1 M PBS for 3 min each time. They were then fixed in 4% paraformaldhyde for 20 min, washed in 0.1 MPBS four times for 3 min each time. The cells were then incubated in 3% H_2O_2 for 10 min to remove endogenous peroxidase, then washed in 0.1 MPBS three times for 3 min each time. The cells were incubated in mouse anti-rat Nestin as primary antibody, at a concentration of 1:200. A blank control group with PBS as primary antibody was set up at 4°C overnight. The cells were washed in 0.1 MPBS three times for 3 min each time and then incubated in goat anti-rabbit IgG antibody-HRP polymer at 37°C for 30 min, washed in 0.1 MPBS three times for 3 min each time. The color was developed by DAB in the dark for 2-3 min, then they were rinsed in tap water for 3 min. They were dehydrated in 75% ethyl alcohol once, 95% ethyl alcohol twice, absolute ethyl alcohol three times for 1 min each time, then washed in xylene three times for 1 min each time. They were the dried and mounted with gum for observation and photographing under microscope.

β-Tubulin staining of neuron after induction was done using cells with differentiated NSCs taken from cover glass which were washed three times in 0.1 M PBS for 3 min each time. They were then fixed in 4% paraformaldhyde

for 20 min, washed in 0.1 MPBS four times for 3 min each time. The cells were then incubated in 3% H_2O_2 for 10 min to remove endogenous peroxidase, then washed in 0.1 MPBS three times for 3 min each time. The cells were incubated in rabbit anti-rat Tubulin as primary antibody, at a concentration of 1:200. A blank control group with PBS as primary antibody was set up at 4°C overnight. The cells were washed in 0.1 MPBS three times for 3 min each time and then incubated in goat anti-rabbit IgG at 37°C for 15 min, washed in 0.1 MPBS three times for 3 min each time. After dripping streptavidin liquid labeled by horseradish peroxidase they were incubated in the liquid at 37°C for 15 min, then washed by 0.1 MPBS three times for 3 min each time. The color was developed by AEC in the dark for 2-3 min, then they were rinsed in tap water for 3 min. They were dehydrated in 75% ethyl alcohol once, 95% ethyl alcohol twice, absolute ethyl alcohol three times for 1 min each time, then washed in xylene three times for 1 min each time. then washed in xylene three times for 1 min each time. They were the dried and mounted with gum for observation and photographing under microscope.

Manufacture of rat hemisected spinal cord model and postoperative nursing

Rats were narcotized by injecting 10% chloral hydrate (0.8 ml/100g). The fur was shaved from the back of the rats, the skin was cut along the midline of the spine and then the muscle was bluntly dissected along the spine. The 8^{th} and 10^{th} spinal cord were exposed by laminotomy. A hemisection was cut on the right side of the 10^{th} spinal cord. 50,000 units of penicillin (0.25 ml) were injected into the dorsolateral muscle group, once a day for 5 days. The bladder was massaged once every 8 hours until the vesical reflex recovered.

Transplantation of NSCs and OECs

Seven days after the intervention, NSC transplantation was performed. Cells were collected by centrifugation before transplantation. Then nutrient solution was removed. Using D-Hank's liquid, the cells were resuspended at a concentration of 1×10^9 /ml. The rats in group A were injected with 10 µl PBS under the condition of general anesthesia, group B was injected with 10 µl NSCs+ OCEs without HPC, and group C was injected with 10 µl NSCs+ HPC that had been pretreated by heat. The ratio of NSCs and OECs was 1:1. Three points on the upper side and lower side of the injured spinal cords were selected to be injected, at depths of 0.5 mm, 1.0 mm and 1.5 mm at intervals of 5min. The syringe remained at those depths for 5 min and was then removed.

Neurological function scale

Morbidity in the nervous system of rats was observed when they regained consciousness. The neurological function scale was used based on time points. Morbidity in the nervous system includes inclination of the body, inability to stand upright, difficulty in crawling, inability to put weight on the injured limb, complete paralysis, slow activity and irritability. Motor function was assessed by Basso-Beatie-Bresnahan (BBB) rating (8), climbing scoring was assessed as in Basso et al. (9) and running time was assessed as in Brailowsky et al. (10).

Statistical analysis

Data of the BBD scale were expressed by mean±SD. SPSS13.0 was used for statistical analysis. Data was first compared by one-way analysis of variance, followed by multiple comparisons. $P<0.05$ meant the difference had statistical significance.

RESULTS

Cultivation and identification of OCEs and NSCs and inducement of NSCs to differentiate to neurons by HPC OECs

OCEs were found in sphere form one day after inoculation. Three days later, morphological characteristics became more obvious, small and as triangles and rhombuses. Six to seven days later, OECs had abundantly grown in oval, fusiform and triangle forms; some cells interlaced into networks. Part of the cells cultured for 7 days were selected for immunocytochemical staining by NGFR p75. Many cells were found to be positive.

NSCs were extracted from adhered fibroblast and then cultured by suspension. One day later, NSCs gathered to form clone spheres, with strong refraction property. Clone sphere tended to be more and larger after four to five days of cultivation, with a strong refraction property. Part of the cells cultured for 7 days were chosen as the subjects for immunocytochemical staining by nestin. A large amount of cells were found to be positive.

It was found that, the rate of NSCs differentiating to neuron 7 days after being induced by HPC OECs supernate was higher than in the control group. Some cells interlaced into a network. Large amounts of neuron were generated after being stained by tubulin.

Recovery of motor function of limbs

BBB score of all groups was assessed one day, two weeks, four weeks, six weeks, eight weeks

Table I. *BBB score one day, two weeks, four weeks, six weeks, eight weeks and twelve weeks after transplantation (mean±SD).*

Time (after transplantation)	Group		
	Group A	Group B	Group C
	(n=8)	(n=8)	(n=8)
1 day	3.375±0.916	5.375±0.916*	5.875±0.641*#
2 weeks	4.500± 0.535	8.375±0.744*	10.625±0.744*#
4 weeks	6.625±0.744	10.250±0.707*	14.250±0.707*#
6 weeks	7.250±0.463	12.625±0.518*	16.125±0.641*#
8 weeks	7.625±0.518	13.375±0.518*	17.125±0.354*#
12 weeks	8.250±0.463	13.875±0.835*	17.875±0.641*#

**: P<0.05 vs "group A"; #: P<0.05 vs "B"*

Table II. *Climbing score one day, one week, two weeks, four weeks and six weeks after transplantation (mean±SD).*

Time (after transplantation)	Group		
	Group A	Group B	Group C
	(n=8)	(n=8)	(n=8)
1 day	21.50 ± 0.53	20.38 ± 0.52	20.25 ± 0.46
1 week	19.50 ± 0.53	17.38 ± 0.52	16.13 ± 0.35*
2 weeks	15.13 ± 0.35	13.50±0.53*	13.37 ± 0.52*
4 weeks	14.13±0.35	9.63±0.52*	6.63 ± 0.52*#
6 weeks	12.38±0.52	6.13±0.35*	5.38± 0.52*#

**: P<0.05 vs "A"; #: P<0.05 vs "B"*

Table III. *Running time one day, one week, two weeks, four weeks and six weeks after transplantation (mean±SD).*

Time (after transplantation)	Group		
	Group A	Group B	Group C
	(n=8)	(n=8)	(n=8)
1 day	10.25 ± 0.46	10.63±0.52	11.13±0.35
1 week	7.63±0.52	11.38±0.52*	13.63±0.52*
2 weeks	7.75±0.46	31.13±0.35*	37.75±0.46*#
4 weeks	14.38±0.52	44.88±0.35*	53.38±0.52*#
6 weeks	16.63±0.52	49.63±0.52*	57.13±0.35*#

**: P<0.05 vs "A"; #: P<0.05 vs "B"*

and twelve weeks after the operation. The results demonstrated that, the rats of group C recovered in most effectively, second was group B, and group A was the least recovered. The details are shown in Table I. It was concluded that, the recovery of motor function of limbs was better in group C than in the other groups.

Climbing test was performed one day, one week, two weeks, four weeks and six weeks after transplantation. One day after modeling, the rats were observed to be unable to climb pole, and sometimes dragged the injured limb. After transplantation,

the climbing score of the rats in the three groups decreased as time went by. The degree of decrease of climbing score in group C was the most obvious, second was group B and group A was the least. Four weeks after transplantation, it was found that, the width between supporting hind legs in group C was greater compared to group B, when climbing the pole; in addition, injured legs of rats in group B were weak and feeble. The score is shown in Table II. These results demonstrated that, rats in group C obtained a higher score than the other groups, indicating the functional recovery in that group was superior to the other groups; however, the climbing score was much lower than the other two groups at the 6th week after transplantation.

Running time on a rotating platform was detected one day, one week, two weeks, four weeks and six weeks respectively after transplantation. The results demonstrated that, the running time became longer as time went by. This was the most obvious in Group C, second was group B and group A was the least long. The details are shown in Table III. It can be seen from the table that, running time of group C was longer than the other two groups two weeks after transplantation; at the 6th week, the running time of group C was 57s, which was remarkably longer than the other two groups.

NSCs combined with HPC OECs promotes recovery of injury tissue

HE staining was performed on spinal cord tissue one day, two weeks and four weeks after transplantation respectively, and then the situation of spinal cord tissue was observed. One day after modeling, edema, bleeding and inflammatory cell infiltrations were found in the injury area. Through continuous observation of sections, it was found in control group that, a large amount of glial scar tissues formed in the injured area fourteen days after injecting PBS; 28 days later, the structure of the spinal cord tissue became disordered. In addition, mass hyperplasia was observed both in group B and C after transplantation, but the two groups were found with fewer scar tissues and cavity compared to the control group; 28 days after transplantation, the structure of the spinal cord in the two groups returned to normal, especially in group C. Group C obtained the best recovery effect, secondary was group B and group C recovered slightly.

Relationship between transplanted cells and recovery of spinal cord

BrdU immunohistochemical labeling was performed on the section of group B and C four weeks after transplantation. Cells that showed positive after BrdU labeling were found distributed in the recovered injury area, both in group B and group C to involve in the repair of injury tissue and promote the injury tissue to return to normal. Obvious edema and inflammatory cells were not found.

DISCUSSION

SCI presents a great problem in the field of neural restoration. Its pathological basis is a direct or indirect injury causing axonal degeneration and neuronal death. As the research in this field deepens, the difficulty of central nerve injury is summarized in two categories. i.e., the lack of component supporting nerve growth (11) such as neurotrophic factors and the existence of mechanical and chemical transplantation factors such as scar tissue and inhibitory growth factor. It has been revealed that, NSCs are a kind of ideal seed cells for repairing SCI. Promotion of its differentiating to neuron has become a key point in repairing the nervous system. However, *in vitro* research found that NSCs could remain in an undifferentiated state in serum-free nutrient solution by adding bFGF. However, when 10% FBS was added, more than 90% NSCs were differentiated into astrocyte in five days. An *in-vivo* study demonstrated that, transplanted NSCs mostly differentiated into astrocyte, which inhibited axonal regeneration. This suggests that, NSCs transplantation has only a limited effect in the treatment of SCI; therefore, it is insufficient for treatment.

During this research, it was found that, compared to OECs supernate without HPC, the supernate that has been treated by HPC at 40°C induced more NSCs to differentiate to neuron. Therefore, NSCs combined with HPC OECs is thought to be more suitable for SCI. For further testing, this study established a SCI rat model and performed cell transplantation treatment one week after the modeling to minimize the negative influence of secondary injury to transplanted cells. The results demonstrated that, one week after operation,

BBB scores of the animals in the three groups were of no statistical significance. Two weeks after operation, the average BBB score of the NSCs+OECs group and the NSCs+HPC OECs group was slightly higher than in the control group. Four weeks later, it was found that, the increase of the score in the NSCs+HPC OECs group was higher than in the other two groups, and twelve weeks after operation, the difference was more obvious. Between the 6th week to the 12th week, the increase of the score was slight. That indicated that, two to four weeks after transplantation was the peak time for recovery of limb function. The results of the climbing tests and rotating tests were similar to the BBB scale. Six weeks after operation, limb functions of the rats was basically restored. Previous studies demonstrated that, transplantation of NSCs combined with OECs has a great promotion function in treating SCI. In this study, rats in the NSCs+ HPC OECs group recovered better than the other two groups, indicating that HPC OECs have an important function in neurological recovery. Besides, immunohistochemical staining for tissue further proved the superiority of HPC combined with transplantation. The results of BedU staining demonstrated that, many transplanted cells gathered around the restored spinal cord and there were no edema and inflammatory cells.

This study also found that, HPC combined with transplantation integrated biological characteristics of NSCs and OECs and strengthened the characteristics of OECs. It has been proved that, limb function recovery of transplantation of NSCs combined with HPC OECs was much better than that of combined transplantation without HPC, in the treatment of hemisected SCI of rats. Moreover, it was found that after OECs supernate was induced by 40°C HPC, the proportion of differentiation of NSCs to neuron increased. One week after transplantation, limb functions were obviously improved, the scope of SCI was also reduced and the reborn nerve fiber passed through the injured area. That further suggested that, HPC could strengthen the collaborative effect of NSCs and OECs in the treatment of SCI.

ACKNOWLEDGEMENTS

National Nature Science Foundation of China (No. 81171171, No. 30970991); Science and Technology Development Foundation of Shandong Province (No. 2014GSF118117).

REFERENCES

1. Duan D, Rong M, Zeng Y, et al. Electrophysiological characterization of nscs after differentiation induced by OEC conditioned medium. Acta Neurochir (Wien) 2011; 153(10):2085-90.
2. Duan ZX, Zhang HY, Chen LH. Changes on three neurotrophic factors expression in rats with spinal cord contusion following olfactory ensheathing cell transplantation. J Chendu Med Col 2010; 5(3):185-89.
3. Liu CL, Wu Y. Advances of stem cells transplantation for spinal cord injury. Chin J Tis Engin Res 2011; 15(32):6051-55.
4. Zhi XD, Lu G. Cotransplantation of rat bone marrow mesenchymal stem cells and Schwann's cells for treating spinal cord injury. Chin J Tis Engin Res 2008; 12(16):3015-18.
5. Lou YL. Clinical research of neural stem cells transplantation. Chin Foreign Med Treat 2012; (2):22.
6. Du F, Wu XM, Gong Q, et al. Hyperthermia conditioned astrocyte-cultured medium protects neurons from ischemic injury by the up-regulation of HIF-1 alpha and the increased anti-apoptotic ability. Eur J Pharmacol 2011; 666(1-3): 19-25.
7. Huang T, Solanl J, He D, Loutfi M, Dietrich DD, Kutltz JW. Traumatic injury activates MAP kinases in astrocytes: mechanisms of hypothermia and hyperthermia. J Neurotrauma 2009; 26(9):1535-45.
8. Chuah M I, Au C. Cultures of ensheathing cells from neonatal rat olfactory bulbs. Brain Res 1993; 601(1-2):213-20.
9. Basso DM, Beattie MS, Bresnahan JC. Graded histological and locomotor outcomes after spinal cord contusion using the NYU weight-drop device versus transaction. Exp Neurol 1996; 140(2):244-56.
10. Brailowsky S, Knight RT, Blood K, Scabini D. Gamma-Aminobutyric Acid-induced Potentiation of Cortical Hemiplegia. Brain Res 1986; 362(2):322-30.
11. Chen LH, Shao B. Biological compatibility of compound bone repairing material. Contem Med Sci 2014; (9):148-49.

LETTER TO THE EDITOR

CLOSED FEMORAL NAILING WITH THE TECHNIQUE OF USING A NEW FEMORAL DISTRACTOR: A PRELIMINARY REPORT

ZG. WANG, K. ZHANG, L. JIA, ZL. WANG, D. LIU, SY. YANG, DC. ZHANG and DG. ZHANG

Department of Traumatic Orthopedics, Affiliated Hospital of Binzhou Medical University, Binzhou, Shandong, China

Received April 9, 2015 – Accepted July 20, 2015

This study introduces the application of a new femoral distractor in the treatment of femoral fracture restoration with internal fixation of intramedullary nail. Sixty-three patients with femoral fracture from the Affiliated Hospital of Binzhou Medical University underwent femoral facture restoration with the new femoral distractor in combination with internal fixation of an intramedullary nail from June 2011 to March 2014. There were 18 cases of proximal femur fractures, 44 cases of middle femoral shaft fractures and 1 case of distal femur fracture. Follow-up was on the 4th, 6th, 8th, 12th, 16th and 24th week after operation. All 63 patients successfully underwent the surgery and the steel needles used did not cause injury to the adjacent vessels or nerves. Five cases had to have steel needles reinserted, as they had failed in the distraction reduction due to being unsteadily fixed because of an improper position. Patients were followed up for 10~24 months (mean 16 months), and the total healing rate was 100%. Operative time was 93.5 minutes averagely. Average time of patients' exposure to X-ray was 26.8 seconds. Bleeding volume was averagely 219.1 ml. There were no complications either during the operations or after them. All cases healed within 12 weeks (average 7.6 weeks). This study proves that, the new femoral distractor can help the closed reduction of fractures in treating femoral fractures with intramedullary nails to avoid the inconvenience of applying traction tables and the occurrence of potential complications.

Femoral closed reduction with internal fixation of an intramedullary nail is a standard therapeutic schedule for treating femoral shaft fractures (1). However, femoral fracture closed-reduction technology still has several difficulties. Traction table-aided reduction is the traditional method used by most orthopedists in the operation for femoral shaft fractures, but the flexibility is limited due to the body position, especially for obese patients. In addition, multiple trauma patients are unable to use a traction table due to the restriction of the position of the body. What is worse, traction-table aided reduction is likely to lead to injury of the pudendal nerve, osteofascial compartment syndrome on contralateral limb and skin injury on the perineum (2-6). The use of special distraction instruments for assisting closed-reduction surgery has been reported (7-9), but they are not widely used due to the complex surgery and high technical requirements. Manual closed-reduction has also been reported (10-17). Both supine position and lateral position are feasible during an operation, which can be beneficial for

Keywords: femur fracture, intramedullary nailing, closed reduction, distraction system for femoral fracture

Mailing address: Dr Zhigang Wang, Department of Traumatic Orthopedics, Affiliated Hospital of Binzhou Medical University, the 2nd Huanghe Road, Binzhou, Shandong, 256603, China
e-mail: wzgbzyxy@163.com

0393-974X (2015)

patients with combined injuries, for surgery of the femoral proximal opening and locking with distal interlocking nailing, but an assistant is required for continuous traction during surgery and the failure rate is high.

In this study, we carried out femoral closed-reduction by applying a self-made femoral distractor in combination with internal fixation of an intramedullary nail to treat femoral fractures. This study reports the application of a new femoral distractor in treating 63 cases of femoral fractures with internal fixation of an intramedullary nail.

MATERIALS AND METHODS

Between September 2010 and March 2014, 63 cases of femoral shaft fractures (51 males and 12 females) were treated in the Department of Traumatic Orthopedics of the Affiliated Hospital of Binzhou Medical University by applying internal fixation of an intramedullary nail in combination with a new femoral distractor. The patients were from 18 to 65 years old (mean 35.9 years). Of the 63 cases, 47 had multiple injuries; 53 were injured in traffic accidents (81.4%), 7 cases due to falling (11.1%), 1 case due to a fall while walking (1.6%) and 2 cases due to pressure from heavy objects (3.2%). The fractures were all located in the femoral shaft below the lesser trochanter of the femur, including 18 cases of femoral proximal fractures (28.6%), 43 cases of proximal femur fractures, 43 cases of middle femoral shaft fractures (68.3%), 1 case of distal femur fracture (1.6%), and 1 case of middle femoral shaft fracture combined with intertrochanteric fracture (1.6%). Of the 63 patients, no one was found with a medullary space less than 8 mm or femoral deformity. Patients with 1/4 middle or lower part of fractures in the femur were not included in this study. According to AO classification, 28 cases (44.4%) were determined as A type fractures, 27 cases (42.9%) were B type fractures and 8 cases (12.7%) were C type fractures. Twenty seven cases (42.9%) had multiple fractures on limbs. Of 27 cases, 14 cases (22.2%) had thoracic closed injuries; 4 cases (6.3%) had abdominal closed injuries (3 cases received small intestine rupture operations and one received conservative treatment); 9 cases (14.3%) had craniocerebral injuries in different degrees (all received conservative treatment). All the patients were hospitalized for 1 to 16 days (mean 7.8 days) before being operated.

Before operation, skeletal traction was continuously performed, reduction in the fractured region was reviewed by X-ray and the weight of the traction regulated until the fractured region was completely opened. X-rays should also cover hip joint and knee joint, to prevent missed diagnosis of femoral neck or femoral intercondylar fractures.

To prevent the formation of deep venous thrombosis on lower limbs, patients who were examined with no coagulation disorders and related bleeding complications 24 hours after injury were given an anticoagulant from 12 to 24 hours after the operation.

The distance from the anterior superior spine to the prominence of the lateral malleolus was measured before the operation and that distance in the healthy limb was compared with that of the injured limb, to prevent type B or C fracture shortening deformity.

The new reduction technology was approved by the medical ethics committee of the Affiliated Hospital of Binzhou Medical University. Moreover, all patients signed informed consent.

On the second day after operation, patients were assisted in long contraction functional exercises for quadriceps femoris on the lower limb and active functional exercises for hip, knee and ankle joint. On the 3rd to 5th day, patients were required to do functional exercises without weight with the help of double crutches. Patients were followed up on the 4^{th}, 6^{th}, 8^{th}, 12^{th}, 16^{th}, 24^{th} week and one year after operation and during follow up visit; they were requested to do weighted functional exercises based on their healing conditions.

Surgical technique

Patients were narcotized with either combined spinal epidural anesthesia or tracheal intubation in combination with intravenous inhaled anesthesia. Patients were placed on the X-ray bed in a horizontal recumbent position with the injured limb raised at 25 to 30 degrees, to enable X-ray examination during the operation.

The upper part of the injured limb was hung on the stent above the bed or placed on a board above the chest while the hip of the injured limb was blocked by a support.

The entire injured limb and perineum were disinfected. A 4 mm steel needle was beaten into the ala of ilium from the position of anterior and superior iliac spine, with an angle of 15 degrees inclining to the upper and inner sides. The steel needle was covered by a cannula and the cannula could rotate around the steel needle; a 4.0 mm steel needle was pierced into the lateral femoral epicondyle paralleling to knee joint and then another was inserted into position, 1-2 cm above the upper patella of the femoral condyle from the anterosuperior medial femoral malleolus to the posterior medial femoral malleolus; the needle end was inclined to the upper side for 20 to 30 degrees, and the semi-ring was used to connect the steel needle to form a distal fixation structure; the proximal cannula structure and distal semi-ring structure were connected through an extension rod in the middle by applying a tubing clip; the

extender was rotated to expose the facture region.

As to type B and C fractures, the distance from the anterior superior spine to the prominence of the lateral malleolus was measured before the operation to confirm that it was consistent with the length of the healthy limb.. Moreover, that the force line between the anterior superior spine on the lower limb and the first and second toe, passed the midline of patella should also be confirmed, in order to prevent femoral rotation deformity.

A 5-6 cm incision was made above the top of the greater trochanter. After the muscle was longitudinally separated, a 4-mm steel needle was penetrated towards the femoral medullary canal from the femoral proximal pyriform sinus with an electric drill. An intramedullary needle with an outward inclination of 6 degrees on the near-end was penetrated inward into the top of the greater trochanter. X-ray examination revealed that, the normotopia and side position of the steel needle both pointed towards the middle of the femoral medullary canal, and at the same time, the fracture region was examined to observe correct alignment.

The pilot sleeve was imbedded through the steel needle and then the end of the sleeve was beaten to make the sleeve fix on the entrance of the proximal femur. After the steel needle extracted, a guide needle was pierced into the medullary space through the pilot sleeve. If necessary, Kirschner wire was used to adjust the proximal fracture percutaneously to help reduction. Monitored by X-ray, it was confirmed that the intramedullary needle had reached the distal metaphysis and was located in the centre, both on the images of normotopia and the side position. Then a hollow drill was used to make a cut in the proximal end.

The femoral medullary canal was reamed until a creaking sound was heard or according to the size of the intramedullary needle, from small to large. The reaming diameter for the medullary canal was 1 to 1.5 mm wider than the intramedullary needle used. When there was difficulty for the type C fracture guide needle to pass through the broken end of the fractured bone, a cut was made in the proximal end first and then pierced into medullary canal with a metal finger to make the needle pass through the broken end. After reaming, an intramedullary needle was inserted along the guide needle. Finally, X-ray was used to examine whether there was deformity of rotation, shortening, separation and angulation on the broken end. If there was, then the distraction device could be adjusted by direction and position for correction.

A magnetic navigation positioning device was used to lock in two interlocking nails in the distal end. With the help of a proximal locator, another two interlocking nails were locked into the proximal end for static fixation. As to type A fractures, one interlocking nail was locked into the proximal end for dynamic fixation. When the fractures occurred within 5 mm below the lesser trochanter, reconstructed intramedullary needle fixation was required, i.e., the interlocking nail was driven in the proximal end into the femoral neck. Next, the distraction device was removed and washed. The incision was staunched and sutured. Drainage was not needed.

RESULTS

All the patients were followed up for 10 to 24 months after the operation, on an average of 16 months, and they were all found to be healed. The operation time was, from the installment of the distraction device to the suture of the cut, an average of 93.5. During the operations, discontinuous X-ray exposure was used, and the average exposure time was 26.8 seconds. Moreover, the amount of bleeding was 219.1 ml averagely. All patients had successful closed reduction after surgery and steel needles used in surgery have not caused injury of the adjacent vessels and nerves. During surgery, however, 5 cases were reinserted with steel needles, as they failed in distraction reduction due to unsteadily fixed steel needles caused by improper positioning. In the one year follow up after surgery, all functions of the knee joints on the injured limbs were found to be normal; shortening deformity over 10 mm and deformity with angulation rotation over 15 degrees were not found, as well as the lateral and front-back angulation deformity over 10 degrees. None of the patients had wound infections. Fractures could be confirmed to be healed when X-ray examinations revealed continuous poroma in the fracture end and patients could walk painlessly with a crutch. Within 16 weeks after the operation (average 7.6 weeks), all the patients were healed and could walk to different extents.

For those with fractures in the upper segment of the femur or trochanter, a reconstructed intramedullary needle was used, i.e., inserting a proximal femoral inter-locking nail through the femoral neck, which increased fixation stability in the fracture region and benefited fracture healing. In addition, one case was also found with a femoral neck fracture on the same side and one case with an intertrochanteric fracture; they were treated with a reconstructed intramedullary needle combined with an extended proximal femoral nail anti-rotation needle. Close-reduction surgery, applying the new femoral distractor was finally found to be successful.

DISCUSSION

Closed-reduction intramedullary nail fixation is currently the standard scheme for treating adult femoral fractures (1). Traditionally, using a traction bed for treating femoral fractures is used by many orthopedists; however, the special position required by a traction bed restrains the flexibility of surgery, especially for large or obese patients. There is also a greater risk in the occurrence of complications compared to other reduction methods, because the insufficient adduction of lower limbs will cause femoral neck fractures when the intramedullary nail is inserted. In addition, the traction bed is likely to cause nerve and soft tissue injury due to the excessive traction force. Injury of the perineal region caused by excessive compression, including genital organ edema and nerve paralysis can influence sexual functions of both male and female, with an occurrence rate of 9% (2-5). Moreover, patients with multiple fractures on lower limbs are forbidden to use traction bed for closed-reduction.

Barmgaertel et al. (7) proposed to treat femoral shaft fractures applying AO femoral distractor in combination with the internal fixation of an intramedullary nail; however, screws of the distractor placed in the lesser trochanter of the femur is likely to injure the femoral nerve and femoral vessels; moreover its application was restricted due to the complex surgery. Reynders et al (8, 9) achieved good effect by treating femoral fractures with unreamed intramedullary nail fixation in combination with a new distractor. With that surgery, a nail was not required to be inserted into the proximal femur, but the perineum still needed to resist traction, which could injure the skin and nerve of then perineum.

Among the cases of this study, the injury in 53 cases was caused by automobile accidents (84.1%), of which, 47 cases had combined injury or multiple fractures. Some patients can not be operated due to the combined life threating injury; and before operation, continuous traction or external fixator were required to maintain the length of the injured limbs to prevent closed-reduction difficulty during operation (18). It has been reported that in the treatment of multiple fractures, including femoral fractures (19, 20), the change of early damage control lowers the occurrence rate of acute respiratory distress syndrome (ARDS) and multiple organ failure (MOF), and the occurrence rate of complications does not increase due to delayed femoral operation.

The new femoral distraction reduction system used in this study is a self-made system applied in femoral fracture operations and it was put into use after being approved by the ethics committee of the Affiliated Hospital of Binzhou Medical University. Differing from traditional distraction system, this system with a supporting point on the anterior superior spine is more conformed to the alignment of lower limbs. The top of a steel nail located in the anterior superior spine can reach the bone on the upper side of acetabulum, with a 15 to 20 degree inclination in the end of the steel needle. Cannula rotating around the steel needle can allow adduction and abduction of lower limbs, which is beneficial in surgery and for the stability of the steel needle. The femoral distractor is suitable for patients with any body type, including obese patients. For patients with multiple fractures and combined injuries, this device presents outstanding advantages.

In this study, patients in the supine position were raised for 30 degrees on the healthy side for a flexible operation during surgery and convenient implantation of the intramedullary needle. Firat et al. (16) reported that, the supine position with the healthy side raised could achieve complete adduction of the injured limb and moreover be helpful for observation; but assistants were still required to maintain manual traction during surgery.

Consistence of the direction of the connecting rod and the axial alignment of the femur in the lower limb is of greater benefit in the reduction of femoral fracture. After the location of the proximal femur is simply adjusted by Kirschner wire, an intramedullary needle can be easier inserted into the fracture end. In addition, positioning the distal femoral nail by a magnetic navigation positioning device is accurate. As a result, X-ray exposure time for medical staff and patients is reduced.

To sum up, closed reduction performed with this new femoral distractor can not only reduce the occurrence of complications with regards to the application of the traction bed but also reduces surgical difficulties compared to similar devices. However, this study still has limitations. The size of samples is small and the safety and reliability of

this surgery remains to be explored with controlled clinical trials.

REFERENCES

1. Wild M, Gehrmann S, Jungbluth P, Hakimi M, Thelen S, Betsch M, Windolf J, Wenda K. Treatment strategies for intramedullary nailing of femoral shaft fractures. Orthopedics 2010; 33(10):726.
2. Brumback RJ, Ellison TS, Molligan H, Molligan DJ, Mahaffey S, Schmidhauser C. Pudendal nerve palsy complicating intramedullary nailing of the femur. J Bone Joint Surg Am1992; 74(10):1450-5.
3. Napal LS, Vallejo NJ, Paz VM, et al. Erectile dysfunction caused by neurapraxia of the pudendal nerve after the use of a traction table for the treatment of traumatic fractures. Report of a case and review of the literature. Arch Esp Urol 1998; 51(3):298-300.
4. Pianezza A, Galas T, Minville V, Destrubé M, Laffosse JM. Femoral intramedullary nailing in men on fracture table: beware of the risk of postoperative erectile dysfunction. Ann Fr Anesth Reanim 2008; 27(1):110-1.
5. Rudloff MI, Smith WR. Intramedullary nailing of the femur: current concepts concerning reaming. J Orthop Trauma 2009; 23(5 Suppl):S12-7.
6. Karadimas EJ, Papadimitriou G, Theodoratos G, Papanikolaou A, Maris J. The effectiveness of the antegrade reamed technique: the experience and complications from 415 traumatic femoral shaft fractures. Strategies Trauma Limb Recon 2009; 4:113-21.
7. Baumgaertel F, Dahlen C, Stiletto R, Gotzen L. Technique of using the AO-femoral distractor for femoral intramedullary nailing. J Orthop Trauma 1994; 8(4):315-21.
8. Reynders P, Broos PL. Unreamed intramedullary nailing of femoral shaft fractures using a traction device. Injury 1998; 29(1):81-4.
9. Reynders P, Broos P. Unreamed intramedullary nailing of acute femoral shaft fractures using a traction device without fracture table. Acta Orthop Belg 1998; 64(2):175-9.
10. Karpos PA, McFerran MA, Johnson KD. Intramedullary nailing of acute femoral shaft fractures using manual traction without a fracture table. J Orthop Trauma 1995; 9(1):57-62.
11. Sirkin MS, Behrens F, McCracken K, Aurori K, Aurori B, Schenk R. Femoral nailing without a fracture table. Clin Orthop Relat Res 1996; (332):119-25
12. Hutson JJ Jr. Femoral nailing without a fracture table. Clin Orthop Relat Res 1997; (344):338-40.
13. Liu HT, Wang IC, Yu CM, Huang JW, Wang KC, Chen CH, Ueng SW. Closed femoral nailing in lateral decubitus position without a fracture table: a preliminary report of fifteen patients. Chang Gung Med J 2005; 28(9):629-35.
14. Carr JB, Williams D, Richards M. Lateral decubitus positioning for intramedullary nailing of the femur without the use of a fracture table. Orthopedics 2009; 32(10).
15. Bishop JA, Rodriguez EK. Closed intramedullary nailing of the femur in the lateral decubitus position. J Trauma 2010; 68(1):231-5.
16. Firat A, Tecimel O, Deveci A, Ocguder A, Bozkurt M. Surgical technique: supine patient position with the contralateral leg elevated for femoral intramedullary nailing. Clin Orthop Relat Res 2013; 471(2):640-8.
17. Stephen DJ, Kreder HJ, Schemitsch EH, Conlan LB, Wild L, McKee MD. Femoral intramedullary nailing: comparison of fracture-table and manual traction. a prospective, randomized study. J Bone Joint Surg Am 2002; 84-A(9):1514-21.
18. Aiyer S, Jagiasi J, Argekar H, Sharan S, Dasgupta B. Closed antegrade interlocked nailing of femoral shaft fractures operated up to 2 weeks post injury in the absence of a fracture table or C-arm. J Trauma 2006; 61(2):457-60.
19. Pape HC, Hildebrand F, Pertschy S, Zelle B, Garapati R, Grimme K, Krettek C, Reed RL 2nd. Changes in the management of femoral shaft fractures in polytrauma patients: from early total care to damage control orthopedic surgery. J Trauma 2002; 53(3):452-61
20. Pape HC. Effects of changing strategies of fracture fixation on immunologic changes and systemic complications after multiple traumas: damage control orthopedic surgery. J Orthop Res 2008; 26(11):1478-84.

LETTER TO THE EDITOR

NEUROENDOCRINE FUNCTIONS OF PUERPERAE WITH POSTPARTUM DEPRESSION AGGRAVATED BY STRESSFUL CHILDBIRTH-RELATED EVENTS

W. SONG and S. YU

Department of Obstetrics, Beijing Obstetrics and Gynecology Hospital, Capital Medical University, Beijing, China

Received June 8, 2015 – Accepted July 24, 2015

In the period of gestation, delivery and post-delivery, fear and tension produced in puerperae are likely to evolve into depression as they worry too much about delivery pain. In recent years, it has been noted that stressful events during this period aggravate postpartum depression. To discuss the effect of these childbirth-related stressful events on neuroendocrine functions of patients with postpartum depression, 300 full-term puerperae who had been admitted to the Beijing Obstetrics and Gynecology Hospital, Capital Medical University between October, 2011 and October, 2013 and who had suffered from stressful childbirth-related events were enrolled as a study group. This group was divided into six subgroups, i.e., A, B, C, D, E and F, based on the number of stressful events they had suffered which were labeled by numbers 1 to 6. Additionally, 100 puerperae from the same hospital who had not suffered from childbirth-related stressful events were taken as controls. Relevant clinical indexes, including serum adrenocorticotropic hormone (ACTH), plasma 5-hydroxytryptamine (5-HT), noradrenaline ELISA (NE), dopamine (DA) and cortisol level were measured and compared. It was found that incidence probability of postpartum depression was significantly different between the study group (13.67%, 41/300) and the control group (7%, 7/100). Moreover, the incidence probability of postpartum depression of puerperae suffering from no less than 4 childbirth-related stressful events was higher than those suffering from no more than 3, and the difference was statistically significant (P<0.05). Thus, stress disorders caused by these events are one of the important pathogenic factors of postpartum depression.

Postnatal depression, one of the most common mental disorders occurring after delivery, is caused by endocrine dyscrasia induced by significant body changes after delivery (1). It has been found that puerperae are generally afraid or nervous about delivery, especially regarding the degree of pain, safety of both mother and infant, and the health of the infant; when these emotions are more intensive and childbirth-related stressful events occur they can lead to postnatal depression (2).

To date, it has been generally believed that neuroendocrine change, i.e., hypothalamic-pituitary-adrenal (HPA) axis hyperfunction, is the leading cause of postnatal depression. However, it is seldom reported how the HPA axis and monoamine neurotransmitter system functions of puerperae change and what the relationship is between the changes and postnatal depression (4, 5). To understand more about the effects of these stressful events on neuroendocrine functions of puerperae, this

Key words: postpartum depression, delivery, childbirth-related stressful events, internal secretion

Mailing address: Dr Song Yu,
Department of Obstetrics,
Beijing Obstetrics and Gynecology Hospital,
Capital Medical University,
No.251, Yaojiayuan Street,
Chaoyang, Beijing 100026, China
e-mail: ysongjbrha@163.com

0393-974X (2015)

study reviewed the clinical data of volunteers from the Beijing Obstetrics and Gynecology Hospital and explored the correlation between childbirth-related stressful events and neuroendocrine functions.

MATERIALS AND METHODS

A total of 300 full-term puerperae who had been admitted to the Beijing Obstetrics and Gynecology Hospital, Capital Medical University between October, 2011 and October, 2013 and who had suffered from childbirth-related stressful events were taken as the study group, and 100 full-term puerperae from the same hospital who had not suffered from stressful events were selected as controls. All puerperae signed an informed consent before the study and the research was approved by the ethics committee of the Beijing Obstetrics and Gynecology Hospital, China. None of the subjects had psychological disorders or psychiatric histories; moreover, they had normal intelligence, without any brain disease. The gestation period of puerperae in the observation group ranged from 37 to 41 weeks (average 38.21±1.61 weeks) and they were aged 21-35 years (average 25.8±1.5 years). In the control group, the puerperae were aged 20-36 years (average 26.12±1.64 years) and had 37-43 gestational weeks (average 26.12±1.64 weeks).

The 300 puerperae who had previously suffered from childbirth-related stressful events were divided into sub-groups: group A (50 cases who had suffered one stressful event), group B (50 cases, two stressful events), group C (50 cases, three stressful events), group D (50 cases, four stressful events), group E (50 cases, five stressful events) and group F (50 cases, six stressful events). One hundred puerperae who had not suffered from any stressful events were taken as controls in the same period. The puerperae had no significant differences in average age, health condition before pregnancy, average years of education, times of gestational examination, delivery means, average weight of newborn between the different groups, therefore they were comparable.

Follow-up

Forty-two days after delivery, the puerperae were re-examined by professionally trained medical workers of the Beijing Obstetrics and Gynecology Hospital, Capital Medical University. A total of 300 questionnaires were filled in, with 100% effective investigation rate. Then the Edinburgh Postnatal Depression Scale (EPDS) was used to compare the possibility of occurrence of postpartum depression aggravated by stressful childbirth-related events of the puerperae in the observation group and the control group. The EPDS is shown in Table I.

Sample collection

Forty-two days after delivery, the puerperae were followed-up at the outpatient department. Between 8 and 9.00 a.m., 12 ml samples of venous blood were taken from each subject on an empty stomach. Six ml blood were pre-cooled in a plastic finger pipe loaded with 50 μl aprotinin and 50 μl Ethylene Diamine Tetraacetic Acid (EDTA) and thoroughly mixed. Then the solution was centrifuged at 3,000r/min at 4°C for 10 min. The plasma remained and was cryo-preserved at -70°C.

Stressful events during gestation

The stressful events during childbirth in this study include extension of the first stage of labor, bad pain, labor complications, severe medical and surgical complications, vaginal instrumental delivery, fetal malformation, intrauterine death, neonatal death, neonatal asphyxia, postpartum lactating difficulty and poor healing of the incision.

Detection method

Radioimmunoassay was used to measure corticotropin releasing hormone (CRH), adrenocorticotrophic hormone (ACTH) and cortisol level. Moreover, a high pressure liquid chromatography (HPLC)/electrochemical method was used to detect the level of monoamine neurotransmitters contained in plasma.

Statistical analysis

SPSS 19.0 statistics were used to calculate data analysis. Measurement data are expressed by mean ± SD. Differences between the two groups was compared using *t*-test. Enumeration data was compared by c^2 test. Differences were considered to be statistically significant if $P<0.05$.

RESULTS

Effect of childbirth-related stressful events on incidence probability of postpartum depression

It was found that 41 (13.67%) cases of postpartum depression occurred in the study group, while only 7 (7%) cases occurred in the control group, and the difference between the two groups was statistically significant ($P<0.05$). Furthermore, the incidence probabilities of postpartum depression were higher in puerperae suffering from more stressful childbirth-related events and their EPDS score was also higher. Compared to puerperae suffering from no more than 3 stressful events, those suffering from no less than 4 were found to have a higher EPDS score and

Table I. *EPDS.*

Item	Level	Score	Total
Happy and can see funny side of things	Same as before	0	
	Not so more as before	1	
	Obviously less than before	2	
	Completely incapable of	3	
Keep positive on future	Same as before	0	
	Not so more as before	1	
	Obviously less than	2	
	Completely incapable of	3	
Unnecessarily blame oneself when things go wrong	Often	3	
	Sometimes	2	
	Rarely	1	
	Never	0	
Be worried and anxious without reason	Never	0	
	Sometimes	1	
	Rarely	2	
	Often	3	
Feel scared and alarmed without reason	Often	3	
	Sometimes	2	
	Rarely	1	
	Never	0	
Feel things out of control	Often	3	
	Sometimes	2	
	Rare	1	
	Never	0	
Bad sleep due to bad emotion	Often	3	
	Sometimes	2	
	Rarely	1	
	Never	0	
Feel sad	Often	3	
	Sometimes	2	
	Rarely	1	
	Never	0	
Cry due to bad emotion	Often	3	
	Sometimes	2	
	Rarely	1	
	Never	0	
Want to hurt oneself			
	Sometimes	2	
	Rarely	1	
	Never	0	

Table II. *Effect of childbirth-related stress events on incidence probability of postpartum depression.*

Group	Number of cases	EPDS score	Incidence rate of postpartum depression [n, (%)]
Control group	100	3.5±1.3	8 (8.0)
A	50	7.1±2.3	5 (10.0)
B	50	8.7±2.7	5 (10.0)
C	50	8.6±2.8	6 (12.0)
D	50	11.5±4.0	8 (16.0)
E	50	12.3±4.7	10 (20.0)
F	50	15.9±3.7	11 (22.0)

(Mean ± SD)

Table III. *Comparison of ACTH, CRH and cortisol level in serum of puerperae under obstetric stress events.*

Group	Number of cases	CRH (pg/ml)	ACTH (pg/ml)	Cortisol level (pg/ml)
Control group	100	28.54±4.32	42.40±10.77	312.77±32.15
A	50	29.31±4.20	43.96±11.04	319.15±33.22
B	50	31.26±4.57	45.12±11.79	328.78±37.12
C	50	34.57±5.78	47.63±12.36	332.14±38.86
D	50	39.91±6.46[b]	51.57±13.32[b]	352.17±43.72[b]
E	50	43.32±7.16[b]	56.24±14.83[b]	367.37±49.67[b]
F	50	46.66±8.27[b]	59.78±15.61[b]	384.81±52.17[b]
Total	400	37.15±5.98[a]	5 0.73±13.34[a]	348.52±42.65[a]

Compared to control group, aP < 0.05; compared to group A, B, C, bP < 0.05 (Mean± SD)

incidence probability of stressful events, and the differences were statistically significant. (Table II).

Effect of stressful childbirth-related events on serum CRH, ACTH and cortisol level

CRH, ACTH and cortisol level of puerperae who had experienced stressful events during childbirth were (37.15±5.98) pg/ml, (50.73±13.34) pg/ml and (348.52±42.65) ng/ml, respectively; these levels were (28.54±4.32) pg/ml, (42.4±10.77) pg/ml, (312.77±32.15) ng/m, respectively, in the control group. The differences between the two groups were statistically significant (P<0.01) (Table III).

Effect of stressful childbirth-related events on plasma 5-HT, DA and NE level

5-HT, DA and NE levels of puerperae who had experienced stressful childbirth-related events were (121.37±52.37) ng/ml, (184.43±82.62) ng/ml and (30.52±12.13) ng/ml, respectively, and in the control group were (153.54±68.12) ng/ml, (239.17±96.41) ng/ml, (41.51±b16.91) ng/ml, respectively. The differences between the two groups were statistically significant (P<0.01) (Table IV).

Table IV. *Comparison of ACTH, CRH and cortisol level in serum of puerperae under obstetric stress events.*

Group	Number of cases	5-HT (ng/ml)	DA (ng/ml)	NE (ng/ml)
Control group	100	153.54± 68.12	239.17±96.41	41.51±16.91
A	50	141.3±62.91	232.16±95.27	41.66±15.50
B	50	139.92±60.64	219.98±92.65	38.54±14.94
C	50	124.64±53.78	187.41±86.94	31.62±12.86
D	50	$108.12±46.46^{b}$	$168.57±75.32^{b}$	$26.32±10.72^{b}$
E	50	$89.87±32.16^{b}$	$152.24±67.83^{b}$	$21.83±7.87^{b}$
F	50	$72.66±24.37^{b}$	$136.25±58.53^{b}$	$17.14±5.67^{b}$
Total	400	$121.37±52.37^{a}$	$184.43±82.62^{a}$	$30.52±12.13^{a}$

(Mean± SD)

Table V. *Correlation analysis of plasma 5-HT, DA, NE, serum CRH, ACTH, cortisol level of puerperae in observation group (r).*

Item	Y_1	Y_2	Y_3	Y_4	Y_5	Y_6
Y_1	1	0.32^{c}	0.45^{d}	-0.37^{c}	-0.47^{d}	-0.39^{d}
Y_2	0.32^{c}	1	0.53^{d}	-0.65^{d}	-0.43^{c}	-0.33^{c}
Y_3	0.45^{d}	0.53^{d}	1	-0.41^{d}	-0.58^{c}	-0.45^{d}
Y_4	-0.37^{c}	-0.65^{d}	-0.41^{d}	1	0.39^{d}	0.44^{d}
Y_5	-0.47^{d}	-0.43^{c}	-0.58^{c}	0.39^{d}	1	0.53^{c}
Y_6	-0.39^{d}	-0.33^{c}	-0.45^{d}	0.44^{d}	0.53^{c}	1

Pc <0.05, Pd <0.01; Y1=5-HT, Y2=DA, Y3=NE, Y4=CRH, Y5=ACTH and Y6=cortisol level

Relationship between plasma 5-HT, DA, NE, CRH, ACTH, cortisol level in observation group

Plasma 5-HT, DA and NE of puerperae in the study group who had experienced stressful childbirth-related events were in positive correlation, and serum CRH, ACTH and cortisol level were also in positive correlation. However, plasma 5-HT, DA, NE and serum CRH, ACTH, cortisol levels were negatively correlated (Table V).

DISCUSSION

Postnatal depression occurring at the 6th week after delivery is characterized by low emotion and feeling along with changes of behavior and of the mind as well as sometimes in the body (6, 7). Medical research has proved that pregnant women have great psychological changes as well as the physical ones. Some researchers have suggested that the probability of having postnatal depression after delivery will increase greatly if stressful childbirth-related events occur (8, 9, 10). In the present study, the number of cases of postnatal depression occurring between the study group and the control group was statistically significant ($P<0.05$). Moreover, EPDS score, CRH, ACTH and cortisol level of the study group were much higher than the control group, suggesting that stressful childbirth-related events were the direct factors leading to postnatal depression and an increase of related serum indexes. Additionally, it was

found that EPDS score and probability of postnatal depression of puerperae suffering from more than four stressful events were significantly higher than those suffering from less than four stressful events ($P<0.05$). Moreover, we found abnormal changes of indexes such as 5-HT, NE and DA were also able to worsen depression.

In conclusion, occurrence of stressful childbirth-related events can lead to hyperfunction of HPA axis of puerperae (11). Therefore, for puerperae who have suffered from difficult labour, pain, and fluctuating emotions, special care should be taken to prevent postnatal depression.

REFERENCES

1. Ngai FW, Ngu SF. Predictors of maternal and paternal depressive symptoms at postpartum. J Psychosom Res 2015; 78(2):156161.
2. Lee DT, Yip SK, Chiu HF, et al. Detecting postnatal depression in Chinese women. Validation of the Chinese version of the Edinburgh Postnatal Depression Scale. Br J Psychiatry 1998; 172:433-37.
3. Cox JL, Holden JM, Sagovsky R. Detection of postnatal depression. Development of the 10-item Edinburgh Postnatal Depression Scale. Br J Psychiatry 1987; 150:782-86.
4. Pearlstein T, Howard M, Salisbury A, Zlotnick C. Postpartum depression. Am J Obstet Gynecol 2009; 200(4):357-64.
5. Zhao Y, Kane I, Wang J, Shen BB, Luo JF, Shi SX. Combined use of the Postpartum Depression Screening Scale (PDSS) and Edinburgh Postnatal Depression Scale (EPDS) to identify antenatal depression among Chinese pregnant women with obstetric complications. Psychiatry Res 2015; 226(1):113-19.
6. Yang FZ, Gardner CO Jr, Bigdeli T, et al. Clinical features and risk factors for major depression with history of postpartum episodes in Han Chinese Women: a retrospective study. J Affect Disord 2015; 183(1):339-46.
7. Dennis CL. Psychosocial interventions for the treatment of perinatal depression. Best Pract Res Clin Obstet Gynaecol 2014; 28(1):97-111.
8. Zhang XL, Wang L, Huang FH, Li JF, Li X, Xue H, Zhang YZ. Gene-environment interaction in postpartum depression: a Chinese clinical study. J Affect Disord 2014; 165(20):208-12.
9. Stowe NZ, Nemeroff BC. Women at risk for postpartum-onset major depression. Am J Obstet Gynecol 1995; 173(2):639-45.
10. Deng AW, Xiong RB, Jiang TT, Luo YP, Chen WZ. Prevalence and risk factors of postpartum depression in a population-based sample of women in Tangxia community, Guangzhou. Asian Pac J Trop Med, 2014; 7(3):244-49.
11. Heh SS. Relationship between social support and postnatal depression. Kaohsiung J Med Sci 2003; 19(10):491-96.

JOURNAL OF BIOLOGICAL REGULATORS & HOMEOSTATIC AGENTS Vol. 29, no. 3, 695-699 (2015)

LETTER TO THE EDITOR

IMP-3 EXPRESSION IN BENIGN MELANOCYTIC NEVI, DYSPLASTIC NEVI AND MALIGNANT MELANOMA: PRELIMINARY FINDINGS IN BULGARIAN PATIENTS

A.A. CHOKOEVA[1], J. ANANIEV[2], U.WOLLINA[3], C. TANA[4], T. LOTTI[5], J.C. CARDOSO[6] and G. TCHERNEV[1]

[1]"Onkoderma" –Policlinic for Dermatology, Venereology and Dermatologic Surgery, Sofia, Bulgaria; [2]Department of General and Clinical Pathology, Medical Faculty, Trakia University, Stara Zagora, Bulgaria; [3]Department of Dermatology and Allergology, Academic Teaching Hospital Dresden-Friedrichstadt, Dresden, Germany; [4]Internal Medicine Unit, Guastalla Hospital, AUSL Reggio Emilia (RE), Italy; [5]University of Rome "G.Marconi" Rome, Italy; [6]Dermatology Department, University Hospital of Coimbra, Coimbra, Portugal

Received June 16, 2015 – Accepted July 17, 2015

IMP-3 is generally considered as an oncofetal protein, which plays a critical role in regulation of cell proliferation via an IGF-II-dependent pathway in K562 leukemia cells. IMP-3 expression has been detected in malignancies with various origins, while its appearance in adult tissue is generally considered abnormal, with some exceptions. IMP3 is also considered a prognostic biomarker in patients with renal cell carcinoma and clear-cell type ovarian carcinoma, hepatocellular carcinoma, pancreatic ductal adenocarcinoma and in patients with poorly differentiated thyroid carcinoma and uterine cervical carcinomas, testicular cancer and malignant melanoma. To our knowledge, no more than 4 PubMed-indexed studies have investigated the expression of IMP-3 in melanocytic lesions, namely its role in the differentiation between benign and malignant neoplasms. We investigated the expression of IMP-3 in a small series of benign melanocytic lesions, dysplastic nevi and melanomas, aiming to establish its significance as a marker for their distinction, comparing the results with those from the literature. IMP-3 immunostaining was performed in 30 melanocytic lesions: 10 malignant melanomas, 10 dysplastic nevi and 10 benign melanocytic nevi. Our results revealed expression in 20% of dysplastic lesions and 40% of melanoma cases, while none of the benign nevi showed positive expression. These data contradict some of the results from other studies and raise some questions regarding the correlation between IMP-3 and the degree of dysplasia of melanocytic nevi, as well as its potential relationship with prognostic parameters in melanoma, including tumor thickness and mitotic rate. Our results suggest that IMP-3 expression could be only an auxiliary marker for differentiation between dysplastic nevi and benign nevi, since although it is not expressed in all dysplastic lesions, staining correlates with the degree of dysplasia/atypia. It seems that IMP-3 expression is not a useful discriminator between dysplastic nevi and melanoma nor a good prognostic marker in melanoma.

Key words: IMP-3 expression, immunohistochemistry, melanocytic lesions, melanoma, prognostic marker

Mailing address: Assoc. Prof. Georgi Tchernev PhD,
"Onkoderma" -Policlinic
for Dermatology and Dermatologic Surgery,
„General Skobelev" 26,
Sofia, Bulgaria
Tel.: +359 885 588 424
e-mail: georgi_tchernev@yahoo.de

0393-974X (2015)

DISCLOSURE: ALL AUTHORS REPORT NO CONFLICTS OF INTEREST RELEVANT TO THIS ARTICLE.

Insulin-like growth factor II (IGF-II) is an embryonic growth factor with autocrine and paracrine action (1). Insulin-like growth factor-II messenger RNA (mRNA)-binding protein-3 (IMP-3), also known as K homology domain-containing protein overexpressed in cancer (KOC) and L523S, is a member of the insulin-like growth factor-II mRNA-binding protein family and it is expressed both during embryogenesis and in some malignancies (1). Insulin-like growth factor-II mRNA-binding proteins 1, 2 and 3 (IMP1, IMP2 and IMP3) belong to a family of RNA-binding proteins implicated in mRNA localization, turnover and translational control (1, 2). IMP-3 is mainly combined with IGF-II leader 3 mRNA. It promotes tumor growth via increasing translation of IGF-II mRNA. It also affects extracellular matrix organization (2, 3).

IMP-3 is a 580 amino-acid protein with 4 K homology domains and 2 RNA recognition motifs and is encoded by a gene on chromosome 7p11.5 (4). IMP3 is normally expressed in lymph node germinal centers, focally in intestinal mucosa, placenta, ovary, testis, and brain (3). IMP3 overexpression is seen in a variety of malignant tumors such as lung cancer, hepatocellular carcinoma and urothelial cancer (3-5). IMP3 has been recently studied as an immunohistochemical marker with potential value in the distinction between melanomas and melanocytic nevi (6-8).

We investigated the expression of IMP-3 in melanocytic lesions – benign and dysplastic melanocytic nevi, and melanomas - with the aim of establishing its significance as a marker for differentiation between them, comparing the results with a literature review.

MATERIALS AND METHODS

IMP-3 immunostaining was performed in 30 melanocytic lesions: 10 malignant melanomas, 10 dysplastic nevi and 10 melanocytic nevi.

Immunohistochemistry

After fixation in 10% buffered formalin, specimens were embedded in paraffin, cut to 4 mm thickness and mounted on glass slides. The material was subsequently deparaffinized twice in xylene, followed by absolute ethanol, 96°C, 70°C and 50°C alcohol series, each for 10 min. The sections were rinsed with 0.1 M phosphate-buffered saline (PBS), pH 7.4, boiled in Tris-buffered saline, pH 9.2 for 20 min at 96°C, cooled at room temperature, incubated in 1.2% hydrogen peroxide in methanol for 30 min, and again rinsed with PBS, pH 7.4, for 15 min. The slides were then incubated with primary IMP-3 antibody for 1 hour and then incubated with marked polymer for 30 min and washed again. After this, tissue samples were incubated with DAB substrate-chromogen and, after washing, counterstained with Mayer's hematoxylin.

The following antibodies were used for the immunohistochemistry: Monoclonal Mouse Anti-Human IMP-3 (Clone 69.1 Code M3626, DAKO Denmark) with dilution 1:100, as well as detection system EnVision™ FLEX, High pH, (Link) (K8000, DAKO Denmark). The analysis was performed according to the manufacturer protocols.

Sections incubated with non-immune sera instead of the primary antibodies were used as negative controls.

RESULTS

All benign lesions (10/10) were negative for IMP-3 (0%). Positive expression was observed in 2 of 10 cases of dysplastic nevi (20%) – one mild (1+) and one moderate (2+). Within the melanoma cases, IMP-3 expression was established in 4 of 10 cases (40%) - in 2 of them mild (1+), in one moderate (2+) and another melanoma demonstrated strong (3+) IMP-3 staining.

DISCUSSION

Several investigations point to IMP-3 as important in human embryogenesis, as it is involved in RNA trafficking and stabilization, cell growth and cell migration (1-3). Expression of IMP-3 has been reported in many fetal tissues, but its expression is generally considered unusual in normal adult tissues, with the exception of brain, placenta, ovary and testis (4, 5).

In contrast, strong and diffuse IMP-3 expression has been reported in several human neoplasms, especially carcinomas - including pancreatic cancer, renal cell carcinoma, germ cell neoplasms, and lung carcinomas (5, 9-11). It plays a role in tumor proliferation, invasion and metastasis (10, 11). IMP3 is a prognostic biomarker in patients with renal cell carcinoma and clear-cell type ovarian carcinoma, hepatocellular carcinoma, pancreatic

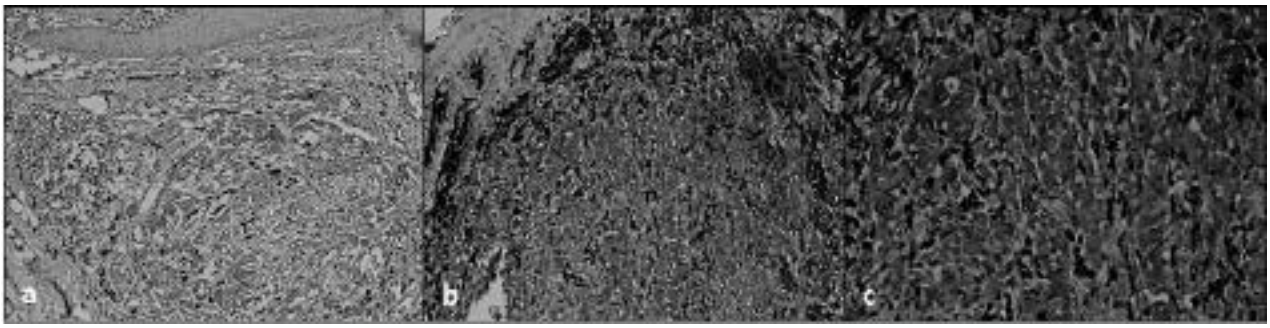

Fig. 1. *Expression of IMP3 in melanomas:* ***a****) Focal weak expression in tumor cytoplasm (x100);* ***b****) diffuse moderate expression in the tumor cytoplasm (x200);* ***c****) diffuse strong expression in tumor cytoplasm and membrane (x400).*

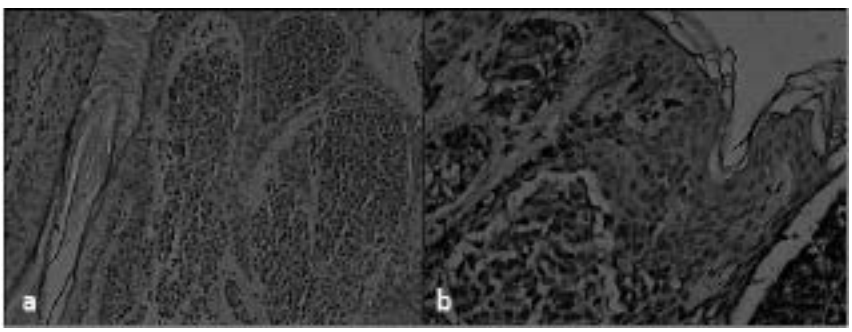

Fig. 2. *Expression of IMP3 in the dysplastic nevi:* ***a****) Diffuse weak expression in the cell cytoplasm (x200);* ***b****) diffuse moderate expression in the cell cytoplasm (x400);*

ductal adenocarcinoma and in patients with poorly differentiated thyroid carcinoma and uterine cervical carcinomas, testicular cancer, where overexpression is associated with poor prognosis (9-11).

To our knowledge, no more than 4 PubMed-indexed studies have addressed the expression of IMP-3 in melanocytic lesions, supporting the hypothesis that it could be a marker for distinction between benign and malignant lesions. A potential prognostic value of IMP-3 in melanocytic lesions has also been considered in several studies, as the majority of them revealed an IMP-3 expression in thick melanomas and almost none in melanoma *in situ* (6-8). IMP-3 expression in metastatic melanoma has been demonstrated to be significantly higher than in primary cutaneous melanoma with a Breslow </=1 mm, while in previous studies none of the benign nevi and dysplastic nevi expressed IMP-3 (6-8). Sheen YS et al. (2015) reported that IMP-3 expression is significantly higher in advanced-stage/metastatic melanomas, suggesting that it is associated with a poor prognosis (12). These data also suggest that IMP-3 is probably involved in melanoma progression.

Our study revealed IMP-3 expression in 20% of dysplastic nevi and in 40% of melanoma cases, while none of the benign nevi showed positive expression. This finding is in contrast to Yu et al. (2010) who found no staining in 8 melanocytic nevi and 8 dysplastic lesions (7) or to the study of Pryor et al. (8).

The expression of IMP-3 in dysplastic melanocytic nevi that we observed argues against a higher diagnostic significance of IMP-3 staining in melanocytic tumors. It can also be argued, that IMP-3 may be of limited prognostic value, which is in line with IGF-II

polymorphism studies on melanomas (13).

IMP-3 is considered helpful in distinguishing benign intranodal nevi from metastatic melanoma in sentinel lymph node biopsy specimens, and it has been suggested as a valuable diagnostic adjunct in sentinel lymph node biopsy (13), which seems to be the only appropriate application of the method at the current state of knowledge. Despite the fact that IMP-3 positive staining is presented in many malignant tumors, it is not a useful marker for distinguishing between carcinomas (1).

Our data showed IMP-3 expression in 4 of the 10 melanomas (40%) and in 2 of 10 dysplastic nevi (20%). No expression was observed in any of the benign nevi, which supports the statement that IMP-3 could be a useful marker for differentiation between benign and dysplastic nevi or melanoma, but it is not a useful marker for distinguishing dysplastic nevi from melanoma, since a positive expression has been observed in both of them. Probably various additional factors play a key role in the relationship between the different IMP-3 expressions in melanocytic lesions with dysplastic features, benign nevi and melanoma, including the severity of cytological atypia, tumor thickness, as well as the metastatic potential of the malignant cells. Further investigations on the correlation between these prognostic factors and IMP-3 expression are needed for confirmation of these suggestions. In further studies it would be important to describe the thickness of the melanomas in the series, and to understand which ones are positive for IMP-3. It would be also important to understand the distribution of the degree of dysplasia in the dysplastic nevi (i.e., how many mildly, moderately and severely atypical cases there were).

In conclusion, IMP-3 expression could be only an auxiliary marker for the distinction between overtly benign and dysplastic melanocytic lesions. However, IMP-3 expression seems to be of limited value in the differentiation between dysplastic nevi and melanoma, and in establishing melanoma prognosis.

REFERENCES:

1. Nielsen J, Christiansen J, Lykke-Andersen J, Johnsen AH, Wewer UM, Nielsen FC. A family of insulin-like growth factor II mRNA-binding proteins represses translation in late development. Mol Cell Biol 1999; 19(2):1262-70.
2. Mueller-Pillasch F, Lacher U, Wallrapp C, et al. Cloning of a gene highly overexpressed in cancer coding for a novel KH-domain containing protein. Oncogene 1997; 14:2729-33.
3. Liao B, Hu Y, Herrick DJ, et al. The RNA-binding protein IMP-3 is a translational activator of insulin-like growth factor II leader-3 mRNA during proliferation of human K562 leukemia cells. J Biol Chem 2005; 280:18517-524.
4. Nielsen J, Christiansen J, Lykke-Andersen J, et al. A family of insulin-like growth factor II mRNA-binding proteins represses translation in late development. Mol Cell Biol 1999; 19:1262-70.
5. Zhang J, Ou Y, Ma Y, et al. Clinical implications of insulin-like growth factor II mRNA-binding protein 3 expression in non-small cell lung carcinoma. Oncol Lett 2015; 9(4):1927-33.
6. Ikeda K, Tate G, Suzuki T, Kitamura T, Mitsuya T. IMP3/L523S, a novel immunocytochemical marker that distinguishes benign and malignant cells: the expression profiles of IMP3/L523S in effusion cytology. Hum Pathol 2010; 41(5):745-50.
7. Yu L, Xu H, Wasco MJ, Bourne PA, Ma L. IMP-3 expression in melanocytic lesions. J Cutan Pathol 2010; 37(3):316-22.
8. Pryor JG, Bourne PA, Yang Q, Spaulding BO, Scott GA, Xu H. IMP-3 is a novel progression marker in malignant melanoma. Mod Pathol 2008; 21(4):431-37.
9. Yantiss RK, Woda BA, Fanger GR, et al. KOC (K homology domain containing protein overexpressed in cancer): a novel molecular marker that distinguishes between benign and malignant lesions of the pancreas. Am J Surg Pathol 2005; 29:188-95.
10. Wang T, Fan L, Watanabe Y, et al. L523S, an RNA-binding protein as a potential therapeutic target for lung cancer. Br J Cancer 2003; 88:887-94.
11. Gu L, Shigemasa K, Ohama K. Increased expression of IGF II mRNA-binding protein 1 mRNA is associated with an advanced clinical stage and poor prognosis in patients with ovarian cancer. Int J Oncol 2004; 24:671-78.
12. Sheen YS, Liao YH, Lin MH, et al. IMP-3 promotes migration and invasion of melanoma cells by modulating the expression of HMGA2 and predicts

poor prognosis in melanoma. J Invest Dermatol 2015; 135(4):1065-73.

13. Soares MR, Huber J, Rios AF, Ramos ES. Investigation of IGF2/ApaI and H19/RsaI polymorphisms in patients with cutaneous melanoma. Growth Horm IGF Res 2010; 20(4):295-97.

LETTER TO THE EDITOR

TOPICAL CORTICOSTEROIDS BUT NOT CALCINEURIN INHIBITORS INDUCED ATROPHY AFTER FOUR WEEKS

A. JIRÁKOVÁ[1], F. ROB[1], Z. SEČNÍKOVÁ[1], K. KOBLOVÁ[1], M. DŽAMBOVÁ[1], L. RAJSKÁ[1], D. GÖPFERTOVÁ[2], G. PELLACANI[3], M. MALÝ[4], T. LOTTI[5] and J. HERCOGOVÁ[1]

[1]Department of Dermatovenerology 2nd Faculty of Medicine Charles University Bulovka Hospital Prague Czech Republic; [2]Department of Epidemiology 2nd Faculty of Medicine Charles University Prague Czech Republic; [3]Department of Dermatology University of Modena and Reggio Emilia Modena Italy; [4]Department of Biostatistics National Institute of Public Health Prague Czech Republic; [5]Department of Dermatology and Venereology of the University of Guglielmo Marconi, Rome, Italy

Received July 2, 2015 – Accepted July 29, 2015

Reflectance confocal microscopy (RCM) is a non-invasive, *in vivo* technique for real-time imaging of the epidermis and superficial dermis at the cellular resolution. We performed a pilot study focusing on the evaluation of the effect of topical corticosteroids and calcineurin inhibitors on the epidermis of patients with atopic dermatitis (AD). The effect was assessed by RCM. A total of 45 patients with AD took part in the study. Patients were selected according to the standardized protocol and divided into two groups. Twenty-three patients used methylprednisolone aceponat topically on the skin with lesions of AD once a day for three months (group A). Twenty-one patients applied topical tacrolimus on the skin with lesions of AD twice a day for three months (B). RCM imaging was performed on the day of intiating the study (T0), then after one (T1), two (T2) and three months (T3). In group A, there was a visible decrease of the stratum corneum and the epidermis thickness which was statistically significant. In comparison, in group B, such changes were not noted and the differences between the groups in time course were statistically significant. In group A, an increase in the percentage of blurred keratinocytes in the stratum spinosum was also recorded, especially between the first (T0) and the second visit (T1). RCM is a useful method for evaluating the changes in epidermis due to the different topical treatment in patients with AD.

Atopic dermatitis (AD) is a chronic inflammatory skin disease often associated with asthma and allergies. Its prevalence appears to be highest in children in developed countries, where it is about 17%, with decreasing trend in higher age groups. Complex pathogenesis involving genetic, immunologic, and environmental factors leads to a dysfunctional skin barrier and dysregulation of the immune system in AD (1). Like other chronic diseases, AD can significantly impair the quality of

Key words: reflectance confocal microscopy, atopic dermatitis, topical corticosteroids, topical calcineurin inhibitors

Mailing address: Anna Jiráková, MD, Ph.D.
2nd Faculty of Medicine,
Charles University and Bulovka Hospital,
Budínova 2,
Praha 8, Czech Republic
Tel.: +420 723 443 481
e-mail: annajirakova@seznam.cz

0393-974X (2015)

DISCLOSURE: ALL AUTHORS REPORT NO CONFLICTS OF INTEREST RELEVANT TO THIS ARTICLE.

life of patients (2, 3).

In managing AD, the role of moisturizers is of a significant importance. Their application should be an integral part of the treatment as there is strong evidence that their use can reduce disease severity and the need for pharmacologic intervention (1).

Topical corticosteroids (TCS) are used in the management of AD in both adults and children and are the mainstay of anti-inflammatory therapy. TCS can be well used both in active inflammation or prevention of relapses (1). Although many studies have been carried out in the past, there is no consensus on the ideal TCS dosing regimen. There are basically two approaches to deal with a flare of AD. Treatment can be started with a short burst of a high-potency TCS, to reach control of flare as soon as possible, with rapid decrease to less potent forms. The second possibility is the initiation of treatment with the lowest-potency TCS which could handle the flare and move to more potent forms only in case of insufficient effect of initially started treatment. For long-term management of AD, the least-potent TCS that is effective should be used, mainly to minimize the risk of side effects of treatment. The most common side effects of TCS treatment include skin atrophy, acneiform-like eruptions, striae, focal hypertrichosis, purpura, teleangiectasias. The risk of the skin thinning increases with the use of higher-potent TCS, occlusion, or application on thinner skin (4). Another significant problem connected with TCS is corticophobia which leads to the undertreatment of a high percentage of patients with AD and consequently to a non-compliance.

Topical calcineurin inhibitors (TCI, pimecrolimus, tacrolimus) are another option of anti-inflammatory therapy for patients with AD (1). Like corticosteroids, their anti-inflammatory mechanism of action inhibits T-cell activation, blocking the production of pro-inflammatory cytokines and affecting mast cell activation. TCI may be used for patients who have failed treatment with other local medication, refused treatment with TCS, or the body area is unsuitable for long-term treatment with TCS (e.g. face, skin folds). In case of TCI, there is no risk of cutaneous atrophy and TCI can be used in reversing skin atrophy. The most frequent side effect is a burning sensation in the application area. TCI have been proven to have a good safety profile during short-term and long-term use. However, they are still relatively new drugs, the side effects of which may not all be known.

Reflectance confocal microscopy (RCM) is one of the non-invasive imagining tools which allow real time examination of the skin with a cellular resolution (5). It enables to make a diagnosis, to observe the development of the disease and finally to observe the effects of the treatment. RCM uses a laser as a source of monochromatic and coherent light. The light passes through a beam splitter, a scanning and focusing optical lens and a skin contact device. Light is focused on the skin in a spot of few microns wide. Reflection occurs between cellular structures with different indexes of refraction, such as membranes, keratohyalin granules and melanosomes. RCM is currently used in the diagnosis of melanoma and non-melanoma skin cancers, but is also increasingly used in inflammatory skin diseases such as contact dermatitis, lupus erythematosus, mycosis fungoides or psoriasis (6).

MATERIALS AND METHODS

Patients

A total of 45 patients with AD took part in our study (15 males and 30 females). Patients were recruited from the Department of Dermatovenerology 2nd Faculty of Medicine, Charles University and Hospital Bulovka in Prague. One female patient was excluded from the study during the second control visit as, due to the deterioration of her AD, systemic treatment with cyclosporine was started. The study was approved by the hospital ethics committee. All the patients signed an informed consent before entering the study. Patients were selected according to the inclusion and exclusion criteria. Inclusion criteria were: age from 2 to 65 years, diagnosis of AD with the lesions on the trunk or limbs, patient willing to take part in all the control visits assessed by the doctor, signed informed consent.

The exclusion criteria were: patients under systemic treatment of AD (except systemic antihistamines) during the study period, patient's noncompliance, another skin disease on the examined lesion, treatment of the examined lesion with other topical medications, history of allergy to the topical treatment used in the study, clinical signs of bacterial, viral or parasitic infection of the skin.

Study protocol

Patients were assigned into two groups according to the block randomization scheme. In group A the patients used TCS (methylprednisolone aceponat), once a day for three months on the examined lesion. In Group B the patients

used TCI (tacrolimus), twice a day on the examined lesion. In each patient one lesion on the limbs or on the trunk was chosen to be examined. Study visits were scheduled at T0 (baseline, before starting the treatment), after 1 month (T1), after 2 months (T3) and after 3 months (T3). At each visit RCM imaging was performed. To minimize the differences connected with product formulation, we used the greasy cream for TCS, since TCI is only vehicled in ointment.

RCM imaging

RCM imaging was performed with Vivascope® 3000 (MAVIG GmbH, Munich, Germany). RCM produces horizontal images of the skin at the cellular resolution from the stratum corneum to the papillary dermis (5). Vivascope® 3000 is a handheld microscope which enables to examine body areas which are difficult to assess. One VivaStack, corresponding to a series of RCM images, each 800x800 µm field-of-view, was captured in the center of examined lesions. Each Vivastack started from above the first visible layer of stratum corneum and finished at 150 µm in depth, corresponding to the superficial dermis with a constant step of 4.5 µm between each layer. The laser intensity was automatically adjusted by the software.

Parameters

For each Vivastack stratum corneum and epidermis thickness was measured according with the method proposed by Ardigò et al. (7).

Keratinocyte contours were evaluated at the level of spinosum on a minimum of 2 single consecutive images per Vivastack. Keratinocyte contours were defined as "clearly defined" or "blurred" according to the cell border outline and degree of brightness between keratinocyte borders (8).

Statistical analysis

For the thickness of the stratum corneum and epidermis, means and standard deviations (SD) were calculated at each study time-point (T0, T1, T2, T3). Analysis of variance for repeated measures (MANOVA) was used to evaluate changes over the time in both groups and to compare the trends between groups. Differences in the proportion of blurred keratinocytes between the two groups were tested by means of logistic regression model with random effects. In all cases, the results were considered as statistically significant when $p<0.05$. Statistical analysis was carried out by statistical software Stata, release 9.2 (Stata Corp LP, College Station, TX).

RESULTS

Patients who were enrolled in the study were followed-up for three months. All patients completed the study except one female patient in group A, who

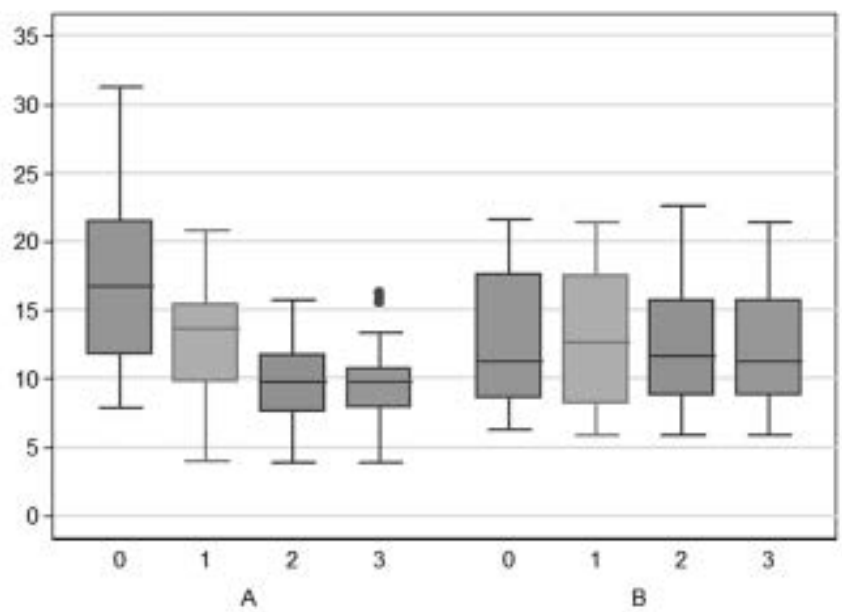

Fig. 1. *Stratum corneum thickness.*

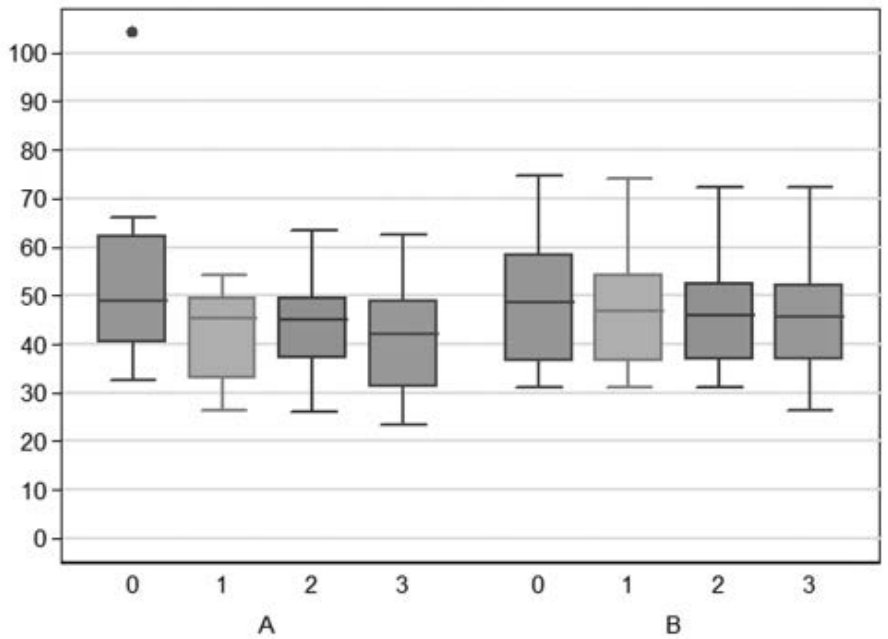

Fig. 2. *Epidermal thickness.*

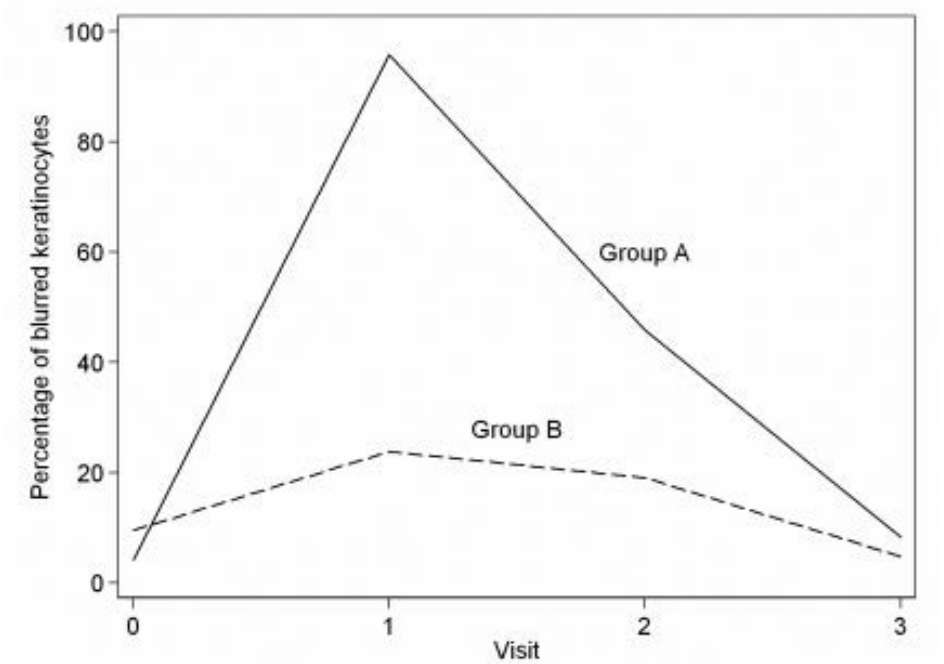

Fig. 3. *Percentage of blurred keratinocytes.*

was excluded from the study at T2, due to therapy shift to systemic treatment for disease progression. The age of the patients varied from 2 to 53 years (mean age was 21.1, SD 13.6).

In the majority of the patients, images were taken on a lesion on the lower or upper limb (90.9%). In a small percentage of participants a lesion on the trunk was selected (9.1%).

In group A (CTS treatment), there was a significant decrease of stratum corneum thickness between T0 (mean ± SD: 16.9±5.8 μm) and T1 (12.4±4.0 μm), T2 (9.5±3.2 μm), and T3 (10.0±3.2 μm) and between T1 and T2 ($p \leq 0.05$). On the other hand, in group B (TCI) no significant decrease of stratum corneum thickness was observed (Fig. 1).

With regard to epidermal thickness, we noticed a significant decrease in group A only between T0 (51.2±15.5) and T1 (42.0±9.1) ($p \leq 0.05$), followed by a plateau. In group B there was no significant decrease of epidermal thickness from baseline to the end of the study, although a borderline reduction was observed between T0 and T1 ($p=0.058$) (Fig. 2).

In group A, an increase was also recorded in the percentage of blurred keratinocytes in the stratum spinosum, especially between baseline (T0) and the first control visit (T1). This phenomenon was not noticed in group B, showing just a very slight, not significant, increment between T1 and T2. The difference between groups was statistically significant ($p < 0.05$) (Fig. 3).

DISCUSSION

Atopic dermatitis remains one of the most common skin disorders throughout all ages. Its first line treatment is TCS therapy. Although these drugs have been used in dermatology for more than 60 years, we still deal with the two major problems. The first one is the side effects caused by TCS especially skin atrophy. The second one is a corticophobia.

Our study proved the novel idea to evaluate *in vivo,* at the cellular resolution, the influence of two different active drugs (i.e. TCS and TCI) on the skin in patients with AD. We registered a significant decrease of the stratum corneum and the epidermis thickness in a group of patients using TCS (methylprednisolone aceponate). In a group of patients using TCI, there was only a slight, non-significant decrease of stratum corneum thickness after 1 month. Similar results were attained by Ardigo et al. in a study comparing the topical effect of steroid cream (betamethasone) and a non-steroidal anti-inflammatory gel (aceclofenac) by RCM in patients with plaque psoriasis (7). To the best of our knowledge there are only two published studies monitoring the effect of the topical treatment of skin condition with RCM. The second study monitors the response to a physical treatment-narrowband UVB (9).

Our data on corneum and epidermal thickness are in line with different studies employing different measurement techniques. Aschoff et al. investigated corticosteroid-induced epidermal thinning using optical coherent tomography (OCT) (10). They used 1% hydrocortisone cream and pimecrolimus 1% cream. The results proved a significant decrease of epidermis in a group using TCS and no significant decrease in a group using pimecrolimus. Shlivko and collegues focused on the morphological differences between phototypes in patients using topical 0.05% clobetasol propionate, hydrocortisone 17-butyrate and tacrolimus. Changes were evaluated by OCT. The results proved thinning in the group using TCS and no epidermal decrease in patient using tacrolimus (11).

In our study, we noticed significant changes of the epidermis thickness had taken place by the second visit. This could be explained either by attaining a steady state on keratinocyte proliferative activity in this time-frame, or by reduced treatment adherence frequently observed in prolonged topical treatment, especially at the achievement of the clinical effect (12).

An increase of the percentage of blurred keratinocytes in the stratum spinosum in the TCS treated group only, particularly remarkable between baseline (T0) and the first control (T1), represents an interesting finding. The same phenomenon was observed by Ardigo et al. who explained it as a result of the effect of TCS on the reduction of metabolic activity of keratinocytes. Combination of the two findings, epidermal layer reduction and increment of blurred keratinocytes, seems to confirm the rapid effect of TCS on keratinocyte proliferation and metabolism that can lead to skin atrophy and barrier impairment in a prolonged treatment. On the other hand, TCI was affecting not the epidermal thickness

nor the keratinocyte contour brightness and outline, probably preserving a more physiological status of the epidermis and its functions.

In conclusion, our study proved that TCS can cause slight but measurable skin atrophy after only 4 weeks and that TCI do not have this effect. It is important to stress that these are the preliminary results. The study is continuing and results on a greater number of patients will be published.

This paper also points out that RCM is an effective non-invasive tool in monitoring and comparing the effect of topical drugs used in patients with AD. Thus, monitoring a treatment with RCM can better individualize the clinical approach through early detection of eventual side effects, such as skin atrophy. Moreover, the objective documentation of the drug effects on the skin can consequently reduce the corticophobia, reassuring the patients on drug safety, increasing compliance and mutual satisfaction.

ACKNOWLEDGEMENTS

This study was supported by the grant from the Czech Ministry of Health IGA NT 13465-4.

REFERENCES

1. Eichenfield LF, Tom WL, Berger TG, et al. Guidelines of care for the management of atopic dermatitis 2014; J Am Acad Dermatol 2014; 71:116-32.
2. Jiráková A, Vojáčková N, Göpfertová D, Hercogová, J. A comparative study of the impairment of quality of life in Czech children with atopic dermatitis of different age groups and their families. Int J Dermatol 2012; 51:688-92.
3. Chernyshov PV, Jirakova A, Ho RC, Moed H, Caldeira AP, Alvarenga TM, Park CW, Hercogova J. An international multicenter study on quality of life and family quality of life in children with atopic dermatitis. Indian J Dermatol Venereol Leprol 2013; 79:52-8.
4. Pariser D. Topical corticosteroids and topical calcineurin inhibitors in the treatment of atopic dermatitis: focus on percutaneous absorption. AM J Ther 2009; 16:264-73.
5. Wurm AMT, Soyer HP. The confocal story. In Reflectance confocal microscopy for skin diseases. Wellenhof RH, Pellacani G, Malvehy J et al. Springer-Verlag, Berlin, 2012; p. 3-10.
6. Ulrich M, Lange-Asschenfeldt S. *In vivo* confocal microscopy in dermatology: from research to clinical application. J Biomed Opt 2013; 18:061212.
7. Ardigò M, Agozzino M, Longo C, Conti A, Di Lernia V, Berardesca E, Pellacani G. Psoriasis plaque test with confocal microscopy: evaluation of different microscopic response pathways in NSAID and steroid treated lesions. Skin Res Technol 2013; 19:417-23.
8. Longo C, Casari A, Beretti F, Cesinaro AM, Pellacani G. Skin aging: *in vivo* microscopic assessment of epidermal and dermal changes by means of confocal microscopy. J Am Acad Dermatol 2013; 68:73-82.
9. Wolberink EA, van Erp PE, de Boer-van Huizen RT, van de Kerkhof PC, Gerritsen MJ. Reflectance confocal microscopy: an effective tool for monitoring ultraviolet B phototherapy in psoriasis.Br J Dermatol 2012; 167:96-403.
10. Aschoff R, Schmitt J, Knuschke P, Koch E, Bräutigam M, Meurer M. Evaluation of the atrophogenic potential of hydrocortisone 1% cream and pimecrolimus 1% cream in uninvolved forehead skin of patients with atopic dermatitis using optical coherence tomography. Exp Dermatol 2011; 20:832-6.
11. Shlivko IL, Kamensky VA, Donchenko EV, Agrba P. Morphological changes in skin of different phototypes under the action of topical corticosteroid therapy and tacrolimus. Skin Res Technol 2014; 20:136-40.
12. Hix E, Gustafson CJ, O'Neill JL, Huang K, Sandoval LF, Harrison J, Clark A, Feldman SR. Adherence to a five day treatment course of topical fluocinonide 0.1% cream in atopic dermatitis. Dermatol Online J 2013; 19:20029.

LETTER TO THE EDITOR

RECTAL IMPACTION DUE TO PRICKLY PEAR SEEDS BEZOAR: A CASE REPORT

S. MARCHESE[1], B. BERTUCCI[1], F. MANTI[1], D. BERRITTO[2], AG. ROPERTO[1] and S. TAMBURRINI[3]

[1]Department of Experimental and Clinical Medicine-Radiology, University of Catanzaro, Catanzaro, Italy; [2]Department of Radiology, Second University of Naples, Naples, Italy; [3]Department of Radiology, Pellegrini Hospital, Naples, Italy

Received February 10, 2015 – Accepted June 4, 2015

Fecal impaction is the third cause of lower gastrointestinal tract obstruction after strictures for colon cancer and postoperative adhesions. A rapid diagnosis is necessary to avoid complications due to intestinal obstruction. Rectal phytobezoar due to prickly pear fruit seeds are an extremely rare entity, in the literature about twenty similar cases are described. Prickly pears are common in many countries, even in the Mediterranean area. When the ingestion of their fruit is excessive, this can be harmful, leading to the formation of phytobezoar causing fecal impaction. We describe the first case of phytobezoar due to prickly pear fruit seeds in continental Europe: a 76-year-old Italian female who ingested almost 40 prickly pear fruit leading to the composition of a large rectal phytobezoar. The patient presented clinically with fecal impaction, diagnosed by imaging and successfully treated by rectal irrigation and manual disimpaction. Our aim is to remind the physicians of these risks in evaluating patients with intestinal obstruction, when there is positive anamnesis for provenience from some areas in which these fruits are eaten. We also want to underline the role of Imaging Multi Detector Computed Tomography (MDCT) in the diagnosis of these very uncommon entities.

Fecal impaction (FI) is a common cause of lower gastrointestinal tract obstruction, lagging behind stricture for colon cancer and postoperative adhesions (1, 2). It occurs at all ages, but is more prevalent in paediatric and elderly populations.

FI is defined as symptoms of constipation in the presence of a hard fecal mass obstructing the rectal vault on digital rectal examination, and/or the presence of a fecal mass or fecaloma in the rectum or colon based on abdominal X-ray or CT-scan, and/or the presence of significant fecal retention or fecal loading in the rectum or colon, either with or without proximal colonic or small bowel dilatation (3). There are various risk factors in the genesis of FI, including chronic or severe constipation, behavioural causes, anatomic anorectal abnormalities, neurological or functional gastrointestinal disorders (4, 5).

The typical symptoms of FI are similar to those of intestinal obstruction: distension, abdominal and anal pain, nausea, vomiting and paradoxical diarrhea with fecal incontinence (6). Its diagnosis is gained by a careful history, physical examination, laboratory tests and especially radiological studies: CT scan, in fact, can show large amounts of fecal matter in

Key words: intestinal obstruction, fecal impaction, phytobezoar, prickly pear fruit seeds

Mailing address: Dr Daniela Berritto,
Second University of Naples,
P.zza L. Miraglia 2,
80132, Naples, Italy
Tel: +39 3932420522
Fax: +39 0815665200
e-mail: berritto.daniela@gmail.com

0393-974X (2015)

DISCLOSURE: ALL AUTHORS REPORT NO CONFLICTS OF INTEREST RELEVANT TO THIS ARTICLE.

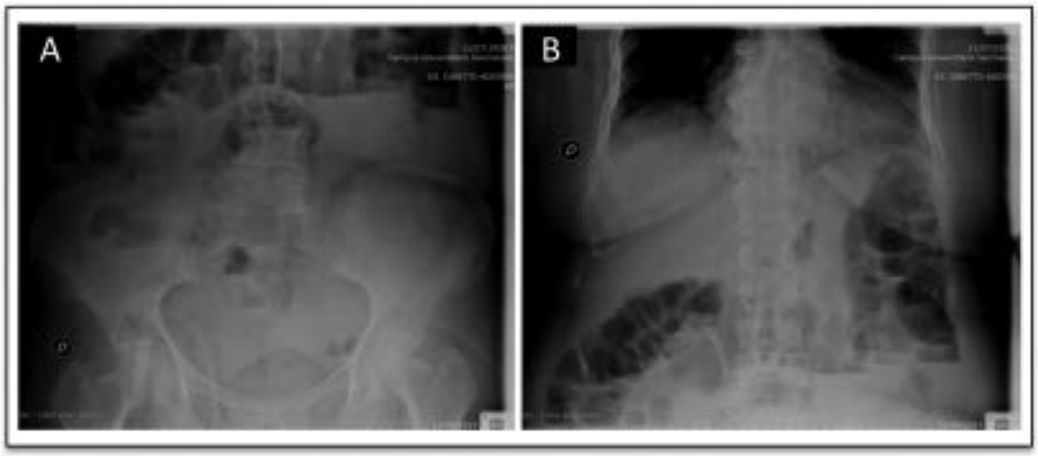

Fig. 1. *Plain abdominal film examination. Plain abdominal film shows some air fluid levels and a colonic overdistension, with no gas in the rectosigmoidal junction, where there is a speckled opacity. Some dilatated small bowel loops suggest an incontinent ileocecal valve (**A**). No subdiaphragmatic air (**B**).*

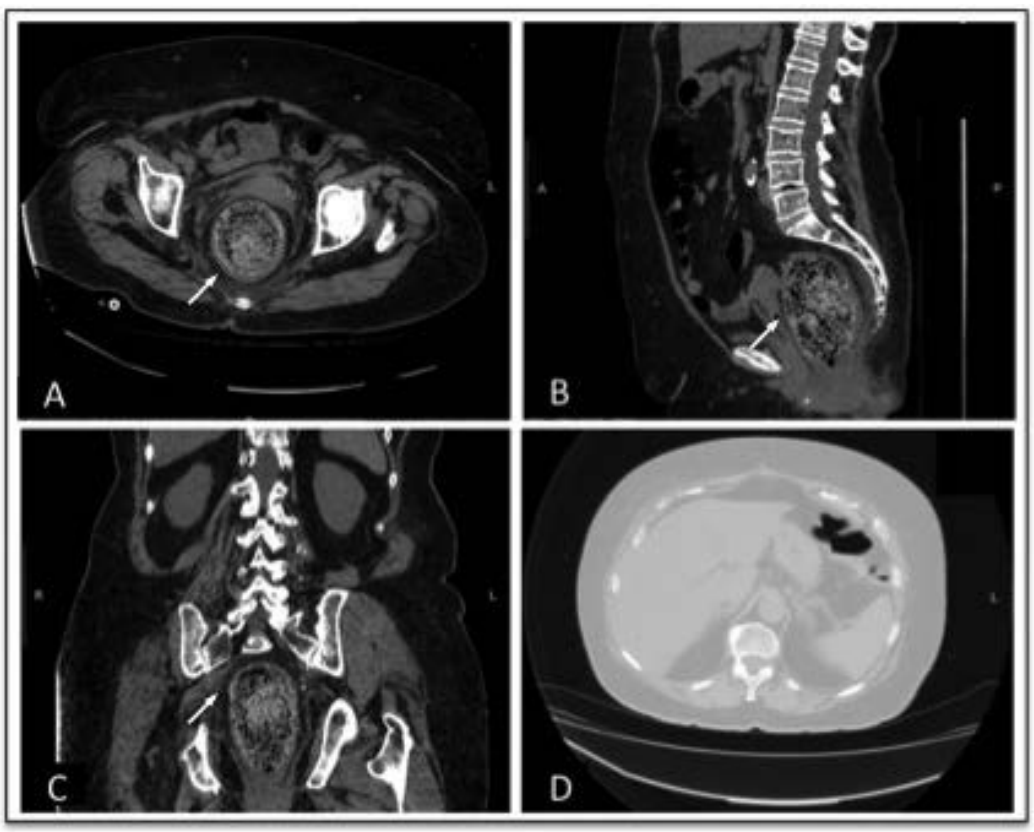

Fig. 2. *Abdominal computed tomography examination. Un-enhanced CT in axial plane (**A**) and multiplanar reconstructions (**B**) sagittal, (**C**) coronal, shows a large mass-like lesion in the rectal vault (white arrow), composed of tightly packed densities having variable HU values (60-120) with interposed air. There were no signs of complications, such as fluid in the peritoneal cavity or small air bubbles (**D**), axial image passing through upper abdominal quadrants and viewed at lung window settings.*

the rectal vault or in the colon, with or without sign of large bowel perforation (7). Prompt diagnosis and treatment helps in the prevention of possible complications of this bowel obstruction, such as stercoral ulcers, perforations and peritonitis (8, 9). Treatment includes disimpaction, followed by a total colonic evaluation by colonoscopy or Colonography-Computed Tomography (CT) and by a regimented treatment program to prevent further obstructions.

Case presentation

We present the case of a 76-year-old female patient. Her past medical history included diabetes, controlled only by diet, and no gastrointestinal surgery. She came to us with a four-day history of dull abdominal pain, spasm, distension and constipation. She reported normal defecation before the onset of the symptoms but when the discomfort worsened, she reported obstructed defecation. She did not report diarrhea, vomiting, melena, hematemesis, and hematochezia. Vital signs of the patient were blood pressure 130/75 mmHg, body temperature 36.2°C, heart rate 80 bpm, respiratory rate 22/min.

Physical examination revealed an abdomen that was distended without rebound pain. There was no evidence of external hernia, organomegaly, abdominal masses or ascites. There was increased bowel sound frequency. In digital rectal examination the rectum was found to be impacted with hardened stool.

Firstly, we gained informed consent from the patient, then carried out a plain abdominal film (Fig. 1) showing dilated small bowel loops with some air fluid levels and colonic air over distension, with no gas in the sigmoid colon, where there were mottled lucencies. Subsequently, we performed a first non-enhanced CT scan of the abdomen (Fig. 2) that revealed the presence of mass-like lesion in the rectal vault involving an approximately 12.5 cm segment. It was composed of multiple tightly packed densities having variable HU values (60-120) with interposed air, giving a mottled appearance. We did not noticed parietal thickening or stranding of the pericolonic fat. No evidence of fluid in the peritoneal cavity, no soft tissue masses nor regional lymphadenopathy were present. Given the findings and because of the absence of any clinical and radiological sign of complications, we did not perform a contrastographic phase, even on the basis of a not confirmed exclusion of allergic history. Therefore on questioning, the patient remembered that she had eaten large quantities of prickly pear fruit, approximately 40, five days previously, without separating the seed from the pulp. Thanks to examinations and to the clarification of the patient's history, there was no need for any further study.

The patient was treated with manual disimpaction and subsequent rectal irrigations (1), followed by spontaneous gas-rich evacuations, with full resolution of symptoms. After a few days the woman was subjected to colonoscopy to reveal anatomic abnormalities, stricture or malignancy with negative results. Therefore, the patient suffered an intestinal obstruction due to a large phytobezoar impacted in the rectum, composed by prickly pear fruit seeds.

DISCUSSION

Bezoars are the conglomeration of partially digested or non-digested foreign material that accumulates in the gastrointestinal tract. The word "bezoar" is derived from the Arabic "badzehr" or from the Persian "panzher" and means "antidote"; animals bezoars were treasured in the sixteenth century as an antidote to poisons (10). Bezoar incidence is low, but should not be underestimated; in fact, mortality rates may be as high as 30% if they remain untreated (10). There are various types of bezoars depending on the material of which they consist, therefore they are classified, in order of frequency, in: phytobezoars, made of vegetable material; trichobezoar, consisting of a large quantity of human hair; lactobezoar, composed of undigested milk, described in infants; pharmacobezoar, made of accumulated masses of medication; lithobezoar, consisting of stones or clay; miscellaneous bezoars or polybezoars (11-15).

Symptoms of bezoars are location-specific. In the stomach they cause anorexia, bloating, early satiety, dyspepsia, malaise, weakness, weight loss, headaches, and a feeling of fullness or heaviness in the epigastrium. In the small bowel they cause obstruction, pancreatitis, obstructive jaundice and perforations (4-6). In the large bowel the rarely-described bezoars caused abdominal pain, constipation, intestinal obstruction, chronic diarrhea, encopresis and perforation.

The most common site of phytobezoar formation is the stomach (16), followed by the small intestine and, rarely, the colon or rectum (17, 18). Watermelon seeds are the most frequent cause of phytobezoar. Rectal phytobezoars of prickly pear fruit seeds are very rare entities.

The prickly pear fruit (*Opuntia ficus indica*) is a cactus fruit widely distributed throughout the world (Australia, Southern Europe, Africa, Southern Asia, Southern USA and some oceanic islands with warm climates). The fruit is edible and contains a sweet pulp and hundreds of little seed coated by a hard and prickly outer skin. This fruit is also used as a popular herbal medicine for diabetes, hypercholesterolemia, obesity and atherosclerosis. Usually, this fruit is eaten without separating the pulp from the indigestible seeds, which pass through the gastrointestinal tract and reach the distal colon, where they are expelled in the feces. However, if eaten in large quantity, the seeds can accumulate and harden by water reabsorption. The larger the amount of fruits eaten, the greater the risk of developing a phytobezoar.

To obtain a diagnosis, radiological studies are necessary. Signs of obstruction or perforation, characterized by dilated loops of small or large bowel with air-fluid levels or free air, respectively, can be seen on abdominal radiographs (19). CT scan is very sensitive and specific in determining the presence of bowel obstruction and should be recommended for patients with suspected bowel obstruction (20). Unenhanced MDCT can show bezoars or fecalomas in the colon and rectum with or without signs of colonic perforation (7). MDCT with intravenous contrast provides superb anatomical detail and diagnostic specificity by directly imaging of the intestinal wall, detecting primary and secondary signs of bowel disease (21).

Bezoars in the rectum will often require digital fragmentation and mechanical removal. A prior distal softening of hardened stool with enemas and suppositories is often helpful, while a proximal oral lavage with solutions to soften or washout a hardened stool is contraindicated when a complete bowel obstruction exists (1).

CONCLUSIONS

We describe the first rectal phytobezoar of prickly pear fruit seeds in Continental Europe. These bezoars are very rare entities. Prickly pears are distributed worldwide, and it is important to emphasize the dangers if their fruit is ingested in excessive doses. Our purpose is to remind the physicians of these risks during the evaluation of patients presenting with intestinal obstruction who live in areas where prickly pears are eaten.

MDCT of the abdomen is extremely useful to detect the specific site and severity of obstruction and also for identifying complications and determining the etiology. Plain film (flat and upright/ left lateral decubitus) can be equivocal, non-specific and misleading, but it is readily available, less expensive, exposes the patient to less radiation and obviates the need for abdominal MDCT in some patients. However, in our department of Radiology, generally, we obtain plain abdominal films prior to proceeding to abdominal MDCT.

REFERENCES

1. Obokhare I. Fecal Impaction: A cause for concern? Clin in Colon Rectal Sur 2012; 25:53-58.
2. Taourel P, Kessler N, Lesnik A, Pujol J, Morcos L, Bruel JM. Helical CT of large bowel obstruction. Abdom Imaging 2003; 28(2):267-75.
3. Hussain ZH, Whitehead DA, Lacy BE. Fecal impaction. Curr Gastroenterol 2014; 16(9):404.
4. Beck DE. Surgical management of constipation. Clin Colon Rectal Surg 2005; 18(2):81-84.
5. De Lillo AR, Rose S. Functional bowel disorders in the geriatric patient: constipation, fecal impaction and fecal incontinence. Am J Gastroenterol 2000; 95(4):901-905.
6. Wrenn K. Fecal Impaction. N Engl J Med 1989; 321(10):658-62.
7. Fragelman D, Warhit JM, Reiter JD, Geiss AC. CT diagnosis of fecaloma. J Comput Assist Tomogr 1984; 8(3):559-561.
8. Maull KI, Kinning WK, Kay S. Stercoral ulcerations. Am Surg 1982; 48:20-4.
9. Sutton R, Blaake JR. Massive rectal bleeding following fecal impaction. Br J Surg 1984; 71(8):631.
10. Williams RS. The fascinating history of bezoars. Med J Aust 1986; 11-12:613-614
11. Taylor JR, Streetman DS, Castle SS. Medication

bezoars: a literature review and report of a case. Ann Pharmacother 1998; 32(9): 940-46.
12. Towery HH, Chan RK Lactobezoar: a case report. Clin Pediatr (Phila) 2004; 43(6):577-78.
13. Mohammad MA. Rectosigmoid lithobezoar in an eight-year-old. Afr J Paediatr Surg 2010; 7(1):38-39.
14. Singhal GD, Bhatia BD, Chooramani S. Case of the month: tricho-phytobezoar. Indian Pediatr 1980; 17(3) 297-98.
15. Holmes TW Jr. Polybezoar and gastrointestinal foreign bodies. Total surgical experience in a large state hospital. Am J Surg 1962; 103:487-93.
16. Chaganti S, Immadisetty M, Botchu R, Chari K. Gastrointestinal trichobezoar: a case report and review of the literature. The Internet J Surgery 2007; 15:2 https://ispub.com/ IJS/15/2/4442.
17. Minty B, Kelly L. Rectal bezoars in children. CMAJ 2010; 182(11):E532.
18. Erzurumlu K, Malazgirt Z, Bektas A, Dervisoglu A, Polat C, Senyurek G, Yetim I, Ozkan K. Gastrointestinal bezoars: A retrospective analysis of 34 cases. World J Gastroenterol 2005; 11(12):1813-17.
19. Grassi R, Di Mizio R, Pinto A, Romano L, Rotondo A. Serial plain abdominal film findings in the assessment of acute abdomen: spastic ileus, hypotonic ileus, mechanical ileus and paralytic ileus. Radiol Med 2004; 108(1-2):56-70. English, Italian.
20. Grassi R, Romano S, D'Amario F, Giorgio Rossi A, Romano L, Pinto F, Di Mizio R. The relevance of free fluid between intestinal loops detected by sonography in the clinical assessment of small bowel obstruction in adults. Eur J Radiol 2004; 50(1):5-14.
21. Reginelli A, Russo A, Pinto A, Stanzione F, Martiniello C, Cappabianca S, Brunese L, Squillace E. The role of computed tomography in the preoperative assessment of gastrointestinal causes of acute abdomen in elderly patients. Int J Surg 2014; S181-86.

LETTER TO THE EDITOR

DENTAL PULP STEM CELLS AND HUMAN PERIAPICAL CYST MESENCHYMAL STEM CELLS IN BONE TISSUE REGENERATION: COMPARISON OF BASAL AND OSTEOGENIC DIFFERENTIATED GENE EXPRESSION OF A NEWLY DISCOVERED MESENCHYMAL STEM CELL LINEAGE

M. TATULLO[1,2], G. FALISI[3], M. AMANTEA[1,2], C. RASTELLI[3], F. PADUANO[1] and M. MARRELLI[1,2]

[1]Tecnologica Research Institute, Biomedical Section, Stem Cells Unit, Crotone, Italy;
[2]Calabrodental Clinic, Biomedicine Unit, Crotone, Italy;
[3]Department of Life, Health and Environmental Sciences, School of Dentistry, University of L'Aquila, L'Aquila, Italy

Received February 25, 2015 – Accepted May 13, 2015

Bone regeneration is an interesting field of biomedicine. The most recent studies are aimed to achieve a bone regeneration using mesenchymal stem cells (MSCs) taken from more accessible sites: oral and dental tissues have been widely investigated as a rich accessible source of MSCs. Dental Pulp Stem Cells (DPSCs) and human Periapical Cysts Mesenchymal Stem Cells (hPCy-MSCs) represent the new generation MSCs. The aim of this study is to compare the gene expression of these two innovative cell types to highlight the advantages of their use in bone regeneration. The harvesting, culturing and differentiating of cells isolated from dental pulp as well as from periapical cystic tissue were carried out as described in previously published reports. qRT-PCR analyses were performed on osteogenic genes in undifferentiated and osteogenic differentiated cells of DPSC and hPCy-MSC lineage. Real-time RT-PCR data suggested that both DPSCs and hPCy-MSCs cultured in osteogenic media are able to differentiate into osteoblast/odontoblast-like cells: however, some differences indicated that DPSCs seem to be directed more towards dentinogenesis, while hPCy-MSCs seem to be directed more towards osteogenesis.

Oral and maxillofacial surgery is focused on treatment of traumatic or degenerative diseases mainly affecting the bone tissue. Bone regeneration is a widely discussed topic, and several research groups have described their techniques to regenerate bone loss in the last twenty years.

Bone regeneration is an interesting field of biomedicine that combines different aspects of medicine and biology of the bone: the more recent performance techniques have investigated the platelet concentrate used in oral and maxillofacial surgery in order to regenerate, repair or replace bone tissue.

Whitman (1) published the first studies on the use of growth factors contained in a platelet gel, called Platelet-Rich Plasma (PRP). Platelet-Rich in Growth

Key words: regenerative medicine, mesenchymal stem cells, bone regeneration, dental pulp stem cells, human periapical cyst mesenchymal stem cells, hPCy-MSCs

Mailing address: Dr. Marco Tatullo, PhD
Scientific Director,
Tecnologica Research Institute,
Biomedical Section,
Stem Cells Unit, Str. E. Fermi,
88900 Crotone, Italy
e-mail: marco.tatullo@tecnologicasrl.com

0393-974X (2015)

DISCLOSURE: ALL AUTHORS REPORT NO CONFLICTS OF INTEREST RELEVANT TO THIS ARTICLE.

Factor (PRGF) is considered an evolution of the PRP (2) and allows to obtain a higher concentration of growth factors in platelet concentrate. Marrelli studied the effects of Choukroun's Platelet Rich Fibrin (PRF) on bone and gingival tissues: PRF has the advantage of being a blood-derived gel, obtained from a simple preparation protocol that does not require any alteration of the blood, containing a three-dimensional matrix of autologous, elastic and flexible fibrin (3).

Tatullo suggested a useful osteoinductive potential of PRF, mainly related to its neo-angiogenic ability and concentration of growth factors (GFs) able to activate the pre-osteoblastic cells resident in the surgical site (4).

The most recent studies have been aimed to achieve a bone regeneration using MSCs taken from more accessible sites: oral and dental tissues have been investigated as a rich accessible source of mesenchymal stem cells (5).

Nowadays, numerous types of MSCs have been isolated from teeth: in 2000, Gronthos discovered an MSC lineage from dental pulp, named Dental Pulp Stem Cells (DPSCs) (6). DPSCs have been long studied and considered the gold standard of MSCs from oral cavity for bone regeneration use, however, DPSCs need to be harvested from a vital pulp, thus requiring the extraction of a healthy tooth (7). To overcome this limitation, recently, Marrelli et al. demonstrated that MSCs derived from human inflamed periapical cysts (hPCy-MSCs) have a mesenchymal stem cell immune-phenotype and the high ability to differentiate into osteogenic lineages (8).

DPSCs and hPCy-MSCs are, respectively, isolatable from dental pulp of every tooth not severely contaminated by bacteria, and from the periapical cystic tissues commonly derived from an acute pulpitis affecting one or more teeth.

DPSCs and hPCy-MSCs represent the new generation MSCs, easily usable in bone tissue regeneration: the aim of this study is to compare the gene expression of these two cell types to highlight the advantages in using of each of them.

MATERIALS AND METHODS

Patient samples

DPSCs and hPCy-MSCs were obtained from healthy volunteers, 2 males aged 34±5 years and 3 females aged 25±2, all suffering from chronic apical periodontitis affecting a third molar tooth showing a cystic formation, but without any clinical sign of development of carious

Table I. *Oligonucleotide primer sequences utilized in the quantitative real-time PCR analysis.*

Gene	Forward Primer	Reverse Primer	Product Size (Bp)
Osteocalcin **(OSC)**	TGAGAGCCCTCACACTCCTC	ACCTTTGCTGGACTCTGCAC	98
Osteonectin **(ON)**	TGCATGTGTCTTAGTCTTAGTCACC	GCTAACTTAGTGCTTACAGGAACCA	188
Osteopontin **(OPN)**	CAGTTGTCCCCACAGTAGACAC	GTGATGTCCTCGTCTGTAGCATC	127
Bone sialoprotein (**BSP)**	GCAGTAGTGACTCATCCGAAGAA	GCCTCAGAGTCTTCATCTTCATTC	121
Dentin Sialophosphoprotein **(DSPP)**	CTGTTGGGAAGAGCCAAGATAAG	CCAAGATCATTCCATGTTGTCCT	129
Runt-related transcription factor 2 **(RUNX-2)**	ATGTGTGTTTGTTTCAGCAGCA	TCCCTAAAGTCACTCGGTATGTGTA	199
Dentin Matrix acid Phosphoprotein **(DMP-1)**	GTGAGTGAGTCCAGGGGAGATAA	TTTTGAGTGGGAGAGTGTGTGC	111

disease on the dental crown. This study was carried out under the approved guidelines of the internal Ethics Committee. Each patient gave signed informed consent, accordingly to the Declaration of Helsinki, Ethical Principles for Medical Research Involving Human Subjects Committee, and Italian laws on the use of human subjects for medical research. Before teeth extraction, each subject was checked for oral diseases, and all subjects were pre-treated with professional dental hygiene one week prior to surgery, followed by daily oral rinses with mouthwash containing 0.12% Chlorhexidine. The culture of cells isolated from dental pulp as well as from periapical cystic tissue was carried out as described in previously published reports (8) .

RNA preparation and qRT-PCR analysis

Undifferentiated DPSC and hPCy-MSC RNA were extracted by means of Purelink™ RNA mini kit (Ambion): the quantification of RNA was carried out with the spectrophotometer Multiskan Go (Thermo Scientific). Following reverse-transcription, cDNAs were amplified by real-time PCR in the Pikoreal 96 (Thermo scientific) machine. The proper specificity of PCR final product was carefully analyzed by melting curve analysis, while the efficiencies of rt-PCRs were calculated by constructing curves with cycle threshold (Ct) and they resulted between 93 and 100%. The gene expression was obtained with the threshold cycle (Ct), while the expression levels were calculated by means of the $^{\Delta\Delta}$Ct method, after the normalization to the expression of the HRPT housekeeping gene. Primer sequences for Osteocalcin (OSC), Osteonectin (ON), Osteopontin (OPN), Bone sialoprotein (BSP), Dentin Sialophosphoprotein (DSPP), Runt-related transcription factor 2 (RUNX-2) and Dentin matrix protein 1 (DMP-1) are listed in Table I. The experiments were performed in triplicate.

Osteogenic differentiation and genes rationale

The osteo-specific gene expression pattern for Osteocalcin (OSC), Osteonectin (ON), Osteopontin (OPN), Bone sialoprotein (BSP), Dentin Sialophosphoprotein (DSPP), Runt-related transcription factor 2 (RUNX-2) and dentin matrix protein 1 (DMP-1) of both DPSCs and hPCy-MSCs were analyzed at mRNA level after 25 days of osteo-induction, following a differentiation protocol previously reported in literature (9).

OPN and DMP-1 proteins are present in mineralized tissues such as bone, dentin, and cementum (10). RUNX-2 is a transcription factor that belongs to the runt-domain gene family: this gene is a master regulator of osteoblast differentiation and bone development (11).

DSPP is essential to the formation and mineralization of dentin and also plays an important role in forming and maintaining a healthy periodontium (12).

The initial distribution of BSP may modify bone formation and mineralization (13), instead, both OPN and BSP are necessary for the initiation of the mineralization process. Finally, OSC and ON are not present in early process of bone mineralization, but both are widely represented in the mature mineralized matrix (14).

Statistical analysis

Results are reported as the mean ± standard deviations of three different experiments. The significance of differences between groups was evaluated by one-way analysis of variance (ANOVA) followed by Dunnett's test for multiple comparisons or a Student's *t*-test. Analyses were conducted using the GraphPad Prism software (San Diego, CA, USA), and differences were considered significant if $P < 0.05$.

RESULTS

Real-time PCR data, expressed as differentiated over undifferentiated and carried out from cultured DPSCs and hPCy-MSCs, showed a growing for all the tested markers (Fig. 1). These results suggest that both DPSCs and hPCy-MSCs cultured in osteogenic media are able to differentiate into osteoblast/odontoblast-like cells. The real-time RT-PCR data, showed a similar behaviour of the gene expression variation in the 2 investigated cell lineages: however, some differences need to be highlighted. Dentin Sialophosphoprotein (DSPP) and Dentin Matrix acid Phosphoprotein (DMP-1) gene showed a different behaviour in DPSCs and hPCy-MSCs: in fact, in DPSCs these genes showed a higher significant increase in differentiated DPSCs compared to the value expressed in differentiated hPCy-MSCs. On the other hand, Osteonectin (ON), Bone sialoprotein (BSP) and Runt-related transcription factor 2 (RUNX-2) genes showed a clearer increase in differentiated hPCy-MSCs compared to the value expressed in differentiated DPSCs. Therefore, the qRT-PCR results suggested that after osteogenic differentiation, hPCy-MSCs express both markers related to dentinogenesis and osteogenesis, even if this new MSC lineage seems to have a commitment towards the bone regeneration; on the other hand, after osteogenic differentiation DPSCs express markers related to dentinogenesis and osteogenesis, with a clear commitment towards the odontogenesis.

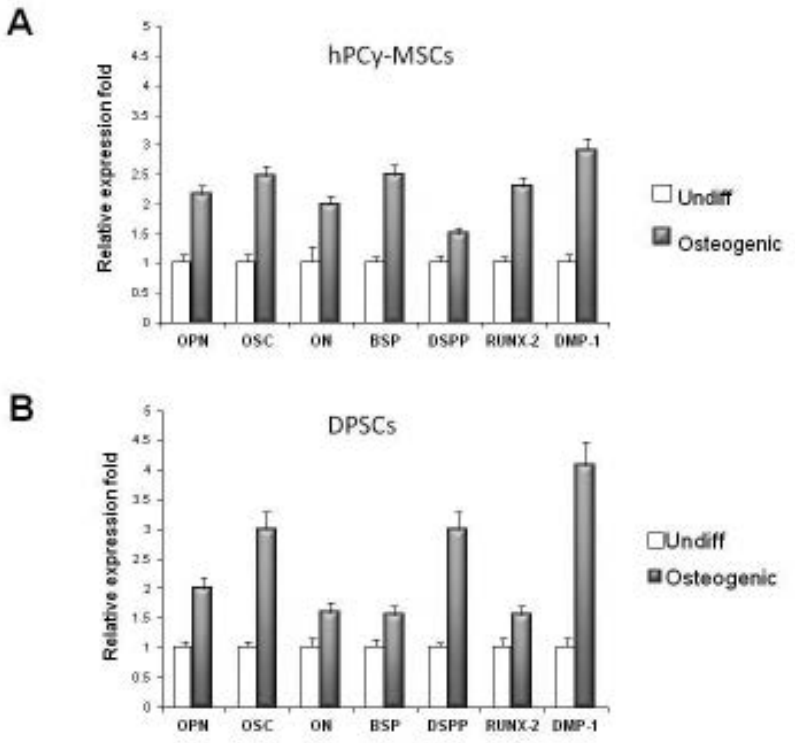

Fig. 1. *Osteogenic differentiation of cells isolated from human oral cyst and dental pulp. qRT-PCR was used to determine the gene expression profiles ratio of osteoblastic specific markers in 25 days osteoblastic-differentiated over undifferentiated cells of both the investigated hPCy-MSCs (**A**) and DPSCs (**B**). Relative expression levels were calculated by using the* $2^{-\Delta\Delta CT}$ *method. Values were expressed as mean ± SD and were normalized using HPRT housekeeping gene. Y-axis shows relative expression fold and X-axis the tested markers, *P < 0.05 compared with CTRL, two tailed Student's t-test.*

DISCUSSION

The oral cavity is a complex environment where MSCs niches have been found in hard and soft tissues: Gronthos first described MSCs from dental pulp (DPSCs) (6). DPSCs were found to be phenotypically similar to Bone Marrow Stem Cells (BMSCs) (15), commonly considered the gold standard for MSC-based cell therapy and they can induce dentinogenesis forming the dentin structure when transplanted into immunocompromised mice (16).

Marrelli et al. discovered a new promising MSC lineage in the wall of inflamed periapical cyst: the authors termed them human periapical cyst mesenchymal stem cells (hPCy-MSCs), easily harvested from a tissue usually considered as biological waste (8, 17). DPSCs and hPCy-MSCs were investigated in this study and their ability to differentiate towards bone or dental tissue was compared: this ability could be topically utilized for bone regeneration. However, the achievement of a good bone regeneration passes through a correct strategy, thus, the tissue reconstruction needs to place *in situ* acellular materials from extracellular matrix (ECM) (18). Moreover, bone regeneration needs to be enhanced by nerve regeneration (19) and by a proper neoangiogenesis, stimulated for example by means of platelet concentrate such as Platelet-Rich Fibrin (PRF) (3, 4).

The use of MSCs in regenerative medicine is an intriguing challenge that needs to become

easily applicable in daily reconstructive surgery: the commitment of hPCy-MSCs make them the perfect candidates for the bone regeneration, even in consideration that hPCy-MSCs are isolated from a tissue that is easily obtainable with minimal discomfort to the patients (17).

DPSCs and hPCy-MSCs are two MSCs lineage isolated from oral cavity, easily usable in bone tissue regeneration and with a strong commitment towards osteogenesis and dentinogenesis.

In this study, the gene expression was compared of these two cell types. In osteogenic differentiation, hPCy-MSCs showed expression levels of osteogenic marker genes clearly increased after differentiation, instead DPSCs seemed to be directed more towards dentinogenesis.

Therefore, hPCy-MSCs could be a useful source of mesenchymal stem cells for bone regeneration and they can represent a good alternative to MSCs from other sources reachable with more difficulty for the surgeon.

ACKNOWLEDGEMENTS

The present study was supported by "ICARE Project - Infrastruttura Calabrese per la medicina Rigenerativa: generazione di biobanche per la criopreservazione di cellule staminali umane e di tessuto osseo per uso clinico e design e sviluppo di bioscaffold innovativi". PON03PE_00009_2

REFERENCES

1. Whitman DH, Berry R, Green D. Platelet gel: an autologous alternative to fibrine glue with applications in oral and maxillofacial surgery. J Oral Maxillofac Surg 1997; 55:1294-9.
2. Weibrich G, Kleis WKG, Hitzler WE, Hafner G. Comparison of the platelet concentrate collection system with the plasma-rich-in-growth-factors kit to produce platelet-rich plasma: a technical report. Int J Oral Maxillofac Implants 2005; 20:118-23.
3. Marrelli M, Tatullo M. Influence of PRF in the healing of bone and gingival tissues. Clinical and histological evaluations. Eur Rev Med Pharmacol Sci 2013; 17: 1958-62.
4. Tatullo M, Marrelli M, Cassetta M, et al. Platelet Rich Fibrin (P.R.F.) in reconstructive surgery of atrophied maxillary bones: clinical and histological evaluations. Int J Med Sci 2012; 9:872-80.
5. Mao JJ, Prockop DJ. Stem cells in the face: Tooth regeneration and beyond. Cell stem cell 2012; 11:291-301.
6. Gronthos S, Mankani M, Brahim J, Robey PG, Shi S. Postnatal human dental pulp stem cells (dpscs) *in vitro* and *in vivo*. Proceedings of the National Academy of Sciences of the United States of America 2000; 97:13625-30.
7. Tatullo M, Marrelli M, Shakesheff KM, White LJ. Dental pulp stem cells: function, isolation and applications in regenerative medicine. J Tissue Eng Regen Med 2014 May 21. doi: 10.1002/term.1899
8. Marrelli M, Paduano F, Tatullo M. Cells isolated from human periapical cysts express mesenchymal stem cell-like properties. Int J Biol Sci 2013; 9:1070-78.
9. Zhang Y, Huang B. Peripheral blood stem cells: Phenotypic diversity and potential clinical applications. Stem Cell Reviews 2012; 8:917-25.
10. Zarrabi M, Mousavi SH, Abroun S, Sadeghi B. Potential uses for cord blood mesenchymal stem cells. Cell Journal 2014; 15:274-81.
11. Geoffroy V, Kneissel M, Fournier B, Boyde A, Matthias P. High bone resorption in adult aging transgenic mice overexpressing cbfa1/runx2 in cells of the osteoblastic lineage. Mol Cell Biol 2002; 22:6222-33.
12. Gibson MP, Jani P, Wang X, Lu Y, Qin C .Overexpressing the NH2-terminal fragment of dentin sialophosphoprotein (DSPP) aggravates the periodontal defects in Dspp knockout mice. J Oral Biosci 2014; 56:143-48.
13. Nagata T, Goldberg HA, Zhang Q, Domenicucci C, Sodek J. Biosynthesis of bone proteins by fetal porcine calvariae *in vitro*. Rapid association of sulfated sialoproteins (secreted phosphoprotein-1 and bone sialoprotein) and chondroitin sulfate proteoglycan (CS-PGIII) with bone mineral. Matrix 1991; 11:86-100.
14. Roach HI. Why does bone matrix contain non-collagenous proteins? The possible roles of osteocalcin, osteonectin, osteopontin and bone sialoprotein in bone mineralisation and resorption. Cell Biol Int 1994; 18:617-28.

15. Shi S, Robey PG, Gronthos S. Comparison of human dental pulp and bone marrow stromal stem cells by cdna microarray analysis. Bone 2001; 29:532-39.
16. Gronthos S, Brahim J, Li W, Fisher LW, Cherman N, Boyde A, DenBesten P, Robey PG, Shi S. Stem cell properties of human dental pulp stem cells. J Dental Res 2002; 81:531-35.
17. Tatullo M, Marrelli M, Paduano F. The regenerative medicine in oral and maxillofacial surgery: the most important innovations in the clinical application of mesenchymal stem cells. Int J Med Sci 2015; 12:72-7.
18. Londono R, Badylak SF. Biologic scaffolds for regenerative medicine: mechanisms of *in vivo* remodeling. Ann Biomed Eng 2014; doi: 10.1007/s10439-014-1103-8
19. Marrelli M, Paduano F, Tatullo M. human periapical cyst-mesenchymal stem cells differentiate into neuronal Cells. J Dent Res 2015; doi: 10.1177/0022034515570316.

LETTER TO THE EDITOR

CLODRONATE: OLD DRUG, NEW USES

G. SAVIOLA, L. ABDI-ALI and M.R. POVINO

Rheumatology and Rehabilitation Unit- Salvatore Maugeri Foundation Irccs- Castel Goffredo, Mantua, Italy

Received March 17, 2015 – Accepted May 8, 2015

Clodronate (CLO) is a bisphosphonate (BP) with proved efficacy in the treatment of osteoporosis. The reason of its activity is the anti-resorptive action, which is a common characteristic of BPs. Contrary to other BPs, CLO has a relatively low affinity for bone and a peculiar mechanism of action. CLO is effective in several diseases associated to excessive bone resorption as bone Paget's disease and CRPS type I. Moreover, there are data showing activity of CLO in the erosive osteoarthritis of the hands, in the osteoarthritis of the knees, in the treatment of extra-articular calcifications and in preventing the mobilization of knee and hip prosthesis.

BPs are the most used class of anti-resorptive drugs in the treatment of osteoporosis and other conditions with excessive bone resorption. On the basis of their chemical structure and on the nature of the R(2) side chain, they can be divided into two groups: nitrogen–containing and non nitrogen-containing BPs. CLO is a first generation BP with a simple halogenated non-nitrogen chemical structure. Therefore its mechanism of action is completely different from that of the nitrogen-containing BPs. CLO, as shown in Fig. 1, is able to produce a "toxic analogue" of AT which inhibits mithocondrial oxygen consumption inducing osteoclast apoptosis (1). The clinical activity of CLO in the prevention and treatment of post-menopausal and glucocorticoid induced osteoporosis is well known (2-4), as well as in the treatment of bone Paget's disease, malignant hypercalcemia, osteolytic bone metastases, primary hyperparathyroidism, algodystrophic syndrome (5). Moreover, CLO has an anti-inflammatory activity, inhibiting cyclooxygenase-2-dependent prostaglandin E2 production. On the contrary, amino-BP can produce, as a side effect, an acute-phase response due to the inhibition of the mevalonate pathway, which is its mechanism of action to reach the anti-resorptive result (6, 8). CLO is generally well-tolerated. Gastrointestinal symptoms have been observed in 2-10% of patients taking oral CLO at high doses, while CLO, contrary to other BPs, seems to be not contraindicated in patients with renal failure (5). Moreover, in osteonecrosis of the jaw (ONJ) which is believed to be a side effect of BPs, CLO has been rarely applied, mainly in patients with a previous history of treatment with amino-BPs (9). Significant beneficial effects of CLO on pain have been shown in patients with rheumatological diseases and malignancies in contrast with reports of severe bone, joint and muscle pain in course of treatment with alendronate or pamidronate (5). CLO is available in Europe as oral (400 and 800 mgs) and intravenous formulations; moreover, in Italy it is available in two different intramuscular injections

Key words: clodronate, osteoarthritis, extra-articular calcifications, aseptic mobilization of prosthesis

Mailing address: Gianantonio Saviola MD,
Rheumatology and Rehabilitation Unit,
Salvatore Maugeri Foundation Irccs,
Via Ospedale, 36,
46042 Castel Goffredo, Mantua, Italy,
Tel.: +390376 77471 Fax: +39 0376 779886,
e-mail: gianantonio.saviola@fsm.it

0393-974X (2015)

DISCLOSURE: ALL AUTHORS REPORT NO CONFLICTS OF INTEREST RELEVANT TO THIS ARTICLE.

(100 mgs and 200 mgs).

CLODRONATE: THE NEW FIELDS OF RESEARCH

Osteoarthritis (OA)

Agents suppressing bone turnover (including BPs) have been associated with reduction of lesions in the subcondral region of patients with OA. Subcondral lesions (including disruption of the connectivity and microarchitecture of trabecular bone) seem to play an important role in the development of OA (10-12). Moreover, there are data showing that CLO is able to exert an anabolic effect on articular chondrocyte culture which could ameliorate cartilage damage. These effects are transducted through the purinergic receptor pathway (13).

Following these hypotheses and the previous clinical observations (14) painful erosive osteoarthritis of the hands was treated with iv CLO, as an attack dose, followed by a maintenance intramuscular dose for 24-month follow-up. The Authors showed reduction in pain (p=0.001), in disability Dreiser score (p= 0.026), in number of tender joints (p=0.011) and an improvement in strength of both hands (p=0.04 of the right; p=0.016 of the left) (15).

Intra-articular CLO was used in knee OA, concluding that the drug provides symptomatic and functional improvements at least as good as those obtained with hyaluronic acid (16). A second double-blind study, with 12 weeks of follow-up, showed that intra-articular CLO at the dose of 2 mgs was more effective than placebo in reducing pain ($p < 0.05$) while in the patients treated with CLO Lequesne functional index was significantly improved (17).

These observations could open a new pathway in the research of an effective treatment for OA, to reduce, not only the symptoms, but also the evolution of the disease.

EXTRA-ARTICULAR CALCIFICATIONS

Hydroxyapatite (HA) crystals are often deposited in the vicinity of joints where they can cause a clinical periarthritis.

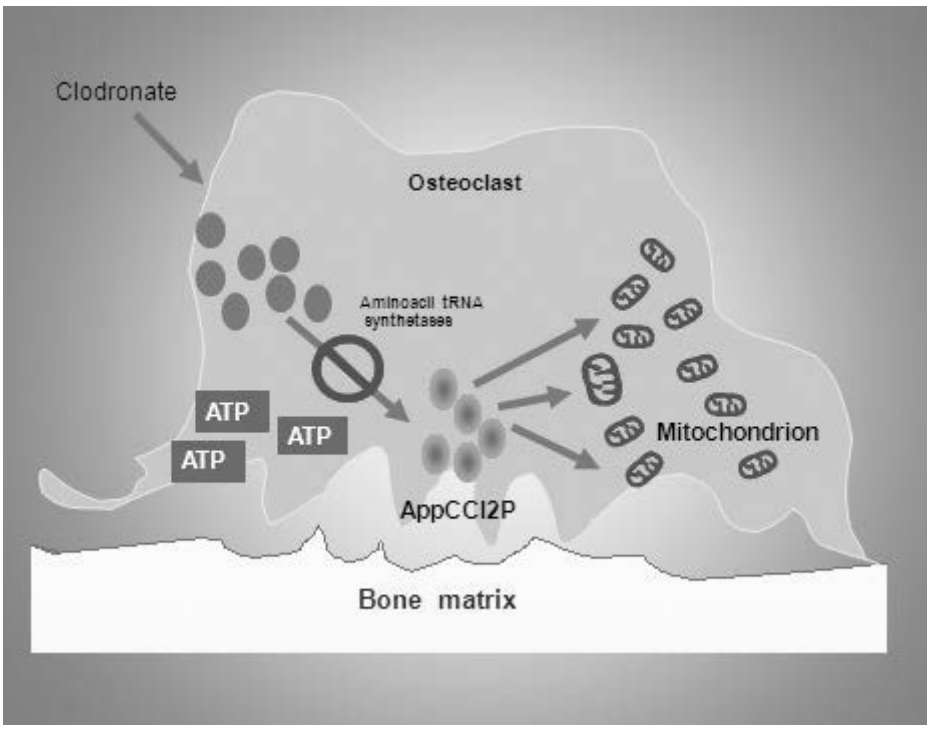

Fig. 1. *The mechanism of action of clodronate. The drug can be metabolized intracellulary to a cytotoxic analog of ATP (AppCCl2p). AppCCl2p is able to inhibit mitochondrial oxygen consumption, causing apoptosis of the osteoclasts.*

BPs are able to bind to HA crystals, thus inhibiting crystal growth (18). CLO, because of its relatively low affinity to bone, is able to inhibit non-skeletal and soft tissues calcifications. Two cases of disabling calcific periarthritis of the shoulders lasting for years and resistant to any traditional drugs (including high dose glucocorticoids), infiltrations and surgical treatments, were successfully treated with CLO in chronic cycles (100 mg im daily for 20 days/ every 3 months) with a sudden clinical and functional result and radiological confirmation after 18 months of therapy (19).

Further study involving a larger number of patients is needed to confirm these data.

PREVENTION OF MOBILIZATION OF HIP AND KNEE PROSTHESIS

Periprosthetic osteolysis and bone loss are the most important causes of the aseptic failures in artroplasty. BPs, because of their anabolic effect on osteoblasts, have the potential to enhance bone ingrowth into implant porosities, prevent bone resorption under adverse conditions, and dramatically extend the long-term durability of joint arthroplasties (20). The database of the United Kingdom General Practice Research of the years 1986-2006 showed that of 41,995 patients undergoing primary hip or knee arthroplasty, 1,912 BPs users were identified. The Authors concluded that, after 5 years, in BP users the implant survival time had increased almost two-fold (21). Moreover, the database of the Danish Nationwide Registries showed that of 80,342 eligible patients with a primary total joint replacement, the BP users had a 59% reduced risk of revision surgery. This association was strongest in patients with the longest duration of treatment and/or the best adherence and only when BP was started after arthroplasty surgery (22).

Oral CLO (1.6 gr/daily), starting 3 weeks before the operation and continuing for 6 months after, reduced the prosthetic migration after total knee prosthesis in a double-blind randomized study with 4-year follow-up. In this paper the Authors showed 25% less migration in the CLO group measured by radiostereometry (23).

Intramuscular CLO (100 mg/weekly) was tested on uncemented stems after total hip arthroplasty. Periprosthetic and contralateral bone mineral density (BMD) scans were performed. After 12 months, in patients treated with CLO versus non-treated, the Authors showed a reduction in bone loss ($p<0.05$) with the exception of Gruen zones 4 and 5 (24). A very similar result was shown in another study. (25).

Following these data, the next step could be the use of CLO to reduce the symptoms in painful prosthesis not yet mobilized, where bone loss is probably the cause of pain.

CONCLUSIONS

As shown, CLO is an old drug with a peculiar mechanism of action and a good safety. For these reasons it should be better studied to prove its efficacy and to extend its use to other fields.

REFERENCES

1. Lehenkari PP, Kellinsami M, Juha P, et al. Further insight into mechanism of action of clodronate: inhibition of mitochondrial ADP/ATP translocase by a nonhydrolyzable, adenine-containing metabolite. Mol Pharmacol 2002; 61(5):1255-62.
2. McCloskey E, Selby P, Davies M, et al. Clodronate reduces vertebral fracture risk in women with postmenopausal or secondary osteoporosis: results from a double-blind, placebo controlled 3-year study. J Bone Miner Res 2004; 19:728-36
3. McCloskey EV, Beneton M, Charlesworth D et al. Clodronate reduces the incidence of fractures in community-dwelling elderly women unselected for osteoporosis: Result of a double-blind placebo-controlled randomized study. J Bone Miner Res 2007; 22:135-41.
4. Frediani F, Falsetti P, Baldi F, Acciai C, Filippou G, Marcolongo R. Effects of 4-year treatment with once-weekly clodronate on prevention of corticosteroid-induced bone loss and fractures in patients with arthritis. Bone 2003; 33:575-81.
5. Frediani B, Cavalieri L, Cremonesi G. Clodronic acid formulations available in Europe and their use in osteoporosis. A review. Clin Drug Invest 2009; 29(6):359-79.
6. Ghonoi V, Brandi ML. Clodronate: mechanism

of action on bone remodelling and clinical use in osteometabolic disorders. Expert Opin Pharmacoter 2002; 3(11): 1643-56.
7. Liu L, IgarashiK, Kenzaki H, Chiba M, Shinoda H, Mitani H. Clodronate inhibits PGE(2) production in compressed periodontal ligament cells. J Dent Res 2006; 85(8):757-60.
8. Hewitt RE, Lissina A, Green AE, Slay ES, Price DA, Sewell AK. The bisphosphonate acute phase response: rapid and copious production of proinflammatory cytokines by peripheral blood γδ T cells in response to aminobisphosphonates is inhibited by statins. Clin Exp Rheumatol 2005; 139(1):101-11
9. Diel IJ, Fogelman I, Al-Nawas B, et al. Pathophysiology risk factors and management of bisphosphonate-associated osteonecrosis of the jaw: is there a diverse relationship of amino and non-aminobisphosphonates? Crit Rev Oncol Hematol 2007; 64(3);198-207.
10. Bergman AG, Willen HK, Lindstrand AL. Osteoarthritis of the knee: correlation of subchondral MR signal abnormalities with histopathologic and radiographic features. Skeletal Radiol 1994; 23(6):445-8.
11. Carbone LD, Nevitt MC, Wildy K, et al. The relationship of antiresorptive drug use to structural finding and symptoms of knee osteoarthritis. Arthritis Rheum 2004; 50(11):3516-25.
12. Zhen G, Wen C, Jia X et al. Inhibition of TGF-β signalling in mesenchymal stem cells of subcondral bone attenuates osteoarthritis. Nature Medicine 2013; 19:704-12.
13. Rosa RG, Collavino K, Lakhani A, Delve E, Weber JF, Rosenthal AK, Waldman SD. Clodronate exerts an anabolic effect on articular chondrocytes mediated through the purinergic receptor pathway. Osteoarthritis Cartilage 2014; 22:1324-36.
14. Saviola G, Santoro L. Clodronate in erosive osteoarthritis of the hand; efficacy for pain and function recovery. G Ital Med Lav Erg 2000; 22(4):328-31.
15. Saviola G, Abdi-Ali L, Campostrini L, et al. Clodronate and hydroxychloroquine in erosive osteoarthritis: a 24 month open randomized pilot study.Mod Rheumatol 2012; 22(2):256-63.
16. Rossini R, Viapiana O, Ramonda R, Bianchi G, Olivieri I, Lapadula G, Adami S. Intra-articular clodronate for the treatment of knee osteoarthritis: dose ranging study vs hyaluronic acid. Rheumatology (Oxford) 2009; 48(7):773-8.
17. Rossini M. Adami S, Fracassi E, et al. Effects of intra-articular clodronate in the treatment of knee osteoarthritis: results of a double-blind, randomized placebo-controlled trial. Rheumatol Int 2015; 35(2):255-63.
18. Fleisch H. Bisphosphonates: mechanism of action. Endocr Rev 1998; 19:80-100.
19. Saviola G, Abdi-Ali L, Baiardi P, Benucci M. Can clodronate be effective in the treatment of disabling hydroxyapatite crystal-deposition disease? A report of two cases. Rheumatol Int 2011; 31(3):415-7.
20. Shanbhag AS. Use of bisphosphonates to improve the durability of total joint replacement. J Am Acad Orthop Surg 2006; 14(4):215-25.
21. Prieto-Alhambra D, Javaid MK, Judge A, Murray D, Carr A, Cooper C. Arden NK, Association between bisphosphonate use and implant survival after primary total arthroplasty of the knee or hip: population based retrospective cohort study. BMJ 2013; 347:f6956
22. Prieto-Alhambra D, Lalmohamed A, Abrahamsen B, Arden NK, de Boer A, Vestergaard P, de Vries F. Oral bisphosphonate use and total knee/hip implant survival: validation of results in an external population-based cohort. Arthritis Rheum 2014; 66:3233-40.
23. Hilding M, Aspenberg P. Postoperative clodronate decreases prosthetic migration. Acta Orthop. 2006; 77(6):912-916.
24. Trevisan S, Ortolani S, Romano P, et al. Decreased periprosthetic bone loss in patients treated with clodronate; a 1-year randomized controlled study. Calcif Tissue Int 2010; 86:436-446.
25. Massari L, De Rito G, Brunoro A, Lo Caputo A, Traina F, Traina GC. Il disodio clodronato riduce il riassorbimento periprotesico in impianti non cementati nelle fasi precoci: studio prospettico con controllo. G.I.O.T.2002; 28:79-87.

LETTER TO THE EDITOR

TELOMERE AND TELOMERASE MODULATION BY BERGAMOT POLYPHENOLIC FRACTION IN EXPERIMENTAL PHOTOAGEING IN HUMAN KERATINOCYTES

S. NISTICÒ[1], J. EHRLICH[2], M. GLIOZZI[3], J. MAIUOLO[3], E. DEL DUCA[1], C. MUSCOLI[3] and V. MOLLACE[2,3]

[1]Department of Health Sciences; University of Catanzaro "Magna Graecia", Italy; [2]Interregional Research Center For Food Safety and Health, Department of Health Sciences, University of Catanzaro "Magna Graecia", Italy; [3]School of Pharmacy; University of Catanzaro "Magna Graecia", Italy

Received December 23, 2014 - Accepted February 10, 2014

Photoageing represents the addition of extrinsic chronic ultraviolet radiation-induced damage on intrinsic ageing and accounts for most age-associated changes in skin appearance. In this study, we evaluated the effect of 38% BPF, a highly concentrated extract of the bergamot fruit (*Citrus bergamia*) on UVB-induced photoageing by examining inflammatory cytokine expression, telomere length/telomerase alterations and cellular viability in human immortalized HaCaT keratinocytes. Our results suggest that 38% BPF protects HaCaT cells against UVB-induced oxidative stress and markers of photoageing in a dose-dependent manner and could be a useful supplement in skin care products. Together with antioxidant properties, BPF, a highly concentrated extract of the bergamot fruit, appears to modulate basic cellular signal transduction pathways leading to anti-proliferative, anti-aging and immune modulating responses.

The alarming increase in the incidence of skin cancer and dermatological conditions related to excessive exposure to solar ultraviolet (UV) radiation has led to a comprehensive search for novel preventive strategies in dermatology and cosmetology.

Photoageing represents the addition of extrinsic chronic ultraviolet radiation-induced damage on intrinsic ageing and accounts for most age-associated changes in skin appearance (1). In addition, epidemiological and experimental data show a direct relationship between ultraviolet radiation and the development of human skin cancers. Numerous studies have described the process of senescence associated with accumulation of oxidative damage, immune/cytokine and telomere alterations resulting in a decline in proliferative potential, depression of cellular integrity and increased likelihood for carcinogenic transformation (2).

In recent years there has been extensive research involving the use of botanical phytochemicals or flavonoids with antioxidant and/or anti-inflammatory properties for use as skin photoprotective agents (3). Clinical and animal studies demonstrating that bergamot polyphenol fraction (38% BPF) has powerful antioxidant and anti-inflammatory activity prompted the current study to examine its potential effect on photoageing and cellular viability (4).

Key words: telomere, telomerases, photoageing, UVB, keratinocytes, bergamot fruit extract

Mailing address: Prof. Steven Nistico,
Dermatologist, Associate Professor of Dermatology,
University Magna Graecia, Catanzaro
Viale Europa, Germaneto (CZ)
88100 Catanzaro, Italy
Tel./Fax: +39 09613694001
e-mail: steven.nistico@gmail.com

0393-974X (2015)

In this study, we evaluated the effect of 38% BPF, a highly concentrated extract of the bergamot fruit (*Citrus bergamia*) on UVB-induced photoageing by examining inflammatory cytokine expression, telomere length/telomerase alterations and cellular viability in human immortalized HaCaT keratinocytes. As UVB radiation is absorbed mostly by the DNA of the epidermal keratinocytes, the current study (focused on photoageing) is also potentially relevant for photocarcinogenesis.

MATERIALS AND METHODS

We used an MTT assay to measure the presence of formazan crystals within metabolically active cells (non-active cells are devoid of these crystals) to reliably examine cellular viability in control, irradiated and BPF treated irradiated cell cultures (at 3 doses). As shown in Fig. 1, UVB irradiation resulted in approximately a 70% loss of cell viability.

Keratinocytes produce various cytokines which are enhanced by UV radiation. Interleukin-1beta (IL-1b) is a pro-inflammatory cytokine involved in the up-regulation of UVR-induced matrix metalloproteinases especially in dermal fibroblasts which contribute to the loss of interstitial collagen structure characteristically found in skin photoaging (5). In our investigation (Fig. 2), a quantitative reverse transcriptase-polymerase chain reaction technique (RT-PCR) was used to examine changes in the messenger RNA expression of IL-1b after UVB irradiation with and without pre-treatment at high and low doses of BPF. We also examined and compared the blunting of cytokine expression between BPF and N-acetyl cysteine (NAC), a powerful anti-oxidant with documented ability to inhibit the production of pro-inflammatory molecules. Fig. 2 shows that BPF dose-dependently reduces IL-1b mRNA expression with BPF 100 mM exceeding the capability of 100 mM NAC to blunt this UV-induced inflammatory response.

Telomere signal alterations are inherently connected to the mechanisms of skin aging. "Intrinsic aging" is associated with progressive telomere shortening while UV irradiation ("extrinsic aging") accelerates telomere damage. To examine whether BPF preserves and/or attenuates UVB-induced telomere shortening, we used a technique involving a telomere length assay kit (Roche) that examines southern blots of terminal restriction fragments (TRFs). After extraction, DNA was inspected for integrity, digested, resolved by gel electrophoresis,

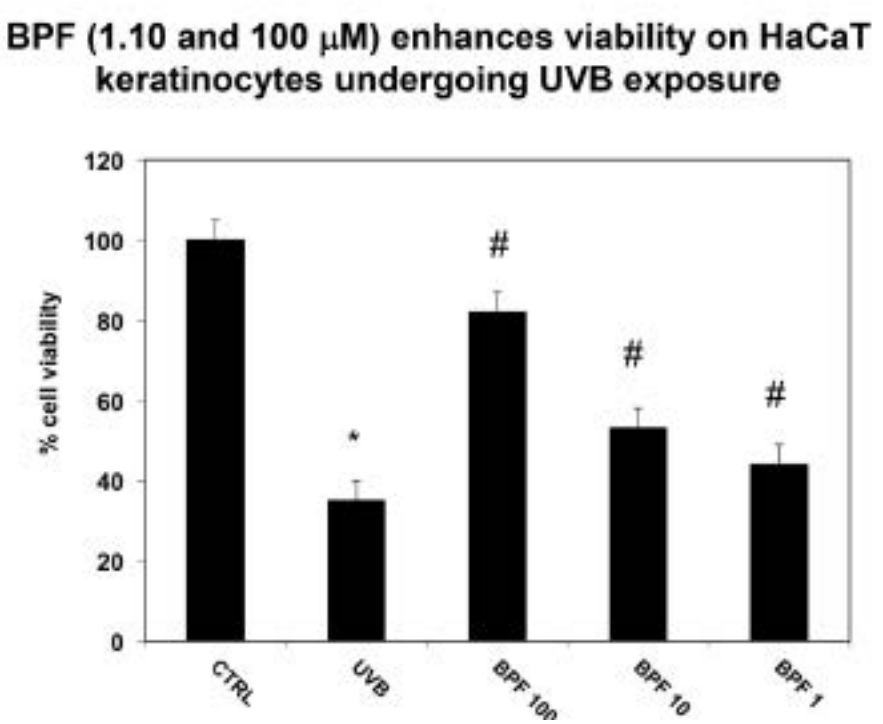

Fig. 1. *BPF and cell viability.*

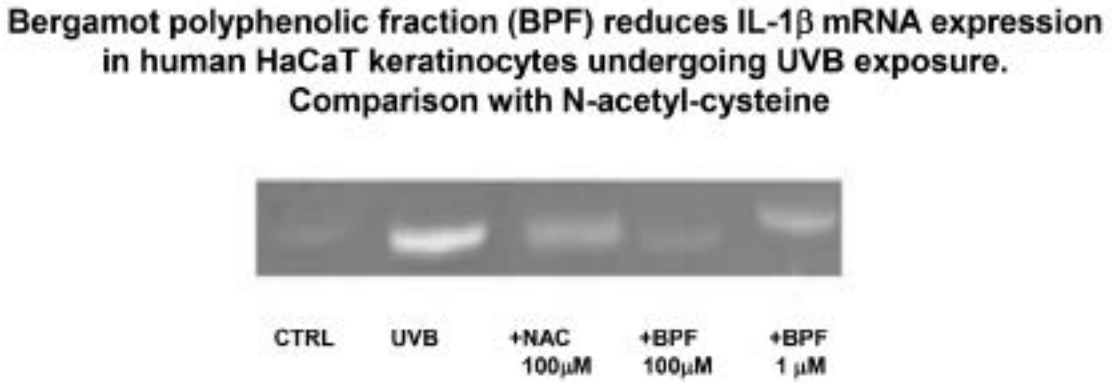

Fig. 2. *BPF and inflammatory cytokine activity.*

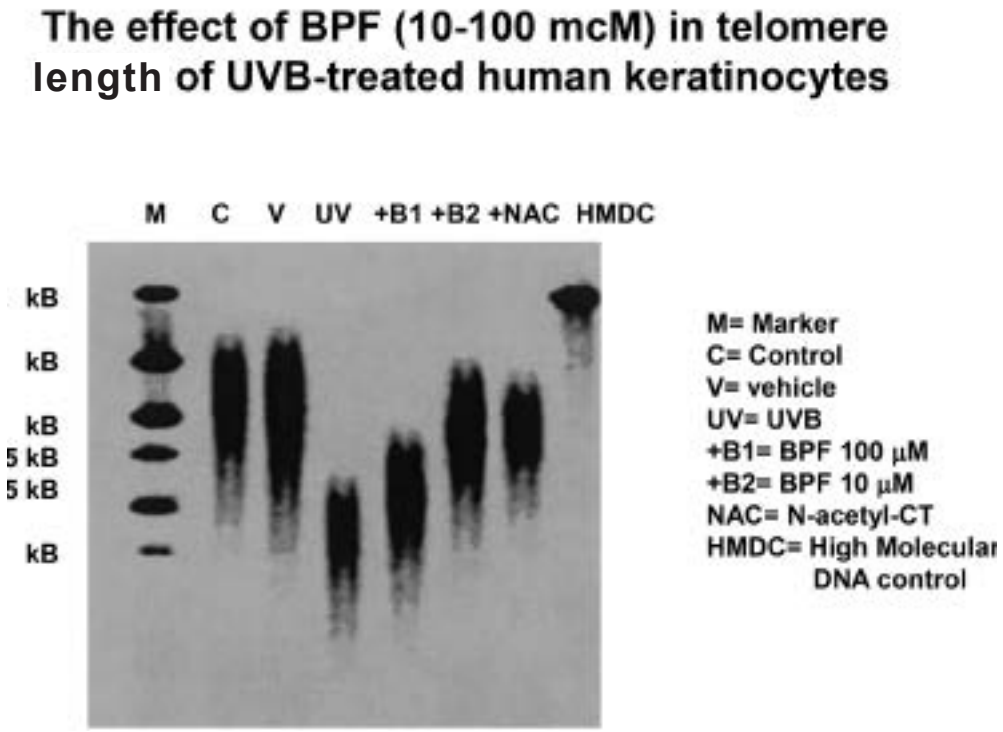

Fig. 3. *BPF and the preservation of telomere length.*

transferred to a membrane, hybridized with labeled probes and exposed to X-ray film using chemiluminescence. As shown in Fig. 3, UVB radiation results in a dramatic reduction in telomere length. BPF treatment of cultured cells dose-dependently restores telomere length after radiation favorably compared to NAC.

The majority of human cells that become immortalized (as in our HaCaT culture) acquire telomerase activity; the expression and amplification of telomerase activity is related to longevity of cells in culture.

RESULTS

In a progressive dose-dependent fashion, BPF substantially restored cell viability towards control levels with the least cytotoxicity demonstrated when keratinocytes were pretreated at higher doses (BPF 100 mM) (Fig. 1).

Fig. 2 shows that BPF dose-dependently reduces IL-1b mRNA expression with BPF 100 mM

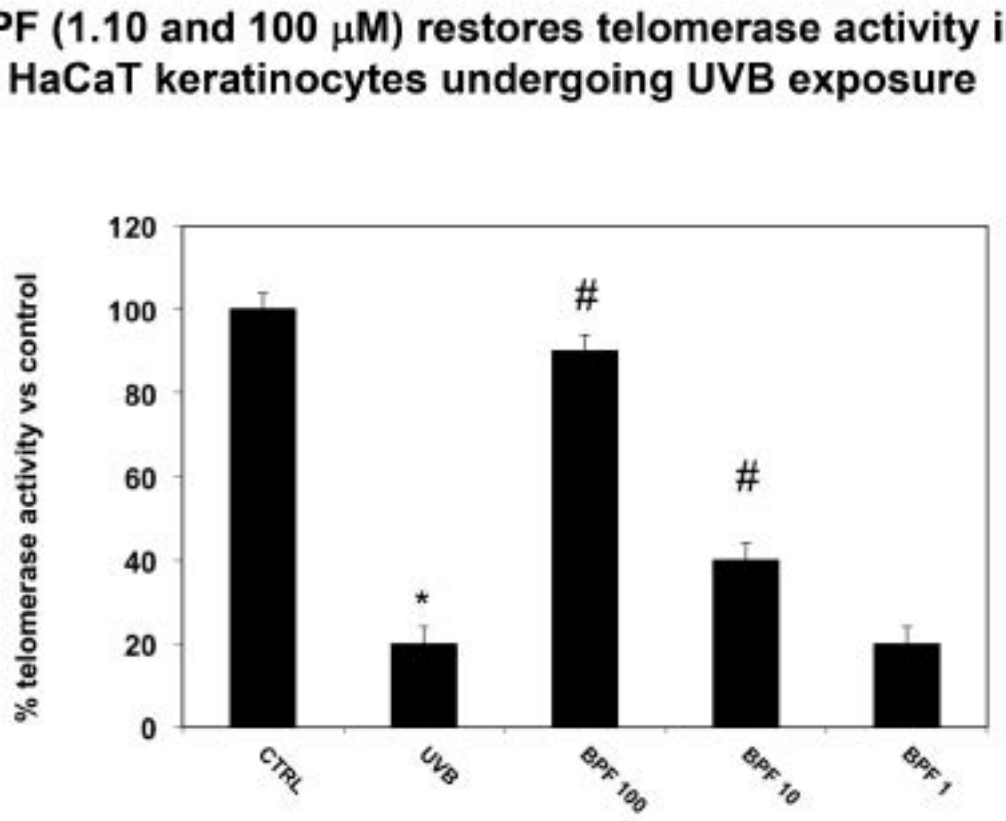

Fig. 4. *BPF and telomerase activity.*

exceeding the capability of 100 mM NAC to blunt this UV-induced inflammatory response.

Telomere signal alterations are inherently connected to the mechanisms of skin aging. "Intrinsic aging" is associated with progressive telomere shortening while UV irradiation ("extrinsic aging") accelerates telomere damage (Fig. 3).

In our investigation, telomerase activity in cell extracts was measured by the PCR-based telomere repeat amplification protocol (TRAP) using TRAPeze kit (Intergen, Gaithersburg, MD, USA), the most widespread assay to detect and measure telomerase activity. As depicted in Fig. 4, UVB radiation resulted in an approximately 80% obliteration of telomerase activity compared to controls. BPF at 100 mM dramatically preserved telomerase activity (about 90% of control) whereas lower doses of BPF were associated with lesser but significant restoration of telomerase activity.

In summary, the present investigation has demonstrated that pretreatment of HaCaT cells with 38% BPF (1-100 mM) dose-dependently inhibits UVB (5, 10, or 15 mJ cm^{-2}) mediated (i) decrease in cell viability, (ii) overexpression of inflammatory cytokine biomarker interleukin-1beta (IL-1b), (iii) telomere shortening and (iv) decreases in telomerase activity. Our research demonstrated that BPF at 100 mM concentration greatly normalizes all 4 parameters under study.

DISCUSSION

There are several interconnected mechanisms involved in photoageing that appear to be addressed by bergamot polyphenols.

Oxidative stress overwhelming endogenous antioxidants

Human skin contains numerous antioxidants to help provide protection from reactive oxidative

species generated during normal cellular metabolism. However, overexposure to UV radiation can overwhelm the skin's antioxidant supply, allowing reactive oxidative species (ROS) to reach damaging levels. UV radiation-induced oxidative stress seems to play a crucial role in the deleterious effects of both UVA and UVB through the generation of such damaging free radicals. It has been consistently demonstrated that acute exposure to ultraviolet radiation (UVR) leads to cellular damage in the face of depletion of endogenous antioxidants (6). Natural polyphenols in BPF have anti-oxidant effects that depend on the free radical scavenging ability of hydroxyl groups linked to carbon aromatic rings (4). In our study, peroxynitrite levels, associated with cytotoxic free radicals from oxidative stress were consistently lowered by BPF at all dose ranges.

Overexpression of inflammatory cytokines

The epidermal cell is a major producer and target of cytokines. Keratinocytes produce a plethora of pro-inflammatory cytokines including interleukin (IL)-1,-6,-8 and tumor necrosis factor alpha (TNF-a) which are consistently overexpressed after UV radiation exposure. Cytokines regulate immunity and inflammation and play an important role in the pathogenesis of various cutaneous disorders including atopy, dermatitis and photoageing (7). Of relevance, IL-1b is involved in the up-regulation of UVA-induced MMP-1 (matrix metalloproteinase) in dermal fibroblasts which contributes substantially to the loss of interstitial collagen, a hallmark of skin photoageing (5). Studying the mRNA expression of cytokine IL-1b by keratinocytes *in vitro* using immortalized cell systems offered our group insights into the capability of a potent antioxidant to modulate inflammatory responses. Inflammation and oxidative stress are interrelated. UV exposure results in an increase in proinflammatory cytokines leading to accelerated oxidative damage through the generation of free radicals and a link to cellular senescence and death (8).

Telomere/telomerase alterations

Telomerase activity is intimately associated with cellular immortality, proliferative activity, cancer and aging. Intrinsic aging is largely controlled by progressive telomere shortening, compounded by oxidative damage to telomeres. In sun-exposed skin, UV irradiation leads to immunosuppression and premature photoageing as a consequence of damage to DNA with rapid telomere shortening. The viability and longevity of the keratinocyte can be improved by slowing down the age-dependent shortening of telomeric DNA. Telomere-dependent replicative senescence is an established response to oxidative stress and is likely to be a link to carcinogenesis, cell death and photoageing (9).

It has been postulated that blocking telomerase by dietary polyphenols is an important mechanism that may also be related to anti-cancer effects. Potent antioxidants like 38% BPF may allow telomeres to suffer from less DNA lesions due to the repression of intracellular oxidative stress.

These results suggest that 38% BPF protects HaCaT cells against UVB-induced oxidative stress and markers of photoageing in a dose-dependent manner and could be a useful supplement in skin care products. Together with antioxidant properties, BPF appears to modulate basic cellular signal transduction pathways leading to anti-proliferative, anti-aging and immune modulating responses. Furthermore, as DNA damages are central to photocarcinogenesis, our results imply a potential value of a bergamot bioflavonoid-based formulation to support the endogenous skin antioxidant system which would favorably modify gene and inflammatory expressions to inhibit both photoageing and its most serious sequelae, skin cancer. From a therapeutic perspective, 38% BPF could be effective given orally or developed into a skin care topical lotion. In recent studies (10-12), the protective effect of two important flavonoids in BPF (hesperetin and naringenin) was studied by a separate research group against UV radiation-induced peroxidation on phosphatidylcholine (PC) vesicles. The flavonoids proved to protect PC liposomes from UV radiation-induced peroxidation, probably by free radical scavenging and demonstrated high anti-lipoperoxidative activity. Importantly, as suitable percutaneous absorption is an essential requirement for a topically applied photo-protective agent, both naringenin and hesperetin were able to permeate through the stratum corneum to the deeper layers of skin. These findings and ours suggest that oral or topically applied bergamot polyphenols could

be excellent candidates for successful employment as protective agents against skin photoageing and potentially, cutaneous carcinomas.

REFERENCES

1. Fisher G, Kang S, Varani J, Bata-Csorgo Z, Wan Y, Datta S, Voorhees JJ. Mechanisms of photoaging and chronological skin aging. Arch Dermatol 2002; 138(11):1462-70.
2. Rabe J, Mamelak A, McElgunn P, Morison W, Sauder DL. Photoaging: mechanisms and repair. J Am Acad Dermatol 2006; 55:1-19.
3. Afaq F, Mukhtar H. Photochemoprevention by botanical antioxidants. Skin Pharmacol Appl Physiol 2002; 5:297-306.
4. Mollace V, Sacco I, Janda E, et al. Hypolipemic and hypoglycaemic activity of bergamot polyphenols: from animal models to human studies. Fitoterapia 2010; 82(3):309-16.
5. Honda A, Abe R, Makino T, et al. Interleukin-1beta and macrophage migration inhibitory factor (MIF) in dermal fibroblasts mediate UVA-induced matrix metalloproteinase-1 expression. J Dermatol Sci 2008; 49(1):63-72.
6. Pandel R, Polsjak B, Godic A, Dahmane R. Skin photoaging and the role of antioxidants in its prevention. ISRN Dermatol 2013; doi: 10.1155/2013/930164.
7. Grone A. Keratinocytes and cytokines. Vet Immunol Immunopathol 2002; 88(1-2):1-12.
8. Groves RW, Rauschmayr T, Nakamura K, Sarkar S, Williams IR, Kupper TS. Inflammatory and hyperproliferative skin disease in mice that express elevated levels of the IL-1 receptor on epidermal keratinocytes. J Clin Invest 1996; 15(2):336-44.
9. Matsui M, Miyasaka J, Hamada K, Ogawa Y, Hiramoto M, Fujimori R, Aioi A. Influence of aging and cell senescence on telomerase activity in keratinocytes. J Dermatol Science 2000; 22(2):80-87.
10. F. Bonina, M. Lanza, L. Montenegro, Salerno L, Smeriglio P, Trombetta D, Saija A. Flavonoids as potential protective agents against photo-oxidative skin damage. Int J Pharm 1996; 145(1-2):87-94.
11. Specchio F, Carboni I, Cannarozzo G, Tamburi F, Nistico S. Excimer UV radiation in dermatology. Int J Immunopath Pharmacol 2014; 27(2):247-49.
12. Muscoli C, Lauro F, Nisticò S, et al. Olea europea-derived phenolic products attenuate antinociceptive morphine tolerance: an innovative strategic approach to treat cancer pain. J Biol Reg Homeost Agents 2014; 28(1):105-16.

JOURNAL OF BIOLOGICAL REGULATORS & HOMEOSTATIC AGENTS Vol. 29, no. 3, 729-736 (2015)

LETTER TO THE EDITOR

NORMAL NUTRITIONAL COMPONENTS AND EFFECTS ON BONE METABOLISM IN PREVENTION OF OSTEOPOROSIS

G. TESTA, V. PAVONE, S. MANGANO, M. RICCIOLI, A. ARANCIO, F.R. EVOLA, S. AVONDO and G. SESSA

Orthopaedic Clinic, University of Catania, Azienda Ospedaliera Universitaria, Policlinico Vittorio Emanuele, Catania, Italy

Received November 8, 2014 – Accepted July 23, 2015

Osteoporosis is the most common bone disease, affecting millions of people and causing a high risk of fractures and a loss of quality of life. It is characterized by low bone mass and microarchitectural deterioration of bone tissue, with a consequent increase in bone fragility and susceptibility to fracture. A primary method of prevention, in order to reduce the risk of fractures, is represented by an appropriate lifestyle and a correct diet. There are potentially numerous nutrients and dietary components that can influence bone health, and these range from macronutrients to micronutrients as well as bioactive food ingredients. The purpose of this review is to overview osteoporosis, including its definition, etiology, and incidence, and then provide some information on possible dietary strategies for optimizing bone health and preventing osteoporosis. A correct diet to prevent osteoporosis should contain adequate amounts of calcium, vitamins D and K, protein, and fatty acids. The effects of these elements are briefly discussed, reporting on their correlation with bone benefits.

Osteoporosis, from the Greek term "porous bone", is the most common bone disease affecting millions of people worldwide. It leads to an increased risk of fracture with consequent high expenditure and a substantial morbidity with a loss of quality of life (1). It is characterized by low bone mass and mineral density and micro architectural deterioration of bone tissue, with a consequent increase in bone fragility and susceptibility to fracture. It was once thought of as a disease commonly affecting women, however, it has become clear that osteoporotic fractures may result in substantial morbidity and mortality also in men (2). Fractures in individuals over the age of 50 can be the first sign of weak bones from osteoporosis. They are particularly common in the spine, hip, and distal forearm (3).

A primary method of prevention, to reduce risks of fractures, is represented by an appropriate lifestyle and a correct diet. Nutrients and food components have a positive or negative impact on bone health. The poor supply of these elements with the diet or under pathological circumstances lead to bone weakness and osteoporosis. These dietary factors range from inorganic minerals (e.g., calcium, magnesium, phosphorus, sodium, potassium, and various trace elements) and vitamins (vitamins A, D, E, K, C, and certain B vitamins), to macronutrients, such as protein and fatty acids (4). The aim of this review is to represent these dietary factors involved in bone metabolism and their role in prevention of

Key words: diet, osteoporosis, prevention, bone mineral density

Mailing address: Vito Pavone MD,
Department of Orthopedics,
AOUOVE- Policlinico,
Viale Vittorio Veneto 106,
95127, Catania, Italy
Tel.: +39 095 7435240 Fax: +39 095 350611
e-mail: vitopavone@hotmail.com

0393-974X (2015)

DISCLOSURE: ALL AUTHORS REPORT NO CONFLICTS OF INTEREST RELEVANT TO THIS ARTICLE.

osteoporosis.

The diet and the skeleton - the way to maintain healthy bone

Bone is a metabolically active structure. Young age and adolescence are the periods of life with the most intensive bone growth: 90% of bone mass will have formed by the end of adolescence. Childhood and adolescence are important for optimal formation of bone and for the prevention of osteoporosis in older age. After the age of 30 years, there is no further increase of bone mass and a gradual natural reduction ensues (5).

A number of factors, in particular calcium intake and metabolism, influence peak bone mass (5). These include genetic, gender, nutrition, endocrine factors (sex hormones, calcitriol), mechanical influences (physical activity, body mass) and negative effects such as smoking, and excessive alcohol intake. Genetic factors influence mainly absorption of calcium from the intestine: the gene responsible for the formation of vitamin D receptors has several variants, which have different effects on absorption of calcium. In fact, Vitamin D has a pleiotropic effect on immune modulation, regulation of skeletal metabolism, and cellular proliferation and differentiation. The sequence of Vitamin D was found to be polymorphic in different individuals. BsmI, ApaI, and TaqI polymorphisms are located in the 3'-regulatory region of the VDR gene, so they are often marked as 1 haplotype; these polymorphisms increase the risk of osteoporosis. On the contrary, Cdx2 is a protective polymorphism that reduces the risk of osteoporosis (3, 5). Genetic differences can, however, be compensated for by adequate supply of calcium in dietary intake (6).

Deposition of calcium into bones is also under the influence of sex hormones, testosterone in men, estrogens in women. Late puberty, early menopause, secondary amenorrhoea and ovarectomy are risk factors for osteoporosis in women. Peak bone mass and bone metabolism are influenced by physical activity (6). Mechanical forces have an essential role on bone mass: not so much weight bearing, but rather pulling forces acting on entheses. Physically fit post-menopausal women have 25% higher intestinal absorption of calcium and calcitriol blood levels than unfit ones. The poor intake of vitamins and other nutrients and the loss of these ingredients in individual saffected by various anomalies which hinder the normal absorption are the main cause of the onset of the osteoporosis (4).

There are many methods to evaluate bone health and the risk of osteoporosis. Standard laboratory tests in a nutrition assessment include investigation of daily urinary excretion of calcium, serum albumin level, total lymphocyte count, and serum 25-hydroxyvitamin D level. Anthropometric values performed through weight-to-height ratio and Body Mass Index (BMI) may give further clinical information.

The following are the targets to be achieved for a good control of osteoporosis. The daily excretion of calcium, carried out on 24-hour urine samples, provides an indirect indication of the amount of calcium taken from the diet and absorbed in the gastrointestinal tract. This excreted amount is reduced when the dietary intake or intestinal absorption are inadequate. The specific goal of nutritional therapy is a daily urinary excretion of calcium < 300 mg (7).

Serum albumin level and total lymphocyte count are biochemical parameters that indicate visceral protein status. The specific goal of nutritional therapy are albumin level > 35 g/L and total lymphocyte count > 1.5 mm^9/L (7).

Another important parameter is the concentration of 25-hydroxyvitamin D, which represents the state of total vitamin D with values ranging from 80 to 150 nmol/L (7).

Body mass index (BMI) provides an estimate of total body fat and can be calculated readily (as kg/m^2). Normal BMI for people aged 65 years and over ranges from 21 to 30 (8). Older adult women with a BMI less than 20.1 and older men with a BMI less than 20.9 have the highest risk of losing basic living skills (8). Furthermore, bone mass improves as BMI goes up because a BMI greater than 26 has been associated with other health risks, therefore patients are encouraged to maintain values in the middle of the range.

Calcium

Ninety-nine % of calcium in the human body is distributed in the skeleton (9). Diet and absorption are two critical factors in determining the availability of calcium for bone development, growth and

maintenance.

Calcium in food occurs as salts or is associated with other dietary constituents in the form of complexes of calcium ions (Ca^{2+}). It must be released in a soluble form before it can be absorbed in the proximal small intestine. There are two routes of absorption: the first consists of an active transcellular vitamin D-dependent pathway (especially when intake is low), with the entry of luminal Ca^{2+} across the microvillar membrane into the enterocyte, according to the electrochemical gradient, through specific ion channels such as CAT1 (calcium transport protein 1). The second route is a non-vitamin D-dependent paracellular pathway (especially when intake is high), when passive calcium is transported through the tight junctions between mucosal cells, nonsaturable, essentially independent of nutritional and physiological regulation, and concentration-dependent (10).

The intake at which the calcium excretion is zero (intake and absorption are equal) would be regarded as the ideal requirement. Though considerable differences exist between results obtained from different researchers, a WHO expert panel has concluded that the correct value is 520 mg per day for adults living in a western environment and consuming a western diet. Loss of calcium from the body occurs through urine and feces, as well as insensible loss. In adults, the minimum urinary loss is up to 140 mg/day. When the amount of calcium introduced by diet is less than 200 mg/day, the net intestinal absorption is practically zero, since approximately the same quantity is daily secreted into gastrointestinal lumen, and lost with the feces (10).

A number of food constituents have been suggested as potential enhancers of calcium absorption. Individual milk components, such as lactose, lactulose, and casein phosphopeptides have in the past attracted considerable attention. In addition, there is a growing body of evidence to show that non-digestible oligosaccharides can improve calcium absorption in some life-stage groups. Fluid milk reduces incident fractures in people who had previously suffered fractures, and bone reduction in postmenopausal women (11).

Calcium is also contained in legumes (soybean, peas, beans, lentils). It is useful to pay attention to cooked spinach, because it contains oxalic acid that interferes with the absorption of calcium (12).

Vitamin D

Vitamin D consists of a group of sterols antirachitic activities, of which only two are nutritionally relevant: ergocalciferol (vitamin D_2) and cholecalciferol (vitamin D_3). Both are produced by the action of ultraviolet radiation on their precursors (7-dehydrocholesterol and ergosterol, respectively). Most of the vitamin D requirement comes from endogenous synthesis in the skin during exposure to sunlight. Sun exposure is effective in late spring and summer from approximately 9 a.m. to 3 p.m. The length of sun exposure varies according to latitude, but exposure of hands, face, and arms three times a week for 5 to 15 minutes is generally adequate to maintain a good intake of Vitamin D.

Food intake plays a key role if sun exposure is insufficient. Vitamin D is contained in very few foods, especially in fish that feed on plankton. Human milk contains a Vitamin D level sufficient for the necessity of the newborn, while bovine milk is extremely poor. Thus cod liver oil, fatty fish and fortified foods (milk and cereals) are recommended in conditions of low sun exposure (13).

Vitamin D is absorbed in the small intestine by simple diffusion. Its absorption is independent of the presence of bile, but is pH-sensitive: it increases with increasing luminal acidity, but it reduces with a neutral luminal pH. After entering the enterocyte, vitamin D passes into the lymphatic circulation.

Calcitriol binds to cytoplasmic receptors in target tissues that translocate the hormone to the nucleus. The interaction of hormone-receptor complex (vitamin D receptor, VDR) with chromatin influences the processes of transcription and promotes protein synthesis. The receptors for the hormone are present in many tissues. In the small intestine calcitriol stimulates calcium absorption and the action is apparently mediated by an increased permeability of the luminal pole of epithelial cells in actively transported calcium to the cell in extracellular fluid. Calcitriol modifies the link between calmodulin and myosin 1, a protein found only in intestinal villi where it binds actin and plasma membrane. Calmodulin-myosin complex 1 promotes the entry of calcium into the intestinal cell, while transporting intracytoplasmic ion requires the intervention of

calbindine, a protein characterized by a high affinity for calcium and the synthesis of which is under the control of vitamin D (13).

The daily requirement of vitamin D varies according to age and also to particular conditions such as gestation or lactation. For an adult subject, in total absence of solar exposition, doses of 600–800 IU per day are needed (12). Vitamin D from the diet, due to its lipo-solubility, will be incorporated in chylomicrons and absorbed through the lymphatic system. Subsequently, it is bound to a vector protein, independently from its origin, and is transported to the liver, where the initial phase of activation takes place, through the formation of 25-OH-cholecalciferol (25-OH vitamin D, or calcifediol). This metabolite then enters the circulation, where it is transported by a globulin. 25-OH vitamin D has a half-life of 2–3 weeks, and its serum levels may be utilized as an indicator of the vitamin D status of the subjects, since it reflects the cumulative effects of vitamin intake and production by sunlight (12, 13).

Some experimental data suggested that $24,25(OH)_2$-D stimulates osteoblast activity and bone formation processes, decreasing fracture risk. It has instead been shown that $1,25(OH)_2$-D may directly inhibit the synthesis and secretion of PTH, resulting in decreased activity of osteoclasts and slowing the process of bone demineralization (13).

Sodium intake

Animal and human studies show that the excretion of calcium in the urine increases as dietary sodium intake increases. The increased urine calcium excretion is estimated at approximately 26 mg per gram of salt ingested. When salt intake is increased, it causes an excess of reabsorption of sodium at the proximal tubule and at Henle's loop, resulting in a reduction of calcium, which is then eliminated in the urine, depleting the calcium pool.

In general, based on data of urinary excretion of sodium, an adult sodium intake ranges from 2,990 to 4,600 mg/day. One study in postmenopausal women found that no hip bone loss occurred at calcium intakes of 1,768 mg/day or urinary sodium excretion of 2,110 mg/day (14).

However, despite evidence that a diet rich in salt increases bone loss, there are no restrictions on common diet.

Protein intake

Protein intake provides the structural matrix of bone, optimizes IGF-1 levels, increases urinary calcium and intestinal calcium absorption.

The volume of bone is composed of 50% protein. This bone protein matrix undergoes continuous turnover and remodeling. Collagen molecules undergo changes in their constituent aminoacids such as lysine and proline hydroxylation. This process prevents the reuse of fragments of collagen formed during proteolysis. This explains the benefits of a daily supply of dietary protein for bone maintenance (15).

Some studies suggest that, as a result of increased urinary calcium excretion with high protein intake, there is an increased risk of fractures or osteoporosis (15). As protein intake increases, there is an increase in urinary calcium, with most subjects developing negative calcium balance. One estimate is that there is a 50% increase in urinary calcium associated with doubling protein intake or roughly 1 mg urinary calcium for every gram of dietary protein (16). However, the increase in urinary calcium observed with purified proteins or amino acid infusions is not readily observed with food sources of protein (16).

However, studies in which diets provided 30% of energy as protein (181–214 g/day) found no increase in calciuria (17). In healthy adults, when protein intake was increased from 0.7 to 2.1 g/kg/day, urinary calcium increased, but intestinal absorption increased as well (17).

Increased calciuria does not necessarily translate to calcium loss, negative calcium balance, and reduced bone. On the contrary, several studies observed a positive association between dietary protein intake and increased bone mineral content or decreased risk of fracture (16).

Insulin-like growth factor (IGF-1) is another important factor that plays a key role in bone metabolism through its action on protein pathway. Higher levels of IGF-1 are osteotrophic. Concentration of IGF-1 in serum decreases with aging. Both the level and type of protein in the diet may have an effect on IGF-1 levels (18). Some, but not all studies (18) have found that meat as a protein source is associated with higher serum levels of IGF-1, which is in turn associated with increased bone mineralization and fewer fractures. Soy foods have been linked with lower levels of IGF-1 (19).

Although a study of Alekel et al. (20) suggested that 40 g soy protein supplementation with 80 mg isoflavones was able to attenuate bone loss from lumbar spine, women still lost 0.2% BMD in six months. Their data (20) imply that soy protein or its isoflavones are incapable of increasing bone mass in perimenopausal women.

Moreover, loss of bone mass (osteopenia) and loss of muscle mass (sarcopenia) that occur with age are closely related. Factors that affect muscle anabolism, including protein intake, also affect bone mass. Maintenance of adequate bone strength and density with aging is highly dependent on the maintenance of adequate muscle mass and function, which is in turn dependent on adequate intake of high-quality protein (21).

It has been suggested that animal protein–based diets might have a greater negative effect on skeletal health than vegetable-based diets because dietary animal protein induces a greater increase in urinary calcium excretion than vegetable protein. However, clinical studies do not support the hypothesis that animal protein has a detrimental effect on bone health or that vegetable-based proteins are better for bone health (21).

The relationship between protein intake and bone is further complicated by the potentially negative effect of overall dietary acid-base balance. Urinary calcium increases with acid-forming foods, such as meat, fish, eggs, and cereal, but decreases with plant foods and is likely determined by the acid-base status of the total diet. Bone loss may be attributable to the mobilization of skeletal salts to balance the endogenous acid generated from acid-forming foods (16). Net renal acid excretion can be predicted from the ratio of dietary protein to potassium because the dietary intake of potassium occurs mainly as salts of weak organic acids and therefore has an alkalizing effect. This explains the beneficial influence of fruit and vegetables, the major dietary source of potassium, on bone health (16). The effect of dietary acidity on the bone has a large impact over time. The positive association between meat intake and bone loss may, in fact, be a reflection more of inadequate intake of fruits and vegetables than overconsumption of meat.

Vitamin K

Vitamin K is a coenzyme for glutamate carboxylase, which mediates the conversion of glutamate (Glu) to gamma-carboxyglutamate (Gla). At least 3 Gla proteins are found in bone tissue (osteocalcin 5 bone Gla Protein, matrix Gla protein, and protein S), the most plentiful and best known of which is osteocalcin (OC). OC, which is synthesized by osteoblasts, is the major noncollagenous protein incorporated in bone matrix during bone formation, and is also released into the blood and used as a marker of bone formation. Gla residues at amino acid positions 17, 21, and 24 of OC can bind Ca^{2+} ions and are responsible for its high affinity for hydroxyapatite. The synthesis of functionally active OC is both vitamin D- and vitamin K-dependent. Vitamin K deficiency results in inadequate carboxylation of OC and leads to high serum levels of undercarboxylated (Glu) OC with low biologic activity. Low dietary vitamin K intake is associated with a decrease in BMD and an increase in fracture risk (22).

There are two types of vitamin K: K_1 (phytomenadione) and K_2 (menatetrenone, menaquinone). Menatetrenone is composed of four isoprene units and its function consists in increasing the amount of osteocalcin in osteoblasts, which leads to an inhibition of the resorption and reduction of blood calcium levels by acting on bones and kidneys. Menaquinone-7 is composed of seven isoprene units and is present in high levels in fermented soybean (natto). The action of menaquinone-7 on bone calcification is the same as menatetrenone (23).

The daily adequate intake (AI) of vitamin K for women is around 90 g (38). Vitamin K is contained in egg yolk, butter, liver and kidneys of beef, pork, cereals, and dark green leafy vegetables such as spinach and kale. This vitamin may be significant in preventing osteoporosis with increasing age. However, the mechanism of action in bone is not elucidated, but prolonged intake of *Natto* diets containing menaquinone-7 (total, 18.8 mg/100 g diet) can prevent osteoporosis (24).

Fatty acids

There are two classes of essential fatty acids (EFAs): omega-3 and omega-6. Humans (like all mammals) are unable to synthesize EFAs so they must be provided in the diet. The parent compound in the omega-6 fatty acid family is linolenic acid

(LA), while the parent compound of the omega-3 fatty acid family is α-linolenic acid (ALA).

The source of n-3 FAs may also have a significant impact on skeletal health. As reported in a study of Orchard et al., (25), when EFAs were given alone (excluding concomitant administration with calcium and vitamins), there was no beneficial effect noted. In contrast, a diet high in ALA from addition of walnuts, walnut oil and flaxseed oil compared to an average American diet pattern decreased NTx, a marker of bone resorption. Additionally, a mixture of plant and marine sources of n-3 FAs, with ALA in highest quantity, was used to fortify dairy products with the resultant decrease in u-Dpyr, a urinary marker of bone resorption (25).

Of the several potential mechanisms whereby n-3 FAs may impact bone, two of the most well-defined involve decreasing pro-inflammatory cytokines, key regulators of the osteoprotegerin/receptor activator of NFKB ligand (OPG/RANKL) ratio in bone (26). RANKL is expressed in osteoblasts and activates its receptor, RANK, which is expressed on osteoclasts, thus promoting osteoclast formation and activation, as well as suppressing apoptosis of osteoclasts. Osteoprotegerin (OPG) is a secretory glycoprotein expressed by osteoblasts which blocks RANKL from activating RANK. The ratio of OPG/RANKL is critical in the pathogenesis of resorptive bone disease, with a higher ratio indicating less bone resorption (26).

A second possible mechanism by which n-3 FAs may influence bone is related to up-regulation of intestinal calcium absorption. Essential FAs are necessary for maximal vitamin D-dependent calcium absorption (27).

Fatty fish are the major source of EPA and DHA in the U.S. diet, while vegetable oils, especially soybean and canola oils, are the primary sources of ALA. Nuts, seeds, vegetables, and some fruit, as well as egg yolk, poultry, and meat contribute small amounts of omega-3 fatty acids to the diet. Factors known to inhibit fatty acid desaturation are aging, smoking, diabetes, high sodium intake, and biotin deficiency, whereas calcium deficiency can impair essential fatty acid elongation (28).

Coffee

As reported in a study of Hallström et al. (29), high coffee consumption (four or more cups per day) plus high calcium intake (more than 1200 mg/day), did not alter BMD compared with those who had high consumption of coffee and low (< 600 mg/day) or intermediate intake (600-1200 mg/day) of calcium. There is still no strong evidence to show that caffeine alone has the capacity to reduce the risk of fractures (30).

DISCUSSION

As reported above, the anomalous intake of important nutrients to the body results in a serious problem, involving several organ areas and also the bone. Calcium and Vitamin D are some of the most important factors in the pathogenesis and prevention of osteoporosis (9). Calcium, contained in legumes, reduces incident fractures in osteoporotic bones (11). Vitamin D, poorly contained in foods, is derived from sun exposure and stimulates osteoblast acitivity and bone formation processes, decreasing fracture risk (13).

The notable importance in the pathogenesis and prevention of osteoporosis is related to metabolism of sodium, absorption of protein and vitamin K. Indeed, increased dietary sodium determines increased urine calcium excretion (14).

Protein has been identified as being both detrimental and beneficial to bone health, depending on a variety of factors, including the level of protein in the diet, the protein source, calcium intake, weight loss, and the acid/base balance of the diet (15). There is growing evidence that vitamin K, which is a nutritional factor, may play a role in the regulation of bone metabolism, because it is a coenzyme for glutamate carboxylase, which mediates the formation of Gla proteins, involving the synthesis of active OC (22).

Other important factors involved in bone metabolism are linked to fatty acids, that decrease the pro-inflammatory cytokines, reducing osteoclast activity (26), and up-regulate the absorption of vitamin D-dependent calcium (27).

Therefore, dietary rules have been suggested to prevent osteoporosis as follows: consume daily at least 3 portions of milk and dairy produce with reduced fat content; choose vegetables with high calcium content (cauliflower, cabbage); drink

mineral water with high calcium content; moderate alcohol intake; limit consumption of foods and drinks with high levels of phosphates; eat fish at least once a week; use spices or herbs (chives, parsley) in place of salt to enhance flavor; eat vegetables and fruit during the day; limit consumption of foods which contains high contents in oxalates; ensure sufficient intake of vitamin D (fish, liver, milk), vitamin K (leafy vegetables, liver, fish) and vitamin C.

In conclusion, osteoporosis is a multifactorial disease, the risk of which can be reduced by adequate nutrition and an appropriate lifestyle. Prevention should start in childhood, as that is the time when bone formation is very intensive, and achievement of optimal peak bone mass is a necessary requirement for optimal bone density in older age. Optimal intake of calcium, vitamins D and K, and fatty acids are important factors in primary as well as in secondary prevention of osteoporosis. Otherwise, it is important to exclude a diet containing large amounts of salt and caffeine. Moreover, an appropriate change of lifestyle, avoiding smoking, low body weight, high alcohol intake and a sedentary lifestyle, allows to maintain a lower fracture risk in the elderly.

REFERENCES

1. Ray N, Chan J, Thamer M, et al. Medical expenditures for the treatment of osteoporotic fractures in the United States in 1995: report from the National Osteoporosis Foundation. J Bone Miner Res 1997; 12:24-35
2. Halling A, Persson GR, Berglund J, Johansson O, Renvert S. Comparison between the Klemetti index and heel DXA BMD measurements in the diagnosis of reduced skeletal bone mineral density in the elderly. Osteoporos Int 2005; 16:999-1003.
3. Gosch M, Kammerlander C, Nicholas JA. Treatment of osteoporosis in older adults. Panminerva Med 2014; 56(2):133-43.
4. Cashman KD. Diet and control of osteoporosis. In: Remacle C, Reusens B, editors. Functional foods, ageing and degenerative disease. Cambridge, UK: Woodhead Publishing Limited; 2004. p. 83-114.
5. Uitterlinden AG, Ralston SH, Brandi ML. The association between common vitamin D receptor gene variations and osteoporosis: a participant-level meta-analysis. Ann Intern Med 2006; 145(4):255-64.
6. Stránský M, Ryšavá L. Nutrition as Prevention and Treatment of Osteoporosis. Physiol Res 2009; 58(Suppl 1):S7-S11.
7. Packard PT, Heaney RP. Medical nutrition therapy for patients with osteoporosis. J Am Diet Ass 1997; 97(4):414-17.
8. Mu M, Wang SF, Sheng J, et al. Dietary patterns are associated with body mass index and bone mineral density in Chinese freshmen. J Am Coll Nutr 2014; 33(2):120-8.
9. Warensjö E, Byberg L, Melhus H, Gedeborg R, Mallmin H, Wolk A, Michaëlsson K. Dietary calcium intake and risk of fracture and osteoporosis: prospective longitudinal cohort study. British Med J 2011; 342:1473.
10. Keller J, Schinke T. The role of the gastrointestinal tract in calcium homeostasis and bone remodeling. Osteoporos Int 2013; 24(11):2737-48.
11. Christakos S. Recent advances in our understanding of 1,25-dihydroxyvitamin D(3) regulation of intestinal calcium absorption. Arch Biochem Biophys 2012; 523(1):73-6.
12. Rossini M, Bianchi G, Di Munno O, et al. Determinants of adherence to osteoporosis treatment in clinical practice. Osteoporos Int 2006; 17(6):914-21.
13. Lips P. Vitamin D physiology. Prog Biophys Mol Biol 2006; 92(1):4-8.
14. Harrington M, Bennett T, Jakobsen J, Ovesen L, Brot C, Flynn A, Cashman KD. The effect of a high-protein, high-sodium diet on calcium and bone metabolism in postmenopausal women and its interaction with vitamin D receptor genotype. Br J Nutr 2004; 91(1):41-51.
15. Noakes M, Keogh J, Foster P, Clifton P. Effect of an energy-restricted, high-protein, low-fat diet relative to a conventional high-carbohydrate, low-fat diet on weight loss, body composition, nutritional status, and markers of cardiovascular health in obese women. Am J Clin Nutr 2005; 81:1298-306.
16. Heaney RP, Layman DK. Amount and type of protein influences bone health. Am J Clin Nutr 2008; 87(suppl):1567S-70S.
17. Nuttall F, Schweim K, Hoover H, Gannon M. Metabolic effect of a LoBAG30 diet in men with type 2 diabetes. Am J Physiol Endocrinol Metab

2006; 291:E786 -91.
18. Budek A, Hoppe C, Michaelsen K, Bügel S, Mølgaard C. Associations of total, dairy, and meat protein with markers for bone turnover in healthy, prepubertal boys. J Nutr 2007; 137:930-34.
19. Arjmandi BH, Lucas EA, Khalil DA, et al. One year soy protein supplementation has positive effects on bone formation markers but not bone density in postmenopausal women. Nutr J 2005; 4:8.
20. Alekel DL, Genschel U, Koehler KJ, et al. Soy isoflavones for reducing bone loss study: effects of a 3-year trial on hormones, adverse events, and endometrial thickness in postmenopausal women. Menopause 2015; 22(2):185-97.
21. Rondanelli M, Guido D, Opizzi A, Faliva MA, Perna S, Grassi M. A path model of sarcopenia on bone mass loss in elderly subjects. J Nutr Health Aging 2014; 18(1):15-21.
22. Shea MK, Booth SL. Update on the role of vitamin K in skeletal health. Nutr Rev 2008; 66(10):549-57.
23. Ehara Y, Takahashi H, Hanahisa Y, Yamaguchi M. Effect of vitamin K2 (menaquinone-7) on bone metabolism in the femoral-metaphyseal tissues of normal and skeletal-unloaded rats: enhancement with zinc. Res Exp Med 1996; 196:171-78.
24. Yamaguchi M, Kakuda H, Gao YH, Tsukamoto Y. Prolonged intake of fermented soybean (natto) diets containing vitamin K2 (menaquinone-7) prevents bone loss in ovariectomized rats. J Bone Miner Metab 2000; 18:71-76
25. Orchard TS, Pan X, Cheek F, Ing SW, Jackson RD. A systematic review of omega-3 fatty acids and osteoporosis. Br J Nutr 2012; 107(Suppl 2):S253-60.
26. Hofbauer LC, Schoppet M. Clinical implications of the Osteoprotegerin/RANKL/RANK system for bone and vascular diseases. JAMA 2004; 292(4):490-95.
27. Haag M, Magada ON, Claassen N, Böhmer LH, Kruger MC. Omega-3 fatty acids modulate ATPases involved in duodenal Ca absorption. Prostaglandins, Leukot Essentl Fatty Acids 2003; 68(6):423-29.
28. Kruger MC, Horrobin DF. Calcium metabolism, osteoporosis and essential fatty acids: a review. Prog Lipid Res 1997; 36:131-51.
29. Hallström H, Wolk A, Glynn A, Michaëlsson K. Coffee, tea and caffeine consumption in relation to osteoporotic fracture risk in a cohort of Swedish women. Osteoporos Int 2006; 17:1055-64.
30. Harter DL, Busnello FM, Dibi RP, Stein AT, Kato SK, Vanin CM. Association between low bone mass and calcium and caffeine intake among perimenopausal women in Southern Brazil: cross-sectional study. Sao Paulo Med J 2013; 131(5):315-22.

JOURNAL OF BIOLOGICAL REGULATORS & HOMEOSTATIC AGENTS Vol. 29, no. 3, 737-743 (2015)

LETTER TO THE EDITOR

METABOLIC BONE CHANGES IN OSTEOARTHRITIS: THE ROLE OF IMAGING AND PATHOGENETIC INTERPRETATION

E. SILVESTRI[1], A. CORAZZA[2], L. MOLFETTA[3] and G. GARLASCHI[2]

[1]Department of Radiology and Interventional Ultrasound, Ospedale Evangelico Internazionale (O.E.I.Ge), Genova, Italy; [2]Department of Health Sciences (Di.S.Sal), Section of Radiology, University of Genova, Genova, Italy; [3]Department of Orthopaedics, University of Genova, Genova, Italy

Received March 17, 2015 – Accepted August 25, 2015

Osteoarthritis (OA) is the most prevalent chronic joint disease and one of the major causes of disability in the adult population. Although OA is considered a progressive degenerative process which involves the whole joint, articular cartilage and subchondral bone play a determinant role in its pathogenesis. In particular, metabolic-triggered subchondral bone damage, together with biochemical markers, are referred as important indicators of the disease. Magnetic resonance (MR) is the best imaging technique to detect and characterize such bone abnormalities. It represents an effective method through which to not only diagnose, describe and follow the course of OA but also to deepen our understanding of the natural history of the disease, with the ultimate purpose of attaining improved outcome in terms of therapy and prognosis. Even though MR has enormous potential, some diagnostic pitfalls may occur in clinical practice, hence an accurate clinical assessment of the patient is mandatory in combination with optimal imaging evaluation.

Osteoarthritis is a common chronic joint disease which results in progressive loss of articular cartilage, subchondral bone changes, synovial proliferation and significant clinical manifestation such as articular pain, loss of joint function and disability (1, 2). Although the actual etiopathogenetic process of OA is still not completely known, genetic predisposition and many environmental risk factors including obesity, gender, aging, previous joint injuries and joint misalignment have been indicated as contributing factors for the onset and the progression of the disease over time (3-5). Subchondral bone and cartilage are essential structures that act as one dynamic complex in load-bearing of joints: despite different OA phenotypes, such structures are referred as the crucial structures for the local and systemic inflammatory mediators involved in the pathogenesis and maintenance of OA (6-8). Bone, synovium and cartilage metabolism and, in particular, subchondral bone turnover and its interaction with the articular cartilage, are commonly considered the underlying pathophysiologic pathways of osteoarthritic disease (8, 9). Bone and cartilage are intimately connected by the 'osteochondral junction' formed by the deeper layer of non-calcified cartilage, the tidemark, calcified cartilage and subchondral bone (7); many authors demonstrated the presence of biomechanical and biochemical cross-talk across this junctional

Key words: osteoarthritis, imaging, bone marrow, magnetic resonance, radiography, subchondral bone, cartilage, edema

Mailing address: Dr Angelo Corazza,
Dipartimento di Scienze della Salute (Di.S.Sal),
Sezione di Radiologia,
Università degli Studi di Genova,
Via L.B. Alberti 4 – 3p, 16132, Genova, Italy
Tel.: +39 0105522213 Fax: +39 0105522348
e-mail: angelcoraz@libero.it

0393-974X (2015)

DISCLOSURE: ALL AUTHORS REPORT NO CONFLICTS OF INTEREST RELEVANT TO THIS ARTICLE.

Table I. *Different pathological conditions associated with the presence of bone marrow edema-like pattern on magnetic resonance examinations.*

	Class	***Pathological condition***
1.	Micro-traumatic	· *Stress-response* · *Impingement* · *Traction enthesopathy* · *Focal overuse associated to intense physical activity* · *Insufficiency fractures*
2.	Macro-traumatic	· *Extrinsic bone contusion* · *'Kissing lesion' (bone vs bone)* · *Tendinous/ligamentous distraction associated* · *Chondral/subchondral/osteochondral fractures*
3.	Flogistic	· *Arthritis* · *Infections*
4.	Iatrogenic	· *Periprosthetic* · *Post-surgery*
5.	Ischemic	· *Osteonecrosis* · *Bone infarcts*
6.	Neoplastic	· *Tumor-associated reaction*
7.	Others	· *Transient osteoporosis of the hip* · *Spontaneous Osteonecrosis of the knee*

area which may be involved at many levels in the disease process, in particular regarding the complex inflammatory pathways which characterize osteoarthritic joints (10, 11). Clinical observations documented the role of bone and, in particular, of subchondral bone in early pathogenesis and progression of OA (5, 7, 12); many structural changes occur at this level and are represented by tidemark duplication, bone marrow lesions, calcified cartilage thickening, subchondral bone sclerosis, subchondral (pseudo-) cysts, and osteophytes (10).

In such setting, imaging plays a determinant role for the detection of early findings and for the monitoring of the disease progression, in association with clinical biomarkers (4, 5). Conventional radiography has been the most used technique in the assessment of OA for decades (12, 13). It allows the evaluation of joint space narrowing which indirectly reflects the loss of the articular cartilage; it also provides a good representation of OA–related bone changes such as undermineralization of trabecular structure and subchondral bone sclerosis (as a consequence of abnormal local high bone turnover) (7), bone cystic lesions or 'geodes' and osteophytes (14, 15). The Kellgreen-Lawrence grading scheme, which has been widely using for several years in many research studies and in clinical practice, and the more recent OARSI atlas are based on radiographic findings (15-18). Despite its important contribution, conventional radiography presents some limitations: it does not allow a direct evaluation of articular cartilage and, most important, it does not visualize bone marrow,

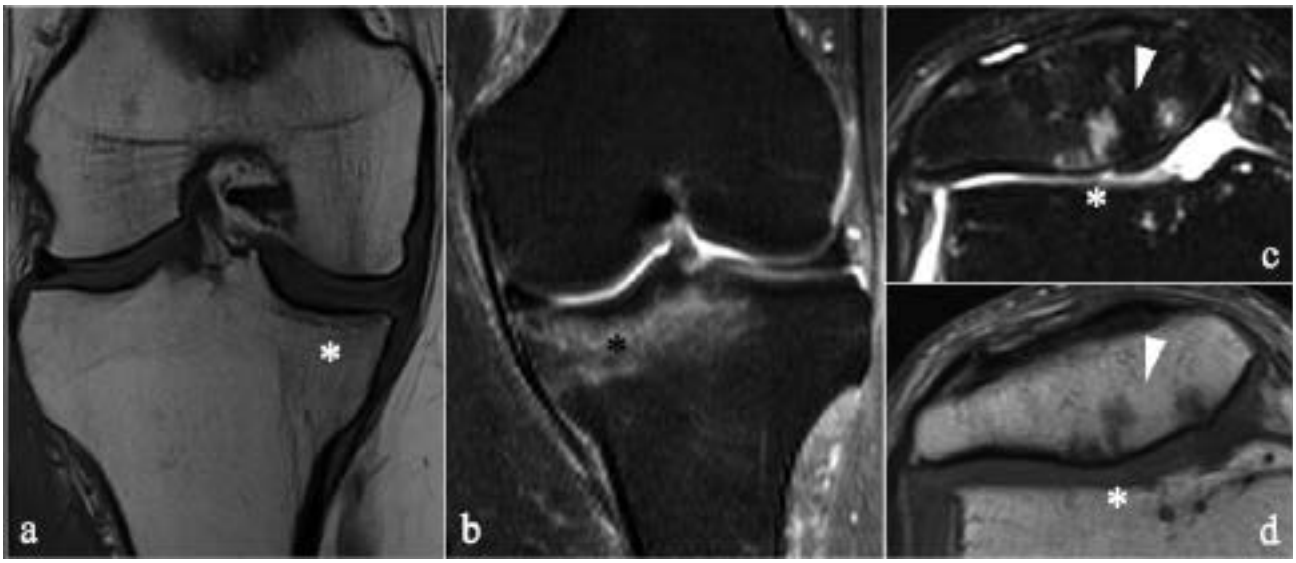

Fig. 1. *Subchondral bone marrow edema (sBME) and magnetic resonance (MR).* ***a)*** *Fast Spin Echo T1-weighted coronal scan of the knee of a 50-year-old woman with tibiofemoral joint OA and previous partial medial meniscus asportation: the image clearly shows a hypointense area of sBME affecting the medial side of the tibial plateau (white asterisk); note the significant extent of such area in particular if compared to the relatively limited articular cartilge damage.* ***b)*** *Proton-density (PD) image with SPectral Attenuated Inversion Recovery (SPAIR) technique. This kind of sequence is made in order to suppress the signal from fat tissue: as the bone marrow in adult epyphisis is fat marrow, MR fat-suppression scans depict it as 'dark' (=no signal). This SPAIR-PD scan shows a hyperintense wide area of sBME affecting the medial side of the tibial plateau (black asterisk) in association with a significant articular cartilage damage, more evident on the medial compartment of the tibio-femoral joint.* ***c)*** *Short-Tau Inversion Recovery axial scan and* ***d)*** *T1-weighted axial scan of a 63 woman with patellofemoral joint OA: these images show the presence of multiple small areas of subchondral bone involvement both on the medial and lateral side of the patella (white arrows), associated high grade articular cartilage damage (white asterisks) is evident; note also other abnormalities such as the femoral throclea irregularities and the marginal osteophytes both at the patellar and femoral side.*

articular and periarticular structures (3, 12, 19); OA is in fact considered a 'whole-organ' disease which progressively involves the entire joint (15). Based on current knowledge, magnetic resonance provides more comprehensive information on articular structures than radiography, but, to date, scientific data have not demonstrated a strong superiority of one technique over another in disease modification efficacy OA trials (20, 21).

Magnetic resonance results as an essential examination in OA, allowing the assessment of several joint components. It not only provides an accurate representation of articular cartilage integrity and subchondral bone abnormalities, but also depicts other joint structure alterations, related with the disease: central and marginal osteophytes, subcortical cysts, subchondral bone sclerosis, synovial hypertrophy and effusion, cruciate and/or collateral ligament injury, meniscal degeneration and/or lesions, intra-articular loose bodies, and periarticular cysts and bursitis (9). Among these, the presence of meniscal damage and/or synovitis are associated with a higher risk of rapid cartilage loss (15, 22, 23). The main strength of magnetic resonance comes from its intrinsic features: elevated contrast resolution, lack of ionizing radiation, multiplanar and multiparametric evaluation, with the possibility to perform both morphologic and high contrast sequences and, consequently, to match multiple data in order to get an accurate 'whole-joint' assessment. In clinical practice, MR examination usually includes Spin Echo, Turbo Spin Echo and Gradient Echo sequences, T1- and T2-weighted, acquired along the three orthogonal planes and/or with 3D isotropic

resolution, with and without fat signal suppression techniques. This standard protocol allows for a comprehensive qualitative evaluation of the joint and its components, as mentioned above. More specific imaging techniques such as compositional MRI (T2 mapping, T1 rho mapping, delayed gadolinium enhanced MR-dGEMRIC-, and sodium MR) could be performed in order to have a quantitative assessment of the biochemical properties of different joint tissues; they are mostly focused on articular cartilage evaluation, in particular dGEMRIC and sodium MR could be performed for the evaluation of the content of glycosaminoglycans, the early depletion of which has been related to the progressive degeneration of cartilage, hence providing useful data even in pre-morphologic changes stage (3, 14, 15, 24, 25). Many studies suggested also semiquantitative scoring methods for joint assessment in OA, among which the whole-organ MR imaging score (or WORMS), the MR imaging osteoarthritis knee score (or MOAKS), the Boston-Leeds osteoarthritis knee score (or BLOKS), the knee osteoarthritis scoring system (or KOSS), the scoring hip osteoarthritis with MRI (or SHOMRI) and the OMERACT hand osteoarthritis magnetic resonance scoring system (or HOAMRIS) are some of the main ones (15, 26).

As mentioned above, MR is crucial for the assessment of bone changes in the subchondral bone. Subchondral bone edema, usually addressed as 'bone marrow edema' (BME) is recognised by many authors as determinant in terms of pain and progression of OA (7, 12, 30). In particular, some studies suggested a correlation between BME detection, extent and pain (31, 32), between BME and the prediction of articular cartilage damage (13), even between BME extent and the increased risk of joint replacement (in osteoarthritic knee studies) (33). To date, the actual underlying histopathologic process of BME has not been completely demonstrated and several different pathological conditions and diseases with different pathogenetic processes result in the same MR pattern commonly referred to as BME (24, 34) (Table I). Such assumption suggests BME should be mentioned only as an MR finding: it is defined as a non-cystic area of the trabecular bone without clear delimitation, with variably high signal intensity on proton density-, intermediate- and T2-weighted sequences and fat suppressed sequences, low signal intensity on T1-weighted sequences (5, 15, 24, 34, 35) (Fig.1).

Some assumptions have to be made in order to properly interpret an MR exam: normally cortical and trabecular bone produce very low or no signal on MR, only bone marrow is represented, in relation to its content of protons, water and fat tissue, which is different in red and yellow marrow. Hence, an essential prerequisite is the knowledge of the normal changes, in terms of entity and distribution, of red and yellow marrow occurring with age (36, 37). Another mandatory prerequisite for the correct evaluation of BME is the exclusion of other conditions which could mimic BME aspect on MR images such as marrow substitution (i.e: neoplastic or infective diseases), marrow depletion (i.e: post radiotheraphy) and yellow-to-red marrow reconversion (i.e: stress, anemia, smokers and post-menstrual period). Some authors investigated the underlying histological changes of BME in OA subchondral bone and demonstrated a variety of findings including vascular congestion, subchondral trabecular thickening, sclerosis and remodeling, bone marrow granulation, edema, fibrosis and necrosis, osseous microfractures (possibly due to overloading) and subchondral intra-osseous cysts. Given such a broad spectrum of findings, some authors proposed to refer to BME as 'bone marrow edema–like lesion' (38, 39). Significant BME lesions could be commonly detected on MR in presence of associated limited articular cartilage damage, representing a useful diagnostic and prognostic element (Fig. 1). Summarizing, BME is widely considered a crucial element in OA, it is a nonspecific reaction which can be found in many pathological conditions: a correct imaging evaluation, together with clinical assessment, is mandatory in order to get an accurate diagnosis. In osteoarthritic patients early MR detection and characterization of BME may provide very useful data in terms of prognosis and therapeutic management.

In conclusion, research has made important steps in the understanding of the complex genetic, mechanical and metabolic factors which contribute to the onset and the progression of OA. To date, although scientific advances have achieved promising results, the road to a full comprehension of OA is still difficult and many issues have yet to be studied

and debated (40-44). The role of imaging and, in particular of the new MR techniques, is fundamental in this process of understanding, especially at early stages of the pathology, with the prospective that future studies may lead to new effective therapies which modify the course of the disease.

REFERENCES

1. Lawrence RC, Felson DT, Helmick CG et al. Estimates of the prevalence of arthritis and other rheumatic conditions in the United States. Part II. Arthritis Rheum 2008; 58:26-35.
2. Bijlsma JW, Berenbaum F, Lafeber FP. Osteoarthritis: an update with relevance for clinical practice. Lancet 2011; 377:2115-26.
3. Ding C, Zhang Y, Hunter D. Use of imaging techniques to predict progression in osteoarthritis. Curr Opin Rheumatol 2013; 25(1):127-35.
4. Wang X, Hunter D, Xu J, Ding C. Metabolic triggered inflammation in osteoarthritis. Osteoarthritis Cartilage 2015; 23(1):22-30.
5. Migliore A, Massafra U. Towards the identification of early stage osteoarthritis. Clin Cases Miner Bone Metab 2014; 11(2):114-6.
6. Sulzbacher I. Osteoarthritis: histology and pathogenesis. Wien Med Wochenschr 2013; 163(9-10):212-9.
7. Li G, Yin J, Gao J, Cheng TS, Pavlos NJ, Zhang C, Zheng MH. Subchondral bone in osteoarthritis: insight into risk factors and microstructural changes. Arthritis Res Ther 2013; 15(6):223.
8. Berembaum F. Osteoarthritis as an inflammatory disease (osteoarthritis is not osteoarthrosis!). Osteoarthritis Cartilage 2013; 21(1):16-21.
9. Karsdal MA, Bay-Jensen AC, Lories RJ, et al. The coupling of bone and cartilage turnover in osteoarthritis: opportunities for bone antiresorptives and anabolics as potential treatments? Ann Rheum Dis 2014; 73(2):336-48.
10. Henrotin Y, Pesesse L, Sanchez C. Subchondral bone and osteoarthritis: biological and cellular aspects. Osteoporos Int 2012; 23 Suppl 8:S847-51.
11. Eckstein F, Kwoh CK, Link TM; OAI investigators. Imaging research results from the osteoarthritis initiative (OAI): a review and lessons learned 10 years after start of enrolment. Ann Rheum Dis 2014; 73(7):1289-300.
12. Jia L, Chen J, Wang Y, Liu Y, Zhang Y, Chen W. Magnetic resonance imaging of osteophytic, chondral, and subchondral structures in a surgically-induced osteoarthritis rabbit model. PLoS One 2014; 9(12):e113707.
13. Roemer FW, Eckstein F, Hayashi D, Guermazi A. The role of imaging in osteoarthritis. Best Pract Res Clin Rheumatol 2014; 28(1):31-60.
14. Roemer FW, Guermazi A. Osteoarthritis year in review 2014: imaging. Osteoarthritis Cartilage 2014; 22(12):2003-12.
15. Huang M, Schweitzer ME. The role of radiology in the evolution of the understanding of articular disease. Radiology 2014; 273(2 Suppl):S1-22.
16. Kellgren J, Lawrence J. Radiological assessment of osteoarthritis. Ann Rheum Dis 1957; 16:494-501.
17. Altman RD, Gold GE. Atlas of individual radiographic features in osteoarthritis, revised. Osteoarthritis Cartilage 2007; 15 suppl A:A1-56.
18. Culvenor AG, Engen CN, Oiestad BE, Engebretsen L, Risberg MA. Defining the presence of radiographic knee osteoarthritis: a comparison between the Kellgren and Lawrence system and OARSI atlas criteria. Knee Surg Sports Traumatol Arthrosc 2014; doi: 10.1007/s00167-014-3205-0 [Epub ahead of print].
19. Leyland KM, Hart DJ, Javaid MK et al. The natural history of radiographic knee osteoarthritis: a fourteen-year population-based cohort study. Arthritis Rheum 2012; 64:2243-51.
20. Eckstein F, Le Graverand MH. Plain radiography or magnetic resonance imaging (MRI): which is better in assessing outcome in clinical trials of disease-modifying osteoarthritis drugs? Summary of a debate held at the World Congress of Osteoatrthritis 2014. Semin Arthritis Rheum 2015; pii: S0049-0172(15)00129-8. doi: 10.1016/j.semarthrit.2015.06.001. [Epub ahead of print].
21. Hunter DJ, Eckstein F, Kraus VB, Losina E, Sandell L, Guermazi A. Imaging biomarker validation and qualification report: sixth OARSI workshop on imaging in osteoarthritis combined with third OA biomarkers workshop. Osteoarthritis Cartilage 2013; 21(7):939-42.
22. Roemer FW, Kwoh CK, Hannon MJ, et al. Can structural joint damage measured with MR imaging

be used to predict knee replacement in the following year?. Radiology 2015 Mar;274(3):810-20.
23. Hunter DJ, Zhang W, Conaghan PG, et al. Systematic review of the concurrent and predictive validity of MRI bio-markers in OA. Osteoarthritis Cartilage 2011; 19:557-88.
24. Xu L, Hayashi D, Roemer FW, Felson DT, Guermazi A. Magnetic resonance imaging of subchondral bone marrow lesions in association with osteoarthritis. Semin Arthritis Rheum 2012; 42(2):105-18.
25. Rautiainen J, Nissi MJ, Salo EN, et al. Multiparametric MRI assessment of human articular cartilage degeneration: correlation with quantitative histology and mechanical properties. Magn Reson Med 2014; doi: 10.1002/mrm.25401. [Epub ahead of print].
26. Guermazi A, Hayashi D, Eckstein F, Hunter DJ, Duryea J, Roemer FW. Imaging of osteoarthritis. Rheum Dis Clin North Am 2013; 39(1):67-105.
27. Alizai H, Roemer FW, Hayashi D, Crema MD, Felson DT, Guermazi A. An update on risk factors for cartilage loss in knee osteoarthritis assessed using MRI-based semiquantitative grading methods. Eur Radiol 2015; 25(3):883-93.
28. Lee S, Nardo L, Kumar D, et al. Scoring hip osteoarthritis with MRI (SHOMRI): a whole joint osteoarthritis evaluation system. J Magn Reson Imaging 2015; 41(6):1549-57.
29. Haugen IK, Ostergaard M, Eshed I, et al. Iterative development and reliability of the OMERACT hand osteoarthritis MRI scoring system. J Rheumatol 2014; 41(2):386-91.
30. Sharkey PF, Cohen SB, Leinberry CF, Parvizi J. Subchondral bone marrow lesions associated with knee osteoarthritis. Am J Orthop (Belle Mead NJ) 2012; 41(9):413-17.
31. Kim IJ, Kim DH, Jung JY, et al. Association between bone marrow lesions detected by magnetic resonance imaging and knee pain in community residents in Korea. Osteoarthritis Cartilage 2013; 21(9):1207-13.
32. Stefanik JJ, Gross KD, Guermazi A, et al. The relation of MRI-detected structural damage in the medial and lateral patellofemoral joint to knee pain: The Multicenter and Framingham Osteoarthritis Studies. Osteoarthritis Cartilage 2015; 23(4):565-70.
33. Scher C, Craig J, Nelson F. Bone marrow edema in the knee in osteoarthrosis and association with total knee arthroplasty within a three-year follow-up. Skeletal Radiol 2008; 37:609-17.
34. Leydet-Quilici H, Le Corroller T, Bouvier C, et al. Advanced hip osteoarthritis: magnetic resonance imaging aspects and histopathology correlations. Osteoarthritis Cartilage 2010; 18(11):1429-35.
35. Roemer FW, Frobell R, Hunter DJ, et al. MRI-detected subchondral bone marrow signal alterations of the knee joint: terminology, imaging appearance, relevance and radiological differential diagnosis. Osteoarthritis Cartilage 2009; 17(9):1115-31.
36. Foster K, Chapman S, Johnson K. MRI of the marrow in the paediatric skeleton. Clinical Radiology 2004; 58:651-73.
37. Bredella MA, Stoller DW. Marrow imaging. In Magnetic resonance imaging in orthopaedics and sports medicine. Stoller DW, ed. Lippincott-Williams and Wilkins. Philadelphia, 2007; p. 1977-2044.
38. Zanetti M, Bruder E, Romero J, Hodler J. Bone marrow edema pattern in osteoarthritic knees: correlation between MR imaging and histologic findings. Radiology 2000; 215(3):835–840.
39. Taljanovic MS, Graham AR, Benjamin JB, et al. Bone marrow edema pattern in advanced hip osteoarthritis: quantitative assessment with magnetic resonance imaging and correlation with clinical examination, radiographic findings, and histopathology. Skeletal Radiol 2008; 37:423-31.
40. Conaghan PG, McQueen FM, Bird P, et al. Update on the OMERACT magnetic resonance imaging task force: research and future directions. J Rheumatol 2014; 41(2):383-5.
41. Jordan JM, Henrotin Y. Osteoarthritis research society international initiative on recommendations for conducting clinical trials in osteoarthritis: overview. Osteoarthritis Cartilage 2015; 23(5):671-3.
42. Gossec L, Paternotte S, Bingham CO 3rd, et al. OARSI/OMERACT initiative to define states of severity and indication for joint replacement in hip and knee osteoarthritis. An OMERACT 10 special interest group. J Rheumatol 2011; 38(8):1765-9.
43. Manno RL, Bingham CO 3rd, Paternotte S, et al. OARSI-OMERACT initiative: defining thresolds for symptomatic severity and structural changes in disease modifying osteoarthritis drugs (DMOAD) clinical trials. Osteoarthritis Cartilage 2012; 20(2):93-101.

44. Guermazi A, Eckstein F, Hunter D, Roemer F. 7th international workshop on osteoarthritis imaging report: "imaging in OA- now is the time to move ahead". Osteoarthritis Cartilage 2015; 23(6):888-96.

ERRATA CORRIGE

In the Supplement of Vo1ume 29 No. 1, page 91, the correct order of the authors should be as follows:
J.R. KALEY, D.R. FULLEN, J.M. GARDNER, J.W. PATTERSON, A.A. CHOKOEVA,
T. LOTTI, U. WOLLINA, G. TCHERNEV and R.M. PATEL